Cranfield Institute of Technology

School of Mechanical Engineering

Ph.D. Thesis

Academic Year 1986-87

Mohammad Mousa Al-Azzawi

AN ADVANCED FINITE ELEMENT SYSTEM FOR STATIC AND DYNAMIC ANALYSIS-WITH APPLICATION TO THE DESIGN OF RADIAL IMPELLERS

Supervisors Professor R.A. Cookson

Dr. A.M. E l-Zafrany

External Examiner Mr. D.A. Thurgood
Chief Mechanical Engineer
British AeroSpace Dynamics Group

July1987

VOLUME CONTAINS CLEAR OVERLAYS

OVERLAYS SCANNED SEPERATELY AND OVER THE RELEVANT PAGE.

To The People of Iraq

ACKNOWLEDGEMENTS

The author is firstly, and mostly, indebted to the people of Iraq to whom education comes before all. The presence of the author, and many others like him, here in the U.K. and around the world, even in these troubled times, proves this point beyond doubt.

The author wishes to express his most sincere gratitude and his true feelings towards Professor Roy Cookson, the Head of the Applied Mechanics Group, for his guidance, valuable advice and unlimited help, without whom the present work could never have been realised.

The author cannot find sufficient words to express his thanks towards Dr. Ali El-Zafrany who assisted and encouraged him at all times. Dr. Ali's deeds will never be erased from the author's memory.

The author wishes to thank the staff and his colleagues in the F.E.M. Group for their multiple help and the friendly atmosphere which they have created.

Last, but by no means least, I wish to express my appreciation to my wife Wisal for the understanding and patience, and to my children Rafal, Saif, Athal, Ienas and Eisa for the courage and amusement they gave me at those times when I needed them most.

SUMMARY

An advanced finite-element package, tailored to the static and dynamic analysis of radial impellers has been produced. Two families of new elements, one for thin and thick plates and the other for thin and thick shells, have been derived and proved to perform very well within a wide range of structural thicknesses. Static and dynamic economical solvers, two- and three-dimensional mesh generation and plotting, sectorial symmetric analysis, steady state response, transient response, and other programs are part of the large number of facilities available in the package.

The finite-element package has been validated by solving a large number of simple case studies and comparing the package results with those obtained from analytical solutions.

Two different radial impeller, experimental validation tests have been carried out, the first being the dynamic analysis of a radial impeller using the time averaged holographic technique, and the second the measurement of the steady-state stresses by means of a strain-gauge/slip ring assembly for a rotating impeller. The experimental results have been shown to be in good agreement with those obtained from the package.

CONTENTS

FIGURES

TABLES

CHAPTER ONE

INTRODUCTION

CHAPTER ONE

INTRODUCTION

A radial impeller, which can be a pump, a centrifugal compressor, or a radial turbine, is a very useful engineering device. Radial impellers have a wide range of applications. They are used in fuel and starting systems for aircraft and rocket engines, they are employed as superchargers for internal combustion engines, and they can be utilised as HP compressors in multi-spool jet engines.

Although designers working in the more conventional areas of industry, for example in some pump companies, may not feel the need for an advanced FEM package for the stress analysis of radial impellers, the situation may well be a little different in the more "High Technology" areas of industry. With the implementation of high speed radial impellers in jet and rocket engines, it is extremely important to have designs based upon rigorous analysis techniques.

Analytical solutions to the stress analysis of radial impellers have been carried out by many investigators, as pointed out by Kikuchi [Ref. 1] and Sham Sunder [Ref. 2]. A finite-difference technique for the stress analysis of rotating discs with asymmetric profile was employed by Thurgood and Givan [Ref. 3], and by Thurgood [Ref. 4].

Thurgood and Givan [Ref. 5] compared their approach [Ref. 3] with a number of earlier analytical techniques and concluded that none of these earlier methods produced satisfactory results for the range of different types of radial impeller.

From the previous literature it is clear that classical analytical methods cannot cope with the wide range of radial impeller design required. This uncertainty in the determination of impeller strength would therefore require the implementation of high safety factors which would, almost certainly lead to overdesign.

Experimental three-D stress and dynamic analysis is an expensive option.

From the early sixties, the finite element method (FEM) has proved to be a very powerful technique for dealing with complex structures such as radial impellers. An early attempt in which two-dimensional axisymmetric finite elements were employed, was that of Kikuchi, [Ref. 1] who himself recommended the use of three-D finite elements, in order to improve the accuracy of the solution. A more recent contribution was that made by Sham Sunder from whose work the following conclusions can be drawn.

- Three-D solid elements may not be the correct type of element for modelling of both thin blades and discs

- The lack of an eigenvalue economisers may limit the practicability of the use of his program for dynamic analysis of radial impellers

- The use of the following equation

$$\theta = \Sigma \theta_i N_i$$

for the representation of the cylindrical coordinate θ, in terms of nodal values and shape functions, is not an isoparametric transformation and may lead to inaccurate solutions.

From the late sixties to the present, a large number of FEM packages have been developed, but to the author's knowledge, there is not an FEM package tailored to the mechanical design of radial impellers. By the same token, versatile packages are too expensive and too complex to be used regularly. The FEM investigator, who would wish to test original ideas related to the FEM theory, has no option but to do so within his own programming system. It was envisaged that the best course for achieving useful original research into FEM

theory, was through the production of a computer package, and by making this package commercially useful, two birds will be hit by one stone.

An early difficulty with the employment of the FEM for the analysis of complex structures, was the generation of thousands of equations which would probably require an enormous amount of computer CPU time for their solution. Hence, it was essential to use economical static and dynamic solvers. With the development of such solvers and improvements in computer technology, it became obvious that a very useful development would be the minimisation of the human effort required for the preparation of FEM data.

Although thousands of papers and technical notes, on the subject of the FEM, are published every year there are still an enormous number of problems to be solved in this field. Paradoxically, it is therefore a little difficult to decide in which direction ones efforts should be aimed. However, when designing a computer package tailored to the analysis of a specific type of structure, the priorities of the task help to define the problems which must be tackled.

Work Objective

In line with the previous considerations, it was decided that the basic objective of this work was the design of an advanced FEM package which would be capable of static and dynamic analysis of radial impellers, or any other similar structure.

Although it appeared that finite element programming could become the major activity in the present work, some degree of originality would be an essential requirement if a competitive package tailored to such an objective was to be developed and if designers were to be offered an alternative which led to better impeller design than could be obtained from the available general purpose packages.

Package Requirements

In order to achieve the previous main objectives the proposed package should satisfy the following basic requirements.

(i) Economical Solver

A principal requirement for a competent FEM package is that it should contain the most economical solver. At the early stages of building the present package, it was not quite clear which solver could be considered to be the best. Banded and Frontal solvers were tried in this work, together with a number of eigenvalue economisers. Naturally, some conclusion will be given later concerning the economical solver recommended for a particular task.

Sectorial symmetry of structures, such as radial impellers, could also save a considerable amount of CPU time and human effort, if it is properly implemented.

(ii) Accuracy of the Finite Element Modelling

For the static and dynamic analysis of radial impellers, with disc and blades of variable thickness, the axisymmetric and/or 3D solid elements would be inadequate.

Thin and thick plate and shell elements should be considered. An attempt to develop accurate new plate and shell elements, which perform well with thin and thick structures, will be made here.

(iii) Minimisation of Human Effort

A versatile 2D-3D mesh generation facility is, without any doubt, essential. At an early stage of this work, the idea of designing a geometrical modeller was considered. However, due to time limitations, it was decided to abandon such an idea and to develop instead some additional techniques which could deal efficiently with

the mesh generation of radial impellers. Fortunately, it is still possible for the present package to be interfaced with commercial geometrical modellers.

(iv) Expandability

It is useful for the future development of a programming package for it to be designed in a way which allows for its expandability. A modular design approach should be adopted in which the package would be divided into a number of suitable modules which can easily be linked together.

(v) Usability

It is little use designing a sophisticated package without facilitating its use. A comprehensive users guide might even discourage designers from using the package. The following basic approaches could be introduced in order to improve the usability of a programming package:

- The implementation of self-explained, user-friendly, data modules.
- The clear display of tabular and graphical output.
- The use of a command procedure for the automatic control of the package operation.

The above points do not, of course, exclude the necessity for producing a well-explained users guide.

(vi) Validation

There is a golden rule set by the IBM company in order to comfort programming beginners that "every program has at least one error". If this is the case, and usually it is, then program

validation is vital. A number of validation cases should be used with the package so as to verify each part, before releasing the package for commercial use.

Thesis Construction

The major part of this thesis represents a detailed guide for the theory and application of the programming package. Chapter 2 deals with the theory of the FEM applied to C^0-elements, whilst old and new plate and shell elements are explained in Chapter 3. A basic review of the package solution procedures is introduced in Chapters 4 and 5, for static and dynamic analysis, respectively.

Mesh generation and plotting, with additional facilities for radial impellers, is illustrated in Chapter 6. A general description of the present programming package is reviewed in Chapter 7. Results and a discussion of the validation of the package together with engineering case studies, including some useful experimental work, are summarised in Chapter 8, whilst the final conclusions are listed in Chapter 9.

Due to the wide range of finite element aspects discussed in this work, it was decided to review the literature in the relevant chapter, for each different subject.

Although it is obviously desirable to make this thesis complete and independent, for such a complex subject the resulting thesis would be very large. Hence, it was decided that the main thesis should contain basic concepts, original derivations and verbal descriptions of the fundamental aspects of the work. Whilst detailed derivations and algorithms are included in a separate Appendix.

CHAPTER TWO

THEORY OF THE FINITE ELEMENT METHOD APPLIED TO $\mathring{C}$-ELEMENTS (TWO-D AND THREE-D SOLID ELEMENTS)

CHAPTER TWO

THEORY OF THE FINITE ELEMENT METHOD APPLIED TO C°-ELEMENTS (TWO-D AND THREE-D SOLID ELEMENTS)

2.1 LITERATURE REVIEW

The label "finite-element" appears to have been used first in a paper on plane elasticity problems [Ref. 6] published by Clough in 1960. The early development of the finite element method (FEM) was continually directed towards engineering applications. Initially, it was a tool designed and developed to solve real engineering problems, even though that outlook is quite distinct from much of the research recently being done in the finite element field. Huebner [Ref. 7] said that the concepts of the FEM began to solidify after 1963 when Besseling [Ref. 8], Melosh [Ref. 9], Fraijs de Veubeke [Ref. 10] and Jones [Ref. 11] recognised that the finite element method was a form of the Ritz method and confirmed it as a general technique to handle elastic continuum problems. In 1965 the finite element method received an even broader interpretation when Zienkiewicz and Cheung [Ref. 12], reported that it was applicable to all field problems that could be cast into variational form.

During the late 1960s and early 1970s (while mathematicians were working on establishing errors, bounds and convergence criteria for finite element approximations), engineers and other appliers of the finite element method were also studying similar concepts for various problems in the area of solid mechanics.

In the years since 1960, the finite element method has received widespread use in engineering. From the 1960's to the present time thousands of papers, and hundreds of books have been published on the subject. The Lagrangian quadrilateral family of finite elements appeared very early in the history of the F.E.M. [Ref. 13]. Melosh [Ref. 9] derived the 4-node rectangular element. Pian [Ref. 14] gave

an algorithm for the direct displacement approach with any number of unknown coefficients.

The concept of arbitrary-noded elements was described by Irons in 1965 [Ref. 15] but his work did not include any interpolation details. Argyris [Ref. 16] derived the 8-node parallelogramic element. Ergatoudis [Ref. 17] derived the shape functions for some Lagrangian and Serendipity elements. However, no general theory for the Serendipity element was produced. Dunne [Ref. 18] showed that two-dimensional shape functions could be complete bivariate polynomials of the m^{th} degree, if the number of element nodes n_o is given by:

$$n_o = \frac{1}{2}(m + 1)(m + 2)$$

This can be satisfied by the m^{th} degree triangular elements.

The hexahedral family is a natural extension to the quadrilateral family. Argyris [Ref. 19] derived the LUMINA element which has been employed for the ASKA system. This element is an isoparametric hexahedral element with m x n x l nodes. Ergatoudis [Ref. 20] derived some serendipity hexahedral elements. Dunne [Ref. 18] showed that the number of nodes required to obtain a complete trivariate polynomial of the m^{th} degree, as a shape function, is

$$n_o = \frac{1}{6}(m + 1)(m + 2)(m + 3)$$

which can be satisfied by the m^{th} degree tetrahedral element.

The triangular element was the first known finite element (but not referred to in those terms), when Turner et al [Ref. 21] published the work on their well-known constant strain triangle in 1956. The triangular element with linearly varying strains was derived by Argyris [Ref. 22]. The general interpolation formula for the

Lagrangian simplexes was given by Taylor [Ref. 23] which was based upon the works of Argyris [Refs. 24, 25, 26].

Fried [Ref. 27] described the mathematical properties of the natural coordinates in the d-dimensional space. A full review of finite element literature was given by Norrie and Vries [Ref. 28].

It is only recently that El-Zafrany and Cookson have derived general theorems for the derivation of Lagrangian and Serendipity shape functions for C^0-Elements [Refs. 29, 30, 31].

2.2 THE FINITE ELEMENT METHOD

The finite element method is a numerical analytical technique for obtaining approximate solutions to a wide variety of engineering problems.

2.2.1 Steps of FEM Applied to Static Analysis

The finite element procedure for the stress analysis of engineering structures can be organised in an algorithm which can be expressed in terms of the following basic steps.

(I) Discretisation of the Domain

The first step of the finite element procedure is to discretise the domain into subdomains (known as finite elements) connected by nodes. The discretised domain is called the finite element mesh and the discretisation process is known as the mesh generation. Techniques of mesh generation for 2D, 3D, plate and shell structures will be explained in Chapter (5).

(II) Formulation of Element Equations

A variational principle may be applied to each element in order to derive the element equations. For structural analysis, the element equations can be written as

$$\underline{K}_{(\bullet)} \quad \underline{\delta}_{(\bullet)} = \underline{F}_{(\bullet)}$$

where

$\underline{\delta}_{(\bullet)}$ is the nodal displacement vector

$\underline{F}_{(\bullet)}$ is the nodal force vector

$\underline{K}_{(\bullet)}$ is the element stiffness matrix.

Details of an element stiffness matrices for C^0- elements are given in this Chapter whilst the plate and shell elements will be explained in the next Chapter.

(III) Assembly of the Equations for the Whole Structure

In order to solve the finite element problem, the equations of all the elements must be assembled together to obtain the complete equations for the structure, and they are usually expressed in the following matrix form:

$$\underline{K}_T \quad \underline{\delta}_T = \underline{F}_T$$

(IV) Application of Boundary Conditions

Taking into account the boundary conditions of the problem, all of the restrained degrees of freedom will be eliminated to obtain a solvable reduced system of equations:

$$\underline{K}\ \underline{\delta} = \underline{F}$$

(V) Solution of the Resulting Equation

The reduced system of equations mentioned previously represents an algebraic system of simultaneous equations which can be solved to obtain $\underline{\delta}$. Efficient techniques for solving such equations will be described in Chapter (4).

(VI) Evaluation of Element Stresses and Strains

From the displacement solution it is possible to find the element nodal displacement vector which can be employed to find the element stresses and strains, as will be explained later.

2.2.2 Steps of FEM Applied to Dynamic Analysis

The finite element method can be applied to the dynamic analysis of structures. The basic types of analysis are; estimation of natural frequencies and natural mode shapes, the analysis of steady-state response and the analysis of transient response. Dynamic analysis using the FEM can also be standardised in the form of the following steps.

(I) Discretisation of the Domain

As mentioned in section (2.2.1)

(II) Formulation of Element Equations

This can be carried out in a way similar to that mentioned in section (2.2.1), except that the element equations for dynamic analysis are in the following matrix form:

$$\underline{M}_{(\bullet)}\ \ddot{\underline{\delta}}_{(\bullet)} + \underline{C}_{(\bullet)}\ \dot{\underline{\delta}}_{(\bullet)} + \underline{K}_{(\bullet)}\ \underline{\delta} = \underline{F}_{(\bullet)}$$

where

$\dot{\underline{\delta}}_{(\bullet)}$ is the nodal velocity vector

$\ddot{\underline{\delta}}_{(\bullet)}$ is the nodal acceleration vector

$\underline{M}_{(\bullet)}$ is the element mass matrix

$\underline{C}_{(\bullet)}$ is the element damping matrix.

(III) Assembly of the Equations for the Whole Structure

The dynamic equations for the whole structure are assembled and expressed in the following matrix form:

$$\underline{M}_T\ \ddot{\underline{\delta}}_T(t) + \underline{C}_T\ \dot{\underline{\delta}}(t) + \underline{K}_T\ \underline{\delta}_T(t) = \underline{F}_T(t)$$

where all nodal vectors are functions of time t.

(IV) Application of Boundary Conditions

Applying the given boundary conditions, the previous system will be reduced (in rows and columns) to the following:

$$\underline{M}\ \ddot{\underline{\delta}}(t) + \underline{C}\ \dot{\underline{\delta}}(t) + \underline{K}\ \underline{\delta}(t) = \underline{F}(t)$$

(V) Dynamic Analysis

The previous reduced system of equations represents a system of simultaneous second order differential equations in time t. The different types of dynamic analysis can be summarised as follows:

(a) Natural Frequency

When the structure is excited by a constant fequency ω, then $\underline{\delta}(t)$ can be written as follows:

$$\underline{\delta}(t) = \hat{\underline{\delta}} \cos\omega t$$

The natural frequency analysis is to find the values of ω required for the non-trivial solution of

$$\underline{M}\,\ddot{\underline{\delta}} + \underline{K}\,\underline{\delta} = \underline{0}$$

(b) Steady-State Response

For this case, it is required to find $\underline{\delta}(t)$, and the corresponding $\underline{\sigma}(t)$ and $\underline{\varepsilon}(t)$ for a cyclically repeated loading, i.e. to find the structure response to a forced excitation.

(c) Transient Response

If the exciting force vector $\underline{F}(t)$ is a general function of time (impulsive loading, random vibration, earthquake excitation etc), then it may be useful to obtain the history of $\underline{\delta}(t)$ through a time-marching scheme.

2.2.3 Element Selection

Finite element analysis of complex structures may require many different types of finite element depending upon the following considerations:

(a) Geometry of the structure
(b) Loading and boundary conditions
(c) Type of analysis required.

The popular types of element employed for the static and dynamic analysis of structures are demonstrated in Fig. 2.1. The basic elements employed in this work are listed as follows:

(a) Two-D Elements

These are plane-stress, plane-strain, and axisymmetric elements explained in section (2.5).

(b) Three-D Elements

These are solid elements used for the full 3-D analysis of structures. Cartesian and cylindrical elements are described in sections (2.3 and 2.6).

(c) Plate-and-Shell Elements

Due to the large number of types and considerations for these elements, they will be discussed in a separate Chapter (Chapter 3).

2.3 STEPS OF ELEMENT STIFFNESS MATRIX DERIVATION APPLIED TO A THREE-D ELEMENT

The stiffness matrix for a finite element can be derived in a systematic procedure. Such a procedure is more-or-less the same for all of the elements based upon the displacement approach. Using such a procedure, the stiffness matrix of an element will be expressed by the following triple product:

$$\underline{K}_{(\bullet)} = \int_{\substack{\text{volume of}\\ \text{the element}}} \int \int \underline{B}^t \, \underline{D} \, \underline{B} \; dV$$

as will be explained later. The difference between elements will appear only in the expression of the $\underline{D}$ and/or the $\underline{B}$ matrices. It is

perhaps best if such a basic procedure is reviewed using a practical example of a three-dimensional element. The steps of such a procedure can be summarised as follows:

Step 1: Definition of nodal parameters

For three-dimensional elasticity problems, the state of displacement at a point is defined in terms of three displacement components u,v,w in the direction of x,y and z axes. The nodal displacement vector for any n-node element can be defined as follows:

$$\underline{\delta} = \{u_1 \; v_1 \; w_1 \;\; u_2 \; v_2 \; w_2 \; \ldots\ldots\ldots \; u_n \; v_n \; w_n\}$$

and the nodal force vector is,

$$\underline{F} = \{F_{x1} \; F_{y1} \; F_{z1} \;\; F_{x2} \; F_{y2} \; F_{z2} \; \ldots\ldots\ldots \; F_{xn} \; F_{yn} \; F_{zn}\}$$

which is equivalent to any real loading system, as will be explained later.

Step 2: Interpolation of displacement components

In this step, the displacement components at any point are interpolated in terms of nodal displacements and shape functions, as follows:

$$u(x,y,z) = \sum_{i=1}^{n} u_i \; N_i(x,y,z)$$

$$v(x,y,z) = \sum_{i=1}^{n} v_i \; N_i(x,y,z)$$

$$w(x,y,z) = \sum_{i=1}^{n} w_i \; N_i(x,y,z)$$

where n_i, i = 1,2, ... n are the element shape functions.

in order to have an intrinsic form for the shape functions, it is essential to tranform the element into one which is uniform in the intrinsic ξ-η-ζ space, and the shape functions will, therefore, be expressed in terms of the intrinsic coordinates (ξ,η,ζ) as will be reviewed in section (2.6).

Step 3: Strain Components

Using the strain-displacement relationships [Ref. 32], strain components at any point are expressed in terms of nodal displacements and shape functions.

Hence, the vector of strain components at any point can be written as follows:

$$\underline{\varepsilon}_{6\times 1} = \underline{B}_{6\times 3n} \quad \underline{\delta}_{3n\times 1}$$

where

$$\underline{\varepsilon} = \{\varepsilon_x \ \varepsilon_y \ \varepsilon_z \ \gamma_{xy} \ \gamma_{yz} \ \gamma_{zx}\}$$

$$\underline{B} = [\underline{b}_1 \ \underline{b}_2 \ \ldots\ldots\ldots \ \underline{b}_n]$$

and

$$\underline{b}_i = \begin{pmatrix} N_{i,x} & 0 & 0 \\ 0 & N_{i,y} & 0 \\ 0 & 0 & N_{i,z} \\ N_{i,y} & N_{i,x} & 0 \\ 0 & N_{i,z} & N_{i,y} \\ N_{i,z} & 0 & N_{i,x} \end{pmatrix}$$

If the shape functions are expressed in terms of intrinsic coordinates (ξ, η, ζ) then the isoparametric transformation can be used to realte x,y,z to ξ, η, ζ as follows:

$$x(\xi,\eta,\zeta) = \sum_{i=1}^{n} x_i \, N_i(\xi,\eta,\zeta)$$

$$y(\xi,\eta,\zeta) = \sum_{i=1}^{n} y_i \, N_i(\xi,\eta,\zeta)$$

$$z(\xi,\eta,\zeta) = \sum_{i=1}^{n} z_i \, N_i(\xi,\eta,\zeta)$$

Considering any function $f(\xi,\eta,\zeta)$ and using the chain rule of partial differentiation, it can be deduced that:

$$\begin{pmatrix} \frac{\partial f}{\partial \xi} \\ \frac{\partial f}{\partial \eta} \\ \frac{\partial f}{\partial \zeta} \end{pmatrix} = \underline{J} \left(\frac{x,y,z}{\xi,\eta,\zeta}\right) \begin{pmatrix} \frac{\partial f}{\partial x} \\ \frac{\partial f}{\partial y} \\ \frac{\partial f}{\partial z} \end{pmatrix}$$

where

$\underline{J}$ is the three-dimensional Jacobian matrix which is defined as follows:

$$\underline{J} \left(\frac{x,y,z}{\xi,\eta,\zeta}\right) = \begin{pmatrix} \frac{\partial x}{\partial \xi} & \frac{\partial y}{\partial \xi} & \frac{\partial z}{\partial \xi} \\ \frac{\partial x}{\partial \eta} & \frac{\partial y}{\partial \eta} & \frac{\partial z}{\partial \eta} \\ \frac{\partial x}{\partial \zeta} & \frac{\partial y}{\partial \zeta} & \frac{\partial z}{\partial \zeta} \end{pmatrix}$$

Hence, the cartesian derivatives of the shape functions, at any point, can be obtained from:

$$\begin{pmatrix} \frac{\partial N_i}{\partial x} \\ \frac{\partial N_i}{\partial y} \\ \frac{\partial N_i}{\partial z} \end{pmatrix} = \underline{J}^{-1} \left(\frac{x,y,z}{\xi,\eta,\zeta}\right) \begin{pmatrix} \frac{\partial N_i}{\partial \xi} \\ \frac{\partial N_i}{\partial \eta} \\ \frac{\partial n_i}{\partial \zeta} \end{pmatrix}$$

Step 4: Stress Components

The stress components at any point can be expressed in terms of nodal displacements and shape functions. Firstly, define the stress vector at any point as follows:

$$\underline{\sigma} = \{\sigma_x \ \sigma_y \ \sigma_z \ \tau_{xy} \ \tau_{yz} \ \tau_{zx}\}$$

let $\underline{\sigma}_o$ be the vector of initial stresses

and $\underline{\varepsilon}_o$ be the vector of initial and/or thermal strains,

then, from the theory of elasticity [Ref. 32], it can be deduced that:

$$\underline{\sigma} = \underline{D}\,(\underline{\varepsilon} - \underline{\varepsilon}_o) + \underline{\sigma}_o$$

where

$$\underline{D} = \frac{E}{(1+\nu)(1-2\nu)} \begin{pmatrix} 1-\nu & \nu & \nu & 0 & 0 & 0 \\ \nu & 1-\nu & \nu & 0 & 0 & 0 \\ \nu & \nu & 1-\nu & 0 & 0 & 0 \\ 0 & 0 & 0 & \frac{1-2\nu}{2} & 0 & 0 \\ 0 & 0 & 0 & 0 & \frac{1-2\nu}{2} & 0 \\ 0 & 0 & 0 & 0 & 0 & \frac{1-2\nu}{2} \end{pmatrix}$$

Step 5: Strain Energy

The strain energy (U) of the element is expressed in terms of nodal displacements.

From the definition of strain energy it can be expressed as follows:

$$U = \int_{\text{element}} \int \int \left(\int_{o}^{\varepsilon} \sigma^t \, d\underline{\varepsilon} \right) dV + U_o$$

$$\int_{o}^{\varepsilon} \underline{\sigma}^t \, d\underline{\varepsilon} = \int_{o}^{\varepsilon} (\underline{\varepsilon}^t D - \underline{\varepsilon}_o^t \, \underline{D} + \underline{\sigma}_o^t) \, d\underline{\varepsilon}$$

$$= \tfrac{1}{2} \, \underline{\varepsilon}^t \, \underline{D} \, \underline{\varepsilon} - \underline{\varepsilon}_o^t \, \underline{D} \, \underline{\varepsilon} + \underline{\sigma}_o^t \, \underline{\varepsilon}$$

$$= \tfrac{1}{2} \, \underline{\varepsilon}^t \, \underline{D} \, \underline{\varepsilon} - \underline{\varepsilon}^t \, \underline{D} \, \underline{\varepsilon}_o + \underline{\varepsilon}^t \, \underline{\sigma}_o$$

$$= \tfrac{1}{2} \, \underline{\delta}^t \, \underline{B}^t \, \underline{D} \, \underline{B} \, \underline{\delta} - \underline{\delta}^t \, \underline{B}^t \, \underline{D} \, \underline{\varepsilon}_o + \underline{\delta}^t \, \underline{B}^t \, \underline{\sigma}_o$$

Hence, it can be shown that

$$U = \tfrac{1}{2} \, \underline{\delta}^t \left(\int_{\text{element}} \int \int \underline{B}^t \, \underline{D} \, \underline{B} \, dV \right) \underline{\delta}$$

$$- \underline{\delta}^t \left(\int_{\text{element}} \int \int \underline{B}^t \, \underline{D} \, \underline{\varepsilon}_o \, dV \right) + \underline{\delta}^t \left(\int_{\text{element}} \int \int \underline{B}^t \, \underline{\sigma}_o \, dV \right) + U_o$$

and

$$U_o = -\int \int \int \left(\int_{o}^{\varepsilon_o} \underline{\sigma}^t \, d\underline{\varepsilon} \right) dV$$

Step 6: Energy Theorem

Apply the minimum total potential energy theorem to derive the equilibrium equations for the element. The total potential energy for the element can be defined as follows:

$$\chi = U + V$$

where V is the potential energy.

If the potential energy is due to mechanical loading only, then

$$V = -W$$

where W is the work done by external loads.

An equivalent loading vector $\underline{F}$ can be found such that

$$W = \underline{\delta}^t \underline{F}$$

Hence

$$\chi = U - \underline{\delta}^t \underline{F}$$

which is a function of $\underline{\delta}$.

The mathematical condition for the minimisation of χ can be defined vectorally as follows:

$$\frac{\partial \chi}{\partial \underline{\delta}} = \underline{0}$$

From the theorems for the differentiation of matrix products [Ref. 33], it can be proved that

$$\frac{\partial \chi}{\partial \underline{\delta}} = \underline{K}_{(\bullet)}\ \underline{\delta} - \underline{F} - \underline{F}_{\varepsilon} - \underline{F}_{\sigma} = \underline{0}$$

which gives

$$\underline{K}_{(\bullet)}\ \underline{\delta} = \underline{F} + \underline{F}_{\varepsilon} + \underline{F}_{\sigma}$$

where

$$\underline{K}_{(\bullet)} = \int_{\text{element}} \int \int \underline{B}^{t}\ \underline{D}\ \underline{B}\ dV$$

$$\underline{F}_{\varepsilon} = \int_{\text{element}} \int \int \underline{B}^{t}\ \underline{D}\ \underline{\varepsilon}_{o}\ dV$$

$$\underline{F}_{\sigma} = -\int_{\text{element}} \int \int \underline{B}^{t}\ \underline{\sigma}_{o}\ dV$$

2.4 STEPS OF ELEMENT MASS MATRIX DERIVATION APPLIED TO A THREE-D ELEMENT

The mass matrix for a finite element can also be derived by using an algorithmic approach which can be summarised as follows:

Step 1: Definition of nodal parameters

These are the nodal velocities which can be defined as follows

$$\dot{\underline{\delta}} = \{\dot{u}_1\ \dot{v}_1\ \dot{w}_1\ \dot{u}_2\ \dot{v}_2\ \dot{w}_2\ \ldots\ldots\ldots\ \dot{u}_n\ \dot{v}_n\ \dot{w}_n\}$$

where

$$\dot{u}_i = \frac{du_i}{dt}, \quad \dot{v}_i = \frac{dv_i}{dt}, \quad \dot{w}_i = \frac{dw_i}{dt}$$

Step 2: Interpolation of Velocity Components

The velocity components at any point are interpolated in terms of nodal velocities as follows:

$$\dot{u} = \sum_{i=1}^{n} \dot{u}_i N_i$$

$$\dot{v} = \sum_{i=1}^{n} \dot{v}_i N_i$$

$$\dot{w} = \sum_{i=1}^{n} \dot{w}_i N_i$$

where N_i are the same shape functions as employed before.

The velocity vector at any point can therefore be defined as follows:

$$\underline{C} = \begin{pmatrix} \dot{u} \\ \dot{v} \\ \dot{w} \end{pmatrix} = \underline{N}_{3 \times 3n} \; \dot{\underline{\delta}}_{3n \times 1}$$

where

$$\underline{N} = \begin{pmatrix} N_1 & 0 & 0 & \ldots\ldots\ldots\ldots & N_n & 0 & 0 \\ 0 & N_1 & 0 & \ldots\ldots\ldots\ldots & 0 & N_n & 0 \\ 0 & 0 & N_1 & \ldots\ldots\ldots\ldots & 0 & 0 & N_n \end{pmatrix}$$

Step 3: Kinetic Energy

The kinetic energy of the element is expressed in terms of the nodal velocities. Generally, the kinetic energy can be defined as follows:

$$KE = \frac{1}{2} \int |\underline{C}|^2 \, dm$$

Hence

$$KE = \frac{1}{2} \int_{element} \int \int \rho \, |\underline{C}|^2 \, dV$$

$$= \frac{1}{2} \int_{element} \int \int \rho \, \underline{C}^t \, \underline{C} \, dV$$

From the previous definition of $\underline{C}$,

$$\underline{C}^t = \dot{\underline{\delta}}^t \, \underline{N}^t$$

therefore

$$KE = \frac{1}{2} \int_{element} \int \int \rho \, \dot{\underline{\delta}}^t \, \underline{N}^t \, \underline{N} \, \dot{\underline{\delta}} \, dV$$

$$KE = \frac{1}{2} \, \dot{\underline{\delta}}^t \left(\int_{element} \int \int \rho \, \underline{N}^t \, \underline{N} \, dV \right) \dot{\underline{\delta}}$$

Step 4: The element mass matrix $\underline{M}_{(\bullet)}$ can be deduced from the following equation

$$KE = \frac{1}{2} \, \dot{\underline{\delta}}^t \, \underline{M}_{(\bullet)} \, \dot{\underline{\delta}}$$

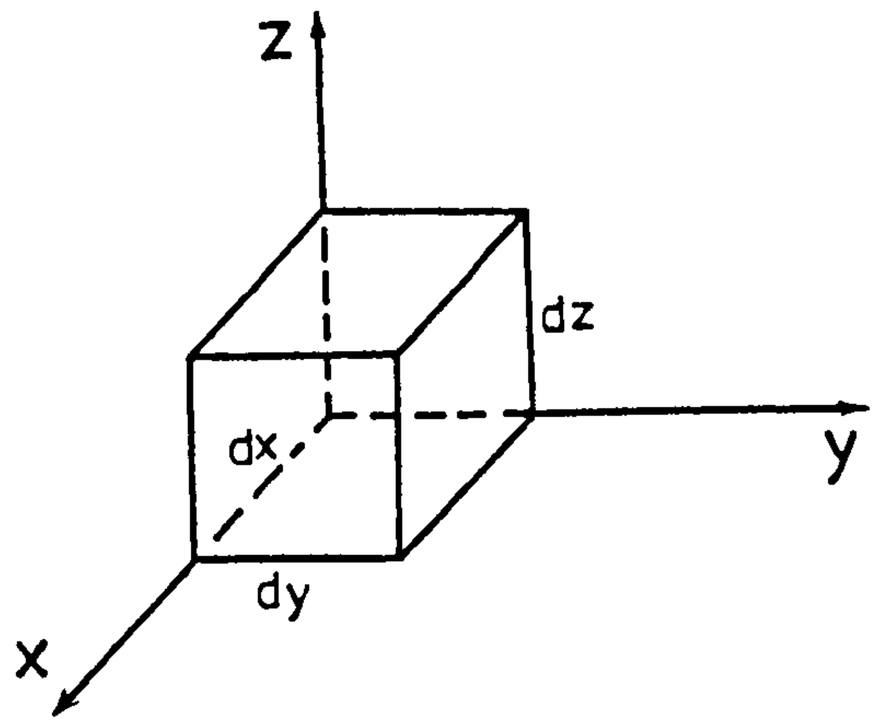

An element of volume dV

Therefore

$$\underline{M}_{(\bullet)} = \int_{\text{element}} \int \int \rho \, \underline{N}^t \, \underline{N} \, dx \, dy \, dz$$

$$dV = dx \, dy \, dz$$

The above expression for $\underline{M}_{(\bullet)}$ is more-or-less the same for most types of element based upon a displacement derivation. The differences between types of element will appear in the $\underline{N}$ matrix, as will be shown later.

2.5 TWO-D AND AXISYMMETRIC ELEMENTS

The steps of element stiffness and mass matrix derivations are the same for all types of displacement elements as explained before. Hence, a brief definition of the basic vectors and matrices employed for two-D, and for axisymmetric elements, will be reviewed.

2.5.1 Two-D Elements

These are the elements which are employed for static and dynamic analysis of plane-stress and plane-stress problems. For an n-node element in the x-y plane, the nodal displacement vector can be defined as follows:

$$\underline{\delta} = \{u_1 \; v_1 \; u_2 \; v_2 \; \ldots\ldots\ldots \; u_n \; v_n\}$$

Defining the strain vector at any point (x,y) as:

$$\underline{\varepsilon}_{3\times 1} = \underline{B}_{3\times 2n}\ \underline{\delta}_{2n\times 1}$$

where

$$\underline{B} = \begin{pmatrix} N_{1,x} & 0 & N_{2,x} & 0 & \cdots\cdots & N_{n,x} & 0 \\ 0 & N_{1,y} & 0 & N_{2,y} & \cdots\cdots & 0 & N_{n,y} \\ N_{1,y} & N_{1,x} & N_{2,y} & N_{2,x} & \cdots\cdots & N_{n,y} & N_{n,x} \end{pmatrix}$$

writing the stress vector as follows

$$\underline{\sigma} = \{\sigma_x \quad \sigma_y \quad \tau_{xy}\}$$

$$\underline{\sigma} = \underline{D}\ \underline{\varepsilon}$$

Instead of using two different $\underline{D}$ matrices for plane-stress and plain strain, one $\underline{D}$ matrix can be used for both of these cases, which is as follows:

$$\underline{D} = \frac{2G}{1-2\nu'} \begin{pmatrix} 1-\nu' & \nu' & 0 \\ \nu' & 1-\nu' & 0 \\ 0 & 0 & \frac{1-2\nu'}{2} \end{pmatrix}$$

where

$$G = \frac{E}{2(1+\nu)}$$

$$\nu' = \nu \quad \text{for plane-strain}$$

$$\nu' = \frac{\nu}{1+\nu} \quad \text{for plane-stress}$$

The $\underline{N}$ matrix for a two-dimensional element is as follows:

$$\underline{N}_{2\times 2n} = \begin{pmatrix} N_1 & 0 & N_1 & 0 & \ldots\ldots & N_n & 0 \\ 0 & N_1 & 0 & N_2 & \ldots\ldots & 0 & N_n \end{pmatrix}$$

Finally, the stiffness and mass matrices for an element can be defined as follows:

$$\underline{K}_{(\bullet)} = \int_{\text{element}} \int t\, \underline{B}^t\, \underline{D}\, \underline{B}\; dx\, dy$$

$$\underline{M}_{(\bullet)} = \int_{\text{element}} \int \rho\, t\, \underline{N}^t\, \underline{N}\, dx\, dy$$

where t is the element thickness.

2.5.2 Axisymmetric Elements

These elements can be employed for the stress analysis of solid structures provided that the following conditions are valid:

(a) The structure is geometrically symmetric w.r.t. an axis (say the z-axis)

(b) There is no loading component normal to the r-z plane

(c) The load distribution in the r-z plane should be the same at any θ.

The use of such elements in dynamic analysis is limited to the evaluation of circular mode shapes of vibration and the response due to an axisymmetric dynamic loading.

From the previous conditions, it can be deduced that

$$\frac{\partial \text{property}}{\partial \theta} = 0$$

and

$$u_\theta = 0$$

where u_θ is the tangential displacement component. The strain vector, for this case, can be defined as follows:

$$\underline{\varepsilon} = \{\varepsilon_r \ \varepsilon_\theta \ \varepsilon_z \ \gamma_{rz}\}$$

Using the displacement-strain relationships with cylindrical polar coordinates, it can be deduced that:

$$\underline{\varepsilon}_{4\times 1} = \underline{B}_{4\times n} \ \underline{\delta}_{n\times 1}$$

where

$$\underline{B} = [\underline{b}_1 \ \underline{b}_2 \ \ldots\ldots\ldots \ \underline{b}_n]$$

such that:

$$\underline{b}_i = \begin{pmatrix} N_{i,r} & 0 \\ \dfrac{N_i}{r} & 0 \\ 0 & N_{i,z} \\ N_{i,z} & N_{i,r} \end{pmatrix}$$

n = number of nodes of the element.

Consequently, the stress vector is defined as follows:

$$\underline{\sigma} = \{\sigma_r \ \sigma_\theta \ \sigma_z \ \tau_{rz}\}$$

and from the stress-strain relationships:

$$\underline{\sigma}_{4\times1} = \underline{D}_{4\times4} \quad \underline{\varepsilon}_{4\times1}$$

where

$$\underline{D} = \frac{E}{(1+\nu)(1-2\nu)} \begin{pmatrix} 1-\nu & \nu & \nu & 0 \\ \nu & 1-\nu & \nu & 0 \\ \nu & \nu & 1-\nu & 0 \\ 0 & 0 & 0 & \frac{1-2\nu}{2} \end{pmatrix}$$

Hence, the stiffness and mass matrices for an axisymmetric element can be expressed as follows:

$$\underline{K}_{(\bullet)} = \int_{\substack{r-z \\ \text{element}}} \int 2\pi r \, \underline{B}^t \, \underline{D} \, \underline{B} \, dr \, dz,$$

$$\underline{M}_{(\bullet)} = \int_{\substack{r-z \\ \text{element}}} \int 2\pi r \, \rho \, \underline{N}^t \, \underline{N} \, dr \, dz$$

The $\underline{N}$ matrix is the same as for the two-dimensional case. From Fig. 2.2, it can be shown that the volume of an infinitesimal axisymmetric element is as follows

$$dV = r \, d\theta \, dr \, dz$$

2.5.3 Review of Families of Isoparametric 2-D Elements

Two families of 2D isoparametric elements are employed in this work, they are summarised as follows:

(a) Quadrilateral Family

Simple 4-node quadrilateral element, together with higher order Lagrangian and Serendipity elements, a total of (7) elements, shown in Tables 2.1 - 2.2 have been employed in the present work.

The intrinsic shape functions for these elements are listed explicitly in terms of (ξ,η) defined in the region [0,1], as given in Appendix (A.1).

(b) Triangular Family

Linear, quadratic and cubic elements, shown in Table 2.3 are employed in the present package. The lists of their intrinsic shape functions in terms of (ξ,η) are given in Appendix (A.1).

2.6 THREE-D SOLID ELEMENTS

Three-dimensional isoparametric elements are employed for the full three-dimensional static and dynamic analysis of solid structures. There are two types of derivation for such elements depending upon the frame of axes. The first type are known as Cartesian elements, which are those derived w.r.t. the Cartesian x-y-z space. The derivation of stiffness and mass matrices for such elements has been described in section (2.3). The second type are known as cylindrical elements which are defined in the cylindrical-polar r-z-θ space. Cylindrical elements are more practical for the modelling of rotating machine components. They are optimum elements for structures with sectorial symmetry such as radial impellers.

2.6.1 Cylindrical 3D Elements

Consider an n-node element in r-z-θ space for example a hexahedral element as shown in Fig. 2.3. The nodal displacement

vector for such an element can be defined as follows:

$$\underline{\delta} = \{(u_r)_1 \ (u_\theta)_1 \ (u_z)_1 \ \ldots\ldots\ldots \ (u_r)_n \ (u_\theta)_n \ (u_z)_n\}$$

where u_r, u_θ, u_z are the displacement components in the r,θ,z directions respectively.

The strain components can be written as follows:

$$\underline{\varepsilon} = \{\varepsilon_r \ \varepsilon_\theta \ \varepsilon_z \ \ \gamma_{r\theta} \ \gamma_{\theta z} \ \gamma_{zr}\}$$

The cylindrical-polar strain-displacement relationships are:

$$\varepsilon_r = \frac{\partial u_r}{\partial r}$$

$$\varepsilon_\theta = \frac{u_r}{r} + \frac{1}{r}\frac{\partial u_\theta}{\partial \theta}$$

$$\varepsilon_z = \frac{\partial u_z}{\partial z}$$

$$\gamma_{r\theta} = \frac{1}{r}\frac{\partial u_r}{\partial \theta} + \frac{\partial u_\theta}{\partial r} - \frac{u_\theta}{r}$$

$$\gamma_{\theta z} = \frac{1}{r}\frac{\partial u_z}{\partial \theta} + \frac{\partial u_\theta}{\partial z}$$

$$\gamma_{zr} = \frac{\partial u_r}{\partial z} + \frac{\partial u_z}{\partial r}$$

The element will be transformed (isoparametrically) into a uniform element in the ξ-η-ζ space, and the displacement components at any (ξ,η,ζ) will be as follows:

$$u_r(\xi,\eta,\zeta) = \sum_{i=1}^{n} (u_r)_i \quad N_i(\xi,\eta,\zeta)$$

$$u_\theta(\xi,\eta,\zeta) = \sum_{i=1}^{n} (u_\theta)_i \quad N_i(\xi,\eta,\zeta)$$

$$u_z(\xi,\eta,\zeta) = \sum_{i=1}^{n} (u_z)_i \quad N_i(\xi,\eta,\zeta)$$

Hence, the strain vector can be expressed in terms of nodal displacements and shape functions as follows:

$$\underline{\varepsilon} = \underline{B} \ \underline{\delta}$$

$$\underline{B} = [\underline{b}_1 \ \underline{b}_2 \ \ldots\ldots\ldots \ \underline{b}_n]$$

and

$$\underline{b}_i = \begin{pmatrix} \frac{\partial N_i}{\partial r} & 0 & 0 \\ \frac{N_i}{r} & \frac{1}{r}\frac{\partial N_i}{\partial \theta} & 0 \\ 0 & 0 & \frac{\partial N_i}{\partial z} \\ \frac{1}{r}\frac{\partial N_i}{\partial \theta} & \left(\frac{\partial N_i}{\partial r} - \frac{N_i}{r}\right) & 0 \\ 0 & \frac{\partial N_i}{\partial z} & \frac{1}{r}\frac{\partial N_i}{\partial \theta} \\ \frac{\partial N_i}{\partial z} & 0 & \frac{\partial N_i}{\partial r} \end{pmatrix}$$

Since the element nodal coordinates should be expressed in terms of (r,θ,z), it would seem reasonable to use the following isoparametric equations:

$$r(\xi,\eta,\zeta) = \sum_{i=1}^{n} r_i N_i(\xi,\eta,\zeta)$$

$$\theta(\xi,\eta,\zeta) = \sum_{i=1}^{n} \theta_i N_i(\xi,\eta,\zeta)$$

$$z(\xi,\eta,\zeta) = \sum_{i=1}^{n} z_i N_i(\xi,\eta,\zeta)$$

However, an early attempt proved not to converge to an accurate answer, a condition which was found to be due to the violation of the constant derivative convergence condition [Ref. 34]. Such a condition will be satisfied automatically for an element with

$$\sum_{i=1}^{n} N_i(\xi,\eta,\zeta) = 1$$

if the following transformation is employed:

$$x(\xi,\eta,\zeta) = \sum_{i=1}^{n} x_i N_i(\xi,\eta,\zeta)$$

$$y(\xi,\eta,\zeta) = \sum_{i=1}^{n} y_i N_i(\xi,\eta,\zeta)$$

$$z(\xi,\eta,\zeta) = \sum_{i=1}^{n} z_i N_i(\xi,\eta,\zeta)$$

which has been adopted here regardless of the type of the global frame of axes.

Using the chain rule of partial differentiation, it can be deduced that:

$$\frac{\partial r}{\partial \xi} = \frac{\partial r}{\partial x}\frac{\partial x}{\partial \xi} + \frac{\partial r}{\partial y}\frac{\partial y}{\partial \xi} + \frac{\partial r}{\partial z}\frac{\partial z}{\partial \xi}$$

$$\frac{\partial r}{\partial \eta} = \frac{\partial r}{\partial x}\frac{\partial x}{\partial \eta} + \frac{\partial r}{\partial y}\frac{\partial y}{\partial \eta} + \frac{\partial r}{\partial z}\frac{\partial z}{\partial \eta}$$

$$\frac{\partial r}{\partial \zeta} = \frac{\partial r}{\partial x}\frac{\partial x}{\partial \zeta} + \frac{\partial r}{\partial y}\frac{\partial y}{\partial \zeta} + \frac{\partial r}{\partial z}\frac{\partial z}{\partial \zeta}$$

which can be written in the following matrix form

$$\begin{pmatrix} \frac{\partial r}{\partial \xi} \\ \frac{\partial r}{\partial \eta} \\ \frac{\partial r}{\partial \zeta} \end{pmatrix} = \underline{J}\left(\frac{x,y,z}{\xi,\eta,\zeta}\right) \begin{pmatrix} \frac{\partial r}{\partial x} \\ \frac{\partial r}{\partial y} \\ \frac{\partial r}{\partial z} \end{pmatrix} \qquad \ldots\ldots (a)$$

where

$\underline{J}\left(\frac{x,y,z}{\xi,\eta,\zeta}\right)$ is the three-dimensional Jacobian matrix defined in section (2.3)

Similarly,

$$\begin{pmatrix} \frac{\partial\theta}{\partial\xi} \\ \frac{\partial\theta}{\partial\eta} \\ \frac{\partial\theta}{\partial\zeta} \end{pmatrix} = \underline{J}\left(\frac{x,y,z}{\xi,\eta,\zeta}\right) \begin{pmatrix} \frac{\partial\theta}{\partial x} \\ \frac{\partial\theta}{\partial y} \\ \frac{\partial\theta}{\partial z} \end{pmatrix} \qquad \ldots\ldots (b)$$

Defining the following cylindrical-polar Jacobian matrix:

$$\underline{J}_c\left(\frac{r,\theta,z}{\xi,\eta,\zeta}\right) = \begin{pmatrix} \frac{\partial r}{\partial\xi} & \frac{\partial\theta}{\partial\xi} & \frac{\partial z}{\partial\xi} \\ \frac{\partial r}{\partial\eta} & \frac{\partial\theta}{\partial\eta} & \frac{\partial z}{\partial\eta} \\ \frac{\partial r}{\partial\zeta} & \frac{\partial\theta}{\partial\zeta} & \frac{\partial z}{\partial\zeta} \end{pmatrix} \qquad \ldots\ldots (c)$$

it can be deduced from equations (a), (b), (c) that

$$\underline{J}_c\left(\frac{r,\theta,z}{\xi,\eta,\zeta}\right) = \underline{J}\left(\frac{x,y,z}{\xi,\eta,\zeta}\right) \begin{pmatrix} \frac{\partial r}{\partial x} & \frac{\partial\theta}{\partial x} & 0 \\ \frac{\partial r}{\partial y} & \frac{\partial\theta}{\partial y} & 0 \\ \frac{\partial r}{\partial z} & \frac{\partial\theta}{\partial z} & 1 \end{pmatrix}$$

Considering a function $f(r,\theta,z)$, using the chain rule of partial differentiation, it can be shown that

$$\begin{pmatrix} \frac{\partial f}{\partial r} \\ \frac{\partial f}{\partial \theta} \\ \frac{\partial f}{\partial z} \end{pmatrix} = \begin{pmatrix} \frac{\partial x}{\partial r} & \frac{\partial y}{\partial r} & \frac{\partial z}{\partial r} \\ \frac{\partial x}{\partial \theta} & \frac{\partial y}{\partial \theta} & \frac{\partial z}{\partial \theta} \\ 0 & 0 & 1 \end{pmatrix} \begin{pmatrix} \frac{\partial f}{\partial x} \\ \frac{\partial f}{\partial y} \\ \frac{\partial f}{\partial z} \end{pmatrix}$$

$$= \begin{pmatrix} \frac{\partial x}{\partial r} & \frac{\partial y}{\partial r} & \frac{\partial z}{\partial r} \\ \frac{\partial x}{\partial \theta} & \frac{\partial y}{\partial \theta} & \frac{\partial z}{\partial \theta} \\ 0 & 0 & 1 \end{pmatrix} \underline{J}^{-1}\left(\frac{x,y,z}{\xi,\eta,\zeta}\right) \begin{pmatrix} \frac{\partial f}{\partial \xi} \\ \frac{\partial f}{\partial \eta} \\ \frac{\partial f}{\partial \zeta} \end{pmatrix}$$

$$= \underline{J}_c^{-1}\left(\frac{r,\theta,z}{\xi,\eta,\zeta}\right) \begin{pmatrix} \frac{\partial f}{\partial \xi} \\ \frac{\partial f}{\partial \eta} \\ \frac{\partial f}{\partial \zeta} \end{pmatrix}$$

where

$$\underline{J}_c^{-1}\left(\frac{r,\theta,z}{\xi,\eta,\zeta}\right) = \begin{pmatrix} \frac{\partial x}{\partial r} & \frac{\partial y}{\partial r} & \frac{\partial z}{\partial r} \\ \frac{\partial x}{\partial \theta} & \frac{\partial y}{\partial \theta} & \frac{\partial z}{\partial \theta} \\ 0 & 0 & 1 \end{pmatrix}$$

Using the following relationships between (x,y,z) and (r,θ,z);

$$x = r\cos\theta$$

$$y = r\sin\theta$$

$$z = z$$

it can be deduced that

$$\underline{J}_c^{-1}\left(\frac{r,\theta,z}{\xi,\eta,\zeta}\right) = \begin{pmatrix} \cos\theta & \sin\theta & 0 \\ -r\sin\theta & r\cos\theta & 0 \\ 0 & 0 & 1 \end{pmatrix} \underline{J}^{-1}\left(\frac{x,y,z}{\xi,\eta,\zeta}\right)$$

Expressing $N_i(\xi,\eta,\zeta)$ as $f(\xi,\eta,\zeta)$, the derivatives of the shape function w.r.t. r,θ and z can be obtained.

The element of volume dV can be defined as follows:

$$dV = \begin{pmatrix} \frac{\partial r}{\partial \xi} & r\frac{\partial \theta}{\partial \xi} & \frac{\partial z}{\partial \xi} \\ \frac{\partial r}{\partial \eta} & r\frac{\partial \theta}{\partial \eta} & \frac{\partial z}{\partial \eta} \\ \frac{\partial r}{\partial \zeta} & r\frac{\partial \theta}{\partial \zeta} & \frac{\partial z}{\partial \zeta} \end{pmatrix} d\xi\, d\eta\, d\zeta$$

Hence, it can be deduced that

$$dV = r \mid \underline{J}_c \mid d\xi\, d\eta\, d\zeta$$

$$\equiv \mid \underline{J} \mid d\xi\, d\eta\, d\zeta$$

The vector of stress components is defined as follows:

$$\underline{\sigma} = \{\sigma_r \quad \sigma_\theta \quad \sigma_z \quad \tau_{r\theta} \quad \tau_{\theta z} \quad \tau_{zr}\}$$

and

$$\underline{\sigma} = \underline{D}\ \underline{\varepsilon}$$

where the $\underline{D}$ matrix is the same as that given in section (2.3).

The element stiffness matrix for this type of element will be as follows:

$$\underline{K}_{(\bullet)} = \int_{\text{element}} \int \int \underline{B}^t \ \underline{D} \ \underline{B} \ dV$$

using the developed form of the $\underline{B}$ matrix. The derivation of the element mass matrix is the same as in section (2.3), and the $\underline{M}_{(\bullet)}$ equation is as follows:

$$\underline{M}_{(\bullet)} = \int_{\text{element}} \int \int \rho \ \underline{N}^t \ \underline{N} \ dV$$

2.6.2 Review of Families of Isoparametric 3-D Elements

The 3-D families employed in the present package, for both the cartesian and cylindrical derivation, are hexahedral, pentahedral and tetrahedral families. A complete list of the intrinsic shape functions, defined in the region [0,1], for all of the isoparametric 3-D elements employed in this work, is given in Appendix (A.2).

Since a fully three-D analysis may require a large number of nodes and elements, elements of too high an order are not recommended. Hence, only the first and second order elements of each family have been employed in this work and they can be summarised as follows:

(a) Hexahedral Family

The hexahedral elements used in this work, are

i) the 8-node Lagrangian element,

ii) the 20-node serendipity element, as shown in Table 2.4.

The equations of $\underline{K}_{(\bullet)}$ and $\underline{M}_{(\bullet)}$ for those elements are as follows:

$$\underline{K}_{(\bullet)} = \int_0^1 \int_0^1 \int_0^1 \underline{B}^t \; \underline{D} \; \underline{B} \; |\underline{J}| \; d\xi \, d\eta \, d\zeta$$

$$\underline{M}_{(\bullet)} = \int_0^1 \int_0^1 \int_0^1 \rho \; \underline{N}^t \; \underline{N} \; |\underline{J}| \; d\xi \, d\eta \, d\zeta$$

(b) Tetrahedral Family

The tetrahedral elements used in this work, are

i) the 4-node tetrahedral element (the linear element)

ii) the 10-node tetrahedral element (the quadratic element), as shown in Table 2.5.

The equations of $\underline{K}_{(\bullet)}$ and $\underline{M}_{(\bullet)}$ for this family are

$$\underline{K}_{(\bullet)} = \int_0^1 \int_0^{1-\zeta} \int_0^{1-\eta-\zeta} \underline{B}^t \; \underline{D} \; \underline{B} \; |\underline{J}| \; d\xi \, d\eta \, d\zeta$$

$$\underline{M}_{(\bullet)} = \int_0^1 \int_0^{1-\zeta} \int_0^{1-\eta-\zeta} \rho \; \underline{N}^t \; \underline{N} \; |\underline{J}| \; d\xi \, d\eta \, d\zeta$$

c) Pentahedral Family

The pentahedral elements employed in this work are:

i) the 6-node Serendipity element

ii) the 15-node Serendipity element, as demonstrated in Table 2.6.

The equations of $\underline{K}_{(\bullet)}$ and $\underline{M}_{(\bullet)}$ for such elements are as follows:

$$\underline{K}_{(\bullet)} = \int_0^1 \int_0^1 \int_0^{1-\eta} \underline{B}^t \, \underline{D} \, \underline{B} \, |\underline{J}| \, d\xi \, d\eta \, d\zeta$$

$$\underline{M}_{(\bullet)} = \int_0^1 \int_0^1 \int_0^{1-\eta} \rho \, \underline{N}^t \, \underline{N} \, |\underline{J}| \, d\xi \, d\eta \, d\zeta$$

CHAPTER THREE

PLATE AND SHELL FINITE ELEMENTS

CHAPTER THREE

PLATE AND SHELL FINITE ELEMENTS

3.1 LITERATURE REVIEW

The bending properties of a plate depend greatly upon its thickness as compared with its other dimensions. For "thin" plates the transverse shear is negligible leading to the validation of the assumption that normals to the neutral surface remain normal after deformation. For "thick" plates there is a considerable shear deformation leading to warping of the plate [Ref. 35].

Thin Plates

Ignoring transverse shear, and assuming that the plate deflection is small compared with its thickness, the state of deformation of the plate can be expressed in terms of a single parameter w, which represents the lateral deformation of the plate midplane, as will be explained later. Unfortunately, continuity conditions between elements should be imposed not only on w, but also on its first order partial derivatives, (at least) to ensure that the deformed plate does not kink [Ref. 34].

Attempts on the finite element analysis of plate bending appeared very early in the literature, however the first convergent element satisfying the C^1-continuity conditions was the 4-node rectangular element published by Melosh in 1963 [Ref. 36]. Zienkiewicz and Cheung in 1964 [Ref. 37] derived Hermitian shape functions for the same element, which are equivalent to the Melosh derivation. The 4-node rectangular element can only be generalised to a parallelogram since its transformation to a general quadrilateral shape will lead to a violation of the constant curvature criterion [Ref. 34]. This disadvantage limited the use of FEM for plate bending to shapes which can be modelled into rectangular or parallelogramic

elements. This was the case until a suitable 3-node triangular element was published in 1965 by Bazeley et al [Ref. 38].

Several attempts were carried out to derive higher order, C^1-continuous elements, and these are reviewed in Zienkiewicz's book [Ref. 34]. Only recently, El-Zafrany and Cookson have introduced a basis for the derivation of general Hermitian triangular elements [Ref. 29] and general Hermitian quadrilateral elements [Ref. 30].

Thick Plates

For the case of thick plates, sandwich construction or cellular plates, the shear deformation is significant, and the classic thin plate theory based on Kirchoff's assumption, will lead to an inaccurate solution. Attempts to correct the theory and basic equations to allow for such deformation are numerous. Love [Ref. 39], Reissner [Ref. 40], Libove and Batdore [Ref. 41], Mindlin [Ref. 42], and Essenburg and Machoi [Ref. 43] described various attempts to formulate more general governing equations.

A general formulation for curved thick shell elements was presented by Ahmad et al [Ref. 44]. The success of this (Ahmad's) element encouraged Hinton et al [Ref. 45] to apply a similar approximation to thick plates and they published details of the first "Mindlin" element in 1974. It was discovered that the solutions obtained from using the Mindlin element were less accurate than those based upon the Kirchoff element, when the plate thickness was reduced, and this source of inaccuracy was referred to as the "shear locking" phenomenon.

Zienkiewicz et al [Ref. 46], Pugh [Ref. 47], Hughes et al [Ref. 48] and others have investigated this phenomenon, and they have used reduced and selective integration schemes to avoid locking. Hughes and Cohen [Ref. 49] derived a 9-node quadrilateral element, known as the Heterosis element, which exhibits improved characteristics in comparison with both the 8-node Serendipity and the 9-node Lagrangian

elements.

El-Zafrany and Cookson [Ref. 50] introduced a general approach to the derivation of plate-bending elements which performs quite well and is independent of the plate thickness.

Facet Shell Elements

For the static and dynamic analysis of radial impellers with straight blades, no new elements are required. Three-D elements given in Chapter two can be employed for very thick impellers. A thin or thick plate bending element can be combined with a two-D element to form a thin or thick facet shell element, as will be described later.

Curved blades can be modelled approximately by facet elements, employing the assumption that the behaviour of a continuously curved surface can be adequately represented by the behaviour of a surface built up of small flat elements [Ref. 34].

Curved Shell Elements

These elements may provide a more accurate facility for the finite element modelling of curved blades. The classical shell element is derived by reducing the 3-dimensional field equations to a particular class of shell equations using analytical integration over the thickness which is governed by the shell assumptions. Common assumptions are based on one or more characteristics of the shell geometry, for example, that the rotation of the cross-section is simply the slope of the shell. This applies only when the shell is relatively thin and where its shear strain is negligible.

The basic equations which describe the behaviour of a thin elastic shell were originally derived by Love [Refs. 39, 51]. There has been considerable literature concerning curved shell elements (see Finite Element Bibliography Ref. 28). Pawsey [Ref. 52] and Dovey

[Ref. 53] explained the basic problems common to most shell elements, and which restrict most elements to one class of shells, either thin or thick, depending on the parent theory used for developing the element.

Several attempts have been made to degenerate 3-dimensional elements for employment as shells. Wilson [Ref. 54] and Dovey [Ref. 53] modified 3-dimensional elements for use as thick shells. However, the convergence of such modified elements was not guaranteed.

The degeneration concept discretises directly the 3-D field equation in terms of midsurface nodal values. This process employs shell assumptions and a formulation which includes transverse shear effects.

This type of element requires only the C^0 continuous shape functions, because the equilibrium equations in terms of independent variables (e.g. displacements and rotations) are second-order differential equations. Irons and Draper [Ref. 55], Melosh [Ref. 56], Ukta [Ref. 57], and Wempner et al [Ref. 58], who developed shell elements based on this concept, obtained unsatisfactory results when these elements were applied to the thin shell regime. Worsak (Ref. 59] explained that such difficulty could be traced to the transverse shear energy which is $0[(L/_h)^2]$ higher than the remaining terms, where $L/_h$ denotes the element length to thickness aspect ratio.

If the thickness approaches zero, the shear stiffness will be completely dominant and no effect of the bending stiffness remains within the finite-element computer word length. From this explanation it can be seen that this element will give a stiff solution which does not reflect the correct bending behaviour. As explained previously, physically, this phenomenon is again shear-locking. Wempner et al [Ref. 58], Zienkiewicz et al [Ref. 46], Ahmad et al [Ref. 44], Zienkiewicz and Hinton [Ref. 60], and other researchers have studied several techniques, in order to solve the shear-locking problem. The interesting problem is to discover a simple shell element, which can

be used for thin and thick shell structures and at the same time yield accurate results. Irons [Ref. 61], and Irons and Ahmad [Ref. 62] explained the Semiloof Beam and shell elements which can be used for thin and thick shells. Irons and Ahmad [Ref. 62] emphasised that the Semiloof shell theory is probably the most difficult on record. They stated that the shape function package was large, forbidding, and relatively slow - although the cost was only a small proportion of the total, particularly for large jobs, and they looked forward to the day when other workers could introduce a new element based on a simpler formulation.

In this Chapter the Hermitian shape functions for a 9-node subparametric quadrilateral element will be derived using the generalised approach of El-Zafrany and Cookson [Ref. 30].

Different elements for the analysis of thin and thick plates are summarised. A new element which uses Hermitian shape functions and takes the transverse shear into consideration, is introduced. Facet shell elements based upon plane-stress, and plate-bending elements are reviewed. A new facet shell element for thin and thick structures is derived. A unified approach, based upon the standard steps for the derivation of stiffness and mass matrices as explained in sections (2.3) and (2.4), is employed here for different plate and shell elements.

3.2 HERMITIAN SHAPE FUNCTIONS

Several different types of finite element, with Hermitian shape functions, are employed for plate and shell analysis. It would perhaps be advantageous to review the shape functions of the basic families of such elements, explicitly here, before going on to describe the details of different types, of element.

3.2.1 Triangular Family

Although triangular elements of very high order are available

in the literature, it was decided to use only the 3-node triangular element in this work. Such an element has proved to be accurate and reliable. The elements of higher order, employ shape functions of very high degree, which may lead to large rounding off errors.

For the 3-node triangular element a field function w(x,y) can be interpolated in terms of the nodal values, w_1, $w_{1,x}$, $w_{1,y}$, ... etc and Hermitian shape functions. Intrinsic expressions for such shape functions can be obtained if the element is transformed into an intrinsic element in the ξ-η plane, as shown in Fig. 3.1.

The following isoparametric equations can be used for such a transformation:

$$x(\xi,\eta) = x_1 + \xi (x_2 - x_1) + \eta (x_3 - x_1)$$

$$y(\xi,\eta) = y_1 + \xi (y_2 - y_1) + \eta (y_3 - y_1)$$

The interpolated field function can, therefore, be expressed as follows:

$$w(x,y) = w_1 N_1 (\xi,\eta) + w_{1,x} N_2 (\xi,\eta) + w_{1,y} N_3 (\xi,\eta) + ...$$

Explicit expressions for N_1, N_2, ... are given in Appendix (B.1).

3.2.2 4-Node Quadrilateral Element

The Hermitian interpolation problem, for a 4-node quadrilateral element, can be simplified if the element is transformed to a square of unit side length in the intrinsic ξ-η plane, in a way similar to that explained in section (2.3). If it is required to express a field function $w(\xi,\eta)$ in terms of its nodal values and intrinsic first order partial derivatives, then the bi-variate Hermitian interpolation formula [Ref. 30], can be applied directly as follows:

$$w(\xi,\eta) = w_1 H_1(\xi,\eta) + w_{1,\xi} H_2(\xi,\eta) + w_{1,\eta} H_3(\xi,\eta) + \ldots\ldots\ldots \quad \text{(a)}$$

Intrinsic Hermitian shape functions H_1, H_2, ... are listed in Appendix (B.1).

Unfortunately, the previous equation, in its present form, cannot be employed for plate and shell problems since the slopes there are expressed in terms of Cartesian derivatives of the lateral displacement. Three cases are summarised as follows:

(a) Rectangular Element

For a 4-node rectangular element, as shown in Fig. 3.2, it can be deduced that the isoparametric equations of the element are as follows:

$$x(\xi,\eta) = x_1 + a\,\xi$$

$$y(\xi,\eta) = y_1 + b\,\eta$$

Using the chain rule of partial differentiation, it can be shown that:

$$w_{i,\xi} = w_{i,x}\left(\frac{\partial x}{\partial \xi}\right) + w_{i,y}\left(\frac{\partial y}{\partial \xi}\right) = a\,w_{i,x} \quad \text{(b)}$$

and

$$w_{i,\eta} = w_{i,x}\left(\frac{\partial x}{\partial \eta}\right) + w_{i,y}\left(\frac{\partial y}{\partial \eta}\right) = b\,w_{i,y}$$

Substituting from equation (b) into (a), it can be proved that:

$$w(x,y) = w_1 N_1(\xi,\eta) + w_{1,x} N_2(\xi,\eta) + w_{1,y} N_3(\xi,\eta) + \ldots\ldots$$

where

$$N_{3i-2} = H_{3i-2}$$

$$N_{3i-1} = a H_{3i-1}$$

$$N_{3i} = b H_{3i} \quad ,$$

$$i = 1,2,3,4$$

(b) <u>Parallelogramic Element</u>

For the case of a 4-node parallelogramic element as shown in Fig. 3.3, it can be proved that the isoparametric equations of the element are given by:

$$x(\xi,\eta) = x_1 + \xi (x_2 - x_1) + \eta (x_4 - x_1)$$

$$y(\xi,\eta) = y_1 + \xi (y_2 - y_1) + \eta (y_4 - y_1)$$

Employing the chain rule of partial differentiation it can be deduced that:

$$\left.\begin{aligned} w_{i,\xi} &= (x_2 - x_1) w_{i,x} + (y_2 - y_1) w_{i,y} \\ w_{i,\eta} &= (x_4 - x_1) w_{i,x} + (y_4 - y_1) w_{i,y} \end{aligned}\right\} \text{---------- (c)}$$

Substituting equation (c) into (a), the required shape functions can be stated as follows:

$$N_{3i-2} = H_{3i-2}$$

$$N_{3i-1} = (x_2 - x_1)\, H_{3i-1} + (x_4 - x_1)\, H_{3i}$$

$$N_{3i} = (Y_2 - Y_1)\, H_{3i-1} + (Y_4 - Y_1)\, H_{3i}$$

where i = 1,2,3,4,

$$w(x,y) = w_1\, N_1 + w_{1,x}\, N_2 + w_{1,y}\, N_3 + \ldots\ldots$$

(c) General Quadrilateral Element

The isoparametric equation for such an element can be expressed in a way similar to that shown in Section (2.3). Hence, it can be deduced that

$$w_{i,\xi} = J_{11}\, w_{i,x} + J_{12}\, w_{i,y}$$

$$w_{i,\eta} = J_{21}\, w_{i,x} + J_{22}\, w_{i,y}$$

where J_{11}, J_{12}, ... are the elements of the Jacobian matrix defined in Section (2.3).

Hence, it can be proved that the shape functions for such an element are:

$$N_{3i-2} = H_{3i-2}$$

$$N_{3i-1} = J_{11}\, H_{3i-1} + J_{21}\, H_{3i}$$

$$N_{3i} = J_{12}\, H_{3i-1} + J_{22}\, J_{3i}$$

However, this element is restricted to shapes which are very nearly parallelogramic because it does not generally satisfy the constant curvature condition [Ref. 34].

3.2.3 The 9-Node Quadrilateral Element

The disadvantages of the 4-node quadrilateral element suggested that there was no Hermitian element suitable for the modelling of arbitrary-shaped plates (such as blades and radial impellers) other than the 3-node triangular element. This motivated the author to derive a new sub-parametric Hermitian 9-node quadrilateral element. Such an element can be used in radial impellers and is more accurate than the 3-node triangular element. The derivation of its shape functions is reviewed here and its implementation to thin and thick plates and facet shells will be explained in subsequent sections. The following two bivariate interpolation theorems are necessary for the derivation of such an element:

(a) Bivariate Lagrangian Interpolation

As shown in Fig. 3.3, a general quadrilateral element in the x-y Cartesian plane has been transformed into a square of unit length in the intrinsic ξ-η plane. This intrinsic element can be described by the following set:

$$\Omega_e = \left\{ (\xi, \eta) \; ; \; 0 \leq \xi \leq 1 \; , \; 0 \leq \eta \leq 1 \right\}$$

Suppose that there exists a field function, in the domain of the element, which satisfies the following interpolatory conditions:

$$w(\xi_r, \eta_s) = w_{r,s}$$

where

$$1 \leq r \leq m$$

$$1 \leq s \leq n$$

Hence, the bivariate Lagrangian interpolation formula can be written as follows [Ref. 13];

$$w(\xi,\eta) = \sum_{r=1}^{m} \sum_{s=1}^{n} \mathcal{L}_r^m(\xi)\, \mathcal{L}_s^n(\eta)\, w_{r,s}$$

where $\mathcal{L}_r^m$ is the r^{th} Lagrangian of order m.

(b) Bivariate Hermitian Interpolation

Consider an m*n intrinsic rectangular element which can be defined by the following set:

$$\Omega_e = \left\{(\xi,\eta);\ 0 \le \xi \le 1\ ,\ 0 \le \eta \le 1 \right\}$$

it is required to solve the following Hermitian interpolation problem

$$D_\xi^s\, D_\eta^t\, \tilde{w}_{ij} = D_\xi^s\, D_\eta^t\, w_{ij}$$

where

$1 \le i \le m$,

$1 \le j \le n$,

$0 \le s \le u$,

$0 \le t \le v$,

and the following notation is used:

$$D_\xi \; D_\eta \; w_{ij} = \left(\frac{\partial^2 \; w(\xi,\eta)}{\partial\xi \; \partial\eta} \right)_{\substack{\text{at } \xi = \xi_i \\ \eta = \eta_j}} ,$$

Using the partial interpolation technique which has been employed for the derivation of the bivariate Lagrangian interpolation formula, it can be proved that [Ref. 30]:

$$w(\xi,\eta) = \sum_{i=1}^{m} \sum_{j=1}^{n} (g_i^m \; (\xi) + h_i^m \; (\xi) \; D_\xi) * (g_j^n \; (\eta) + h_j^n \; D_\eta) * w_{ij} \qquad (d)$$

The shape functions of 9-node quadrilateral element can be obtained by using the superposition theory, as shown in Fig. 3.4

$$\tilde{w}(\xi,\eta) = w_\xi + w_\eta - \hat{w}$$

From the previous theorems, the following expressions can be deduced:

$$w_\xi = \sum_{i=1}^{m} \sum_{j=1}^{n} (g_i^m \; (\xi) + h_i^m \; (\xi) \; D_\xi) \cdot \int_j^n (\eta) \; w_{ij}$$

$$w_\eta = \sum_{i=1}^{m} \sum_{j=1}^{n} \int_i^m (\xi) \cdot (g_j^n \; (\eta) + h_j^n \; (\eta) \; D_\eta) \cdot w_{ij}$$

$$\hat{w} = \sum_{i=1}^{m} \sum_{j=1}^{n} \int_i^m (\xi) \int_j^n (\eta) \; w_{ij}$$

where

$$\omega_i = \sum_{\substack{i=1 \\ i \neq r}}^{m} \left(\frac{1}{z_i - z_r} \right)$$

$$g_i^m(z) = \left[1 - 2\omega_i\ (z-z_i)\right]\left[\ell_i^m(z)\right]^2$$

$$h_i^m(z) = (z-z_i)\left[\ell_i^m(z)\right]^2 \qquad i = 1,2,3$$

As shown in the figure below, the resulting interpolation formula can be expressed as follows:

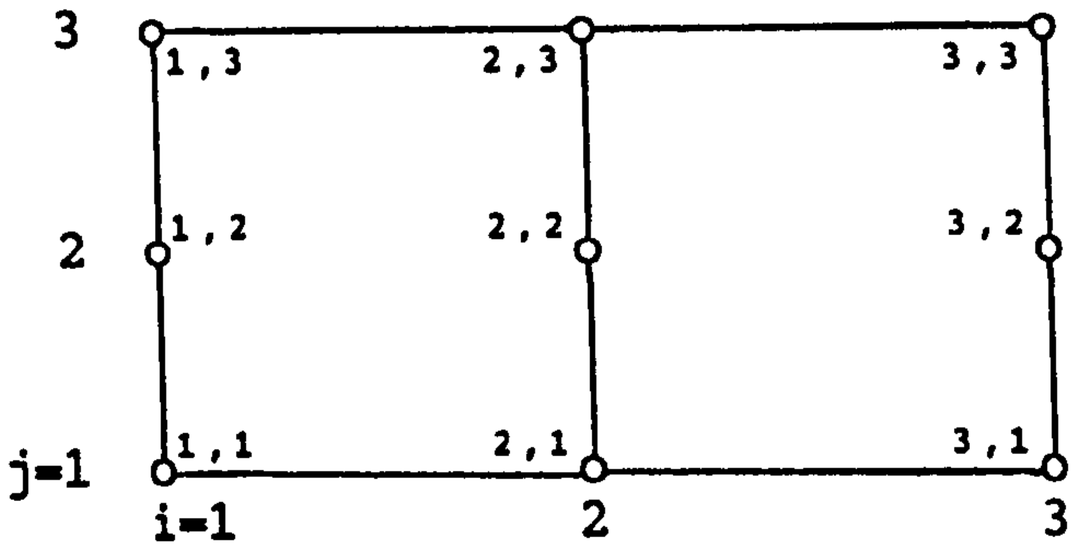

$$w(\xi,\eta) = \sum_{i=1}^{m}\sum_{j=1}^{n}\left[f_{ij}\ w_{ij} + g_{ij}\ w_{ij,\xi} + h_{ij}\ w_{ij,\eta}\right]$$

where

$$f_{ij} = g_i^m(\xi)\ell_j^n(\eta) + \ell_i^m(\xi)\ g_j^n(\eta) - \ell_i^m(\xi)\ell_j^n(\eta)$$

$$g_{ij} = h_i^m(\xi)\ell_j^n(\eta)$$

$$h_{ij} = \ell_i^m(\xi)\ h_j^n(\eta)$$

For the 9-node quadrilateral element as shown in the figure above, and from the above equations, for

$$i = 1, 2, 3$$
$$j = 1, 2, 3$$

the f_{ij}, g_{ij} and h_{ij} are defined as follows:-

$$f_{11} = g_1^3(\xi)\mathcal{L}_1^3(\eta) + \mathcal{L}_1^3(\xi)\, g_1^3(\eta) - \mathcal{L}_1^3(\xi)\,\mathcal{L}_1^3(\eta)$$

$$f_{21} = g_2^3(\xi)\mathcal{L}_1^3(\eta) + \mathcal{L}_2^3(\xi)\, g_1^3(\eta) - \mathcal{L}_2^3(\xi)\,\mathcal{L}_1^3(\eta)$$

$$f_{31} = g_3^3(\xi)\mathcal{L}_1^3(\eta) + \mathcal{L}_3^3(\xi)\, g_1^3(\eta) - \mathcal{L}_3^3(\xi)\,\mathcal{L}_1^3(\eta)$$

$$f_{32} = g_1^3(\xi)\mathcal{L}_2^3(\eta) + \mathcal{L}_3^3(\xi)\, g_2^3(\eta) - \mathcal{L}_3^3(\xi)\,\mathcal{L}_2^3(\eta)$$

$$f_{33} = g_1^3(\xi)\mathcal{L}_3^3(\eta) + \mathcal{L}_3^3(\xi)\, g_3^3(\eta) - \mathcal{L}_3^3(\xi)\,\mathcal{L}_3^3(\eta)$$

$$f_{23} = g_2^3(\xi)\mathcal{L}_3^3(\eta) + \mathcal{L}_2^3(\xi)\, g_1^3(\eta) - \mathcal{L}_2^3(\xi)\,\mathcal{L}_3^3(\eta)$$

$$f_{13} = g_1^3(\xi)\mathcal{L}_3^3(\eta) + \mathcal{L}_1^3(\xi)\, g_3^3(\eta) - \mathcal{L}_1^3(\xi)\,\mathcal{L}_3^3(\eta)$$

$$f_{12} = g_1^3(\xi)\mathcal{L}_2(\eta) + \mathcal{L}_1(\xi)\, g_2^3(\eta) - \mathcal{L}_1(\xi)\,\mathcal{L}_2(\eta)$$

$$f_{22} = g_2^3(\xi)\mathcal{L}_2^3(\eta) + \mathcal{L}_2^3(\xi)\, g_2^3(\eta) - \mathcal{L}_2^3(\xi)\,\mathcal{L}_2^3(\eta)$$

$$g_{1\,1} = h_1^3(\xi)\int_1^3(\eta)$$

$$g_{2\,1} = h_2^3(\xi)\int_1^3(\eta)$$

$$g_{3\,1} = h_3^3(\xi)\int_1^3(\eta)$$

$$g_{3\,2} = h_3^3(\xi)\int_2^3(\eta)$$

$$g_{3\,3} = h_3^3(\xi)\int_3^3(\eta)$$

$$g_{2\,3} = h_2^3(\xi)\int_3^3(\eta)$$

$$g_{1\,3} = h_1^3(\xi)\int_3^3(\eta)$$

$$g_{1\,2} = h_1^3(\xi)\int_2^3(\eta)$$

$$g_{2\,2} = h_2^3(\xi)\int_2^3(\eta)$$

$$h_{1\,1} = \int_1^3(\xi)\ h_1^3(\eta)$$

$$h_{2\,1} = \int_2^3(\xi)\ h_1^3(\eta)$$

$$h_{3\,1} = \int_{3}^{3} (\xi)\ h_1^3\ (\eta)$$

$$h_{3\,2} = \int_{3}^{3} (\xi)\ h_2^3\ (\eta)$$

$$h_{3\,3} = \int_{3}^{3} (\xi)\ h_3^3\ (\eta)$$

$$h_{2\,3} = \int_{2}^{3} (\xi)\ h_3^3\ (\eta)$$

$$h_{1\,3} = \int_{1}^{3} (\xi)\ h_3^3\ (\eta)$$

$$h_{1\,2} = \int_{1}^{3} (\xi)\ h_2^3\ (\eta)$$

$$h_{2\,2} = \int_{2}^{3} (\xi)\ h_2^3\ (\eta)$$

Explicit expressions for the above functions are listed in Appendix (B.1).

The Hermitian interpolation formula useful for plate and shell applications should be expressed in terms of Cartesian derivatives of the field function, as explained before for the 4-node element. In order that the 9-node Hermitian element satisfies the C^1-continuity condition it should not be a parabolically curved quadrilateral element. A sub-parametric transformation must be employed in which the geometry of the element can be described in terms of the corner nodes only. Consider the corners of the element to be as shown in Fig. 3.5. Hence, the sub-parametric transformation of the 9-node element can be expressed as follows:

$$x\ (\xi,\eta) \;=\; N_a\ x_1 + N_b\ x_3 + N_c\ x_5 + N_d\ x_7$$

$$y\ (\xi,\eta) \;=\; N_a\ y_1 + N_b\ y_3 + N_c\ y_5 + N_d\ y_7$$

where

$$N_a \;=\; (1 - \xi)\ (1 - \eta)$$

$$N_b \;=\; \xi\ (1 - \eta)$$

$$N_c \;=\; \xi\ \eta$$

$$N_d \;=\; (1 - \xi)\ \eta$$

using the chain rule of partial differentiation, it can be proved that:

$$w_{i,\xi} \;=\; J_{11}\ w_{i,x} + J_{12}\ w_{i,y}$$

$$w_{i,\eta} \;=\; J_{21}\ w_{i,x} + J_{22}\ w_{i,y}$$

where

$$J_{11} \;=\; \frac{\partial x}{\partial \xi} \;=\; \left(\frac{\partial N_a}{\partial \xi}\right) x_1 + \left(\frac{\partial N_b}{\partial \xi}\right) x_3 + \ldots\ldots$$

$$J_{12} \;=\; \frac{\partial y}{\partial \xi} \;=\; \left(\frac{\partial N_a}{\partial \xi}\right) y_1 + \ldots\ldots\ldots\ldots, \text{ etc.}$$

Substituting the above equations into the intrinsic Hermitian interpolation equation (d), it can be deduced that:

$$w(x,y) = \sum_{i=1}^{m} \sum_{j=1}^{n} \Big\{ f_{ij}\, w_{ij} + g_{ij}\, [J_{11}\, w_{ij,x} + J_{12}\, w_{ij,y}] + h_{ij}\, [J_{21}\, w_{ij,x} + J_{22}\, w_{ij,y}] \Big\}$$

$$w(x,y) = \sum_{i=1}^{m} \sum_{j=1}^{n} [F_{ij}\, w_{ij} + G_{ij}\, w_{ij,x} + H_{ij}\, w_{ij,y}]$$

where

$$F_{ij} = f_{ij}$$

$$G_{ij} = J_{11}\, g_{ij} + J_{21}\, h_{ij}$$

$$H_{ij} = J_{12}\, g_{ij} + J_{22}\, h_{ij}$$

Explicit expressions for the final shape functions, given in the above equation, are listed in Appendix (B.1), also a complete derivation of the second order Jacobian used in this element is given in Appendix (B.2).

3.3 PLATE BENDING ELEMENT

Lagrangian and Hermitian families of elements given in Sections (2.5, 3.2), have been employed for the derivation of different plate and shell elements. The type of element depends upon the basic assumptions involved in the derivation of its stiffness and mass matrices. The stiffness and mass matrices for the different elements are derived using generalised steps explained in Sections (2.3), (2.4) respectively. The different elements employed in this work are summarised as follows:-

(a) Kirchoff Plate-Bending Element

This element is based upon Kirchoff's theory of plate-bending in which transverse shear is ignored and normals to the midplane of the plate remain normal after deformation. The element which is suitable for thin plates is based upon Hermitian shape functions described in Section (3.2), and consequently three different elements are available in this work:

(i) The 3-node triangular element

(ii) The 4-node quadrilaterial element

(iii) The 9-node subparametric quadrilateral element.

The details of the derivation of stiffness and mass matrices for a typical n-node element is reviewed in Appendix (B.3)

(b) Mindlin Plate-Bending Element

In this element, the transverse shear is taken into consideration and warping of the cross-section is approximated by assuming that the normals to the midsurface remain straight, but not necessarily normal, after deformation. Due to the shear effect, lateral displacement and slope angles can be interpolated in terms of Lagrangian shape functions, and all 2D families of elements given in Section (2.5.3), can be employed for the Mindlin element. This element is suitable for thick plates only. The derivation of stiffness and mass matrices for a typical n-node element is described in Appendix (B.4).

(c) A New Plate-Bending Element

This element is based upon the approach of El-Zafrany and

Cookson [Ref. 50] in which Mindlin's theory is applied with Hermitian interpolation. Their approach is applied to the 9-node subparametric element derived in this work to obtain an efficient new element which should perform well irrespective of the plate thickness as will be verified later. The basic modification to the standard Mindlin element is the addition of shear angles ϕ_x and ϕ_y to the nodal degrees of freedom. Hence, for an n-node element, it can be deduced that:

$$w(x,y) = \sum_{i=1}^{n} \left[f_i w_i + g_i .(\theta_x)_i + h_i . (\theta_y)_i - g_i .(\phi_x)_i - h_i .(\phi_y)_i \right]$$

$$\phi_x(x,y) = \sum_{i=1}^{n} N_i .(\phi_x)_i$$

$$\phi_y(x,y) = \sum_{i=1}^{n} N_i .(\phi_y)_i$$

where

f_i , g_i , h_i are Hermitian shape functions

N_i are Lagrangian shape functions

From the previous two sections the displacement components at any point (x,y,z) are given as follows:

$$u(x,y,z) = - z\, \theta_x (x,y)$$

$$v(x,y,z) = - z\, \theta_y (x,y)$$

$$w(x,y,z) = w(x,y)$$

All of the values w, θ_x ,θ_y are at the midplane of the plate.

Using the above definition of displacement components, the relevant strain components in the Cartesian directions can be expressed as follows:-

$$\varepsilon_x = \frac{\partial u}{\partial x} = - z \frac{\partial \theta_x}{\partial x}$$

$$\varepsilon_y = \frac{\partial v}{\partial y} = - z \frac{\partial \theta_y}{\partial y}$$

$$\gamma_{xy} = \frac{\partial u}{\partial y} + \frac{\partial v}{\partial x} = - z \left(\frac{\partial \theta_x}{\partial y} + \frac{\partial \theta_y}{\partial x} \right)$$

$$\gamma_{xy} = \frac{\partial w}{\partial y} + \frac{\partial v}{\partial z} = - \phi_y$$

$$\gamma_{zx} = \frac{\partial w}{\partial x} + \frac{\partial u}{\partial z} = - \phi_x$$

If the nodal displacement vector $\underline{\delta}$ is defined as

$$\underline{\delta} = \{w_1 \ (\theta_x)_1 \ (\theta_y)_1 \ (\phi_x)_1 \ (\phi_y)_1 \ \ldots\ldots\ldots\ldots (\phi_x)_n \ (\phi_y)_n\},$$

and using the shape function expressions, it can be shown that

$$\underline{\varepsilon} = \underline{B} \, \underline{\delta}$$

where

$$\underline{B} = [\underline{b}_1 \ \underline{b}_2 \ \ldots\ldots\ldots\ldots\ldots\ldots \underline{b}_n]$$

$$\underline{b}_i = \begin{bmatrix} z\,f_{i,xx} & z\,g_{i,xx} & z\,h_{i,xx} & z\,(N_{i,x}-g_{i,xx}) & -z\,h_{i,xx} \\ z\,f_{i,yy} & z\,g_{i,yy} & z\,h_{i,yy} & -z\,g_{i,yy} & z\,(N_{i,y}-h_{i,yy}) \\ 2z\,f_{i,xy} & 2z\,g_{i,xy} & 2z\,h_{i,xy} & z(N_{i,y}-2g_{i,xy}) & 2(N_{i,x}-2h_{i,xy}) \\ 0 & 0 & 0 & 0 & -N_i \\ 0 & 0 & 0 & -N_i & 0 \end{bmatrix}$$

The $\underline{D}$ matrix (stress-strain matrix) is the same as for the Mindlin element, given in Appendix (B.4).

The $\underline{B}$ matrix and stiffness matrix can be partitioned in a way similar to that explained in Appendix (B.4), hence:

$$\underline{K} = \underline{K}_b + \underline{K}_s \ ,$$

$$\underline{K}_b = \int\int_{\substack{\text{Intrinsic}\\\text{Element}}} \hat{\underline{B}}_b^t \, \hat{\underline{D}}_b \, \hat{\underline{B}}_b \, |J| \, d\xi \, d\eta$$

$$\underline{K}_s = \int\int_{\substack{\text{Intrinsic}\\\text{Element}}} \underline{B}_s^t \, \hat{\underline{D}}_s \, \underline{B}_s \, |J| \, d\xi \, d\eta$$

where $\hat{\underline{D}}_b$, $\hat{\underline{D}}_s$ are as defined in Appendix (B.4),

$$(\hat{\underline{b}}_i)_b = \begin{bmatrix} f_{i,xx} & g_{i,xx} & h_{i,xx} & (N_{i,x}-g_{i,xx}) & -h_{i,xx} \\ f_{i,yy} & g_{i,yy} & h_{i,yy} & -g_{i,yy} & (N_{i,y}-h_{i,yy}) \\ 2f_{i,xy} & 2g_{i,xy} & 2h_{i,xy} & (N_{i,y}-2g_{i,xy}) & (N_{i,x}-h_{i,xy}) \end{bmatrix}$$

$$(\underline{b}_i)_s = \begin{bmatrix} 0 & 0 & 0 & 0 & -N_i \\ 0 & 0 & 0 & -N_i & 0 \end{bmatrix}$$

From the analysis given in Appendix (B.4), the Kinetic energy of the element can be defined as follows:

$$KE = \frac{1}{2} \iint \hat{\dot{q}}^t \, \underline{D}_M \, \hat{\dot{q}} \, dA$$

where $\hat{\dot{q}}$ is the modified velocity vector defined as follows:

$$\hat{\dot{q}} = \{\dot{w} \; \dot{\theta}_x \; \dot{\theta}_y\}$$

Defining the nodal velocity vector $\underline{\delta}$ as:

$$\dot{\underline{\delta}} = \{\dot{w}_1 \; (\dot{\theta}_x)_1 \; (\dot{\theta}_y)_1 \; (\dot{\phi}_x)_1 \; (\dot{\phi}_y)_1 \; \ldots\ldots\ldots\ldots\ldots\ldots\}$$

then, it can be deduced that:

$$\dot{w} = \sum_{i=1}^{n} \left[f_i \; \dot{w}_i + g_i \; .(\dot{\theta}_x)_i + h_i \; .(\dot{\theta}_y)_i - g_i \; .(\dot{\phi}_x)_i - h_i \; .(\dot{\phi}_y)_i \right]$$

$$\dot{\theta}_x = \frac{\partial \dot{w}}{\partial x} + \dot{\phi}_x$$

$$\dot{\theta}_y = \frac{\partial \dot{w}}{\partial y} + \dot{\phi}_y$$

$$\dot{\phi}_x = \sum_{i=1}^{n} N_i \; .(\dot{\phi}_x)_i$$

$$\dot{\phi}_y = \sum_{i=1}^{n} N_i \; .(\dot{\phi}_y)_i$$

Hence, it can be proved that

$$\hat{\dot{q}} = \underline{N} \, \dot{\underline{\delta}} \; ,$$

$$\underline{N} = [\underline{n}_1 \quad \underline{n}_2 \ \ldots\ldots\ldots \ \underline{n}_n]$$

where

$$\underline{n}_i = \begin{bmatrix} f_i & g_i & h_i & -g_i & -h_i \\ f_{i,x} & g_{i,x} & h_{i,x} & (N_i - g_{i,x}) & -h_{i,x} \\ f_{i,y} & g_{i,y} & h_{i,y} & -g_{i,y} & (N_i - h_{i,y}) \end{bmatrix}$$

From the definition of Kinetic energy:

$$KE = \frac{1}{2} \dot{\underline{\delta}}^t \ \underline{M} \ \dot{\underline{\delta}}$$

it can be shown that:

$$\underline{M} = \int\int_{\substack{\text{Intrinsic} \\ \text{Element}}} \underline{N}^t \ \underline{D}_M \ \underline{N} \ |J| \ d\xi \ d\eta$$

where $\underline{D}_M$ is as defined in Appendix (B.4).

3.4 FACET SHELL ELEMENTS

The flat or facet shell element has the following advantages:

(a) It does not require any new derivation. Generally speaking, a facet element is a combination of a plane-stress element and a plate-bending element.

(b) It is the appropriate element for the analysis of corrugated plates, and radial impellers with straight blades.

(c) It is easily employed for curved shells.

In this section, two basic facet shell elements are reviewed. The first one is formulated from the Kirchoff plate-bending element,

and is suitable for the analysis of thin shells, whilst the second one is based upon the Mindlin plate-bending element so as to take account of transverse shear, which is significant in thick shells. Some simplification of the derivations is achieved.

However, in using such elements for the analysis of radial impellers some difficulties arose and the author was motivated to derive a modified element with which such difficulties can be overcome.

The presence of Coplanar nodes may lead to singularity of the structure's stiffness and mass matrices, simply because the rows and columns corresponding to θ_z are zeros in the local element stiffness and mass matrices, as realised by Zienkiewicz [Ref. 34], who proposed the use of a fictitious rotational stiffness to overcome such a difficulty. A modified element has been derived here which will never lead to such a problem because it is based upon 5 degrees of freedom (3 displacement components and two rotations) in a way similar to that employed by Ahmad et al [Ref. 44].

A structure, such as a radial impeller, may have zones with variable thickness where it is difficult to use one element type (Kirchoff or Mindlin). If a Mindlin facet element is employed for a thin structure, shear locking will occur and will lead to inaccurate results. In order to have a Hermitian element which includes transverse shear, the new plate-bending element explained in Section (3.3), was combined with a plane-stress element and a new facet element which is capable of accurate analysis of thin and thick shells was derived.

A review of the elements mentioned above is summarised as follows:

3.4.1 Thin Facet Element

This element is generally capable of resisting, in full, 3-D

force and moment components. Hence, there must be provision for 6 degrees of freedom at each node. These six degrees-of-freedom are the displacement components u, v, w, and the rotation components θ_x, θ_y, θ_z, in x, y, z directions respectively, as shown in Fig. 3.6(a). Derivation of the element matrices could be simpler if a system of local matrices were selected. Generally speaking, for such a system, the x-y plane is employed as the element midplane, as shown in Fig. 3.6(b).

The Kirchoff facet shell element is based upon a combination of the 2D plane-stress element discussed in Section (2.5), and the thin plate-bending element illustrated in Appendix (B.3).

The nodal displacement components, with respect to local axes can be defined for an n-node element, as follows

$$\underline{\delta}_L = \{u_1 \; v_1 \; w_1 \; \theta_{x1} \; \theta_{y1} \; \theta_{z1} \; \ldots\ldots\ldots\ldots \; \theta_{zn}\}$$

The displacement component at any point (x,y,z) inside the element can be expressed as follows:

$$u = u_m + u_b$$

$$v = v_m + v_b$$

$$w = w_b$$

where

$(\;)_m \equiv$ membrane or in-plane effect

$(\;)_b \equiv$ bending effect.

From Appendix (B.3) it can be shown that:

$u_b = z\,\theta_y$,

$$v_b = -z\,\theta_x \ ,$$

since

$$\theta_x = \frac{\partial w}{\partial y} \ ,$$

$$\theta_y = -\frac{\partial w}{\partial x}$$

then, it can be shown that

$$u_b = -z\frac{\partial w}{\partial x}$$

$$v_b = -z\frac{\partial w}{\partial y}$$

From plane-stress theory, described in Section (2.5), it can be deduced that

$$u_m = \sum_{i=1}^{n} u_i\, N_i$$

$$v_m = \sum_{i=1}^{n} v_i\, N_i$$

where N_i , i=1, 2, ..., n are the Lagrangian shape functions.

From Kirchoff plate theory, given in Appendix (B.3) it can be shown that

$$w = \sum_{i=1}^{n} [f_i\, w_i + g_i\, w_{i,x} + h_i\, w_{i,y}]$$

$$= \sum_{i=1}^{n} [f_i \; w_i - g_i \; \theta_{yi} + h_i \; \theta_{xi}]$$

where f_i, g_i, h_i are the Hermitian shape functions. Defining the strain vector

$$\underline{\varepsilon} = \{\varepsilon_x \; \varepsilon_y \; \gamma_{xy}\} = \underline{\varepsilon}_m + \underline{\varepsilon}_b$$

where

$$\underline{\varepsilon}_m = \{\varepsilon_x \; \varepsilon_y \; \gamma_{xy}\}_m$$

is the membrane part, and

$$\underline{\varepsilon}_b = \{\varepsilon_x \; \varepsilon_y \; \gamma_{xy}\}_b$$

is the bending part, it can be proved that:

$$\underline{\varepsilon}_m = \begin{bmatrix} \dfrac{\partial u_m}{\partial x} \\ \dfrac{\partial v_m}{\partial y} \\ \dfrac{\partial u_m}{\partial y} + \dfrac{\partial v_m}{\partial x} \end{bmatrix}$$

$$\underline{\varepsilon}_b = \begin{bmatrix} \dfrac{\partial u_b}{\partial x} \\ \dfrac{\partial v_b}{\partial y} \\ \dfrac{\partial u_b}{\partial y} + \dfrac{\partial v_b}{\partial x} \end{bmatrix} = - z \begin{bmatrix} \dfrac{\partial^2 w}{\partial x^2} \\ \dfrac{\partial^2 w}{\partial y^2} \\ 2 \dfrac{\partial^2 w}{\partial x \partial y} \end{bmatrix}$$

Two $\underline{B}$ matrices can be defined such that

$$\underline{\varepsilon}_m = \underline{B}_m \underline{\delta} \quad ,$$

$$\underline{\varepsilon}_b = \underline{B}_b \underline{\delta}$$

and $$\underline{\varepsilon} = \underline{B} \underline{\delta}$$

where $$\underline{B} = \underline{B}_m + \underline{B}_b$$

and $$\underline{B}_m = [\underline{b}_1 \ \underline{b}_2 \ \ldots\ldots\ldots \ \underline{b}_n]_m$$

$$\underline{B}_b = - z \hat{\underline{B}}_b = - z [\hat{\underline{b}}_1 \ \hat{\underline{b}}_2 \ \ldots\ldots\ldots \ \hat{\underline{b}}_n]_b$$

where

$$(\underline{b}_i)_m = \begin{bmatrix} \dfrac{\partial N_i}{\partial x} & 0 & 0 & 0 & 0 & 0 \\ 0 & \dfrac{\partial N_i}{\partial y} & 0 & 0 & 0 & 0 \\ \dfrac{\partial N_i}{\partial y} & \dfrac{\partial N_i}{\partial x} & 0 & 0 & 0 & 0 \end{bmatrix}$$

$$(\underline{b}_i)_b = \begin{bmatrix} 0 & 0 & \frac{\partial^2 f_i}{\partial x^2} & \frac{\partial^2 h_i}{\partial x^2} & -\frac{\partial^2 g_i}{\partial x^2} & 0 \\ 0 & 0 & \frac{\partial^2 f_i}{\partial y^2} & \frac{\partial^2 h_i}{\partial y^2} & -\frac{\partial^2 g_i}{\partial y^2} & 0 \\ 0 & 0 & 2\frac{\partial^2 f_i}{\partial x \partial y} & 2\frac{\partial^2 h_i}{\partial x \partial y} & -\frac{\partial^2 g_i}{\partial x \partial y} & 0 \end{bmatrix}$$

The stress components can be partitioned in a way similar to the strains,

i.e. $\underline{\sigma} = \underline{\sigma}_m + \underline{\sigma}_b$

Hence, it can be shown that

$$\underline{\sigma}_m = \underline{D}\,\underline{\varepsilon}_m \quad , \quad \underline{\sigma}_b = \underline{D}\,\underline{\varepsilon}_b$$

and $\underline{\sigma} = \underline{D}\,\underline{\varepsilon}$

where

$$\underline{D} = \frac{E}{1-\nu^2} \begin{bmatrix} 1 & \nu & 0 \\ \nu & 1 & 0 \\ 0 & 0 & \frac{1-\nu}{2} \end{bmatrix}$$

From the definition of strain energy:

$$U = \frac{1}{2} \iiint_{\text{Element}} \underline{\varepsilon}^t \, \underline{\sigma} \, d\,V$$

it can be deduced that

$$U = \frac{1}{2} \underline{\delta}^t \left(\iiint \underline{B}^t \underline{D} \underline{B} \, dV \right) \underline{\delta}$$

$$= \frac{1}{2} \underline{\delta}^t \underline{K}_L \underline{\delta}$$

where $\underline{K}_L$ is the local stiffness matrix of the element defined as follows

$$\underline{K}_L = \iiint_{-t/2}^{t/2} (\underline{B}_m^t - z \hat{B}_b^t) \underline{D} (\underline{B}_m - z \hat{B}_b) \, dz \, dx \, dy$$

Hence, it can be proved that:

$$\underline{K}_L = \underline{K}_m + \underline{K}_b$$

where

$$\underline{K}_m = \iint t \underline{B}_m^t \underline{D} \underline{B}_m \, dx \, dy$$

$$\underline{K}_b = \iint \frac{t^3}{12} \hat{\underline{B}}_b^t \underline{D} \underline{B}_b \, dx \, dy$$

An alternative approach, which is based upon a single $\underline{B}$ matrix, can be derived as follows:

$$U = \frac{1}{2} \underline{\delta}^t \left(\iiint \underline{B}^t \underline{D} \underline{B} \, dV \right) \underline{\delta}$$

$$= \frac{1}{2} \underline{\delta}^t \underline{K} \underline{\delta}$$

Hence, the element stiffness matrix can be defined as follows:

$$\underline{K} = \iiint \underline{B}^t \underline{D} \underline{B} \, dV$$

where $\underline{B} = \underline{B}_m + \underline{B}_b$

The z-integration in the above equation can be carried out as follows:

From $\int_{-t/2}^{t/2} f(z) \, dz = \int_0^1 t \, f(\zeta) \, d\zeta$

it can be deduced that

$$z = \zeta t - t/2 = t\,(\zeta - 0.5)$$

Using the 2-point Gauss-Quadrature formula, it can be shown that:

$$\int_0^1 t\, f\,(\zeta)\, d\,\zeta = \frac{t}{2}\,[f\,(z_1) + f\,(z_2)]$$

$$\zeta_1 = 0.5 - \frac{1}{2\sqrt{3}} \qquad z_1 = -\frac{t}{\sqrt{12}}$$

$$\zeta_2 = 0.5 + \frac{1}{2\sqrt{3}} \qquad z_2 = +\frac{t}{\sqrt{12}}$$

$$\text{i.e.} \quad \int_{-t/2}^{t/2} f\,(z)\, dz = \frac{t}{2}\left[f\left(-\frac{t}{\sqrt{12}}\right) + f\left(+\frac{t}{\sqrt{12}}\right)\right]$$

Hence, it can be proved that:

$$\underline{K}_L = \int\int \frac{t}{12}\,[\underline{B}_1^t\ \underline{D}\ \underline{B}_1 + \underline{B}_2^t\ \underline{D}\ \underline{B}_2]\ dx\ dy$$

where

$$\underline{B}_1 = \underline{B}_m - \frac{t}{\sqrt{12}}\,\hat{B}_b$$

$$\underline{B}_2 = \underline{B}_m + \frac{t}{\sqrt{12}}\,\hat{B}_b$$

The relationships between local and global systems are reviewed in Appendix (B.5), from which it can be proved that:

$$\underline{K}_G = \underline{R}^t\ \underline{K}_L\ \underline{R}$$

where the $\underline{R}$ matrix is a 6n x 6n matrix defined as follows:

$$\underline{R} = \lceil \underline{R}_{3x3} \; \underline{R}_{3x3} \; \cdots\cdots \; \underline{R}_{3x3} \rfloor$$

where $\underline{R}_{3x3}$ is the rotation matrix of the axes defined in Appendix (B.5). From the equation of $\underline{K}_L$, it can be shown that

$$\underline{K}_G = \iiint (\underline{B}\ \underline{R})^t\ \underline{D}\ (\underline{B}\ \underline{R})\ dV$$

$$= \iiint \underline{B}_G^t\ \underline{D}\ \underline{B}_G\ dV$$

where

$$\underline{B}_G = \underline{B}\ \underline{R}$$

Defining

$$(\underline{B}_G)_1 = \underline{B}_1\ \underline{R}$$

$$(\underline{B}_G)_2 = \underline{B}_2\ \underline{R}$$

it can be shown that

$$\underline{K}_G = \iint \overset{t}{-} [(\underline{B}_G^t)_1\ \underline{D}\ (\underline{B}_G)_1$$

$$+ (\underline{B}_G^t)_2\ \underline{D}\ (\underline{B}_G)_2]\ dx\ dy$$

The vector of nodal velocities for an n-node element can be defined as follows:

$$\dot{\underline{\delta}}_L = \{\dot{u}_1\ \dot{v}_1\ \dot{w}_1\ \dot{\theta}_{x1}\ \dot{\theta}_{y1}\ \dot{\theta}_{z1}\ \cdots\cdots\ \dot{\theta}_{zn}\}$$

The velocity components, at any point (x,y,z) inside the element, can be expressed as follows:

$$\dot{u}\ (x,y,z) = \dot{u}_m + \dot{u}_b$$

$$\dot{v}\ (x,y,z) = \dot{v}_m + \dot{v}_b$$

$$\dot{w}\ (x,y,z) = \dot{w}_b$$

where $\dot{u}_m$, $\dot{v}_m$ are the velocity components at (x,y) of the midplane,

$$\dot{u}_b = - z\ \dot{\theta}_y = - z\ \frac{\partial \dot{w}}{\partial x}$$

$$\dot{v}_b = - z\ \dot{\theta}_x = - z\ \frac{\partial \dot{w}}{\partial y}$$

The velocity vector is defined as:

$$\underline{\dot{q}} = \{\dot{u}\ \dot{v}\ \dot{w}\}$$

which can be partitioned as follows:

$$\underline{\dot{q}} = \dot{q}_m + \dot{q}_{bT} + \dot{q}_{bR}$$

where

$$\underline{\dot{q}}_m = \{\dot{u}_m\ \dot{v}_m\ 0\}$$

the membrane part,

$$\underline{\dot{q}}_{bT} = \{0\ \ 0\ \ \dot{w}_b\}$$

the bending part,

$$\underline{\dot{q}}_{bR} = - z \left\{ \frac{\partial \dot{w}}{\partial x}\ \ \frac{\partial \dot{w}}{\partial y}\ \ 0 \right\}$$

the rotatary inertia part.

From 2-D and plate-bending analysis:

$$\dot{u}_m = \sum_{i=1}^{n} \dot{u}_i \, N_i$$

$$\dot{v}_m = \sum_{i=1}^{n} \dot{v}_i \, N_i$$

$$\dot{w} = \sum_{i=1}^{n} \{f_i \, \dot{w}_i + h_i (\dot{\theta}_x)_i - g_i (\dot{\theta}_y)_i\}$$

where

N_i , i=1,2,....., n are the Lagrangian shape functions

f_i , g_i , h_i are the Hermitian shape functions.

Hence it can be shown

$$\underline{\dot{q}}_m = \underline{N}_m \, \underline{\dot{\delta}}$$

$$\underline{\dot{q}}_T = \underline{N}_{bT} \, \underline{\dot{\delta}}$$

$$\underline{\dot{q}}_{bR} = \underline{N}_{bR} \, \underline{\dot{\delta}}$$

$$\underline{N}_m = \begin{bmatrix} N_1 & 0 & 0 & 0 & 0 & 0 & \cdots \\ 0 & N_1 & 0 & 0 & 0 & 0 & \cdots \\ 0 & 0 & 0 & 0 & 0 & 0 & \cdots \end{bmatrix}$$

$$\underline{N}_{bT} = \begin{bmatrix} 0 & 0 & 0 & 0 & 0 & 0 & \cdots \\ 0 & 0 & 0 & 0 & 0 & 0 & \cdots \\ 0 & 0 & f_1 & h_1 - g_1 & 0 & \cdots \end{bmatrix}$$

$$\underline{N}_{bR} = - z \, \hat{\underline{N}}_{bR}$$

where

$$\hat{\underline{N}}_{bR} = \begin{bmatrix} 0 & 0 & \frac{\partial f_1}{\partial x} & \frac{\partial h_1}{\partial x} - \frac{\partial g_1}{\partial x} & 0 & \cdots \\ 0 & 0 & \frac{\partial f_1}{\partial y} & \frac{\partial h_1}{\partial y} - \frac{\partial g_1}{\partial y} & 0 & \cdots \\ 0 & 0 & 0 & 0 & 0 & \end{bmatrix}$$

The Kinetic energy of the element can be expressed as follows:

$$KE = (KE)_m + (KE)_b$$

where

$$(KE)_m = \frac{1}{2} \iiint \rho \, \dot{\underline{q}}_m^t \, \dot{\underline{q}}_m \, dx \, dy \, dz$$

$$(KE)_b = \frac{1}{2} \iiint \rho \, \dot{\underline{q}}_{bT}^t \, \dot{\underline{q}}_{bT} \, dx \, dy \, dz$$

$$+ \frac{1}{2} \iiint \rho \, \dot{\underline{q}}_{bR}^t \, \dot{\underline{q}}_{bR} \, dx \, dy \, dz$$

with $KE = \frac{1}{2} \, \dot{\underline{\delta}}^t \, \underline{M} \, \dot{\underline{\delta}}$

it can be shown that

$$\underline{M} = \underline{M}_m + \underline{M}_b$$

where

$$\underline{M}_m = \iint \underline{N}_m^t \, \underline{D}_m \, \underline{N}_m \, dx \, dy$$

$$\underline{M}_b = \iint \underline{N}_b^t \, \underline{D}_b \, \underline{N}_b \, dx \, dy$$

$$\underline{D}_m = \rho t \begin{bmatrix} 1 & 0 & 0 \\ 0 & 1 & 0 \\ 0 & 0 & 1 \end{bmatrix}$$

$$\underline{D}_b = \rho t \begin{bmatrix} \frac{t^2}{12} & 0 & 0 \\ 0 & \frac{t^2}{12} & 0 \\ 0 & 0 & 1 \end{bmatrix}$$

$$\underline{N}_b = \underline{N}_{bT} + \hat{N}_{bR}$$

$$\underline{N}_b = \begin{bmatrix} 0 & 0 & \frac{\partial f_1}{\partial x} & \frac{\partial h_1}{\partial x} & -\frac{\partial g_1}{\partial x} & 0 & \cdots\cdots \\ 0 & 0 & \frac{\partial f_1}{\partial y} & \frac{\partial h_1}{\partial y} & -\frac{\partial g_1}{\partial y} & 0 & \cdots\cdots \\ 0 & 0 & f_1 & h_1 & -g_1 & 0 & \cdots\cdots \end{bmatrix}$$

An alternative approach in which one $\underline{N}$ matrix is employed, can be described as follows:

$$KE = \frac{1}{2} \iiint \rho \, \dot{q}^t \, \dot{q} \, dx \, dy \, dz$$

where

$$\dot{\underline{q}} = \dot{q}_m + \dot{q}_{bT} + \dot{q}_{bR}$$

$$= (\underline{N}_m + \underline{N}_{bT} + \underline{N}_{bR})\ \dot{\underline{\delta}}$$

or $$\dot{\underline{q}} = \underline{N}\ \dot{\underline{\delta}}$$

where $$\underline{N} = \underline{N}_m + \underline{N}_{bT} - z\ \hat{N}_{bR}$$

Then:

$$KE = \frac{1}{2}\ \dot{\underline{\delta}}^t\ (\iiint \rho\ \underline{N}^t\ \underline{N}\ dx\ dy\ dz)\ \dot{\underline{\delta}}$$

$$= \frac{1}{2}\ \dot{\underline{\delta}}^t\ \underline{M}\ \dot{\underline{\delta}}$$

Hence

$$\underline{M} = \iiint \rho\ \underline{N}^t\ \underline{N}\ dx\ dy\ dz$$

Integrating with respect to z, it can be shown that:

$$\underline{M} = \iint \frac{\rho t}{2} \{\underline{N}_1^t\ \underline{N}_1 + \underline{N}_2^t\ \underline{N}_2\}\ dx\ dy$$

where

$$\underline{N}_1 = \underline{N}_m + \underline{N}_{bT} - \frac{t}{\sqrt{12}}\ \hat{\underline{N}}_{bR}$$

$$\underline{N}_2 = \underline{N}_m + \underline{N}_{bT} + \frac{t}{\sqrt{12}}\ \hat{\underline{N}}_{bR}$$

The global mass matrix can be obtained directly from the global $\underline{N}$ matrix, as follows:

Defining $\underline{N}_G = \underline{N}\ \underline{R}$

then $\underline{M}_G = \iiint \rho\ \underline{N}_G^t\ \underline{N}_G\ dx\ dy\ dz$

$$= \iint \frac{\rho t}{2} \left[(\underline{N}_G^t)_1\ (\underline{N}_G)_1 + (\underline{N}_G^t)_2\ (\underline{N}_G)_2 \right] dx\ dy$$

where

$$(\underline{N}_G)_1 = \underline{N}_1\ \underline{R}$$

$$(\underline{N}_G)_2 = \underline{N}_2\ \underline{R}$$

3.4.2 Thick Facet Element

This element is based upon a combination of the 2-D plane-stress element, given in Section (2.5), and the Mindlin element, explained in Appendix (B.4). The element employs a nodal displacement vector similar to that used in the previous element. The displacement components at any point in the element can be expressed as follows:

$$u(x,y,z) = u_m\ (x,y) + u_b\ (x,y,z)$$

$$v(x,y,z) = v_m\ (x,y) + v_b\ (x,y,z)$$

$$w(x,y,z) = w_b\ (x,y)$$

where u_m, v_m are the membrane or in-plane effects,

u_b, v_b, w_b, are the bending effect,

$$u_b = + z\ \theta_y$$

$$v_b = - z\ \theta_x$$

From plane-stress theory, it can be shown that

$$u_m = \sum_{i=1}^{n} u_i N_i$$

$$v_m = \sum_{i=1}^{n} v_i N_i$$

and from Mindlin plate theory;

$$\theta_x = \sum_{i=1}^{n} (\theta_x)_i N_i$$

$$\theta_y = \sum_{i=1}^{n} (\theta_y)_i N_i$$

$$w = \sum_{i=1}^{n} w_i N_i$$

Defining the strain vector

$$\underline{\varepsilon} = \{\varepsilon_x \ \varepsilon_y \ \gamma_{xy} \ \gamma_{yz} \ \gamma_{zx}\} ,$$

it can be partitioned as follows:

$$\underline{\varepsilon} = \underline{\varepsilon}_m + \underline{\varepsilon}_b + \underline{\varepsilon}_s$$

where $\underline{\varepsilon}_m = \{\varepsilon_x \ \varepsilon_y \ \gamma_{xy} \ 0 \ 0\}_m$

is the membrane part due to in-plane deformation

$\underline{\varepsilon}_b = \{\varepsilon_x \ \varepsilon_y \ \gamma_{xy} \ 0 \ 0\}_b$

is the bending part without transverse shear

$$\underline{\varepsilon}_s = \{ 0 \quad 0 \quad 0 \quad \gamma_{yz} \quad \gamma_{zx} \}_s$$

is the transverse shear strain. $\underline{\varepsilon}_s$ is taken into consideration for Mindlin thick plates.

From 2-D elasticity and plate-bending theories, it can be shown that:

$$\underline{\varepsilon}_m = \begin{bmatrix} \dfrac{\partial u_m}{\partial x} \\ \dfrac{\partial v_m}{\partial y} \\ \dfrac{\partial u_m}{\partial y} + \dfrac{\partial v_m}{\partial x} \\ 0 \\ 0 \end{bmatrix}$$

$$\underline{\varepsilon}_b = \begin{bmatrix} z \dfrac{\partial \theta_y}{\partial y} \\ -z \dfrac{\partial \theta_x}{\partial y} \\ z \left(\dfrac{\partial \theta_y}{\partial y} - \dfrac{\partial \theta_x}{\partial x} \right) \\ 0 \\ 0 \end{bmatrix}$$

$$\underline{\varepsilon}_s = \begin{bmatrix} 0 \\ 0 \\ 0 \\ \dfrac{\partial w}{\partial y} - \theta_x \\ \dfrac{\partial w}{\partial x} + \theta_y \end{bmatrix}$$

Hence, three $\underline{B}$ matrices can be defined such that

$$\underline{\varepsilon}_m = \underline{B}_m \, \underline{\delta}$$

$$\underline{\varepsilon}_b = \underline{B}_b \, \underline{\delta}$$

$$\underline{\varepsilon}_s = \underline{B}_s \, \underline{\delta}$$

where:

$$\underline{B}_m = \begin{bmatrix} \dfrac{\partial N_1}{\partial x} & 0 & 0 & 0 & 0 & 0 & \cdots \\ 0 & \dfrac{\partial N_1}{\partial y} & 0 & 0 & 0 & 0 & \cdots \\ \dfrac{\partial N_1}{\partial y} & \dfrac{\partial N_1}{\partial x} & 0 & 0 & 0 & 0 & \cdots \\ 0 & 0 & 0 & 0 & 0 & 0 & \cdots \\ 0 & 0 & 0 & 0 & 0 & 0 & \cdots \end{bmatrix}$$

$$\underline{B}_b = z \, \hat{\underline{B}}_b ,$$

$$\underline{\hat{B}}_b = \begin{bmatrix} 0 & 0 & 0 & 0 & \frac{\partial N_1}{\partial x} & 0 & \cdots \\ 0 & 0 & 0 & \frac{\partial N_1}{\partial y} & 0 & 0 & \cdots \\ 0 & 0 & 0 & \frac{\partial N_1}{\partial y} & \frac{\partial N_1}{\partial x} & 0 & \cdots \\ 0 & 0 & 0 & 0 & 0 & 0 & \cdots \\ 0 & 0 & 0 & 0 & 0 & 0 & \cdots \end{bmatrix}$$

$$\underline{B}_s = \begin{bmatrix} 0 & 0 & 0 & 0 & 0 & 0 & \cdots \\ 0 & 0 & 0 & 0 & 0 & 0 & \cdots \\ 0 & 0 & \frac{\partial N_1}{\partial y} & -N_1 & 0 & 0 & \cdots \\ 0 & 0 & \frac{\partial N_1}{\partial x} & 0 & N_1 & 0 & \cdots \end{bmatrix}$$

Finally

$$\underline{\varepsilon} = \underline{\varepsilon}_m + \underline{\varepsilon}_b + \underline{\varepsilon}_s$$

$$= (\underline{B}_m + \underline{B}_b + \underline{B}_s)\ \underline{\delta}$$

$$= \underline{B}\ \underline{\delta}$$

where

$$\underline{B} = \underline{B}_m + \underline{B}_b + \underline{B}_s$$

Similarly, the stress components can be defined as follows:

$$\underline{\sigma} = \{\sigma_x \ \sigma_y \ \tau_{xy} \ \tau_{yz} \ \tau_{zx}\}$$

$$= \underline{\sigma}_m + \underline{\sigma}_b + \underline{\sigma}_s$$

where

$$\underline{\sigma}_m = \{\sigma_x \ \sigma_y \ \tau_{xy} \ 0 \ 0\}_m$$

$$\underline{\sigma}_b = \{\sigma_x \ \sigma_y \ \tau_{xy} \ 0 \ 0\}_b$$

$$\underline{\sigma}_s = \{0 \ 0 \ 0 \ \tau_{yz} \ \tau_{zx}\}_s$$

Hence, $\underline{\sigma}_m = \underline{D}\ \underline{\varepsilon}_m$, $\underline{\sigma}_b = \underline{D}\ \underline{\varepsilon}_b$, $\underline{\sigma}_s = \underline{D}\ \underline{\varepsilon}_s$

where

$$\underline{D} = \frac{E}{(1-\nu^2)} \begin{bmatrix} 1 & \nu & 0 & 0 & 0 \\ \nu & 1 & 0 & 0 & 0 \\ 0 & 0 & \frac{1-\nu}{2} & 0 & 0 \\ 0 & 0 & 0 & \frac{1-\nu}{2\alpha} & 0 \\ 0 & 0 & 0 & 0 & \frac{1-\nu}{2\alpha} \end{bmatrix}$$

$\alpha = 1.2$

The strain energy of the element can be defined as follows:

$$U = U_m + (U_b + U_s)$$

where

$$U_m = \frac{1}{2} \iiint \underline{\sigma}_m^t \, \underline{\varepsilon}_m \, dV$$

$$U_b = \frac{1}{2} \iiint \underline{\sigma}_b^t \, \underline{\varepsilon}_b \, dV$$

$$U_s = \frac{1}{2} \iiint \underline{\sigma}_s^t \, \underline{\varepsilon}_s \, dV$$

Hence

$$U_m = \frac{1}{2} \underline{\delta}^t \left(\iiint \underline{B}_m^t \, \underline{D} \, \underline{B}_m \, dV \right) \underline{\delta}$$

$$U_b = \frac{1}{2} \underline{\delta}^t \left(\iiint \underline{B}_b^t \, \underline{D} \, \underline{B}_b \, dV \right) \underline{\delta}$$

$$U_s = \frac{1}{2} \underline{\delta}^t \left(\iiint \underline{B}_s^t \, \underline{D} \, \underline{B}_s \, dV \right) \underline{\delta}$$

From

$$U = U_m + U_b + U_s = \frac{1}{2} \underline{\delta}^t \, \underline{K}_L \, \underline{\delta}$$

it can be shown that the element stiffness matrix, with respect to local system of coordinates, is

$$\underline{K}_L = \underline{K}_m + \underline{K}_b + \underline{K}_s$$

where

$$\underline{K}_m = \iint t \, \underline{B}_m^t \, \underline{D} \, \underline{B}_m \, dx \, dy$$

$$\underline{K}_b = \iint \frac{t^3}{12} \hat{\underline{B}}_b^t \, \underline{D} \, \hat{\underline{B}}_b \, dx \, dy$$

$$\underline{K}_s = \iint t\ \underline{B}_s^t\ \underline{D}\ \underline{B}_s\ dx\ dy$$

Using an approach similar to that explained in Section (3.4.1), it can be proved that:

$$\underline{K} = \iiint \underline{B}^t\ \underline{D}\ \underline{B}\ dx\ dy\ dz$$

$$= \iint \frac{t}{2} [\underline{B}_1^t\ \underline{D}\ \underline{B}_1 + \underline{B}_2^t\ \underline{D}\ \underline{B}_2]\ dx\ dy$$

where

$$\underline{B}_1 = \underline{B}_m - \frac{t}{\sqrt{12}}\ \hat{B}_b + \underline{B}_s$$

$$\underline{B}_2 = \underline{B}_m + \frac{t}{\sqrt{12}}\ \hat{B}_b + \underline{B}_s$$

Similarly, the global stiffness matrix can be stated as follows:

$$\underline{K}_G = \underline{R}^t\ \underline{K}_L\ \underline{R}$$

$$= \iiint (\underline{B}_L\ \underline{R})^t\ \underline{D}\ (\underline{B}\ \underline{R})\ dV$$

$$= \iiint \underline{B}_G^t\ \underline{D}\ \underline{B}_G\ dV$$

where $\underline{B}_G = \underline{B}\ \underline{R}$

Defining

$$(\underline{B}_G)_1 = \underline{B}_1\ \underline{R}$$

$$(\underline{B}_G)_2 = \underline{B}_2\ \underline{R}$$

then it can be shown that:

$$\underline{K}_G = \iint \frac{t}{2} [(\underline{B}_G^t)_1 \ \underline{D} \ (\underline{B}_G)_1 + (\underline{B}_G^t)_2 \ \underline{D} \ (\underline{B}_G)_2] \ dx \ dy$$

The vector of nodal velocities for an n-node element can be explained as follows:

$$\dot{\underline{\delta}}_L = \{\dot{u}_1 \ \dot{v}_1 \ \dot{w}_1 \ (\dot{\theta}_x)_1 \ (\dot{\theta}_y)_1 \ (\dot{\theta}_z)_1 \ \ldots\ldots\ldots\ldots \ (\dot{\theta}_z)_n\}$$

The velocity components at any point (x,y,z) inside the element can be expressed as follows:

$$\dot{u} = \dot{u}_m + \dot{u}_b$$

$$\dot{v} = \dot{v}_m + \dot{v}_b$$

$$\dot{w} = \dot{w}_b$$

where $\dot{u}_m$, $\dot{v}_m$ are the velocity components at (x,y) of the midplane,

$$\dot{u}_b = z \ \dot{\theta}_y$$

$$\dot{v}_b = - z \ \dot{\theta}_x$$

The velocity vector $\dot{q}$ can be defined as

$$\dot{\underline{q}} = \{\dot{u} \ \dot{v} \ \dot{w}\} = \dot{\underline{q}}_m + \dot{\underline{q}}_{bT} + \dot{\underline{q}}_{bR}$$

where

$$\dot{\underline{q}}_m = \{\dot{u}_m \ \dot{v}_m \ 0\}$$

$$\dot{\underline{q}}_{bT} = \{0 \quad 0 \quad \dot{w}_b\}$$

$$\dot{\underline{q}}_{bR} = z \ \{\dot{\theta}_y \quad -\dot{\theta}_x \quad 0\}$$

From 2-D and plate-bending analysis:

$$\dot{u}_m = \sum_{i=1}^{n} \dot{u}_i \, N_i$$

$$\dot{v}_m = \sum_{i=1}^{n} \dot{v}_i \, N_i$$

$$\dot{\theta}_x = \sum_{i=1}^{n} (\dot{\theta}_x)_i \, N_i$$

$$\dot{\theta}_y = \sum_{i=1}^{n} (\dot{\theta}_y)_i \, N_i$$

Hence, it can be shown that

$$\underline{\dot{q}}_m = \underline{N}_m \, \underline{\dot{\delta}}$$

$$\underline{\dot{q}}_{bT} = \underline{N}_{bT} \, \underline{\dot{\delta}}$$

$$\underline{\dot{q}}_{bR} = \underline{N}_{bR} \, \underline{\dot{\delta}}$$

where

$$\underline{N}_m = \begin{bmatrix} N_1 & 0 & 0 & 0 & 0 & 0 & \cdots \\ 0 & N_1 & 0 & 0 & 0 & 0 & \cdots \\ 0 & 0 & 0 & 0 & 0 & 0 & \cdots \end{bmatrix}$$

$$\underline{N}_{bT} = \begin{bmatrix} 0 & 0 & 0 & 0 & 0 & 0 & .... \\ 0 & 0 & 0 & 0 & 0 & 0 & .... \\ 0 & 0 & N_1 & 0 & 0 & 0 & .... \end{bmatrix}$$

$\underline{N}_{bR} = z\,\hat{\underline{N}}_{bR}$, where

$$\underline{N}_{bR} = \begin{bmatrix} 0 & 0 & 0 & 0 & N_1 & 0 & .... \\ 0 & 0 & 0 & -N_1 & 0 & 0 & .... \\ 0 & 0 & 0 & 0 & 0 & 0 & .... \end{bmatrix}$$

In order to derive the element mass matrix ($\underline{M}$) for the thick element, the same approach as is explained in Section (3.4.1) can be used.

3.4.3 Modified Facet Shell Element

The basic idea of this element is to prevent singularity of the structure stiffness and mass matrices. The nodal displacement components (u,v,w) will always be defined with respect to the global system of axes. For rotation angles two cases will be considered. Local rotation angles are used for coplanar nodes, whilst global rotation angles are used for nodes on discontinuous boundaries. To ensure slope continuity on the common boundaries of elements, a system of local axes similar to that employed by Ahmad et al [ref. 44] is used.

Local Axes for an Element

Let (1), (2), and (3) be three non colinear nodes in an element where x,y,z are its global axes and x', y', z' are its local axes, as shown in Fig. 3.7. The corresponding elemental nodes for (1), (2) and (3) are shown in Fig. 3.8. Let the x''-axis be the line 12 and define y''-axis to be in the 1-2-3 plane and normal to the x''-axis.

The local z' axis is selected normal to the 1-2-3 plane, i.e. normal to the x'', and y'' axes. The local x' axis is selected to be normal to the global x axis and the local z' axis. Finally, the local y' axis is selected normal to the local z' and x' axes. Directional cosines for such axes can be obtained as follows;

(a) Directional cosines of z'-axis

Let $\underline{V}_{12}$ be a vector in the x''-axis direction,

$$\underline{V}_{12} = (x_2-x_1)\,\hat{i} + (y_2-y_1)\hat{j} + (z_2-z_1)\,\hat{K}$$

A vector $\underline{V}_{13}$ can be defined in the 13 direction as follows:

$$\underline{V}_{13} = (x_3-x_1)\,\hat{i} + (y_3-y_1)\,\hat{j} + (z_3-z_1)\,\hat{K}$$

Hence, from the definition of the z'-axis, a vector along it can be obtained as follows:

$$\underline{V}_z = \underline{V}_{21} \wedge \underline{V}_{31}$$

$$\underline{V}_z = \begin{vmatrix} \hat{i} & \hat{j} & \hat{K} \\ x_2-x_1 & y_2-y_1 & z_2-z_1 \\ x_3-x_1 & y_3-y_1 & z_3-z_1 \end{vmatrix}$$

$$= (V_1)_z \hat{i} + (v_2)_z \hat{j} + (V_3)_z \hat{K}$$

where

$$(V_1)_z = (Y_2-Y_1)(z_3-z_1) - (Y_3-Y_1)(z_2-z_1)$$

$$(V_2)_z = (z_2-z_1)(x_3-x_1) - (z_3-z_1)(x_2-x_1)$$

$$(V_3)_z = (x_2-x_1)(Y_3-Y_1) - (x_3-x_1)(Y_2-Y_1)$$

Hence

$$\hat{K}' = \frac{\underline{V}_z}{|\underline{V}_z|} \quad l_3 \hat{i} + m_3 \hat{j} + n_3 \hat{K}$$

where

$$|\underline{V}_z| = \sqrt{(V_1)_z^2 + (V_2)_z^2 + (V_3)_z^2}$$

$$l_3 = (V_1)_z / |\underline{V}_z|$$

$$m_3 = (V_2)_z / |\underline{V}_z|$$

$$n_3 = (V_3)_z / |\underline{V}_z|$$

(b) Direction cosines of x'-axis

There are two special cases for the z'-axis, which should be taken into consideration:

(i) The z'-axis is not parallel to the x-axis

This is the case where

$$|l_3| < 1$$

For that case, a vector in the x'-axis direction is defined as follows:

$$\underline{V}_x = \hat{i} \wedge \underline{V}_z$$

Thus:

$$\hat{i}' = \frac{\hat{i} \wedge \hat{K}'}{|\underline{V}_x|} = \begin{vmatrix} i & j & K \\ 1 & 0 & 0 \\ l_3 & m_3 & n_3 \end{vmatrix} \Big/ |\underline{V}_x|$$

$$\hat{i}' = l_1 \hat{i} + m_1 \hat{j} + n_1 \hat{K}$$

i.e. $l_1 = 0$

$$m_1 = \frac{-n_3}{\sqrt{m_3^2 + n_3^2}}$$

$$n_1 = \frac{m_3}{\sqrt{m_3^2 + n_3^2}}$$

(ii) The z'-axis is parallel to the x-axis

This is the case where

$$l_3 = 1$$

and $m_3 = n_3 = 0$

A vector in the x'-axis direction is

$$\underline{V}_x = \hat{K} \wedge \underline{V}_z$$

$$= \begin{vmatrix} i & j & K \\ 0 & 0 & 1 \\ 1 & 0 & 0 \end{vmatrix} = \hat{j}$$

and $l_1 = 0, \quad m_1 = 1, \quad n_1 = 0$

(c) Direction Cosines of y'-Axis

From the definition of the y'-axis, a unit vector in its direction is:

$$\hat{j}' = \hat{K}' \wedge \hat{i}' \quad ,$$

Hence $l_2 = m_3 \; n_1 - m_1 \; n_3$

$$m_2 = n_3 \; l_1 - n_1 \; l_3 = - n_1 \; l_3$$

$$n_2 = l_3 \; m_1 - l_1 \; m_3 = l_3 \; m_1$$

Rotation of the Modified Facet Shell Element

If the rotation matrix $\underline{R}$ is defined as follows

$$\underline{R} = \begin{bmatrix} l_1 & m_1 & n_1 \\ l_2 & m_2 & n_2 \\ l_3 & m_3 & n_3 \end{bmatrix}$$

then

$$\begin{bmatrix} u \\ v \\ w \end{bmatrix}_{Local} = \underline{R} \begin{bmatrix} u \\ v \\ w \end{bmatrix}_{Global}$$

also

$$\begin{bmatrix} \theta_x \\ \theta_y \\ \theta_z \end{bmatrix}_{Local} = \underline{R} \begin{bmatrix} \theta_x \\ \theta_y \\ \theta_z \end{bmatrix}_{Global}$$

and for the i^{th} node

$$\underline{\delta}_i = \{u_i \; v_i \; w_i \; (\theta_x)_i \; (\theta_y)_i \; (\theta_z)_i\}$$

The $(\underline{\delta}_i)$ Global is defined as follows:

For nodes of type (a) on continuous surfaces

$$(\underline{\delta}_i)_{Global} = \begin{bmatrix} (u_i)_{Global} \\ (v_i)_{Global} \\ (w_i)_{Global} \\ (\theta_x)_{i\ Local} \\ (\theta_y)_{i\ Local} \\ (\theta_z)_{i\ Local} \end{bmatrix}$$

(a)

For nodes of type (b) on discontinuous surfaces

$$(\underline{\delta}_i)_{Global} = \{u_i\ v_i\ w_i\ (\theta_x)_i\ (\theta_y)_i\ (\theta_z)_i\}_{Global}$$

(b)

From the above equations it can be shown that for nodes of type (a)

$$(\underline{\delta}_i)_{Local} = (\underline{R}_a)_i\ (\underline{\delta}_i)_{Global}$$

(a)

and for nodes of type (b)

$$(\underline{\delta}_i)_{Local} = (\underline{R}_b)_i\ (\underline{\delta}_i)_{Global}$$

(b)

where

$$\underline{R}_a = \begin{bmatrix} l_1 & m_1 & n_1 & 0 & 0 & 0 \\ l_2 & m_2 & n_2 & 0 & 0 & 0 \\ l_3 & m_3 & n_3 & 0 & 0 & 0 \\ 0 & 0 & 0 & 1 & 0 & 0 \\ 0 & 0 & 0 & 0 & 1 & 0 \\ 0 & 0 & 0 & 0 & 0 & 1 \end{bmatrix}$$

$$\underline{R}_b = \begin{bmatrix} l_1 & m_1 & n_1 & 0 & 0 & 0 \\ l_2 & m_2 & n_2 & 0 & 0 & 0 \\ l_3 & m_3 & n_3 & 0 & 0 & 0 \\ 0 & 0 & 0 & l_1 & m_1 & n_1 \\ 0 & 0 & 0 & l_2 & m_2 & n_2 \\ 0 & 0 & 0 & l_3 & m_3 & m_3 \end{bmatrix}$$

For an n-node element

$$\underline{R} = \lceil \underline{R}_1 \ \underline{R}_2 \ \ldots\ldots\ldots \underline{R}_n \rfloor$$

according to the given data, each $\underline{R}_i$ must be checked to discover whether it is of type (a) or type (b).

3.4.4. The New Thin and Thick Facet Shell Element

The basic idea is to divide each slope angle into its two constituent parts due to bending and to shear, respectively. Hence, it can be assumed, as shown in Fig. 3.9, that

$$\theta_x = \frac{\partial w}{\partial y} + \phi_x \quad \ldots\ldots\ldots \text{(a)}$$

$$\theta_y = -\left(\frac{\partial w}{\partial x} + \phi_y\right) \quad \ldots\ldots\ldots \text{(b)}$$

$$\theta_z = \phi_z = 0$$

where ϕ_x, ϕ_y, ϕ_z represent the transverse shear effects.

At any node, 9-degrees - of - freedom are required :

$$(u, v, w, \theta_x, \theta_y, \theta_z, \phi_x, \phi_y, \phi_z)$$

The use of ϕ_x, ϕ_y and ϕ_z will allow the displacement component w to be expressed in terms of Hermitian shape functions. The additional shear angles will be expressed in terms of Lagrangian shape functions. Hence, it can be shown that

$$u_m = \sum_{i=1}^{n} u_i \cdot N_i \quad \ldots\ldots\ldots (c)$$

$$v_m = \sum_{i=1}^{n} v_i \cdot N_i \quad \ldots\ldots\ldots (d)$$

$$\phi_x = \sum_{i=1}^{n} (\phi_x)_i \cdot N_i \quad \ldots\ldots\ldots (e)$$

$$\phi_y = \sum_{i=1}^{n} (\phi_y)_i \cdot N_i \quad \ldots\ldots\ldots (f)$$

$$w = \sum_{i=1}^{n} [F_i \cdot w_i + h_i \cdot (\theta_{xi} - \phi_{xi}) - g_i (\theta_{yi} + \phi_{yi})] \ldots\ldots (g)$$

Substituting equation (e) and the differentiation of equation (g) w.r.t. y, into equation (a), it can be shown that

$$\theta_x = \sum_{i=1}^{n} [f_{i,y} w_i + h_{i,y} \cdot (\theta_x)_i + (N_i - h_{i,y}) (\phi_x)_i$$

$$- g_{i,y} \cdot (\theta_y)_i - g_{i,y} \cdot (\phi_y)_i]$$

$$\theta_y = \sum_{i=1}^{n} [f_{i,x} w_i + h_{i,x} \cdot (\theta_x)_i - h_{i,x} \cdot (\phi_x)_i$$

$$- g_{i,x} \cdot (\theta_x)_i + (N_i - g_{i,x}) (\phi_y)_i]$$

The displacement components at any point can be expressed as follows:

$$u = u_m + z\,\theta_y$$

$$v = v_m - z\,\theta_x$$

$$w = w(x,y)$$

The strain components are similar to the previous thick element, i.e.

$$\underline{\varepsilon} = \{\varepsilon_x \;\; \varepsilon_y \;\; \gamma_{xy} \;\; \gamma_{yz} \;\; \gamma_{zx}\}$$

Using the same approach as was used for the previous thick element, it can be shown that

$$\underline{\varepsilon} = \underline{\varepsilon}_m + \underline{\varepsilon}_b + \underline{\varepsilon}_s$$

and

$$\underline{\varepsilon}_m = \underline{B}_m\,\underline{\delta} \;\;,$$

$$\underline{\varepsilon}_b = \underline{B}_b\,\underline{\delta} = -z\,\underline{B}_b\,\underline{\delta} \;\;,$$

$$\underline{\varepsilon}_s = \underline{B}_s\,\underline{\delta} \;\;,$$

$$\underline{\varepsilon} = \underline{B}\,\underline{\delta} \;\;,$$

where

$$\underline{B} = \underline{B}_m + \underline{B}_b + \underline{B}_s \;\;,$$

$$\underline{\delta} = \{u_1 \;\; v_1 \;\; w_1 \;\; \theta_{x1} \;\; \theta_{y1} \;\; \theta_{z1} \;\; \phi_{x1} \;\; \phi_{y1} \;\; \phi_{z1} \;\; \cdots\cdots \}$$

Using the above interpolation expressions it can be proved that

$$(\underline{b}_i)_m = \begin{bmatrix} N_{i,x} & 0 & 0 & 0 & 0 & 0 & 0 & 0 & 0 \\ 0 & N_{i,y} & 0 & 0 & 0 & 0 & 0 & 0 & 0 \\ 0 & N_{i,x} & 0 & 0 & 0 & 0 & 0 & 0 & 0 \\ 0 & 0 & 0 & 0 & 0 & 0 & 0 & 0 & 0 \\ 0 & 0 & 0 & 0 & 0 & 0 & 0 & 0 & 0 \end{bmatrix}$$

$$(\hat{\underline{b}}_i)_b = \begin{bmatrix} 0 & 0 & f_{i,xx} & h_{i,xx} & -g_{i,xx} & 0 & -h_{i,xx} & (N_{i,x}-g_{i,xx}) & 0 \\ 0 & 0 & f_{i,yy} & h_{i,yy} & -g_{i,yy} & 0 & (N_{i,y}-h_{i,yy}) & -g_{i,yy} & 0 \\ 0 & 0 & 2f_{i,xy} & 2h_{i,xy} & -2g_{i,xy} & 0 & (N_{i,x}-2h_{i,xy}) & (N_{i,y}-2g_{i,xy}) & 0 \\ 0 & 0 & 0 & 0 & 0 & 0 & 0 & 0 & 0 \\ 0 & 0 & 0 & 0 & 0 & 0 & 0 & 0 & 0 \end{bmatrix}$$

$$(\underline{b}_i)_s = \begin{bmatrix} 0 & 0 & 0 & 0 & 0 & 0 & 0 & 0 & 0 \\ 0 & 0 & 0 & 0 & 0 & 0 & 0 & 0 & 0 \\ 0 & 0 & 0 & 0 & 0 & 0 & 0 & 0 & 0 \\ 0 & 0 & 0 & 0 & 0 & 0 & -N_i & 0 & 0 \\ 0 & 0 & 0 & 0 & 0 & 0 & 0 & -N_i & 0 \end{bmatrix}$$

The final expression for the element stiffness matrix is similar to that deduced for the previous thick element, with the new $\underline{B}$ matrix.

The velocity components at any point can be obtained in a way similar to that used for displacement components. Hence, it can be shown that:

$$\dot{\theta}_x = \frac{\partial \dot{w}}{\partial y} + \dot{\phi}_x$$

$$\dot{\theta}_y = -\left(\frac{\partial \dot{w}}{\partial x} + \dot{\phi}_y\right)$$

From the analysis given in Section (3.4), it can be deduced, for an n-node element, that

$$\dot{u}_m\ (x,y) = \sum_{i=1}^{n} \dot{u}_i\ N_i$$

$$\dot{v}_m\ (x,y) = \sum_{i=1}^{n} \dot{v}_i\ N_i$$

$$\dot{\phi}_x\ (x,y) = \sum_{i=1}^{n} (\dot{\phi}_x)_i\ .\ N_i$$

$$\dot{\phi}_y\ (x,y) = \sum_{i=1}^{n} (\dot{\phi}_y)_i\ .\ N_i$$

$$\dot{w}_b\ (x,y) = \sum_{i=1}^{n} \{f_i\ \dot{w}_i + h_i\ .\ [(\dot{\theta}_x)_i - (\dot{\phi}_x)_i]$$

$$- g_i\ .\ [(\dot{\theta}_y)_i + (\dot{\phi}_y)_i]\}$$

If the velocity vector at any point (x,y,z) is partitioned as shown before, then for the case of the new elements, it can be proved that

$$(\underline{n}_i)_m = \begin{bmatrix} N_i & 0 & 0 & 0 & 0 & 0 & 0 & 0 & 0 \\ 0 & N_i & 0 & 0 & 0 & 0 & 0 & 0 & 0 \\ 0 & 0 & 0 & 0 & 0 & 0 & 0 & 0 & 0 \end{bmatrix}$$

$$(\underline{n}_i)_{bT} = \begin{bmatrix} 0 & 0 & 0 & 0 & 0 & 0 & 0 & 0 & 0 \\ 0 & 0 & 0 & 0 & 0 & 0 & 0 & 0 & 0 \\ 0 & 0 & f_i & h_i & -g_i & 0 & -h_i & -g_i & 0 \end{bmatrix}$$

$$(\hat{n}_i)_{bR} = \begin{bmatrix} 0 & 0 & f_{i,x} & h_{i,x} & -g_{i,x} & 0 & -h_{i,x} & (N_i - g_{i,x}) & 0 \\ 0 & 0 & f_{i,y} & h_{i,y} & -g_{i,y} & 0 & (N_i - h_{i,y}) & -g_{i,y} & 0 \\ 0 & 0 & 0 & 0 & 0 & 0 & 0 & 0 & 0 \end{bmatrix}$$

and $\quad \underline{N} = \underline{N}_m + \underline{N}_{bT} + \underline{N}_{bR}$

The mass matrix derivation shown in Section (3.4.1), can be employed for such a case.

A simplified expression for the element mass matrix can be obtained, if the rotary inertia terms can be expressed as follows:

$$\dot{\theta}_x = \sum_{i=1}^{n} (\dot{\theta}_x)_i \cdot N_i$$

$$\dot{\theta}_y = \sum_{i=1}^{n} (\dot{\theta}_y)_i \cdot N_i$$

This will only affect $\underline{N}_{bR}$ and it can be deduced that the modified expression will be as follows:

$$(\underline{n}_i)_{bR} = \begin{bmatrix} 0 & 0 & 0 & 0 & zN_i & 0 & 0 & 0 & 0 \\ 0 & 0 & 0 & -zN_i & 0 & 0 & 0 & 0 & 0 \\ 0 & 0 & 0 & 0 & 0 & 0 & 0 & 0 & 0 \end{bmatrix}$$

The rotation matrix for the new element is explained in Appendix (B.5).

3.5 CURVED SHELL ELEMENT

There are numerous curved shell elements in the literature, and due to time limitations it was decided to select from those available a reasonable element with which to make the package complete. The Ahmad's curved shell element is simple and efficient for thick shells and it can also be employed for thin shells, if a selective quadrature scheme is employed. Hence, it was included in the present work after some simplification of the original derivation, published by Ahmad et al [Ref. 44).

The geometry of the element is defined in terms of

(a) midsurface, with geometric nodes

(b) thickness t which is in the direction of the normal to the midsurface.

If the midsurface is transformed into the intrinsic ξ-η plane and $\zeta = 0.5$, then, any point (ξ, η, 0.5) has

$$x_m = \sum_{i=1}^{n} x_i \cdot N_i (\xi,\eta)$$

$$y_m = \sum_{i=1}^{n} y_i \cdot N_i (\xi,\eta)$$

$$z_m = \sum_{i=1}^{n} z_i \cdot N_i (\xi, \eta)$$

All the details concerning the local axes, the relationship between the local and global coordinates, and the Jacobian matrix were explained in Appendix (B.6). The displacement components at any point are defined as follows:

u, v, w along global x, y, z axes,

α rotation about local y'-axis

β rotation about local x'-axis,

as shown in Fig. 3.10.

Considering an n-node element, the nodal displacement vector can be defined as follows:

$$\underline{\delta} = \{u_1 \; v_1 \; w_1 \; \alpha_1 \; \beta_1 \; \ldots\ldots\ldots \beta_n\}$$

The most important aspect for this element is the use of Lagrangian shape functions for the interpolation of displacement components, as follows:

$$u_m = \sum_{i=1}^{n} u_i \cdot N_i (\xi, \eta)$$

$$v_m = \sum_{i=1}^{n} v_i \cdot N_i (\xi, \eta)$$

$$w_m = \sum_{i=1}^{n} w_i \cdot N_i (\xi, \eta)$$

$$\alpha = \sum_{i=1}^{n} \alpha_i \cdot N_i (\xi, \eta)$$

$$\beta = \sum_{i=1}^{n} \beta_i \cdot N_i (\xi, \eta)$$

From the geometric definition of the Jacobian matrix $\underline{J}$, explained in Appendix (B.6), it can be shown that:

$\frac{\partial x}{\partial \xi}$, $\frac{\partial y}{\partial \xi}$, $\frac{\partial z}{\partial \xi}$ are the directional ratios of the ξ-axis

$\frac{\partial x}{\partial \eta}$, $\frac{\partial y}{\partial \eta}$, $\frac{\partial z}{\partial \eta}$ are the directional ratios of the η-axis

and the ζ-axis is normal to the ξ-η plane. Hence, it can be shown that:

$$l_3 = \frac{\partial x}{\partial \zeta} / K \ ,$$

$$m_3 = \frac{\partial y}{\partial \zeta} / K \ ,$$

$$n_3 = \frac{\partial z}{\partial \zeta} / K \ ,$$

where

$$K = \sqrt{\left(\frac{\partial x}{\partial \zeta}\right)^2 + \left(\frac{\partial y}{\partial \zeta}\right)^2 + \left(\frac{\partial z}{\partial \zeta}\right)^2}$$

$$= t$$

and $$l_3 \frac{\partial x}{\partial \xi} + m_3 \frac{\partial y}{\partial \xi} + n_3 \frac{\partial z}{\partial \xi} = 0$$

$$l_3 \frac{\partial x}{\partial \eta} + m_3 \frac{\partial y}{\partial \eta} + n_3 \frac{\partial z}{\partial \eta} = 0$$

Defining

$$\underline{R}^t = \begin{bmatrix} l_1 & l_2 & l_3 \\ m_1 & m_2 & m_3 \\ n_1 & n_2 & n_3 \end{bmatrix}$$

therefore, it can be shown that

$$(J\, R^t) = \alpha$$

where $\alpha_{13} = \alpha_{23} = \alpha_{31} = \alpha_{32} = 0$

$$\alpha_{11} = l_1 \frac{\partial x}{\partial \xi} + m_1 \frac{\partial y}{\partial \xi} + n_1 \frac{\partial z}{\partial \xi}$$

$$\alpha_{12} = l_2 \frac{\partial x}{\partial \xi} + m_2 \frac{\partial y}{\partial \xi} + n_2 \frac{\partial z}{\partial \xi}$$

$$\alpha_{21} = l_1 \frac{\partial x}{\partial \eta} + m_1 \frac{\partial y}{\partial \eta} + n_1 \frac{\partial z}{\partial \eta}$$

$$\alpha_{22} = l_2 \frac{\partial x}{\partial \eta} + m_2 \frac{\partial y}{\partial \eta} + n_2 \frac{\partial z}{\partial \eta}$$

$$\alpha_{3\,3} = l_3 \frac{\partial x}{\partial \zeta} + m_3 \frac{\partial y}{\partial \zeta} + n_3 \frac{\partial z}{\partial \zeta}$$

$$= \sqrt{\left(\frac{\partial x}{\partial \zeta}\right)^2 + \left(\frac{\partial y}{\partial \zeta}\right)^2 + \left(\frac{\partial z}{\partial \zeta}\right)^2} = t$$

A matrix $\underline{A}$ is defined such that

$$\underline{A} = \alpha^{-1} = \underline{R}\,\underline{J}^{-1}$$

The displacement components (u, v, w) at any point (x, y, z) in the element can now be stated as follows:

$$\begin{bmatrix} u \\ v \\ w \end{bmatrix} = \Sigma N_i \begin{bmatrix} u_i \\ v_i \\ w_i \end{bmatrix} + \Sigma N_i \,.\, t \,.\, (\zeta - 0.5) \begin{bmatrix} l_1 \alpha_i - l_2 \beta_i \\ m_1 \alpha_i - m_2 \beta_i \\ n_1 \alpha_i - n_2 \beta_i \end{bmatrix}$$

The $\underline{B}$ matrix is defined, such that

$$\underline{\varepsilon}' = \underline{B}\,\underline{\delta}$$

Hence, it can be expressed as follows:

$$\underline{B} = [\underline{b}_1 \quad \underline{b}_2 \quad \ldots\ldots \underline{b}_n]$$

where

$$\underline{b}_i = \begin{bmatrix} l_1 C_{1,i} & m_1 C_{1,i} & n_1 C_{1,i} & \Delta t C_{1,i} & 0 \\ l_2 C_{2,i} & m_2 C_{2,i} & n_2 C_{2,i} & 0 & -\Delta t C_{2,i} \\ (l_1 C_{2,i} & (m_1 C_{2,i} & (n_1 C_{2,i} & \Delta t C_{2,i} & -\Delta t C_{1,i} \\ +\, l_2 C_{1,i}) & +\, m_2 C_{1,i}) & +\, n_2 C_{1,i}) & & \\ l_3 C_{2,i} & m_3 C_{2,i} & n_3 C_{2,i} & 0 & -C_{3,i} \\ l_3 C_{1,i} & m_3 C_{1,i} & n_3 C_{1,i} & C_{3,i} & 0 \end{bmatrix}$$

and

$$C_{1,i} = A_{11} \frac{\partial N_i}{\partial \xi} + A_{12} \frac{\partial N_i}{\partial \eta}$$

$$C_{2,i} = A_{21} \frac{\partial N_i}{\partial \xi} + A_{22} \frac{\partial N_i}{\partial \eta}$$

$$C_{3,i} = A_{33}\, t\, N_i$$

$$\Delta t = t\,(\zeta - 0.5)$$

The velocity component, at any point (x,y,z) inside the element, can be defined in a way similar to that employed for the displacement components, i.e.

$$\dot{u}(\xi,\eta,\zeta) = \sum_{i=1}^{n} N_i(\xi,\eta)\,[\dot{u}_i + t(\zeta-0.5)(l_1\,\dot{\alpha}_i - l_2\dot{\beta}_i)]$$

$$\dot{v}(\xi,\eta,\zeta) = \sum_{i=1}^{n} N_i(\xi,\eta)\,[\dot{v}_i + t(\zeta-0.5)(m_1\,\dot{\alpha}_i - m_2\dot{\beta}_i)]$$

$$\dot{w}(\xi,\eta,\zeta) = \sum_{i=1}^{n} N_i(\xi,\eta)\,[\dot{w}_i + t(\zeta-0.5)(n_1\,\dot{\alpha}_i - n_2\dot{\beta}_i)]$$

Hence, the kinetic energy of the element can be defined as follows:

$$KE = \frac{1}{2} \iiint \rho \dot{q}^2 \, dV = \frac{1}{2} \iiint \rho \dot{q}'^2$$

$$\dot{q}'^2 = \dot{q}^2 = \dot{u}^2 + \dot{v}^2 + \dot{w}^2$$

from the above equation, it is clear that the reference has no effect on the $\underline{M}$ matrix. Defining

$$\dot{q} = \{\dot{u}\ \dot{v}\ \dot{w}\} = \underline{N}\ \underline{\dot{\delta}}$$

it can be shown that

$$\underline{N} = [\underline{n}_1\ \underline{n}_2\ \ldots\ldots\ \underline{n}_n]$$

where

$$\underline{n}_i = \begin{bmatrix} N_i & 0 & 0 & l_1 t(\zeta-0.5)N_i & -l_2 t(\zeta-0.5)N_i \\ 0 & N_i & 0 & m_1 t(\zeta-0.5)N_i & -m_2 t(\zeta-0.5)N_i \\ 0 & 0 & N_i & n_1 t(\zeta-0.5)N_i & -n_3 t(\zeta-0.5)N_i \end{bmatrix}$$

CHAPTER FOUR

STATIC ANALYSIS OF STRUCTURES

CHAPTER FOUR

STATIC ANALYSIS OF STRUCTURES

4.1 INTRODUCTION

The objective of static analysis is to obtain the stress, strain and/or deformation for a given structure, subject to a given steady load.

The basic procedure of the FEM applied to the static analysis of structures has been described earlier in section (2.2.1).

Using the FEM, the continuum is represented in terms of parameters at specified nodes (nodal values). The nodal load-deflection equations are assembled in terms of elemental stiffness matrices. Techniques for the derivation of the element stiffness matrix have been reviewed in Chapters 2 and 3 for a wide range of old and new elements.

Actual loads may be distributed (non-nodal) and require special techniques to be converted into equivalent nodal loads.

The finite-element static analysis of a real structure is usually based upon the solution of a very large system of simultaneous equations, and the need to employ an efficient solver is essential. Under certain conditions, it is possible to reduce the number of required equations by using a small part of the structure in the analysis.

In this chapter, a technique for the evaluation of equivalent nodal systems, with emphasis on radial impellers, will be discussed. Some economical solvers will be explained together with techniques for dealing with sectorially symmetric structures.

4.2 EQUIVALENT NODAL LOADING

Using the finite element method, the structure should be discretised into a suitable number of elements. Considering external actual loads, an equivalent nodal loading vector for each element will be obtained, and assembled, so as to find the nodal loading vector for the whole structure. Elemental nodal loading vectors equivalent to the initial stresses and strains are explained in section (2.3).

For structures, such as radial impellers, the basic source of loading is inertial loading. Aerodynamic loading will not be considered here, since it has much less effect than inertial loading and may unduly complicate the finite element modelling.

Load-Equivalence Theorem

This theorem, which was introduced by El-Zafrany [Ref. 31], states that, "The necessary and sufficient condition for obtaining a nodal loading vector which is mechanically equivalent to a given load is that the equivalent load does the same virtual work as would be done by the actual load for all virtual displacements, consistent with the structures constraints".

Two basic examples relevant to radial impellers will be explained.

(a) Load Due to Translational Inertia

Considering the case of a three-dimensional structure moving with a translational acceleration:

$$\vec{a} = a_x \hat{i} + a_y \hat{j} + a_z \hat{k}$$

Using D'Alembert's Law, each infinitesimal mass Δm of the structure, as shown in the figure below

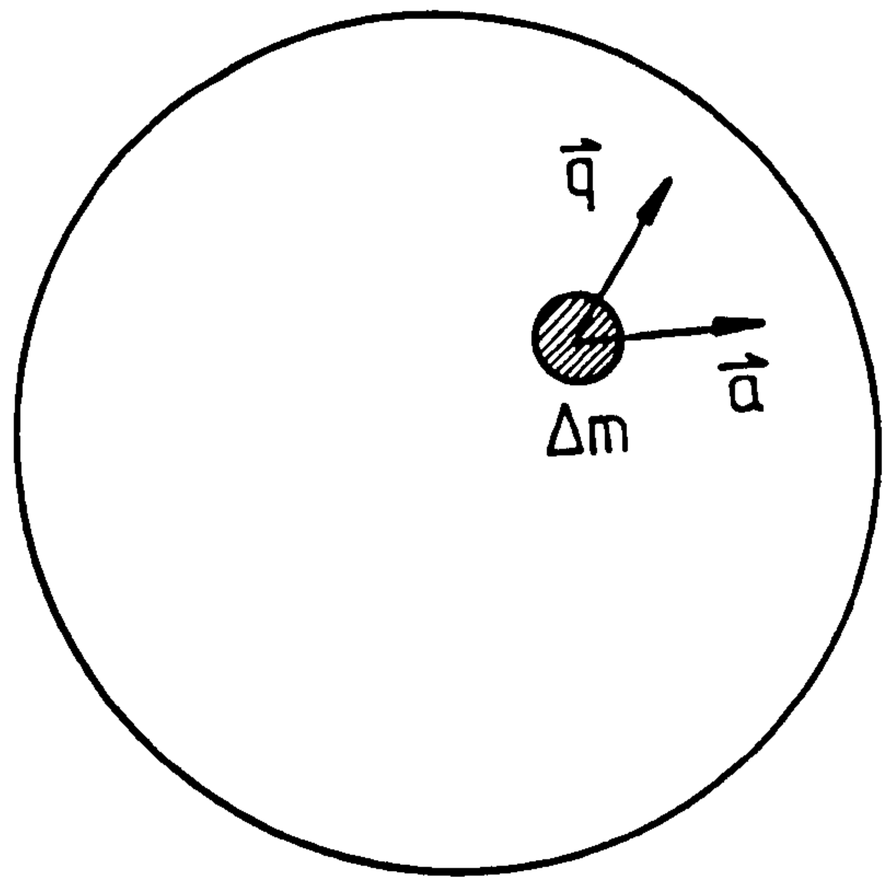

is subject to an inertial force:

$$\Delta\vec{F} = -\vec{a}\,\Delta m = -\rho\,\vec{a}\,\Delta vol$$

If the displacement vector of such an infinitesimal mass is

$$\vec{q} = u\,\hat{i} + v\,\hat{j} + w\,\hat{k}$$

then the work done on that mass is

$$\Delta W = \Delta F \cdot q$$

$$= -\rho(u\,a_x + v\,a_y + w\,a_z)\Delta vol$$

The total work done due to the translational inertial force on a given finite element within the structure is, therefore, as follows:

$$W = -\iiint_{element} \rho(u\,a_x + v\,a_y + w\,a_z)\,dvol \qquad \ldots (a)$$

If there exists an equivalent nodal loading vector $\underline{F}$, then the corresponding work done by that force on the element is:

$$W = \underline{\delta}^t\,\underline{F} \qquad \ldots (b)$$

where $\underline{F}$ and $\underline{\delta}$ are the nodal force vector and nodal displacement vector respectively defined for the element as follows:

$$\underline{F} = \{(F_x)_1 \quad (F_y)_1 \quad (F_z)_1 \quad \ldots\ldots\ldots\ldots \}$$

$$\underline{\delta} = \{u_1 \quad v_1 \quad w_1 \quad \ldots\ldots\ldots\ldots \}$$

In order to obtain a correlation between equations (a) and (b), the following elemental interpolation equations are employed:

$$\left.\begin{aligned} u &= \sum_i u_i \; N_i \\ v &= \sum_i v_i \; N_i \\ w &= \sum_i w_i \; N_i \end{aligned}\right\} \qquad \ldots \text{(c)}$$

where $N_i (i = 1,2, \ldots\ldots)$ are the elemental shape functions.

Substituting equations (c) into equation (a) and comparing the result with equation (b), it can be deduced that

$$\left.\begin{aligned} (F_x)_i &= -\iiint_{\text{element}} \rho \; a_x \; N_i \; \text{dvol} \\ (F_y)_i &= -\iiint_{\text{element}} \rho \; a_y \; N_i \; \text{dvol} \\ (F_z)_i &= -\iiint_{\text{element}} \rho \; a_z \; N_i \; \text{dvol} \end{aligned}\right\} \qquad \ldots \text{(d)}$$

(b) Load Due to Rotational Inertia

If a structure is rotating about a given axis, with a constant angular velocity vector $\vec{\omega}$, as shown in Fig. 4.1, where

$$\vec{\omega} = \omega_x \hat{i} + \omega_y \hat{j} + \omega_z \hat{k}$$

then each infinitesimal mass Δm is subjected to a centrifugal acceleration:

$$\vec{a} = \vec{\omega} \wedge (\vec{\omega} \wedge \vec{r})$$

Let (x_o, y_o, z_o) be a point on the axis of rotation, then at any other point (x,y,z), the position vector $\vec{r}$ is defined as follows:

$$\vec{r} = (x - x_o) \hat{i} + (y - y_o) \hat{j} + (z - z_o) \hat{k}$$

Hence, it can be deduced that

$$\vec{\omega} \wedge \vec{r} = [\omega_y(z - z_o) - \omega_z(y - y_o)] \hat{i}$$

$$+ [\omega_z(x - x_o) - \omega_x(z - z_o)] \hat{j}$$

$$+ [\omega_x(y - y_o) - \omega_y(x - x_o)] \hat{k}$$

and

$$\vec{a} = a_x \hat{i} + a_y \hat{j} + a_z \hat{k}$$

where

$$\left.\begin{aligned} a_x &= - (x - x_o)(\omega_y^2 + \omega_z^2) \\ &\quad + \omega_x [\omega_y (y - y_o) + \omega_z (z - z_o)] \\ a_y &= - (y - y_o)(\omega_z^2 + \omega_x^2) \\ &\quad + \omega_y [\omega_z (z - z_o) + \omega_x (x - x_o)] \\ a_z &= - (z - z_o)(\omega_x^2 + \omega_y^2) \\ &\quad + \omega_z [\omega_x (x - x_o) + \omega_z (y - y_o)] \end{aligned}\right\} \quad \ldots (e)$$

The equivalent nodal loading vector can be obtained by substituting equations (e) into equations (d). For the special case of a structure rotating about the z-axis,

$$\vec{\omega} = \omega_z \hat{k}$$

and using cylindrical-polar coordinates, it can be deduced that

$$a_r = - \omega_z^2 r ,$$

$$a_\theta = a_z = 0$$

i.e.

$$(F_r)_i = \int\int\int_{\text{element}} \rho \omega_z^2 r N_i \, \text{dvol} ,$$

$$(F_\theta)_i = (F_z)_i = 0$$

which is suitable for employment in the analysis of radial impellers.

Equivalent nodal loading vectors for other types of element can be similarly obtained.

4.3 SOLUTION OF LOAD-DEFLECTION EQUATIONS

4.3.1 Ordinary Solvers

The major problem in structural analysis, using the FEM, is the solution of a set of simultaneous algebraic equations. Equations can be solved by either direct methods or iterative schemes, some details about direct methods have been reviewed by Weaver [Ref. 63]. The conjugate-gradient method which is an efficient iterative scheme has been described by Fox and Stanton [Ref. 64] and Fried [Ref. 65, 66]. A state-of-the-art for different solvers was given by Meyer [Ref. 67]. The Gaussian elimination method, although dating as far back as 1826, is still the most efficient one [Ref. 68]. The Choleski square-root method has its importance in the case of multiple loading systems because the decomposition of the matrix is carried out only once for all of the loading systems.

4.3.2 Economical Solvers

The effect of the solution of equations on the efficiency and economy of the FEM has been explained by many investigators. Meyer [Ref. 67], Melosh [Ref. 68] and Irons and Kan [Ref. 69] have shown that the assembly and solution of equations may require up to 80%, or even more, of the total execution time depending on the size of the problem. For a structure with a very large finite element mesh thousands of equations could be generated which may require an enormous CPU time for their solution, perhaps presenting an impossible task for existing computers. Hence, the implementation of economical solvers is vital. Two basic economical solvers are summarised as follows:

(a) Banded Solver

If the stiffness matrix, which is often symmetric, has a band of non-zero values around the leading diagonal and zeros elsewhere, as shown in Fig. 4.2, then the upper (or lower) half of this band is only required to be stored. Algorithms for ordinary solvers can be adapted so as to deal with banded matrices [Refs. 63, 70]. Banded solvers can be more efficient, if the structure nodes are renumbered in a way which minimises the band width [Ref. 71]. Unfortunately, the banded solvers which are available in the present work, whilst being the most efficient of such solvers available, are not recommended for use with ring structures, such as radial impellers, because the band-width cannot be reduced efficiently.

(b) Frontal Solver

The frontal equation-solution technique was originated by Irons [Ref. 72]. The main theme of the frontal solution is to assemble the equations and eliminate the variables at the same time, as shown in Fig. 4.3 [Ref. 73]. As soon as the coefficients of an equation are completely assembled, from the contributions of all relevant elements, the corresponding variables can be eliminated.

A frontal solver with a dynamic front-width developed originally by the Applied Mechanics Group, and shown to be very efficient for use with virtual-memory computers (such as VAX), has been employed in this work.

It is perhaps desirable to use the frontal solver for the analysis of radial impellers, and other large structures, for the following reasons:

(i) The frontal technique uses less storage and arithmetic than the best Gaussian band algorithm.

(ii) In a ring structure, the band algorithm requires an artificial order of node number in order to achieve a small bandwidth, but the order of elements for the frontal technique is a natural one.

(iii) Mesh refinement using higher order elements, is much easier with the frontal algorithm, since node numbers do not effect the front width.

(iv) The part of the coefficient-matrix required in the direct access store (the front) is very small. In computers with a pagination system, this will lead to an enormous saving in CPU time lost due to page faults.

4.4 ANALYSIS OF STRESS AND STRAIN

An important and useful output from the finite element static analysis is the stress distribution. Once the set of simultaneous equations relating the acting loads and displacements are solved, the nodal displacements for any element are available.

The strains and stresses at any point within an element can then be calculated using the strain-displacement equations and stress-strain equations as explained in Chapter Two, as follows:

$$\underline{\varepsilon}\ (x,y,z) = \underline{B}\ (x,y,z)\ \underline{\delta}_{(e)}$$

$$\underline{\sigma}\ (x,y,z) = \underline{D}\ \underline{\varepsilon}\ (x,y,z)$$

The $\underline{B}$ and $\underline{D}$ matrices for different types of element have been reviewed in Chapters Two and Three. An interesting problem arises when choosing the points at which stresses should be calculated. Two types of stress locations are available in this package, as follows:

(a) Nodal Location

Stresses can be obtained at a certain node within the structure as the average of the stresses calculated from the elements meeting at the node. Using the procedure described in the preceding paragraph, it is possible to calculate the stresses at the nodes of an element directly. Generally speaking, the accuracy of stress determination is less than that obtained when determining nodal displacements [Ref. 34].

(b) Optimal Location

It has been suggested that improved accuracy could be achieved by evaluating the stresses at optimal sampling points [Refs. 74,75]. Barlow [Ref. 74] proved that more accurate stresses can be obtained at Gaussian quadrature points, a technique which is also available in the present work.

The present package also produces stresses for all types of element. Details concerning the evaluation of the principal stresses are given in Appendix (C).

4.5 STRESS ANALYSES OF SECTORIALLY-SYMMETRIC STRUCTURE

Structures such as axial compressors, axial turbines, and radial impellers, usually consist of a number of symmetric sectors. If the applied forces and the boundary conditions are the same for each sector, then the stress distribution and deformation for each sector will be the same. Therefore, finite-element stress analysis of such structures can be simplified by considering only one sector as representative of the whole structure, [Ref. 76].

Consider the i^{th} sector of a sectorially symmetric structure, as shown in Fig. 4.4. Discretising the sector into a suitable number of finite elements, the nodal displacement vector for the sector can be partitioned as follows:

$$\underline{\delta}_{sector} = \{\underline{\delta}_1 , \underline{\delta}_0 , \underline{\delta}_2\}$$

where $\underline{\delta}_1$ is the displacement vector for the nodes which are common between the sector under consideration and the previous one [$(i-1)^{th}$ sector],

$\underline{\delta}_2$ is the displacement vector for the nodes which are common between the sector under consideration and the next one [$(i+1)^{th}$ sector], and

$\underline{\delta}_o$ is the displacement vector for all of the internal nodes of the sector.

A sector can be isolated from the whole structure with internal forces acting at nodes common between the sector and other sectors. Hence, the nodal force vector of the sector can be partitioned as follows:

$$\underline{F}_{sector} = \{\underline{F}_1 + \underline{R}_1 , \underline{F}_o , \underline{F}_2 + \underline{R}_2\}$$

where $\underline{F}_1$, $\underline{F}_o$, $\underline{F}_2$ denote external loading, $\underline{R}_1$, $\underline{R}_2$ denote internal loading and subscripts indicate nodes as defined above for $\underline{\delta}$.

The matrix equation of the sector:

$$\underline{K}_{sector} \ \underline{\delta}_{sector} = \underline{F}_{sector}$$

can, therefore, be partitioned as follows:

$$\begin{pmatrix} \underline{K}_{11} & \underline{K}_{10} & \underline{K}_{12} \\ \underline{K}_{01} & \underline{K}_{00} & \underline{K}_{02} \\ \underline{K}_{21} & \underline{K}_{20} & \underline{K}_{22} \end{pmatrix} \begin{pmatrix} \underline{\delta}_1 \\ \underline{\delta}_0 \\ \underline{\delta}_2 \end{pmatrix} = \begin{pmatrix} \underline{F}_1 \\ \underline{F}_0 \\ \underline{F}_2 \end{pmatrix} + \begin{pmatrix} \underline{R}_1 \\ \underline{0} \\ \underline{R}_2 \end{pmatrix}$$

From the necessary and sufficient conditions for sectorial symmetry, it can be deduced that:

$$\underline{\delta}_1 = \underline{\delta}_2$$

$$\underline{R}_1 = -\underline{R}_2$$

Hence, the two "unknown" internal force vectors, $\underline{R}_1$, $\underline{R}_2$, can be eliminated from the above partitioned matrix equation, leading to the following equation:

$$\begin{pmatrix} \underline{K}_{00} & (\underline{K}_{01} + \underline{K}_{02}) \\ (\underline{K}_{10} + \underline{K}_{20}) & (\underline{K}_{11} + \underline{K}_{21} + \underline{K}_{12} + \underline{K}_{22}) \end{pmatrix} \begin{pmatrix} \underline{\delta}_0 \\ \underline{\delta}_1 \end{pmatrix} = \begin{pmatrix} \underline{F}_0 \\ 2\underline{F}_1 \end{pmatrix}$$

Applying the boundary conditions in the usual manner, the above equation can be solved and the sector nodal displacement vector can be obtained. Hence, using the approach described in section (4.3), the stress and strain distribution can be evaluated for the sector.

This technique has been implemented in the present work and can be used with any type of element for any sectorially-symmetric structure.

For the special case of radial impellers (or similar structures) subject to rotational inertia, three-dimensional analysis can be even more simplified by employing cylindrical-polar 3D elements. As described in section (2.6.1) and using the following condition:

$u_\theta = 0$ at all of the nodes common between the sector and other sectors.

This condition will lead to a direct solution of the stiffness equation of the sector without the need to employ the above technique.

CHAPTER FIVE

DYNAMIC ANALYSIS OF STRUCTURES

CHAPTER FIVE

DYNAMIC ANALYSIS OF STRUCTURES

5.1 INTRODUCTION

The finite element method applied to the dynamic analysis of structures has been explained briefly in section (2.2.2). Discretising the structure into a suitable number of elements connected by nodes, nodal dynamic equations can be derived in the following form:

$$\underline{M}\,\ddot{\underline{\delta}}(t) + \underline{C}\,\dot{\underline{\delta}}(t) + \underline{K}\,\underline{\delta}(t) = \underline{F}(t)$$

The basic problem with different types of dynamic analysis is the need to deal with the large matrices usually associated with real structures, such as radial impellers. Economical solvers are essential.

Three basic types of analysis are implemented in this work and they are summarised as follows.

5.2 DYNAMIC EIGENVALUE PROBLEM

5.2.1 Introduction

If there are no external forces acting on a structure, and if the initial conditions are properly imposed, it is possible to induce vibration in any one of several natural modes which are characteristic of the structure. In a natural mode each point of the structure executes harmonic oscillation about the position of static equilibrium and with the same frequency. Generally speaking, damping forces have little effect on the natural frequencies of structures such as radial impellers.

Considering the dynamic equations of a structure without damping and force terms:

$$\underline{M}\ \ddot{\underline{\delta}}(t) + \underline{K}\ \underline{\delta}(t) = \underline{0} \qquad \ldots (a)$$

at a natural mode of vibration with a frequency ω, it is possible to assume that:

$$\underline{\delta}(t) = \underline{\delta}\ \cos\omega t$$

Differentiating with respect to t, then it can be shown that:

$$\dot{\underline{\delta}}(t) = -\omega\ \underline{\delta}\ \sin\omega t$$

$$\ddot{\underline{\delta}}(t) = -\omega^2\ \underline{\delta}\ \cos\omega t$$

substituting $\underline{\delta}(t)$ and $\ddot{\underline{\delta}}(t)$ expressions into equation (a), it can be deduced that

$$-\omega^2\ \underline{M}\ \underline{\delta} + \underline{K}\ \underline{\delta} = 0$$

i.e.

$$\underline{K}\ \underline{\delta} = \omega^2\ \underline{M}\ \underline{\delta}$$

or

$$\underline{K}\ \underline{\delta} = \lambda\ \underline{M}\ \underline{\delta}$$

where

$$\lambda = \omega^2$$

The above equation is a typical eigenvalue problem the roots of which define the natural frequencies of vibration.

5.2.2 Literature Review

Classical methods for the solution of the algebraic eigenvalue problem, as defined above, have been reviewed by Wilkinson [Ref. 77].

Bathe and Wilson [Ref. 78] introduced a survey of probably the most efficient solution methods currently in use for the ordinary dynamic eigenvalue problem.

The numerical advantages of each solution technique, operation counts and storage requirements, are given to establish guidelines for the selection of the appropriate algorithm. One of the popular standard algorithms is the simple iteration, which has been explained in many different ways in the literature [Refs. 79 - 84]. This algorithm has many advantages some of which are given below:

(i) It is direct and uses minimum manipulation

(ii) There is no need to determine all of the eigenvalues if they are not all required.

(iii) It may be suitable for non-positive definite matrices.

(iv) It can be acclerated to a solution.

One of the disadvantages of the simple iteration solver is that it requires large CPU time, if the finite element mesh is large, in which case an economiser should be employed.

The subspace iteration solution is very efficient in the calculation of the lowest eigenvalues and corresponding eigenvectors for large structures [Ref. 31, 85].

Banded and frontal techniques can be employed for the subspace method and result in a considerable reduction in the computer CPU time.

An efficient economiser is dynamic condensation which was introduced by Irons [Ref. 86] and described by other investigators [Refs. 84, 87, 88].

Shah [Ref. 89] has recently introduced a method for automatic condensation. The algorithm of this method is based upon a guideline of Kidder [Ref. 90] which assumes that the associated Guyna [Ref. 91] reduction process is valid.

5.2.3 Standard Eigenvalue Solvers

Two basic algorithms have been employed in the present work:

a) Simple Iteration Solver
b) Jacobi Solver

Their details are available in Reference 92, and are summarised in Appendix (D.1).

5.2.4 Eigenvalue Economisers

Three methods have been used in this work for eigenvalue economisation and they are summarised as follows:

(a) Subspace Iteration

If $\underline{K}$ and $\underline{M}$ are very large matrices whilst relatively few eigenvalues are required, then the subspace-iteration algorithm can be employed. The method is based upon reducing the $\underline{K}$ and $\underline{M}$ matrices whilst retaining the lowest eigenvalues.

The basic steps of the subspace-iteration algorithm can be summarised as follows [Ref. 31, 78].

Step 0

In this step, the following load vectors

$$Y_1 \ , \ Y_2 \ , \ \ldots\ldots\ldots\ldots \ Y_p$$

or the matrix

$$\underline{Y}_{n \times p} = [Y_1 \quad Y_2 \quad \ldots\ldots\ldots\ldots \ Y_p]$$

will be assumed

where n = the total number of degrees of freedom

$$p << n$$

An acceptable assumption is to define:

$$Y_{i,j} = \delta_{ij} \quad \text{(Kronecker delta)}$$

Step 1

The following systems of equations

$$\underline{K} \ \underline{\delta}_r = Y_r \qquad \ldots \text{(a)}$$

where r = 1,2, ... , p

will be solved. It is interesting to note that the above equations are very similar to the static load-deflection equations.

Step 2

Define the matrix of the mode shapes:

$$\underline{X}_{n\,x\,p} = [\underline{\delta}_1 \quad \underline{\delta}_2 \quad \ldots\ldots\ldots\ldots \quad \underline{\delta}_p]$$

which is a rectangular matrix.

Step 3

Obtain the reduced subspace stiffness matrix $\underline{K}^*$,

$$\underline{K}^*_{p\,x\,p} = \underline{X}^t_{p\,x\,n} \quad \underline{K}_{n\,x\,n} \quad \underline{X}_{n\,x\,p}$$

Step 4

Obtain the reduced subspace mass matrix $\underline{M}^*$,

$$\underline{M}^*_{p\,x\,p} = \underline{X}^t_{p\,x\,n} \quad \underline{M}_{n\,x\,n} \quad \underline{X}_{n\,x\,p}$$

Step 5

For this step the system is reduced from the n^{th} order to the order of the following equation

$$\underline{K}^*_{p\,x\,p} \quad \underline{\delta}^*_{p\,x\,1} = \lambda \quad \underline{M}^*_{p\,x\,p} \quad \underline{\delta}^*_{p\,x\,1}$$

And now once this step is achieved it is simple to use any standard eigenvalue solver, such as the simple iteration or Jacobi solvers, to obtain

$\lambda_1, \lambda_2, \ldots\ldots\ldots\ldots, \lambda_p,$ and

$\underline{\delta}^*_1, \underline{\delta}^*_2, \ldots\ldots\ldots\ldots, \underline{\delta}^*_p$

Step 6

Define the matrix of the subspace mode shapes,

$$\underline{X}^{*}_{p \times p} = [\underline{\delta}^{*}_{1} \quad \underline{\delta}^{*}_{2} \quad \ldots\ldots\ldots\ldots \quad \underline{\delta}^{*}_{p}]$$

Step 7

A more accurate matrix of mode shapes can be obtained as follows,

$$\underline{X}_{p x p_{new}} = \underline{X}_{n x p_{old}} \underline{X}^{*}_{p x p}$$

Step 8

A new load matrix is obtained as follows

$$\underline{Y}_{n x p} = \underline{M}_{n x n} \underline{X}_{n x p}$$

Step 9

Calculate the maximum error

$$Er_{max} = Max(|\lambda_{i\ new} - \lambda_{i\ old}|, \quad i = 1,2, \ldots, p)$$

If the maximum error is greater than a given premissible error then return to Step 1.

The solution of the load-deflection equations (a) in Step 1, is the most CPU time consuming part of the algorithm. However, banded or frontal solvers can be introduced in a way similar to that explained for static analysis, in section (4.3). In this work an even faster frontal solver has been developed for subspace iterations in which the elimination of the stiffness matrix $\underline{K}$ will only be carried out once during the first iteration. Special routines, for dealing with the triple products given in Steps 3 and 4 with frontal $\underline{K}$ and $\underline{M}$ matrices,

have been developed. The frontal subspace-iteration algorithm developed in this work has proved to be extremely efficient for virtual-memory computers, such as the VAX.

(b) Dynamic Condensation

This technique retains only a small proportion of the nodal displacements which are called "masters". The remaining "slaves" are assumed to minimise the strain energy, regardless of what effect this has on the kinetic energy [Ref. 86].

The dynamic condensation technique can be used with eigenvalue and response programs. The selection of masters for the present package can be achieved as explained below.

Algorithm for Automatic Masters

An efficient and reliable approach for the automatic selection of masters has been developed from that introduced by Shah [Ref. 89]. Let λ_c be a cut-off eigenvalue which is higher than all the significant eigenvalues. The algorithm to eliminate the slave degrees of freedom can be summarised as follows.

(i) Find the S^{th} degree of freedom, for which the ratio K_{ss}/M_{ss} is largest.

(ii) If this ratio is greater then λ_c, then this S^{th} degree of freedom is assumed to be one of the slaves and it can be eliminated as follows:

Define

$$P_r = K_{rs}$$

$$Q_r = -(M_{ss}/K_{ss})P_r + M_{rs}$$

where

$r = 1, 2, \ldots\ldots, n$

n = the order of the current $\underline{K}$ and $\underline{M}$ matrices.

The reduced matrices can now be defined as:

$$K_{uv}^{reduced} = K_{ij} - P_i P_j / K_{ss}$$

$$M_{uv}^{reduced} = M_{ij} - (P_i Q_j + M_{is} P_j)/K_{ss}$$

where

$i = 1,2, \ldots\ldots, s-1, s+1, \ldots\ldots, n$

$j = 1,2, \ldots\ldots, s-1, s+1, \ldots\ldots, n$

$u = i$ for $i < s$

$u = i - 1$ for $i > s$

$v = j$ for $j < s$

$v = j - 1$ for $j > s$

(iii) Apply steps (i) and (ii) until the largest ratio found in Step (i) is less than or equal to λ_c. At this point the degrees of freedom, associated with the resultant reduced matrices, represent the selected masters.

(c) Double Economiser

This is a combined process of dynamic condensation and subspace iteration. The dynamic condensation technique is firstly employed to eliminate some of the degrees of freedom. Then, the condensed equations are solved by subspace iteration.

5.3 RESPONSE TO DYNAMIC LOADING

Deformation, stress and strain for an engineering structure subjected to a dynamic loading (a loading which is a function of time t) can be obtained by means of the FEM matrix equation of the structure:

$$\underline{M}\,\ddot{\underline{\delta}}(t) + \underline{C}\,\dot{\underline{\delta}}(t) + \underline{K}\,\underline{\delta}(t) = \underline{F}(t) \qquad \ldots (a)$$

According to the nature of the exciting force, there are two different types of analysis available in this work and these are summarised as:

(a) Transient Dynamic Analysis

For the case where a structure is subject to a general exciting force, whether periodic or not, it may be useful for the designer to investigate the history of the structures response (deformation, stresses and strain) to the given excitation, and such an analysis is known as "Transient Dynamic Analysis". Using the FEM, an equivalent nodal loading vector $\underline{F}(t)$, corresponding to the actual excitation, will be evaluated at different time intervals. Then, by applying a suitable time-marching scheme to equation (a), the nodal displacement vector, and the stress- and strain- vectors can be obtained at such time intervals.

There are many time-marching or time-integration schemes which can be employed with the FEM [Ref. 34]. Some weighted-residual Lagrangian schemes have been employed in the package presented here, and their details are demonstrated in Appendix (D.3).

(b) Steady-State Dynamic Analysis

If the structure is subject to a periodic exciting force with time period T, then the corresponding equivalent nodel force can be expanded in terms of the following Fourier series:

$$\underline{F}(t) = \sum_{n=0}^{\infty} \underline{F}_n \ ,$$

$$\underline{F}_o = \frac{1}{2} \underline{A}_o \ ,$$

$$\underline{F}_n = \underline{A}_n \cos(n\omega t) + \underline{B}_n \sin(n\omega t)$$

where

$\omega = 2\pi/T$ and

$\underline{A}_n$, $\underline{B}_n$ are Fourier coefficients.

For such a case, the dynamic FEM equations for the structure can be reduced to a system of algebraic equations by using complex variables, as is explained in detail in Appendix (D.4).

Using such an approach the term $\underline{F}_n$ and the corresponding displacement-vector term $\underline{\delta}_n$ can be expressed as follows:

$$\underline{F}_n(t) = R(\hat{\underline{F}}_n \ e^{-Jn\omega t}) \ ,$$

$$\underline{\delta}_n(t) = R(\hat{\underline{\delta}}_n \ e^{-Jn\omega t}) \ ,$$

where $R(\ ) =$ Real part of $(\ )$,

$$\hat{\underline{F}}_n = \underline{A}_n + J \underline{B}_n \ ,$$

$$J = \sqrt{-1}$$

and the complete answer will be:

$$\underline{\delta}(t) = \sum_{n=0}^{\infty} \underline{\delta}_n(t)$$

The modified dynamic equations for the n^{th} term of $\underline{F}$ and $\underline{\delta}$ can now be stated as follows:

$$[\underline{K} - (n\omega)^2 \underline{M} - J(n\omega) \underline{C}] \hat{\underline{\delta}}_n = \hat{\underline{F}}_n$$

If the structure is manufactured from a single block of material, i.e. no welded or bolted joints, then the structural damping can be introduced by modifying the stiffness matrix in the above equation as follows:

$$[(1 + J\mu) \underline{K} - (n\omega)^2 \underline{M} - J(n\omega) \underline{C}] \hat{\underline{\delta}}_n = \hat{\underline{F}}_n$$

where

μ is known as the hysteretic damping factor, and is equal to about 0.05 for steel and cast iron and about 0.01 for Aluminium and Aluminium alloys.

Using the modern facilities of FORTRAN 77, no new solver is required for the above equations. Ordinary, banded, or frontal solvers used in static analysis, as explained in section (4.3), can be employed with variables being declared complex wherever required. Dynamic stresses and strains can be obtained in a way similar to that employed for static analysis in section (4.4)

5.4 NATURAL FREQUENCY FOR DAMPED SYSTEM

Although the effect of structural damping on the values of natural frequencies for a structure, is negligible, a technique has been introduced here for the estimation of the natural frequencies in the presence of viscous and/or structural damping. This technique is based upon the following complex equation equivalent to the dynamic equation of a structure excited by a frequency ω:

$$[-\omega^2 \underline{M} - J\omega \underline{C} + (1 + J\mu) \underline{K}] \hat{\underline{\delta}} = \underline{0}$$

For the non-trivial solution of the above equation:

$$| -\omega^2 \underline{M} - J\omega\underline{C} + (1 + J\mu) \underline{K} | = 0$$

which generally gives complex eigenvalues.

From the engineering point-of-view, the natural frequencies can be obtained from the following resonance condition.

$$R | -\omega^2 \underline{M} - J\omega\underline{C} + (1 + J\mu) \underline{K} | = R(\omega) = 0$$

The values of ω, which make the real function $R(\omega)$ equal to zero, define the natural frequencies, as shown in the figure below

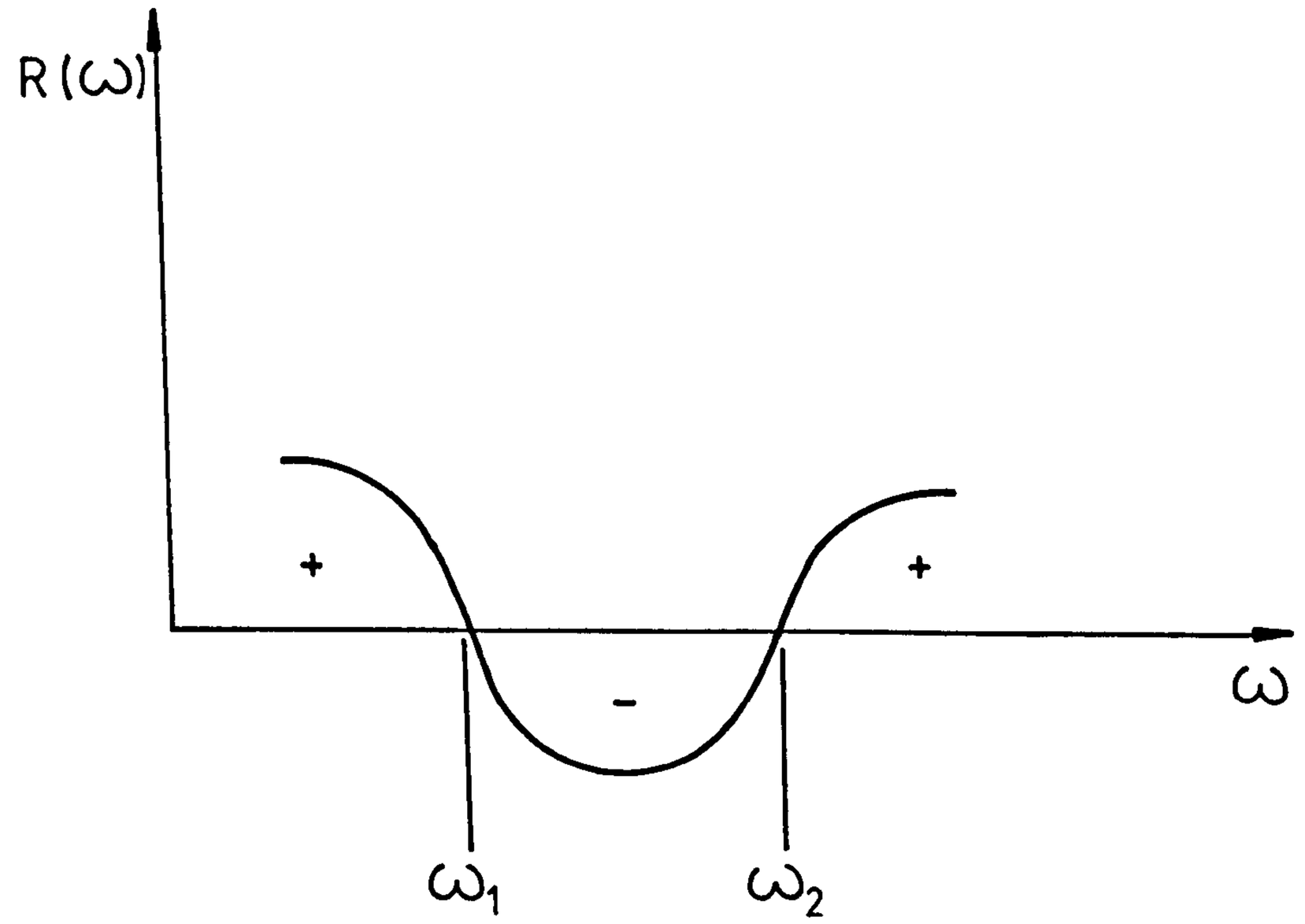

A suggested procedure for determining such ω's is based upon "the determinant search" technique. In this technique, the values of the residual function $R(\omega)$ are to be calculated for a given number of ω. Whenever the sign of $R(\omega)$ changes (either from positive to negative or vice versa) a critical ω can be found at the point where:-

$$R(\omega) = 0$$

as shown in the figure below

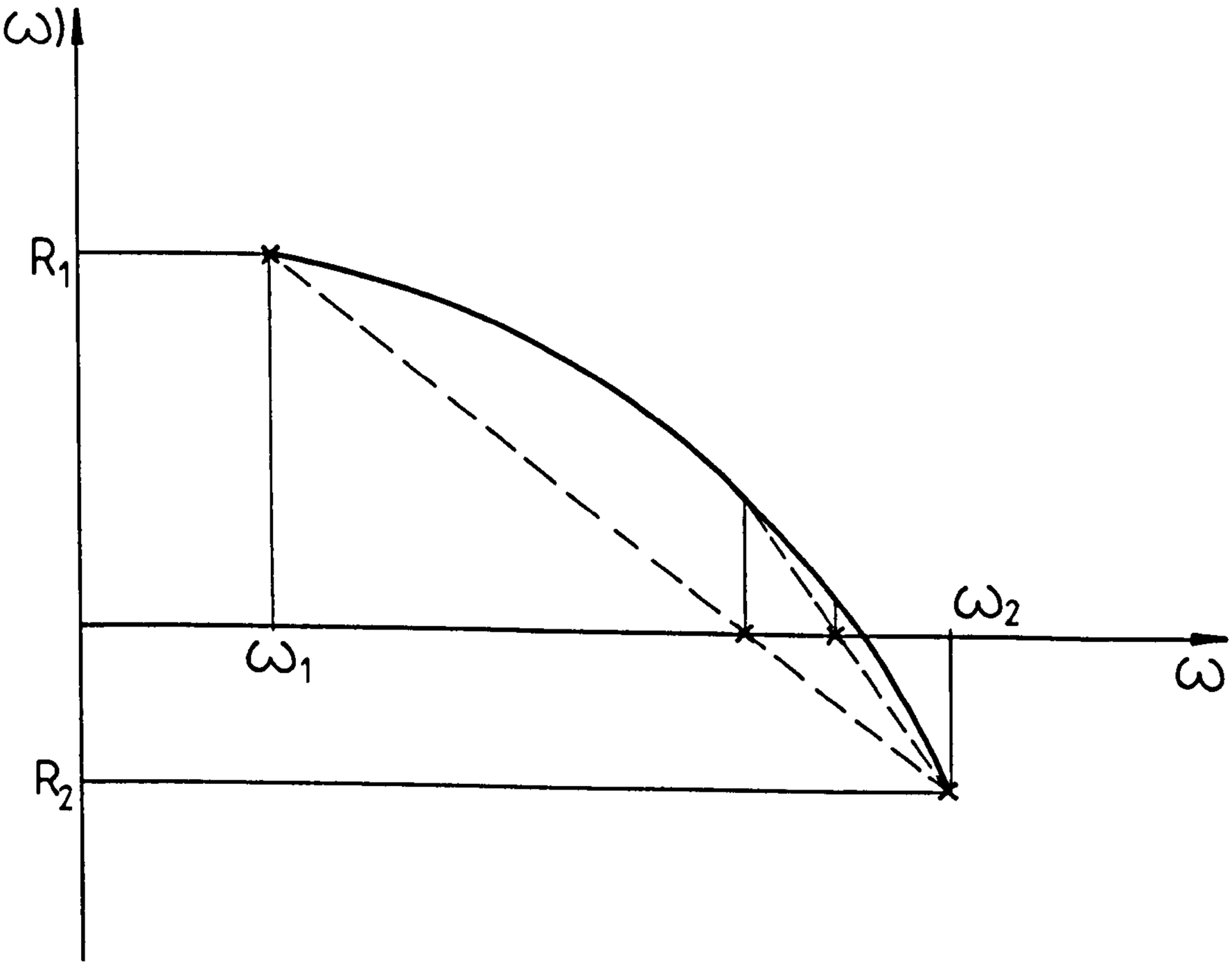

where

$$\frac{\omega - \omega_1}{\omega_2 - \omega_1} = \frac{0 - R_1}{R_2 - R_1}$$

i.e.
$$\omega = \omega_1 - R_1 \left(\frac{\omega_2 - \omega_1}{R_2 - R_1}\right)$$

special techniques for dealing with overflow problems have been introduced, and are as follows:

(a) The logarithm of the residual function $R(\omega)$ is calculated in terms of the logarithms of Gaussian-Elimination pivots.

(b) Before restoring the value of $R(\omega)$ from its logarithm a scale factor will be used. The division by this implys a subtraction of its logarithm from that of $R(\omega)$.

The present package has a facility for calculating the most suitable scaling factor automatically. However, the evaluation of natural frequencies by using such a technique is only recommended if it is thought that the damping may have a considerable effect on the values of the natural frequencies, otherwise, the economical techniques described in section (5.2) should be employed.

CHAPTER SIX

MESH GENERATION AND PLOTTING

CHAPTER SIX

MESH GENERATION AND PLOTTING

6.1 INTRODUCTION

From the early 1960's, the finite element method has proved to be a very powerful technique for dealing with complex structures. An early difficulty with such structures, was the need to solve thousands of simultaneous equations which could require an enormous computer-storage memory and very large CPU time. It was recognised that the solution of equations could consume more than 80% of the total CPU time whenever a large structure was analysed.

With the development of solver routines (such as the frontal solver), and the improvements in computer technology, it became apparent, during the late seventies, that a large amount of the cost for an FEM solution was not due to the computer cost itself but due to the cost of the human effort required for the data preparation. In fact, in order to model a complex structure, the coordinates and topology for thousands of nodes and elements, must be specified. Hence, it became clear that in order to make the FEM more economical the required human effort should be minimised.

The use of an automatic (or computed) method for the generation of the finite element mesh can, of course, reduce such human effort. For that case, the structure may be defined in terms of some basic data parameters and by use of some standard approach for subdivision, a mesh can be generated. Much work has been done recently in the field of interactive generation of the required data (for mesh generation) and some powerful pre-processors which are capable of geometrical modelling of complex structures are now available on the market. Unfortunately, these general-purpose packages are too complex and require considerable skill in order that they be used efficiently.

In order to allow the package presented here to be employed for a wide range of structures, without very large human effort, it was essential to design, at least, a versatile mesh generator for two- and three- dimensional structures. Of course the human effort could further be minimised, if the present package was interfaced with a commercial geometrical-modelling package.

In order to make the present package suitable for use in radial impellers (or similar structures), some additional mesh-generation facilities have been introduced, as will be explained in this chapter. The package also has its own facility for plotting original and deformed meshes.

The mesh generation theory employed in this work was based upon the approach introduced by El-Zafrany [Ref. 31] which was a development of that given by Zienkiewicz and Phillips [Ref. 93]. The basic procedure for the mesh generation is based upon a manual modelling of the structure into the minimum possible number of cells or blocks which can themselves be described as standard finite elements. Using the isoparametric transformation, each block can be transformed to a more uniform shape in an intrinsic space where it is easier for it to be divided into elements. The final mesh is obtained by transforming the generated intrinsic elements back to global space.

Although the mesh generator presented here requires some basic data for the definition of structural block modelling, it is very simple and practical, and it does not require a large computer memory.

6.2 TWO-DIMENSIONAL BLOCKS

Using a recursive approach, every block is transformed into a uniform standard element in its intrinsic ξ,η plane. The block may be divided into simple 4-node quadrilateral, or 3-node triangular, intrinsic elements. A standard procedure can be employed for fitting

real elements inside the simple ones. Any quadrilateral element can be fitted into the domain of the 4-node intrinsic quadrilateral element by means of isoparametric transformation.

This procedure reduces the mesh generation problem to one of generating intrinsic simple elements.

6.2.1 Steps of Mesh Generation

The complete steps for mesh generation will be explained for the first type of blocks, (the uniform quadrilateral block) as an example. Generation of elements for other types of block can be dealt with similarly.

(a) Block Geometry

Consider the example of a uniform quadrilateral block which may have the geometrical shape of any Lagrangian or Serendipity quadrilateral finite element, as shown in Fig. 6.1(a). The block can be transformed into a square of unit side length in its intrinsic ξ-η plane, by means of the following isoparametric transformation:

$$x = \sum_{i=1}^{n_g} x_i \, N_i \, (\xi,\eta)$$

$$y = \sum_{i=1}^{n_g} y_i \, N_i \, (\xi,\eta)$$

where

n_g = number of geometric points of the block

x_i, y_i = cartesian coordinates of block local i^{th} node

N_i .., i=1,2, ... , n_g are the shape functions of the block.

(b) Generation of Quadrilateral Elements

This process can be carried out by using the following steps.

(i) Division into Simple Elements

The division can be performed in the ξ-η plane, in terms of the following data

m = the number of divisions along the ξ-axis

n = the number of divisions along the η-axis

$R_x(1), R_x(2), \ldots, R_x(m+1)$ = division ratios along the ξ-axis

$R_y(1), R_y(2), \ldots, R_y(n+1)$ = division ratios along the η-axis.

Defining:

$$\xi_r = \sum_{i=1}^{r} R_x(i) \Big/ \sum_{i=1}^{m+1} R_x(i)$$

$$\eta_s = \sum_{j=1}^{s} R_y(j) \Big/ \sum_{j=1}^{n+1} R_y(j)$$

$r = 1,2, \ldots, m+1$

$s = 1,2, \ldots, n+1$

then the straight lines of the following equations

$\xi = \xi_r$, $r = 1,2, \ldots, m+1,$

$\eta = \zeta_s$, $s = 1,2, \ldots, n+1$

intersect at the corners of simple rectangular element as shown in Fig. 6.1(b). If the numbering of the nodes and elements starts from the origin and along the ξ-axis:

then

the node with intrinsic coordinates (ξ_r, η_s) has the following number:

$$(s-1)(m+1) + r$$

The element abcd such that:

$$a = (\xi_r, \eta_s)$$

$$b = (\xi_{r+1}, \eta_s)$$

$$c = (\xi_{r+1}, \eta_{s+1})$$

$$d = (\xi_r, \eta_{s+1})$$

has a number = $(s-1)m+r$

Number of generated nodes = $(m+1)(n+1)$

Number of generated elements = $m*n$

(ii) <u>Fitting of Real Elements</u>

Any n_o-node quadrilateral element can be fitted into the domain of the generated 4-node simple elements. Each fitted element can be described as a square of unit side length in its local intrinsic ξ'-η' system, as shown in Fg. 6.1(c). In order to obtain the intrinsic coordinates of the element nodes with respect to the block ξ-η system, an isoparametric transformation can be employed as follows:

$$\xi_i = \sum_{k=1}^{n_c} N_k (\xi_i', \eta_i') \xi_k$$

$$\eta_i = \sum_{k=1}^{n_c} N_k (\xi_i', \eta_i') \eta_k$$

where

(ξ_i', η_i') are the coordinates for the i^{th} local node of the element w.r.t. $\xi' - \eta'$ system.

(ξ_i, η_i) are the corresponding coordinates in $\xi - \eta$ system.

$i = 1,2, \ldots, n_o$

n_c = number of simple-element nodes

n_o = number of fitted-element nodes

N_k = the k^{th} shape function of the simple element.

The simple element abcd is a rectangular element, in ξ,η plane, hence it can be proved that

$$\xi_i = \xi_a + \xi_i' (\xi_b - \xi_a)$$

$$\eta_i = \eta_a + \eta_i' (\eta_d - \eta_a)$$

i.e.

$$\xi_i = \xi_r + \xi_i' (\xi_{r+1} - \xi_r)$$

$$\eta_i = \eta_s + \eta_i' (\eta_{s+1} - \eta_s)$$

(c) Generation of Triangular Elements

(i) Division into Simple Elements

The first step is to divide the block into mxn 4-node elements as shown before. Each e^{th} quadrilateral element can be divided into two triangular elements in two different ways, as shown in Fig. 6.2(a), (b). In order to have well-conditioned triangular elements, the shortest diagonal, in the cartesian system should be joined.

A general procedure can be written for dividing any generated 4-node quadrilateral into two 3-node triangles, for any type of block.

(ii) Fitting of Real Elements

Any n_o-node triangular element can be fitted into the domain of generated 3-node elements. The element (say ABC), can be transformed into a uniform one, in its local ξ'-η' system as shown in Fig. 6.2(c). For any local (ξ_i', η_i') node, the corresponding (ξ_i, η_i) can be obtained by the following isoparametric transformation:

$$\xi_i = (1 - \xi_i' - \eta_i')\xi_A + \xi_i' \xi_B + \eta_i' \xi_c$$

$$\eta_i = (1 - \xi_i' - \eta_i')\eta_A + \xi_i' \eta_B + \eta_i' \eta_c$$

$$i = 1,2, \ldots\ldots , n_o$$

(d) Description in the Cartesian System

The previous processes generate either quadrilateral or triangular elements in the ξ-η plane of the block. In order to describe the generated nodes in cartesian space, the following isoparametric transformation can be used

$$x_j = \sum_{i=1}^{n_g} x_i \; N_i(\xi_j, \eta_j)$$

$$y_j = \sum_{i=1}^{n_g} y_i \; N_i(\xi_j, \eta_j)$$

$$z_j = \sum_{i=1}^{n_g} z_i \; N_i(\xi_j, \eta_j)$$

$$t_j = \sum_{i=1}^{n_g} t_i \; N_i(\xi_j, \eta_j)$$

n_g = number of geometric nodes of the block

N_i = shape functions of the block

t_i = thickness of the element at the i^{th} node.

(e) Generated Element Topology

For the j^{th} node of the e^{th} generated element, j=1,2, ... , n_o the following steps should be carried out:

(i) determine ξ_j', η_j' (for the j^{th} local node of the element)

(ii) find the corresponding ξ_j, η_j as described above

(iii) calculate the corresponding x_j, Y_j, z_j, using the isoparametric transformation, shown above

(iv) compare the generated (x_j, Y_j, z_j) with all (x_g, Y_g, z_g) arrays

if the point is the r^{th} point in (x_g, Y_g, z_g) then

$$TA(e,j) = r$$

if the point is not found, add it, as the last point, to (x_g, Y_g, z_g) and update the number of points N, as

$$N_{new} = N_{old} + 1$$

then,

$$TA(e,j) = N_{new}$$

6.2.2. Review of Two-Dimensional Blocks

In this work, 7 different types of two-dimensional blocks have been introduced in order to provide facilities for an efficient mesh generation, such as transition and zooming. The details of the mathematical procedure for generating elements inside each type of block are reviewed in Appendix (E.1). A brief description of these types follows:

Type 1: Uniform Quadrilateral Block

This block has been described earlier.

Type 2: Uniform Triangular Block

This block can have the geometrical shape of any triangular element. Each side of it is divided into the same number (say n) of uniform divisions generating n^2 similar triangular elements, as shown in Fig. 6.3.

Type 3: Quadrilateral Zooming Block

Mesh generation zooming is a facility by which it is possible to generate a very fine mesh in a local zone surrounding a given node.

Such a facility requires special types of block such as the present one and type 6. The present block is a quadrilateral block which allows a two-directional transition. The block can be divided into quadrilateral or triangular elements as shown in Fig. 6.4.

Type 4: Single-Layer Transition Block

Transition blocks are required to be inserted between fine and coarse meshing in order to maintain compatibility between different blocks. The single-layer transition block is a quadrilateral block which has one layer of elements with two different divisions at two opposite sides as shown in Fig. 6.5.

Type 5: Central Triangular Block

This is a triangular block which can be divided into a number of triangular elements with one common vertex, as shown in Fig. 6.6.

It is useful, for a structure such as a circular disc, to allow a uniform quadrilateral meshing with central triangles as demonstrated in Fig. 6.7.

Type 6: Triangular Zooming Block

This is a triangular block which is divided into triangular elements as shown in Fig. 6.8. The block can be employed for mesh zooming as demonstrated in Fig. 6.9.

Type 7: Multi-Layer Transition Block

This block is a quadrilateral block which consists of more than one layer each of which is similar to the single-layer transition block, as shown in Fig. 6.10.

The multi-layer block is very useful for providing a smooth transition from a very fine mesh to a very coarse one with well-conditioned elements.

6.3 THREE-DIMENSIONAL BLOCKS

A useful idea, developed in this work, is the generation of a standard procedure by which it is possible to fit the actual element into a simple intrinsic element. The direct result of this is the reduction of the mesh generation procedure to one of dealing only with the problem of generating simple intrinsic elements.

A second useful idea is the extension of the two-dimensional, ξ-η, intrinsic mesh in the ζ direction, generating a three-dimensional intrinsic mesh. This process can be carried out for all types of two-dimensional blocks, by using the same procedure. Two additional types of 3D blocks are reviewed in Appendix (E.2).

Finally, a standard procedure has been written for dividing the 8-node intrinsic hexahedral into two 6-node intrinsic pentahedral elements. Another procedure has been written for the division of the 6-node pentahedral element into three 4-node tetrahedral elements.

6.3.1 Generation of 3D Blocks from 2D Blocks

Consider any one of the 2D blocks discussed previously. Let the block be generated into simple intrinsic triangular or quadrilateral elements, in the ξ-η plane.

Define

$$\zeta_t = \sum_{k=1}^{t} R_z(K) \Big/ \sum_{k=1}^{l+1} R_z(K)$$

where

l = number of divisions in the ζ direction,

R_z = division ratio in the ζ direction

Describing the 2D mesh in the planes

$$\zeta = \zeta_t,$$

$$\zeta = \zeta_{t+1}$$

in the same way, and joining the similar nodes, a three-dimensional layer will be generated. The triangular element generates a pentahedral element, and the quadrilateral element generates a hexahedral element, as shown in Fig. 6.11.

The node numbers on plane $\zeta = \zeta_{t+1}$ are to be increased by n above those of the nodes on plane $\zeta = \zeta_t$, where n is the total number of nodes for the 2D block.

If n_e is the number of elements of the 2D block, then the same element numbers can be employed for the first three-dimensional layer. The 3D elements of the layer between planes (ζ_t, ζ_{t+1}) have numbers increased by n_e above those for the elements of the layer between planes (ζ_{t-1}, ζ_t).

Using this approach, all two dimensional blocks given in section (6.2) can be employed for the generation of corresponding three-dimensional blocks.

A review of such generated three-dimensional blocks is shown in Figures 6.12 - 6.18.

6.3.2 Generation of Simple Pentahedra in a Hexahedral Element

This process can be carried out in two different ways, as shown in Fig. 6.19, where each hexahedral element is divided into two

pentahedral elements. Although actual lengths of diagonals in the cartesian x-y-z space, are to be checked, the process is to be carried out on simple intrinsic elements, generating simple intrinsic pentahedra. Then the standard procedure, developed in this work, can be employed to fit the actual cartesian elements.

6.3.3 Generation of Simple Tetrahedra in a Pentahedral Element

The process of dividing a pentahedron into three tetrahedra can be carried out in many different ways. The easiest approach is as shown in Fig. 6.20 where the pentahedral element 123456 is divided into the tetrahedral elements 1234, 2345 and 3456. The process is to be carried out, in intrinsic space, for pentahedral elements. For hexahedral elements, they should be divided first into pentahedral elements, as described above.

6.4 ADDITIONAL MESH GENERATION FACILITIES

These facilities have been introduced to simplify the mesh generation for structures such as radial impellers, and they can be summarised as follows:

6.4.1 Generation of Full Mesh for Axisymmetric Shell Structures

Axi-symmetric shells have practical importance and have attracted the attention of many investigators. If both the shell and the loading are axisymmetric, then the finite element analysis can be reduced to a one-dimensional analysis [Ref.34]. For engineering cases where only a part of the structure can be considered as an axisymmetric shell (for example the disk of a radial impeller), or if it is required to investigate the full three-dimensional vibration mode shapes, it will be found to be impossible to employ axisymmetric analysis. However, the axisymmetry of the geometry can be utilised to simplify the mesh generation for the full structure.

A one-D mesh for the meridian curve of the axisymmetric part should be specified first. Using cylindrical polar coordinates, a full mesh for this part can be generated in terms of curved shell or facet elements, as demonstrated in Fig. 6.21, and linked with the elements of other parts of the structure.

For the example of a radial impeller, the above technique can be employed for the modelling of the disc (using thick curved-shell or facet-elements), and the generated mesh will be linked with that of the blades (using thin facet shell elements).

6.4.2 Generation of a Full 3D Mesh from a 2D Axisymmetric Mesh

Axisymmetric static and dynamic analysis of axisymmetric solids is available in this package. However, the dynamic analysis is limited to the investigation of circular modes of vibration. For full dynamic analysis and/or for a solid structure, where only some parts of the structure are axisymmetric, a full three-dimensional mesh is essential.

For an axisymmetric part of a solid structure, a two-dimensional mesh for the cross-section can be obtained either manually or by using the two-D mesh generation facilities of the present package in a preprocessing step before the full generation. Then, by using some mathematical rotation techniques, the full 3D mesh can be generated by rotating the given 2D mesh one complete revolution with respect to the axis of symmetry, as demonstrated in Fig. 6.22.

6.4.3 Generation of a Full Mesh for a Sectorially-Symmetric Structure

The static analysis of sectorially-symmetric structures may be simplified if the applied forces and the boundary conditions are the same for every sector. For such a case, only one sector is necessary for the analysis, as explained in section 4.5. For the case of general loading, or a full dynamic analysis, a semi-analytical technique may be used but the plotting of the deformed mesh and mode

shapes will be found to be very difficult. An alternative technique is to use the FEM for the full mesh of the structure. This technique can even be more practical if the mesh of only one sector is used.

Hence, a facility has been introduced in this work, by which it is possible to generate the full mesh for sectorially-symmetric structures from that given for one sector. The finite element mesh of the sector can be obtained by the mesh generation facilities available in the package, and it can be modelled by, two-dimensional, facet-shell, curved-shell or three-dimensional elements. The sector will then be rotated with respect to an axis of symmetry so as to generate the finite element mesh for other sectors, as shown in Fig. 6.23.

6.5 MESH PLOTTING

Plotting of a generated mesh is very useful for checking that the mesh is compatible and does not contain ill-conditioned elements (over-distorted elements). The plotting of the deformed structure and mode shapes offers a qualitative facility for reviewing the results of the FEM analysis. Hence, a mesh plotter has been developed in this work in order to plot all types of elements available in the package with or without their deformations. Two-dimensional meshes can be plotted either in the two-dimensional plane, or in three-dimensional space. Three dimensional plots can be projected on any arbitrary plane and the user can therefore examine the finite element mesh from any view.

The theory of mesh plotting was based upon the general approach introduced by El-Zafrany [Ref. 31] and was applied to the different elements available in this work. The plotting approach is reviewed in Appendix (E.3), where simple projection theorems were used for the definition of basic pen movements required for the drawing of a finite element mesh.

The program, used in the present package, was based upon such an approach together with the basic routines of the Gino-F package [Ref. 94] required for character and straight-segments plotting.

CHAPTER SEVEN

FINITE-ELEMENT PROGRAMING SYSTEM

CHAPTER SEVEN

FINITE-ELEMENT PROGRAMMING SYSTEM

7.1 INTRODUCTION

An advanced finite element package, which is capable of static and dynamic analysis of radial impellers, or of any similar structure, was designed on the basis of the theory described in the previous chapters. It is not possible to explain the different parts and segments of the package in this limited context, and a brief review of the package structure will, therefore, be given in this chapter.

Generally speaking the above finite element package has the following basic characteristics:

(i) Package Design Approach

A modular design approach has been adopted for the present package. The package consists of several modules which are stored as separate computer files. Any program required for a particular task will be linked from one or more of these files according to the task specified. Such an approach facilitates the development and expansion of the package.

(ii) User-Friendly Data

Data required for the package, consists of simple data modules with self-explained titles. The package contains a number of subroutines for the interpretation and error-diagnosis of such data modules. For the case of illogical data parameters, descriptive messages will be printed and the program will be terminated after checking all other data modules.

(iii) Pre-Processing Facility

The package has its own mesh generator which runs as a pre-processor and is capable of generating two- and three- dimensional finite-element meshes with all of the types of element available in the package. Additional facilities which simplify the mesh generation for radial impellers, and other similar structures, are also available.

(iv) Sophisticated Library of Finite Elements

The package contains a large library of finite elements including new elements developed in this work. Such a library may help the user to select an optimum element for his job.

(v) Range of Applications

The package is capable of performing static and dynamic analysis for a wide range of structural types; plane-stress, plane-strain, axisymmetrical solids, three-D solids, plates, facet shells and curved shells.

(vi) Solution Accuracy

The accuracy of a finite-element solution depends upon many parameters, including the theory of element derivation, the size of the finite-element mesh, the number of Gauss-quadrature points, etc. The package contains many facilities which allow the user to obtain an accurate convergent solution. New plate-bending and facet-shell elements, which perform well within a wide range of structure thicknesses, are available. Gauss-quadrature points can be modified, etc.

(vii) Computational Economy

Finite element analysis for a real structure usually requires the solution of a very large system of equations. The package contains many economical solvers which can deal efficiently with large structures. A frontal solver is available for static analysis. For vibration analysis, there are many eigenvalue economisers; dynamic condensation, subspace iteration and a double economiser. The subspace-iteration economiser program is also available with a frontal solver.

(viii) Package Output

Tabular and graphical displays of output are available. Generated and deformed meshes can be plotted with different views. Plotting of modal shapes of vibration is also available.

(ix) Package Control

There is a VAX command procedure which controls interactively, the different operations of the package.

(x) Competency

The package, with all of its facilities, provides programs tailored to the users requirements and is therefore very competent in comparison with other packages available on the market.

The package consists of three basic streams as demonstrated in Fig. 7.1, and summarised as follows:

a) Pre-processor

This stream is responsible for reading and checking the job data and, whenever required, it generates a finite element mesh.

b) Finite-element analysis

This is the principal stream through which the required finite element analysis is carried out.

c) Post-processor

After obtaining the results of a finite element analysis, this stream may be used for plotting a deformed mesh or the vibration mode shapes.

7.2 MESH GENERATION AND PLOTTING

The package contains a number of programs for mesh generation and plotting. Each program is a complete unit which carrys out a specific task, as will be explained later. Activation of the appropriate program can be achieved in a simple manner by use of an interactive VAX command procedure which will instruct the user through a compact menu of options.

Mesh generation programs are used as pre-processors whenever an automatically-generated mesh is required. A special data file, which describes the block modelling of the structure and the division ratio, should be defined, after which the mesh generator will be used before the FEM-analysis program is run.

The results of the mesh generation are stored in computer files to be used directly for the analysis and/or mesh plotting.

Mesh-plotting programs may be used immediately after generating a mesh in order to check the generated mesh and define nodal numbers for boundary and loading conditions. A deformed-mesh plotting program may be activated as a post-processor in order to plot the deformed structure, or its vibration mode shapes.

The basic programs for mesh generation and plotting are summarised as follows and shown in Fig. 7.2.

7.2.1 Two-Dimensional Mesh Generation Program (2DMESH)

This program, which is based upon the theory given in section (6.2), generates a mesh of two-D elements in two- or three-dimensional space for two-dimensional, plate-bending, facet-shell and curved shell structures. The program contains seven different types of blocks, as shown in Fig. 7.2, and only the generation of simple intrinsic elements for the blocks requires programming. A generalised "FITTER" subroutine is used to fit the real cartesian elements in the generated intrinsic ones. A simple "SEARCH" subroutine is employed to verify that the generated nodes are unique. For plates and shells with variable thickness, the block thickness is interpolated so as to obtain a reasonable thickness distribution for every generated element.

7.2.2. Three-Dimensional Mesh Generation Program (3DMESH)

This program is capable of generating three-dimensional meshes with cartesian or cylindrical-polar elements. No intrinsic-generation subroutines are required for its seven blocks as shown in Fig. 7.2. The same 2D subroutines are used with one expander subroutine which generates the 3D intrinsic mesh by moving the ξ-η mesh in the ζ-direction. The same "FITTER" and "SEARCH" subroutines are employed. Additional subroutines for generating pentahedra in a hexahedron and tetrahedra in a pentahedron are included.

7.2.3 Additional Mesh Generation Facilities

The following programs which provide additional useful mesh generation facilities are available in the package.

(a) program AXISHELL

This program generates a complete mesh for an axisymmetric plate- or shell- structure. It reads a one-dimensional mesh defining the meridian curve for the midsurface of the structure and generates the required two-D mesh by rotating the meridian curve around the axis of symmetry.

(b) program AXI3D

This program uses a two-dimensional mesh which is manually- or automatically- generated (using program 2DMESH) for the cross-section of an axisymmetric solid structure, in order to generate a full three-dimensional mesh for such a structure using cartesian or cylindrical-polar 3D elements.

(c) program SECTMESH

The input to this program is the mesh for one sector of a sectorially symmetric structure. The sector mesh could be 2D, plate, shell or 3D, manually- or automatically-generated mesh. The program is capable of generating the mesh for the complete structure of any number of its sectors.

7.2.4 Mesh Plotting Programs

Some programs for the plotting of the original and/or the deformed mesh are available with the following facilities:

(i) plotting of two-, or three-dimensional structures

(ii) the mesh plotting can be projected on any arbitrary plane with specified directional cosines

(iii) plotting of nodal symbols and nodal numbers

(iv) plotting of a 2-line title defined interactively

(v) plotting of coloured plots

(vi) magnification of structure deformation, if required.

(a) Two-Dimensional Programs

These are 2DPLOTO and 2DPLOTD which are used for the plotting of original and deformed two-D meshes, respectively. Plots can be obtained with respect to 2D plane or three-D cartesian space for two-D, plate and shell structures. An additional facililty is available for plates and shells, with which it is possible to plot the upper and/or lower surface of the structure.

(b) Three-Dimensional Programs

Programs 3DPLOTO and 3DPLOTD are available for the plotting of original and deformed three-D meshes, respectively.

7.3 FINITE ELEMENT LIBRARY

The package contains a comprehensive finite element library in order to deal with a wide range of structures, namely; two-dimensional, plate, facet and curved shell, and three-dimensional structures. Subroutines for the derivation of intrinsic shape functions and their derivatives are available for 20 basic elements. In the FEM library presented here, the same intrinsic element may be used for the derivation of different types of elements.

Two-D Lagrangian intrinsic elements are employed for two-D, axisymmetric, mindlin plate, and curved shell elements, whilst three-D

Lagrangian intrinsic elements are used for cartesian and cylindrical-polar elements, as demonstrated in Fig. 7.3.

The above facility explains why, with only 20 intrinsic elements, the package can use up to 78 different types of elements as listed in Table 7.1.

A complete description of the intrinsic elements available in the package has already been given in Chapters 2 and 3.

Element Code

In order to help the user to employ the proper type of intrinsic element, a three-digit code is defined for each element as:

d_1 d_2 d_3

where

d_1 is the intrinsic family number, as defined in Table 7.2,

d_2 is a serial number within the same family,

d_3 is the number of Gaussian-quadrature points, in one-dimension, required.

The type of element, with respect to finite element analysis, is usually defined interactively when activating the package command procedure.

7.4 STATIC ANALYSIS

Using its sophisticated library of elements, the package is capable of carrying out static analysis for different types of structure, including radial impellers, with nodal and/or inertial loading. Following the modular programming approach, the static

analysis programs are composed of different files each of which has a specified task. With the aid of the package command procedure it is possible to link the necessary files for a particular job. The basic modules for the static analysis, as demonstrated in Fig. 7.4, can be summarised as follows.

7.4.1 Element Matrices Generator

The stiffness matrix for an element can generally be defined as follows:

$$\underline{K}_{(\bullet)} = \int_{\text{element}} \int \int \underline{B}^t \; \underline{D} \; \underline{B} \; \text{dvol}$$

A unified approach has been adopted in this work for the generation of the element stiffness matrix. An approach which requires the following basic subroutines, as illustrated in Fig. 7.5.

(i) D - Matrix generator

(ii) B - Matrix generator which requires Jacobian-Matrix, Intrinsic derivatives, and Cartesian derivatives subroutines

(iii) Rotation-matrix generator, for facet and curved shell elements

(iv) Matrix-Manipulation subroutines, for the following basic operations:

- Matrix-Initiation
- Matrix-by-matrix product
- Matrix transpose

- Matrix summation
- Matrix-by-vector product
- Matrix inversion

A number of files have been designed for the generation of element stiffness matrices, and whenever applicable, the element equivalent nodal loading vector. Each file contains its own subroutines as defined above and the basic files for element stiffness matrix generation (E.S.M.G) can be summarised as follows:

(a) Two-D and Axisymmetric Structures

File 2DAX is designed for plane-stress, plane-strain and axisymmetrix structures, and a single data parameter is required in order to differentiate between each type.

(b) Three-D Structures

Two files are available; 3DCAR for the E.S.M.G. of three-dimensional cartesian elements, and 3DCYL for the E.S.M.G. of cylindrical-polar elements.

(c) Plates in Bending

Three files have been designed for the E.S.M.G. of plate-bending elements which are as follows:

(i) MINPLATE: for Mindlin elements which are recommended for thick plates

(ii) KIRPLATE: for Kirchoff elements which are suitable for thin plates

(iii)NEWPLATE: for the E.S.M.G. of new plate-bending elements which are efficient for thin and/or thick plates, as explained in Chapter 3.

(d) Facet-Shell Structures

The following files are available in the package:

(i) MINFACET: for thick facet elements with 6 or 5 degrees-of-freedom

(ii) KIRFACET: for thin facet elements with 6 or 5 degrees-of-freedom

(iii)NEWFACET: This file is used for the E.S.M.G. of the new facet elements derived in this work for thin and/or thick facet shell structures.

(e) Curved-Shells

A file named AHMAD is available for the derivation of an element stiffness matrix for AHMAD's element which is suitable for the analysis of curved thick shell structures.

A facility is also available in the package with which the number of quadrature points used for the derivation of the element stiffness matrix can arbitrarily be selected.

7.4.2 Assembly and Solution of Load Deflection Equations

The following basic procedures are available for the assembly and solution of load-deflection equations.

(a) Banded Solver

Using banded matrices, separate subroutines are designed for the assembly and solution of load-deflection equations, as follows:

(i) Assembler

This subroutine calls the element-stiffness-matrix generator and the element-equivalent, nodal, loading-vector generator in order to formulate the stiffness matrix $\underline{K}$ (in a banded form) and the nodal loading vector $\underline{F}$ for the whole structure.

(ii) Reducer

Rows and columns in $\underline{K}$ and $\underline{F}$, corresponding to restrained degrees-of-freedom, are eliminated by subroutine REDUCER in order to formulate the reduced stiffness matrix $\underline{K}_{RED}$ (in a banded form) and the reduced loading vector $\underline{F}_{RED}$, for the structure.

(iii) Solver

In this subroutine, the Gauss-elimination or Choleski-factorisation method is employed for the solution of the banded system of equations:

$$\underline{K}_{RED} \quad \underline{\delta}_{RED} = \underline{F}_{RED}$$

(b) Frontal Solver

When using a frontal solver, it is not possible to separate equations assembly and reduction from the solution process, as explained in section (4.3.2). A frontal solver based upon the Gauss-elimination method is adopted in this work and consists mainly of the following subroutines.

(i) Initiator

This subroutine initiates a number of vectors and matrices required for the frontal operation and also estimates the maximum front width.

(ii) Eliminator

Through this subroutine, each element stiffness matrix is assembled, reduced, and eliminated (whenever applicable) in a step-by-step procedure. In this procedure, an eliminated equation is stored immediately in the back-up store, keeping only a small matrix (the front) in the direct access store.

(iii) Solver

In this subroutine, the eliminated equations are restored, one-by-one, in a reverse order from the direct access store in order to perform the Gaussian backward substitution which leads to the final solution.

7.4.3 Nodal Displacements and Reactions

Having calculated the reduced displacements, a subroutine is employed to calculate and list the total nodal displacements $\underline{\delta}$ for the structure. Another subroutine is used to calculate the nodal reactions, or residuals, according to the following equations:

$$\underline{R} = \underline{F} - \underline{K}\,\underline{\delta}$$

7.4.4 Stresses and Strains

Subroutines for the calculation of stress- and strain-distributions at either nodal locations or optimal locations are

available. Listings of stresses and strains with respect to relevant and principal axes are obtained.

7.5 DYNAMIC ANALYSIS

It is possible to carry out different types of dynamic analysis for different structures, including radial impellers, in a way similar to that explained for the static analysis. There are also many files for such an objective and the program relevant to a specified job can be linked with those files by means of the VAX command procedure. The fundamental modules for dynamic analysis are demonstrated in Fig. 7.6 and can be summarised as follows.

7.5.1 Element Matrices Generators

Both the element stiffness matrix and the element mass matrix are required for any finite-element dynamic analysis. Subroutines for the element stiffness matrix are the same as those used for static analysis as given in section (7.4.1).

The mass matrix for a finite element is defined in a unified approach as follows:

$$\underline{M}_{(\bullet)} = \int_{\text{element}} \int \int \underline{N}^t \quad \underline{D}_D \quad \underline{N} \quad \text{dvol}$$

Hence, unified subroutines have been designed for the generation of the mass matrix for every type of element, in a way similar to that explained for the element stiffness matrix in section (7.4.1). These subroutines are introduced in the same files referred to in section (7.4.1).

7.5.2 Natural Frequency Analysis

Two basic approaches have been adopted depending upon whether the structural damping is to be considered or not.

(a) Undamped Structure

Subroutines for the assembly and reduction of banded stiffness and mass matrices are available. Eigenvalue solver subroutines for such matrices are as follows:

(i) Ordinary Solvers

(ii) Dynamic Condensation

(iii) Subspace Iteration

(iv) Double Economiser

based upon the theory described in Chapter 5.

It was realised, during the early tests of the package, that the most efficient eigenvalue solver is subspace iteration with a frontal solver. Hence, files for such a solver have been implemented for all types of elements available in this package.

(b) Damped Structure

If it is thought that the structural damping will have a significant effect on the natural frequencies of a structure, a facility is available by which it is possible to determine the natural frequencies taking damping into consideration. From a programming point-of-view, this facility, which is based upon the determinant search technique, is a direct application to the steady-state response program.

7.5.3 Response Analysis

Subroutines are available for the dynamic response analysis as follows:

(a) Steady-State Response

A subroutine is capable of assembling a complex stiffness matrix for an element, as follows:

$$\hat{\underline{K}}_{(\bullet)} = (1 + J\mu)\ \underline{K}_{(\bullet)} - \omega^2\ \underline{M}_{(\bullet)}$$

where

$\underline{K}_{(\bullet)}$ and $\underline{M}_{(\bullet)}$ are the element stiffness and ,mass matrices respectively obtained from subroutines described earlier.

Using the facilities of FORTRAN 77, it is possible to write assembler, reducer, and solver subroutines which can deal with banded complex matrices and vectors in a way similar to that used for static analysis.

A complex frontal solver, which is also based upon the static frontal solver, is available.

(b) Transient Response

Subroutines for transient-response analysis based upon the Lagrangian weighted-residual time-marching technique, as explained in section (5.3), have been written for two- and three-dimensional structures.

7.6 PACKAGE CONTROL

The package consists of a very large number of FORTRAN files and linking the appropriate files for a specific task would be

extremely difficult for any user. Using VAX/VMS facilities, a sophisticated VAX command procedure has been designed in order to control package linking and execution. The command procedure file, when activated, presents interactive, self-explained menus to the user, by which the procedure will link the relevant program from the package files, as demonstrated in Fig. 7.7.

CHAPTER EIGHT

RESULTS AND DISCUSSION

CHAPTER EIGHT

RESULTS AND DISCUSSION

8.1 VERIFICATION CASE STUDIES

The finite-element package presented in this work has a large number of facilities and employs a sophisticated library of elements, containing some new elements introduced in this thesis. It is clear from previous chapters that those new elements were based upon rigorous mathematical derivations which makes it vital to verify them. On the other hand, it is essential to validate each other facility of the package before employing it for the analysis of a large structure such as the radial impeller.

A direct approach for the validation of the finite-element package presented here is by comparing its results with those obtained by employing other reliable packages, provided that they contain the same facilities, which was not always possible. Hence, it was decided to use an independent measure for the package verification, by employing it for the analysis of problems with known analytical solutions and comparing results. By the same token, some experimental work has also been carried out and the experimental results so produced have been compared with those obtained from use of the package, as explained in the next sections.

Thousands of very simple cases with known analytical solutions have, in fact, been tested and their results have verified each facility and each subroutine in the present package. Some interesting cases, including those dealing with new elements, are summarised in this section.

8.1.1 New Plate-Bending Element

A simple case of a cantilever plate, as shown in Fig. 8.1, was employed for static and dynamic analysis. A coarse mesh with four 9-node elements, as demonstrated in Fig. 8.2. was used with Mindlin-, Kirchoff- and New-Plate-Bending elements. Cases with different thicknesses were tested, and the nomenclature "thin" as used, for example, in the titling of the result figures, is for thickness/width ratios (h/b) less than or equal to 0.1, whereas "thick" plates signify a thickness/width ratio greater than 0.1.

a) Static-Analysis Results

The free edge of the plate was subjected to a uniform lateral line-pressure simulating a cantilever beam under a concentrated lateral load at its free end.

The corresponding lateral displacement w at the free end of the plate, normalised by dividing it by the value of w obtained by using the beam-bending theory, was plotted versus (h/b) for the thin and thick ranges in Figures 8.3-a and 8.3-b, respectively.

The Mindlin-element has shown "shear locking" at $h/b < 0.025$ by giving meaningless answers. It can be seen from Figures 8.3-a,b that the new plate-bending elements performs like the thin Kirchoff-element within the thin range, and performs like the thick Mindlin-element (including the effect of transverse shear) within the thick range.

On the other hand, it is clear that the derivations for 9-node subparametric elements presented in this work, for both Kirchoff- and new-plate-bending elements have proved to be correct.

It was noticed, through the course of running the previous cases, that the values of the stresses at elemental nodes were much

less accurate than their values at optimal points (Gaussian-quadrature points), and it is strongly recommended that stresses be evaluated at such optimal points only.

The distribution of the bending stress σ_y (at the optimal points) was plotted along the plate y-axis (defined in Fig. 8.1) for the plate with h/b = 0.1, as shown in Fig. 8.4. It is clear from that figure that the Kirchoff- and the New-Plate-Bending elements give a more uniform distribution along the beam axis than the Mindlin element.

The values of $\sigma_y/(\sigma_y)_{analytical}$, at the optimal point nearest to the fixed end of the plate, were plotted versus h/b for different types of 9-node elements as shown in Figures 8.5-a and 8.5-b. It is clear from these figures that the 9-node subparametric Kirchoff and new elements are capable of predicting very accurate values for stress and that the new element has a very stable and accurate performance within a very wide range of thickness.

b) Dynamic-Analysis Results

The natural freuquency analysis has been carried out for the same cases used previously in the static analysis. The non-dimensional frequency λ was plotted against h/b. It is worth mentioning that λ is defined for beams as follows:

$$\lambda = \frac{\omega}{\sqrt{\frac{E\, b^2}{12\, \rho\, L^4}}} \Big/ (h/b)$$

where

ω is the natural frequency of the plate,

E is the Young's Modulus of the plate material,

ρ is the density of the plate material, and

h,b,L are as defined in Fig. 8.1.

The results for the first natural frequency (1B) are shown in Figures 8.6-a and 8.6-b whilst those for the second natural frequency (2B) are illustrated in Figures 8.7-a and 8.7-b.

Note that the values of λ obtained from the beam-theory solution (thin beams) are as follows

$$\lambda_{1B} = 3.515,$$

$$\lambda_{2B} = 20.03$$

It is clear from those figures that the mass matrix derivations for the sub-parametric 9-node Kirchoff-and New-Plate-Bending elements are correct. It is also obvious that the new-plate-bending elements does not lock for plates with very small thickness as does the Mindlin element. For the thick range, the new element converges with the Mindlin element, with both elements including the effect of transverse shear and rotary inertia, which explains their deviation from the beam-theory answers for larger plate thicknesses.

8.1.2 Facet-Shell Elements

A circular plate which can be considered as a curved circular cantilever beam, as shown in Fig. 8.8, was used for the evaluation of the performance of old and new facet-shell elements, for a wide range of plate thicknesses.

Two basic meshes have been tested, the first using 4-noded elements, as shown in Fig. 8.9 whilst the second employs 9-noded

elements as shown in Fig. 8.10. Each mesh was tested with Kirchoff facet-shell elements, Ahmad curved-shell elements, and the new facet-shell element for static and dynamic analysis, and the results can be summarised as follows:

a) Static-Analysis Results

The circular plate was subjected to a vertical load (in the z-direction) at its free end and $w/w_{(anal)}$ at that end has been plotted versus h/b. Results for 4-noded elements are as shown in Fig. 8.11, whilst those for 9-noded elements are demonstrated in Fig. 8.12.

It is clear from these curves that the new facet shell element behaves well in a wide range of thicknesses and is capable of accounting for the transverse shear effect without locking in the thin range of plate-thickness.

It is worth mentioning that all of the tested elements became numerically unstable for $h/b < 0.05$. This phenomenon is due to the round-off errors between the in-plane and out-of-plane terms in the element stiffness matrix [the first are $0(h/L)$ and the second are $0(h/L)^3$]. This problem could be eliminated by employing double-precision arithmetic in the FORTRAN programs.

b) Dynamic-Analysis Results

The natural frequency analysis has been carried out for the cantilever circular plate using the same cases as have been used for the static analysis.

The non-dimensional frequency for the 1B and 2B modes have been plotted for 4-noded elements in Figures 8.13 and 8.14, respectively and for 9-noded elements in Figures 8.15 and 8.16.

It is clear from these figures that the new facet shell element behaves very well within a wide range of thicknesses. For thin plates

it converges with the Kirchoff facet-shell element and for thick plates it converges with Ahmad's element which is known to suffer from shear locking at small h/b.

8.1.3 Cylindrical Elements and Sectorial Symmetry

Cylindrical-polar, three-dimensional solid elements have been derived to be employed for sectorially-symmetric structures. At an early stage of the work, the following isoparametric equations suggested by [Ref. 2] were used:

$$r(x,y) = \Sigma\, r_i\, N_i(x,y)$$

$$\theta(x,y) = \Sigma\, \theta_i\, N_i(x,y)$$

A simple validation case for a rotating solid disc with a uniform thickness has been tested. Unfortunately, there was considerable deviation between the analytical and the FEM results. Then the previous equations were replaced by the following isoparametric x-y equations:

$$r\cos\theta = \Sigma\, r_i \cos\theta_i\, N_i(x,y)$$

$$r\sin\theta = \Sigma\, r_i \sin\theta_i\, N_i(x,y)$$

and the results were found to be satisfactory. The FEM results for a complete disc, with the mesh shown in Fig. 8.17, based upon the two concepts together with the corresponding analytical solution have been plotted. The radial displacement, the radial stress and the hoop stress are demonstrated in Figures 8.18-8.20, and it is obvious from these figures that the derivations introduced in this work lead to more accurate results than those produced with the aid of the previous derivations.

Having completed the results for the whole disc, one-sector was tested only, using the sectorially symmetric facility. The mesh for

the sector is shown in Fig. 8.21, and radial displacement, radial stress, and hoop stress are plotted versus the radius of the disc as shown in Figures 8.22, 8.23 and 8.24 respectively. These figures confirm the accuracy of both the sectorially symmetric facility and the derivation of the three-D cylindrical-polar element presented here.

To illustrate the effect of sectorially symmetry on CPU time, the same disc was analysed for a varying number of sectors and the CPU time is plotted against the number of sectors, as illustrated in Fig. 8.25. It is obvious that the sectorial symmetric facility can save an enormous amount of CPU time.

8.1.4 Economical Solvers

The case of a circular plate, with the mesh shown in Fig. 8.26, has been employed in order to investigate the economy of static and dynamic solvers before using the package for the investigation of radial impellers.

a) Static Analysis

It was clear from the different static tests that the most economical solver for static analysis is the frontal solver. The banded-solver could still be used for small structures.

b) Dynamic Analysis

The natural frequencies obtained by using dynamic condensation, subspace iteration and the double economiser have been plotted versus the number of master degrees-of-freedom, in Figures 8.27 - 8.30, which indicates that subspace iteration can provide accurate answers irrespective of the number of subspace degrees-of-freedom selected, whilst the dynamic condensation and the double economiser require a minimum number of masters before converging to an accurate answer.

The CPU time for the previous cases was plotted against the master degrees-of-freedom as shown in Fig. 8.31 and it is obvious that the most economical eigenvalue solver is the subspace iteration solver provided that it is based upon the frontal concept.

8.2 EXPERIMENTAL WORK

8.2.1. Holographic Interferometry

The technique of dynamic time-averaged interferometric holography was employed for the present investigation. The time-averaged technique is a valuable tool in vibration analysis because it allows for the production of a pictorial representation of any specific mode of vibration for the whole surface of a vibrating component [Ref. 95,96]. The modal pattern at a natural frequency can be studied using only one holographic exposure which provides information about the amplitude of vibration and the locations of the vibratory nodes.

A test rig as shown in Fig. 8.32 - 8.33, and as explained in Appendix (F.1), has been used. The test rig has been used to study the mode patterns of a radial impeller using time-averaged holography, through the following three stages:

a) The Production of a Transmission Hologram

A transmission hologram can be defined as a diffraction grating produced by a photographic emulsion when exposed to an interference pattern produced by two coherent wave fronts, coming together at an angle of not more than 45° on the same side of the photographic plate. To produce two coherent wave fronts at the plate using a HE-NE laser, the difference in path lengths of the object and reference wave front must be less than the coherence length of the HE-NE laser. With these considerations in mind the apparatus was set up as shown in Fig. 8.34, it was then found that to produce the brightest hologram, the light intensities of the object and reference beam had to be equal, this was achieved using a variable density filter/beam splitter. Since the HE-NE laser had a power output of 15 mw it was necessary to paint the object matt white so as to produce maximum reflection of the object wave front.

b) The Excitation of the Impeller at Natural Frequencies

Piezo-electric crystals were used to excite the radial impeller because contact between the whole crystal face and the disc or the blade of the radial impeller could be obtained and because the piezo-electric crystals had very low mass. This meant that energy losses were very small since spurious noise was eliminated. Since the mass of the piezo-electric crystals was negligible, compared with the mass of the disc, the resonant frequencies could be accurately tuned.

c) The Production of a Time-Averaged Hologram

Before a mode shape could be produced, the natural frequency for that mode shape had to be found. This was achieved by monitoring the change across the signal crystal and comparing it with the change in voltage across a crystal cemented on to the impeller to pick-up its frequency response. Both signals were displayed on an oscilloscope simultaneously, it would then be seen when for a particular frequency a maximum peak-to-peak voltage across the "pick-up" crystal was produced for a constant peak-to-peak voltage across the signal crystal. This particular frequency was accurately monitored using a frequency counter connected through the oscilloscope to the signal generator.

To produce the time-averaged hologram, the impeller was vibrated at a natural frequency while recording a transmission hologram.

Radial Impeller Case Study

The radial impeller demonstrated in Fig. 8.35, has been analysed using the previous technique. The mode shape was obtained at ω = 2550.4 Hz as shown in Fig. 8.36. The result has been compared with that obtained by the package as explained in section 8.3.

8.2.2 Stress Analysis of Rotating Radial Impeller

While the holographic technique was used for evaluating the accuracy of the dynamic results obtained from the radial impeller package, the accuracy of the steady stress results, obtained from the same package, was checked by means of a combined strain-gauge/slipring assembly applied to a real rotating radial impeller.

The rotating impeller test-rig was simple as can be seen from Fig. 8.37-a,b, where the impeller was driven by an electric motor and strain gauges were fixed at critical points over the disc and blades. The radial impeller shown in Fig. 8.38-a,b was, in fact, produced by the Elta Fan Company who had asked the Applied Mechanics Group to determine the steady-state stresses produced at specific rotational speeds. The results obtained from the strain-gauges have been compared with the FEM results obtained from the radial impeller, and the comparison is given in the next section. An explanation of the details of this rig is given in Appendix (F.2).

8.3 RADIAL IMPELLER CASE STUDIES

8.3.1 Case 1

The radial impeller tested by using the holographic technique, as explained in section 8.2.1, has been analysed using the FEM package in order to assess the efficiency of the package and the results can be summarised as follows:

a) Blade Vibration

The blade of the impeller was analysed by the package assuming that it is rigidly fixed to the impeller disc and the mode shapes are as shown in Fig. 8.39-a,c and Fig. 8.40-a,c. The theoretical results have been compared with those obtained by (Holography) as shown in Table 8.1. It is clear from that table that a difference of about 4%

to 14% has been obtained between numerical and experimental results. This difference is probably due to the flexibility of the disc which is not considered in the FEM analysis.

b) Vibration of the Whole Impeller

The mode shape observed experimentally, as shown in Fig. 8.36, has been obtained theoretically by using two different meshes as demonstrated in Fig. 8.41-a,b and 8.42-a,b. The comparison between the numerical and the analytical results is given in Table 8.2, where it is clear that the results of the fine FEM mesh are within about 5% of those obtained from the experimental work, and it is possible that even greater accuracy could have been obtained for a more fine mesh still.

8.3.2 Case 2

The second radial impeller as shown in Fig. 43 has been analysed to evaluate the steady-state stresses due to rotational inertia. The FEM results have been plotted together with experimental results obtained by using the technique explained in section 8.2.2. The radial and hoop stress distributions at different locations are shown in Figure 8.44 - 8.47. It is clear from those figures that there is good agreement between the numerical and the experimental results.

CHAPTER NINE

CONCLUSIONS AND RECOMMENDATIONS

CHAPTER 9

CONCLUSIONS AND RECOMMENDATIONS

CONCLUSIONS

It is clear that the major objective of this work has been achieved. An advanced finite-element package, which is capable of static and dynamic analysis for radial impellers, and similar structures, has been designed and proved to be efficient and reliable.

A new sub-parametric, 9-node, plate-bending, element, which takes the transverse shear and rotary inertia into consideration, has been introduced and has proved to perform very well within a wide range of plate thicknesses.

A similar new element has been derived for facet shells and its accuracy and reliability has been confirmed for the static and dynamic analysis of curved shell structures.

An alternative derivation for the 3D cylindrical-polar solid element has been introduced and proved to be more accurate than the conventional one given in the literature.

The package's own mesh-generation and plotting techniques, including the additional facilities for axially- and sectorially-symmetric structures, have proved to be very useful for the minimisation of human effort required for the modelling of radial impellers.

Static and dynamic economical solvers introducd in the package, namely the static frontal solver and the subspace-iteration eigenvalue frontal solver, have proved to save an appreciable amount of computer CPU time when dealing with large structures such as radial impellers.

A good agreement between the dynamic results of a radial impeller obtained by the package and by the holographic experimental technique has been observed. The steady-state stresses measured for another rotating radial impeller have been close to those obtained by the finite-element package.

Finally, the package presented here with its command procedure, user-friendly-data, error diagnosis, sophisticated library of finite elements, mesh generation and plotting, and other facilities has proved to be a very powerful tool for the static and dynamic analysis of turbomachine components.

RECOMMENDATION FOR FUTURE WORK

The package as it stands is a very compact and cheap facility which might interest small radial-impeller manufacturers. However, it may be useful for large establishments if the package could be interfaced with a versatile geometrical modeller such as the SDRC-IDEAS.

Three-dimensional plotting could be improved by introducing a hidden-line facility and variable area contouring.

REFERENCES

R E F E R E N C E S

1. KIKUCHI, H. — 'Stresses in Radial Impellers', Ph.D. Thesis, Cranfield Institute of Technology, SME, 1978.

2. SHAM SUNDER, K. — 'Finite Element Analysis of Centrifugal Impellers', Ph.D. Thesis, Cranfield Institute of Technology, SME, 1981.

3. THURGOOD, D.A. and GIVAN, V.E.F. — 'Stress Analysis of the Asymmetric Profile Rotating Disc', Hawker Siddeley Dynamic Ltd., Stress Office Report No. 619 (parts I and II) January 1967.

4. THURGOOD, D.A. — 'Stresses in Asymmetric Discs', Journal of Strain Analysis, 4, 65-73, 1969.

5. THURGOOD, D.A. and GIVAN, V.E.F. — 'Comparison of Stress Analysis Methods for Radial Flow Rotors', Hawker Siddeley Dynamic Ltd., Stress Office Report No. 630, January 1969.

6. CLOUGH, R.W. — 'The Finite Element Method in Plane Stress Analysis', Proceedings of 2nd ASCE Conference on Electronic Computation, Pittsburgh, Sept. 8 and 9, 1960.

7. HUEBNER, K.H. and THORNTON, E.A. — 'The Finite Element Method for Engineers', John Wiley & Sons, 1982.

8. BESSELING, J.F. — 'The Complete Analogy between the Matrix Equations and the Continuous Field Equations of Structural Analysis', International Symposium on Analogue and Digital Techniques Applied to Aeronautics, Liege, Belgium, 1963.

9. MELOSH, R.J. — 'Basis for Derivation of Matrices for the Direct Stiffness Methods', AIAAJ., Vol.1, pp 1631-1637, 1963.

10. FRAEIJS de VEUBEKE, B. — 'Upper and Lower Bound in Matrix Structural Analysis', in AGARD-Ograph 72, B.F. de Veubeke, Pergamon Press, New York, 1964.

11. JONES, R.E. — 'A Generalization of the Direct-Stiffness Method of Structural Analysis', AIAAJ., Vol.2, pp 821-826, 1964.

12. ZIENKIEWICZ, O.C. and CHEING, Y.K. 'Finite Elements in the Solution of Field Problems', Int. J. Num. Meth. Eng., Vol. 220, 1965.

13. EL-ZAFRANY, A.M.A. 'A Finite Element System for Efficient Static and Dynamic Analysis of Gas Turbine Engines Structures', M.Sc. Thesis, Cranfield Institute of Technology, SME, 1978.

14. PIAN, T.H. 'Derivation of Element Stiffness Matrices by Assumed Stress Distributions AIAAJ, Vol. 2, pp 1333-1336, 1964.

15. IRON, B.M. 'Engineering Applications of Numerical Integration in Stiffness Methods', AIAAJ, Vol. 4, pp 2035-2037, 1966.

16. ARGYRIS, J.H. 'Continua and Discontinua', Proc. Conf. Matrix Methods in Struct. Mech., Air Force Inst. of Tech., Wright Patterson A.F. Base, 1965.

17. ERGATOUDIS, I. IRONS, B. and ZIENKIEWICZ, O.C. 'Curved Isoparametric Quadrilateral Elements for Finite Element Analysis', Int. J. Num. Meth. Eng., Vol. 4, pp 31-42, 1968.

18. DUNNE, P.C. 'Complete Polynomial Displacement Fields for the Finite Element Method', Trans. Roy. Aero. Soc., Vol. 72, pp 245-246, 1968.

19. ARGYRIS, J.H. 'The LUMINA Element for Matrix Displacement Methods', Aer. J. Vol. 72, pp 514-517, 1968.

20. ERGATOUDIS, I. 'Isoparametric Finite Elements in Two and Three Dimensional Stress Analysis', Ph.D. Thesis, Univ. of Wales, 1968.

21. TURNER, M.J. CLOUGH, R.J. MARTIN, H.C. and TOPP, L.J. 'Stiffness and Deflection Analysis of Complex Structures', J. Aero. Sci., Vol. 23, pp 805-823, 1956.

22. ARGYRIS, J.H. 'Triangular Element with Linearly Varying Strain for the Matrix Displacement Method', J. Aero. Sci., Vol. 69, 1965.

23. TAYLOR, R.L. 'On Completeness of Shape Functions for Finite Analysis', Int. J. Num. Meth. Eng., Vol. 4, pp 17-22, 1972.

24. ARGYRIS, J.H. 'Matrix Displacement Analysis of Plates and Shells', Ing. Archiv, band 35, Heft 2, 1966.

25. ARGYRIS, J.H. and SCHARPF, D.W. 'The Curved Tetrahedral and Triangular Elements TEC and TRIC for the Matrix Displacement Method', Aero. J. Vol. 73, pp 55-65, 1969.

26. ARGYRIS, J.H. FRIED, I and SCHARPF, D.W. 'The TET 20 and TEA 8 Elements for the Matrix Displacement Method', Aero. J. Vol. 72, pp 618-623, 1968.

27. FRIED, I. 'Some Aspects of the Natural Coordinate System in the Finite Element Method', AIAAJ, Vol. 7, pp 1366-1368, 1969.

28. NORRIE, D. and VRIES, G.D.E. 'Fnite Element Bibliography', PUB IFI/Plenum N,Y, 1976.

29. EL-ZAFRANY, A.M. and COOKSON, R.A. 'Derivation of Lagrangian and Hermitian Shape Functions for Triangular Elements', Int. J. Num. Meth. Eng., Vol. 23, pp 275-285, 1986.

30. EL-ZAFRANY, A.M. and COOKSON, R.A. 'Derivation of Lagrangian and Hermitian Shape Functions for Quadrilateral Elements', Int. J. Num. Meth. Eng., Vol. 23, pp 1939-1958, 1986.

31. EL-ZAFRANY, A.M. 'An Advanced Finite Element System for Engineering Analysis', Ph.D. Thesis, Cranfield Institute of Technology, SME, 1983.

32. TIMOSHENKO, S.P. and GOODIER, J.N. 'Theory of Elasticity', New York, McGraw-Hill Book Co. 1951.

33. EL-ZAFRANY, A.M. and COOKSON, R.A. 'Finite Element Techniques for Engineering Analysis', (a book to be published).

34. ZIENKIEWICZ, O.C. 'The Finite Element Method', McGraw-Hill Book Co. 1973.

35. TIMOSHENKO, S.P. and WOINOWSKY-KRIEGER, S. 'Theory of Plates and Shells', McGraw-Hill, 2nd Edn., 1959.

36. MELOSH, R.J. 'Basis for Derivation of Matrices for Direct Stiffness Method', AIAAJ, Vol. 1, No. 7, pp 1631-1637, July 1963.

37. ZIENKIEWICZ, O.C. and CHEUNG, Y.K. 'The Finite Element Method for Analysis of Elastic Isotropic and Orthotropic Slabs', Proc. Instn. Civ. Eng., 1964, 28, pp 471-488, Aug.

38. BAZELEY, G.P. CHEUNG, Y.K. IRONS, B.M. and ZIENKIEWICZ, O.C. 'Triangular Elements in Plate Bending-Conforming and Non-Conforming Solutions', Proc. of First Conference on Matrix Methods in Structural Mechanics at Wright Patterson Air Force Base, Ohio, 1965.

39. LOVE, A.E.H. 'A Treatise on the Mathematical Theory of Elasticity', 4th ed., Dover Publication, New York, 1927.

40. REISSNER, E. 'The Effect of Transverse Shear Deformation on the Bending of Elastic Plates', J. Appl. Mech., A69-A77, 1945.

41. LIBOVE, C. and BATDORE, S.B. 'A General Small-Deflexion Theory for Flat Sandwich Plates', TN 1526, National Advisory Committee on Aeronautics, Washington, 1948.

42. MINDLIN, R.D. 'Influence of Rotatory Inertia and Shear on Flexural Motion of Isotropic Elastic Plates', J. Appl. Mech. 1951, 18, Mar., No. 1, pp 31-38.

43. ESSENBURG, F. and MACHOI, P.M. 'On Elastic Plates of Variable Thickness', Prac. 3rd U.S. Nat. Congr. Appl. Mech., pp 313-319, 1958.

44. AHMAD, S. IRONS, B.M. and ZIENKIEWICZ, O.C. 'Analysis of Thick and Thin Shell Structures by Curved Finite Elements', Int. J. Num. Meth. Eng., Vol. 2, pp 419-451, 1970.

45. HINTON, E. RAZZAQUE, A. ZIENKIEWICZ, O.C. and DAVIES, J.D. 'A Simple Finite Element Solution for Plates of Homogeneous Sandwich and Cellular Construction', Proc. Inst. Engrs. Part 2, 1975.

46. ZIENKIEWICZ, O.C. TAYLOR, R.C. and TOO, J.M. 'Reduced Integration Technique in General Analysis of Plates and Shells', Int. J. Num. Meth. Eng., Vol. 3, pp 275-290, 1971.

47. PUGH, E.D. 'A Study of Quadrilateral Plate Bending Elements with Reduced Integration', Int. J. Num. Meth. Eng., Vol. 12, pp 1059-1079, 1978.

48. HUGHES, T.
COHEN, M. and
HAROUN, M.
'Reduced and Selective Integration Techniques in the Finite Element Analysis of Plates', Nuclear Engineering and Design, Vol. 46, pp 203-222, 1978.

49. HUGHES, T. and
COHEN, M.
'The Heterosis Finite Element for Plate Bending', Computers and Structures, Vol. 9, pp 445-450, 1978.

50. EL-ZAFRANY, A.M. and
COOKSON, R.A.
'An Efficient Plate-Bending Finite Element for Thin and Thick Plates. (To be published)

51. LOVE, A.E.H.
'On the Small Free Vibrations and Deformations of Thin Elastic Shells', Phil. Trans. Roy. Soc. (London), 17A, pp 491-546, 1888.

52. PAWSEY, S.F.
'The Analysis of Moderately Thick to Thin Shells by the Finite Element Method', SESM Report No. 70-12, Dept. of Civil Engineering, U.C. Berkeley (1970).

53. DOVEY, H.H.
'Extension of Three-Dimensional Analysis to Shell Structures Using the Finite Element Idealisation', SESM Report No. 74-2, Dept. of Civil Engineering, U.C. Berkeley, 1974.

54. WILSON, E.L.
'Incompatible Displacement Models', in Numerical and Computer Methods in Structural Mechanics (Ed. S.J. Fenves et al), Academic Press, New York, 1973.

55. IRONS, B.M. and
DRAPER, K.J.
'Inadequacy of Nodal Connections in Stiffness Solution for Plate Bending', AIAAJ, Vol.3, 965, 1965.

56. MELOSH, R.J.
'A Flat Triangular Shell Element Stiffness Matrix', Proc. Conf. Matrix Meth. Struct. Mech., Wright-Patterson A.F.B., Ohio. AFFDL-TR-66-80, 503-514 (1965).

57. UTKU, S.
'Stiffness Matrices for Thin Triangular Elements of Non-Zero Gaussian Curvature' AIAAJ-5, 1659-1667 (1967).

58. WEMPNER, G.A.
ODEN, J.T., and
KROSS, D.A.
'Finite-Element Analysis of Thin Shell', J. Engng. Mech. Div., ASCE, 94, EM6, pp 1273-1293 (1968).

59. WORSAK, K.N. 'A Simple and Efficient Finite Element for Shell Analysis', Int. J. Num. Meth. Eng., Vol. 14, pp 179-200, 1978.

60. ZIENKIEWICZ, O.C. and HINTON, E. 'Reduced Integration Function Smoothing and Non-Conformity in Finite Element Analysis', J. Franklyn Inst. 302, 443-461 (1976)

61. IRONS, B.M. The Semiloof Shell Element. Chapter 11, 'Finite Elements for Thin Shells and Curved Membranes', Ashwell and R.H. Gallagher, John Wiley, 1976.

62. IRONS, B.M. and AHMAD, S. 'Techniques of Finite Elements', Ellis Horwood, 1980.

63. WEAVER, W. 'Computer Program for Structural Analysis, Van Norstrant, 1967.

64. FOX, R.L. and STANTON, E.L. 'Developments in Structural Analysis by Direct Energy Minimization', AIAAJ Vol. 6, pp 1036-1042, 1968.

65. FRIED, I. 'More on Gradient Iterative Methods in Finite-Element Analysis', AIAAJ, Vol. 7, pp 505-567, 1969.

66. FRIED, I. 'A Gradient Computational Procedure for the Solution of Large Problems Arising from the Finite Element Discretization Method', Int. J. Num. Meth. Eng., Vol.2, pp 477-494, 1970.

67. MEYER, C. 'Solution of Linear Equations, State-of-the-Art, ASCE J. of Struc. Div., Vol. 99, pp 1507-1526, 1973.

68. MELOSH, R.J. and BAMFORD, R.M. 'Efficient Solution of Load Deflection Equations', ASCE J. of Struc. Div., Vol. 95, pp 661-676, 1969.

69. IRONS, B.M. and KAN, D.K.Y. 'Equation-Solving Algorithms for the Finite-Element Method', Numerical and Computer Methods in Structural Mechanics editors Fenves, S.J. et al, Academic Press, 1973.

70. RAO, S.S. 'The Finite Element Method in Engineering', Pergamon Press, 1982.

71. AKHRAS, G. and DHATTO, G. 'An Automatic Node Relabelling Scheme for Minimising a Matrix or Network Bandwidth', Int. J. Num. Meth. Eng., Vol. 10, pp 787-797, 1976.

72. IRONS, B.M. 'A Frontal Solution Program for Finite Element Method', Int. J. Num. Meth. Eng., Vol.2, pp 5-32, 1970.

73. HINTON, E. and OWEN, D.R. 'Finite Element Programming', Academic Press, 1977.

74. BARLOW, J. 'Optimal Stress Locations in Finite Element Models', Int. J. Num. Meth. Eng., Vol. 10, pp 243-251, 1976.

75. HINTON, E. and CAMPBELL, J. 'Local and Global Smoothening of Discontinuous Finite Element Functions Using a Least Square Method', Int. J. Num. Meth. Eng., Vol. 8, pp 461-480, 1974.

76. ZIENKIEWICZ, O.C. and SCOTT, F.C. 'On the Principle of Repeatability and its Application in Analysis of Turbine and Pump Impellers', Int. J. Num. Meth. Eng., Vol. 4, pp 445-448, 1972.

77. WILKINSON, J.H. 'The Algebraic Eigenvalue Problem, Oxford University, 1965.

78. BATHE, K. and WILSON, E.L. 'Solution Methods for Eigenvalue Problems in Structural Mechanics', Int. J. Num. Meth. Eng., Vol. 6, pp 213-226, 1973.

79. BATHE, K and WILSON, E.L. 'Numerical Methods in Finite Element Analysis', Prentice-Hall, Inc., Englewood Cliffs, New Jersey, 1976.

80. CLINT, M. and JENNINGS, A. 'The Evaluation of Eigenvalues by Simultaneous Iterations', Computer Journal, Vol. 13, pp 76-80, 1970.

81 JENNINGS, A. and ORR, D.R. 'Application of the Simultaneous Iteration Method to Undamped Vibration Problems', Int. J. Num. Meth. Eng., Vol. 3, pp 13-24, 1971.

82. DOWNS, B. 'Direct Iteration of Ascending Natural Frequencies of Vibration Without Inversion of the Stiffness Matrix', Int. J. Num. Meth. Eng., Vol. 7, pp 554-556, 1973.

83. CORR, R.B. and JENNINGS, A. — 'A Simultaneous Iteration Algorithm for Symmetric Eigenvalue Problem', Int. J. Num. Meth. Eng., Vol. 10, pp 647-663, 1976.

84. ANDERSON, R.G. — "A Finite Element Eigenvalue Solution System', Ph.D. Thesis, University of Wales, 1968.

85. BATHE, K. and WILSON, E.L. — 'Eigenvalue of Large Structural Systems with Small Bandwidth', Journal of the Engineering Mechanics Divisions, pp 467-479, 1973.

86. IRONS, B. — "Structural Eigenvalue Problems Elimination of Unwanted Variables', AIAA J. Vol. 3, pp 961-962, 1965.

87. JENNINGS, A. — 'Mass Condensation and Simultaneous Iteration for Vibration Problems', Int. J. Num. Meth. Eng., Vol. 6, pp 543-552, 1973.

88. WRIGHT, G.C. and MILES, G.A. — 'An Economical Method for Determining the Smallest Eigenvalues of Large Linear Systems', Int. J. Num. Meth. Eng., Vol. 3, pp 25-33, 1971.

89. SHAH, V.N. and RAYMUND, M. — 'Analytical Selection of Masters for the Reduced Eigenvalue Problem', Int. J. Num. Meth, Eng., Vol. 18, pp. 89-98, 1982.

90. KIDDER, R.L. — 'Reduction of Structural Frequency Equations', AIAAJ. Vol. 13, No. 5, pp 701-703, 1975.

91. GUYAN, R.J. — 'Reduction of Stiffness and Mass Matrices', AIAA J. Vol. 3, pp 380, 1965.

92. AZZAWI, M.M. — 'Steady and Vibratory Stresses in Centrifugal Impeller', M.Sc. Thesis, Cranfield Institute of Technology, SME, 1983.

93. ZIENKIEWICZ, O.C. and PHILLIPS, D.V. — 'An Automatic Mesh Generation Scheme for Plane and Curved Surfaces by Isoparametric Co-ordinates', Int. J. Num. Meth. Eng., Vol. 3, pp 519-528, 1971.

94. CADCENTER LTD. 'Gino-F User Guide', The General Purpose Graphics Package, Gino-F, 2.7R, CADCENTER LTD.

95. JONES, R. and WYKES, C. 'Holographic and Speckle Interferometry' Cambridge University Press, 1983.

96. LIZUKA, K. 'Engineering Optics', Springer Series in Optical Sciences, Vol. 35, 1985.

FIGURES AND TABLES

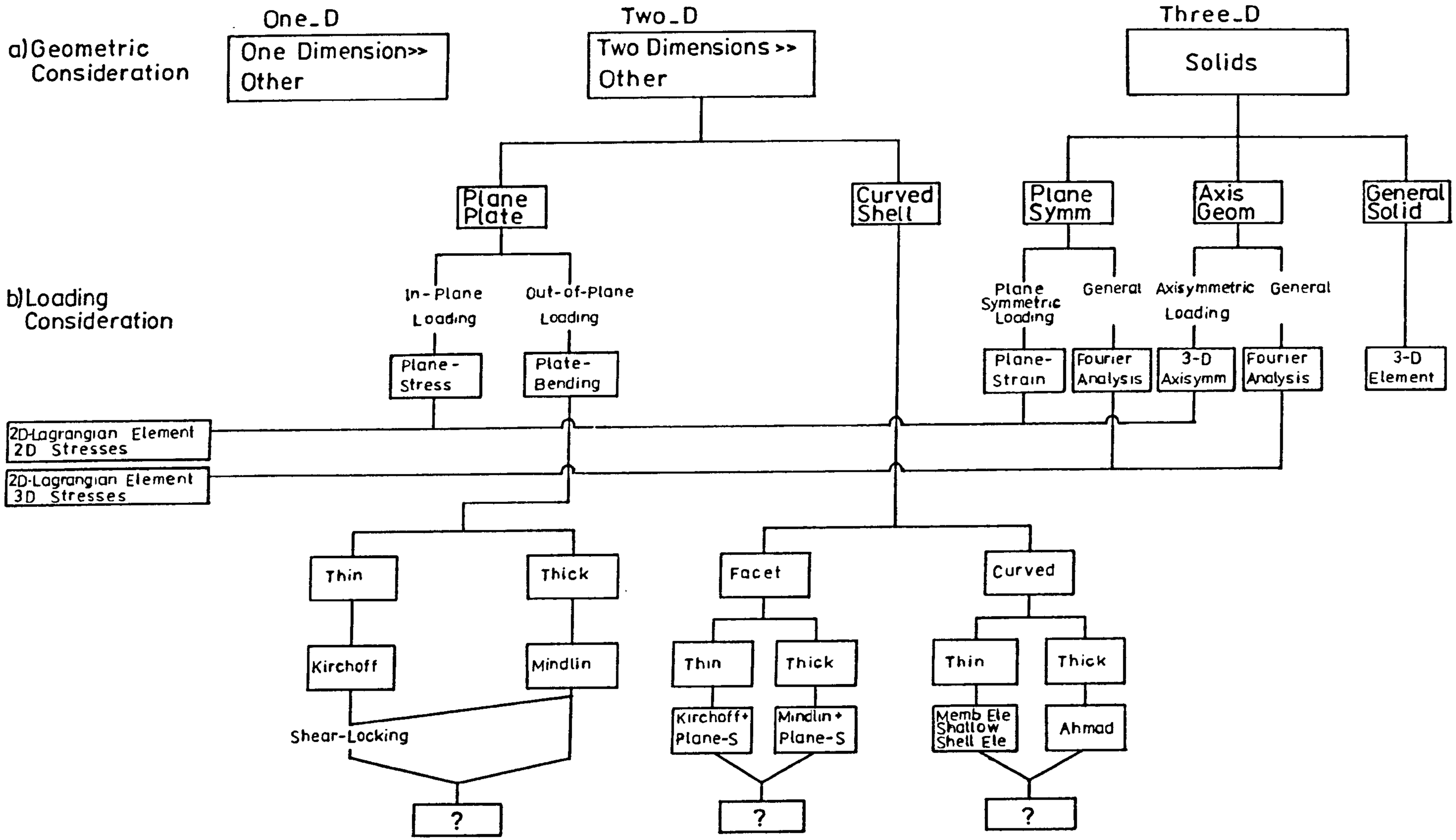

Figure. 2.1 Block Diagram for Element Selection

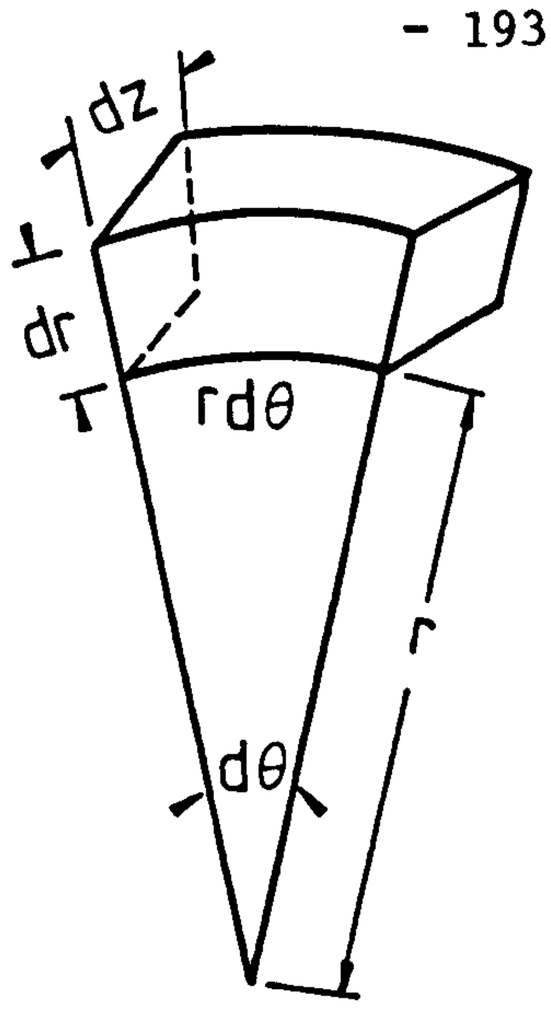

FIGURE 2.2. AN ELEMENT OF VOLUME dV

FIGURE 2.3 20 - NODE HEXAHEDRAL ELEMENT

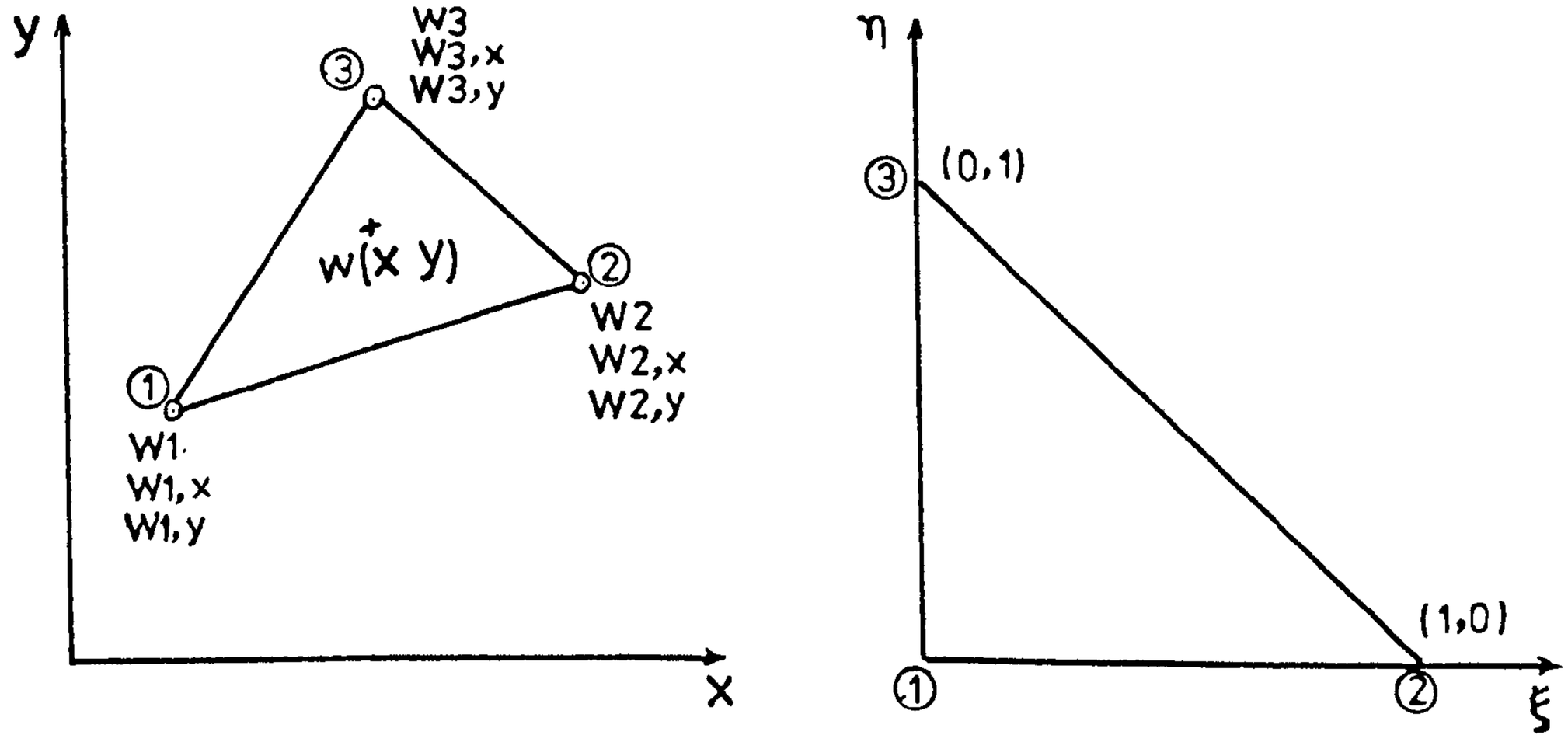

Figure 3.1 Intrinsic Element 3-Node Hermitian Triangular Element

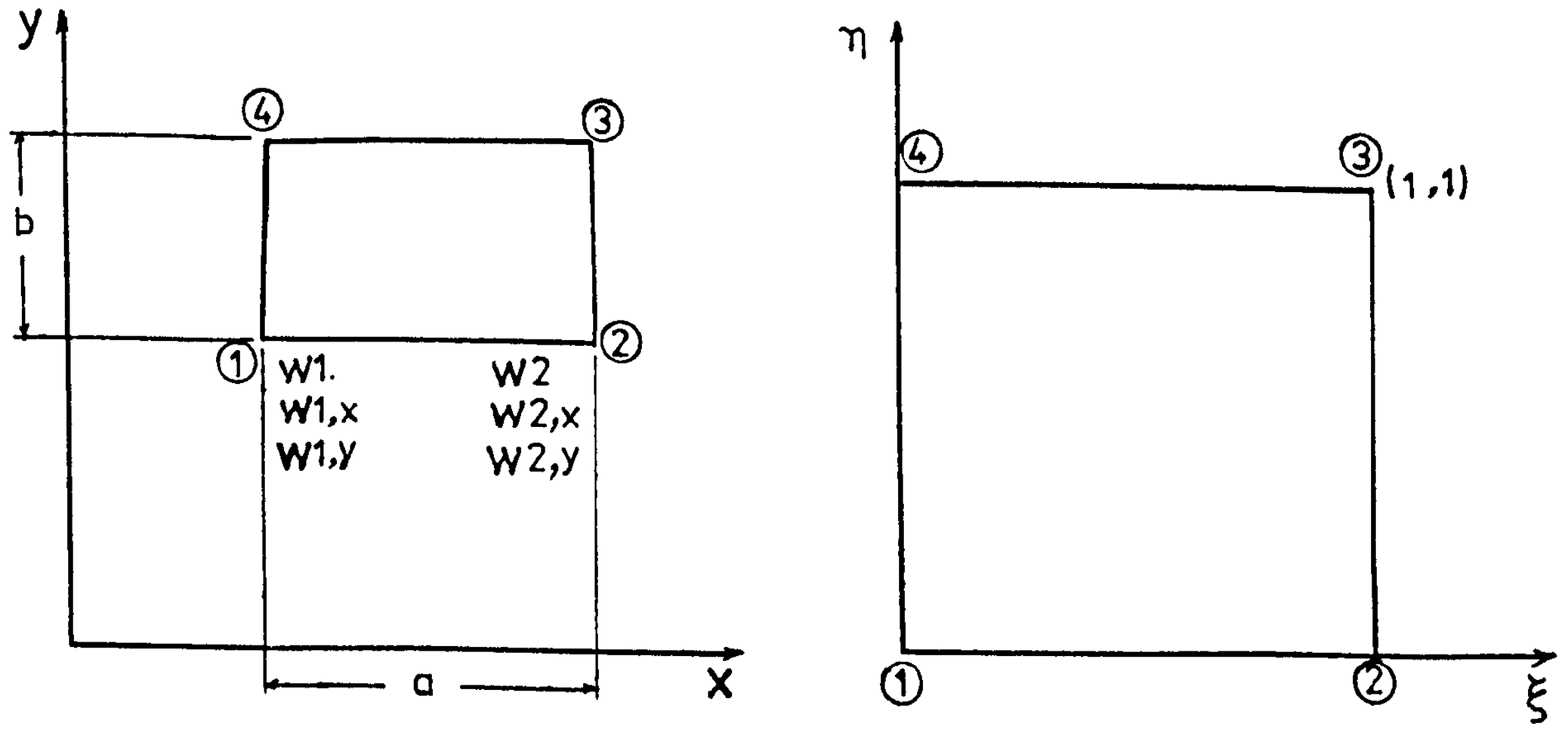

Figure 3.2 Four-Node Hermitian Rectangular Element

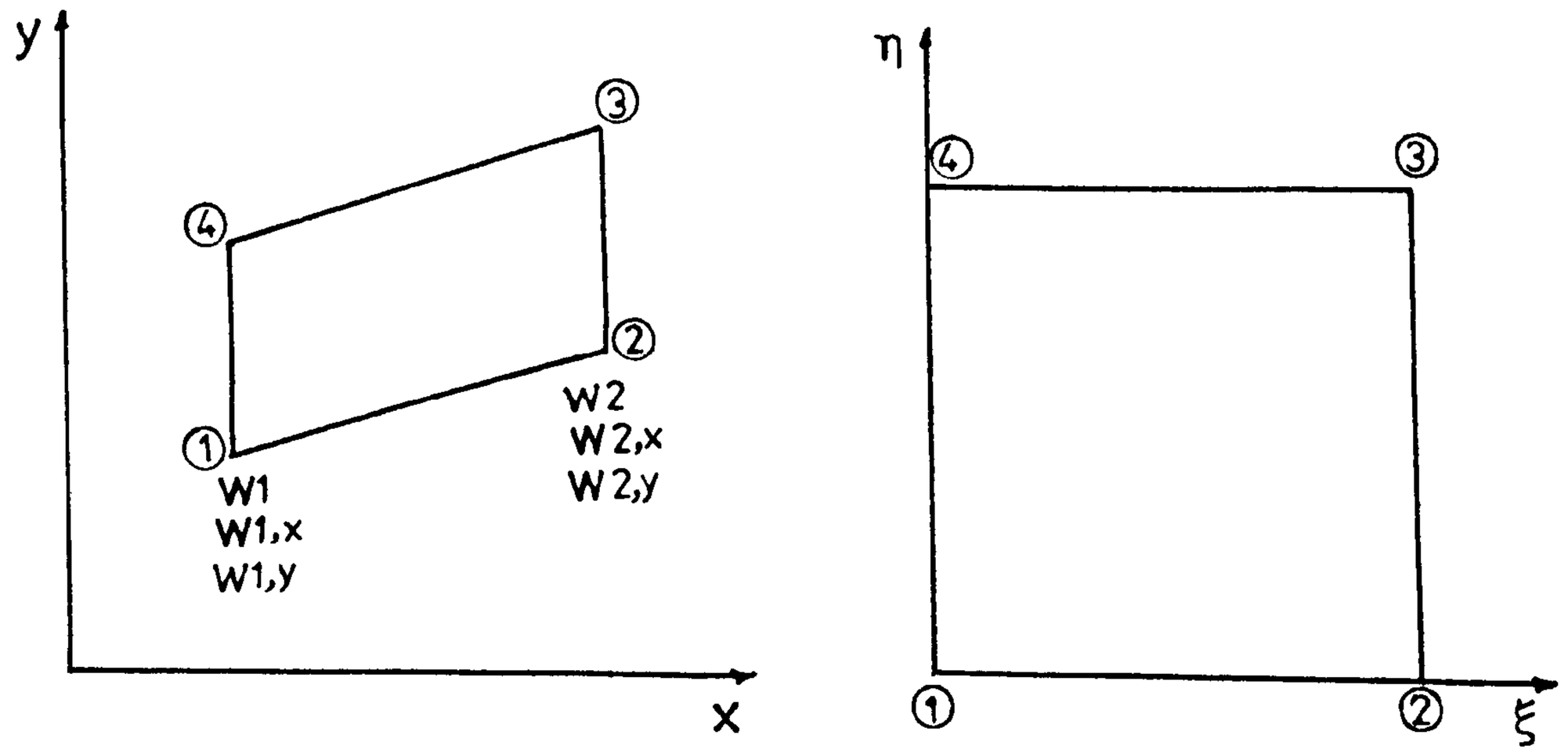

Figure 3.3 Four-Node Hermitian Parallelogramic Element

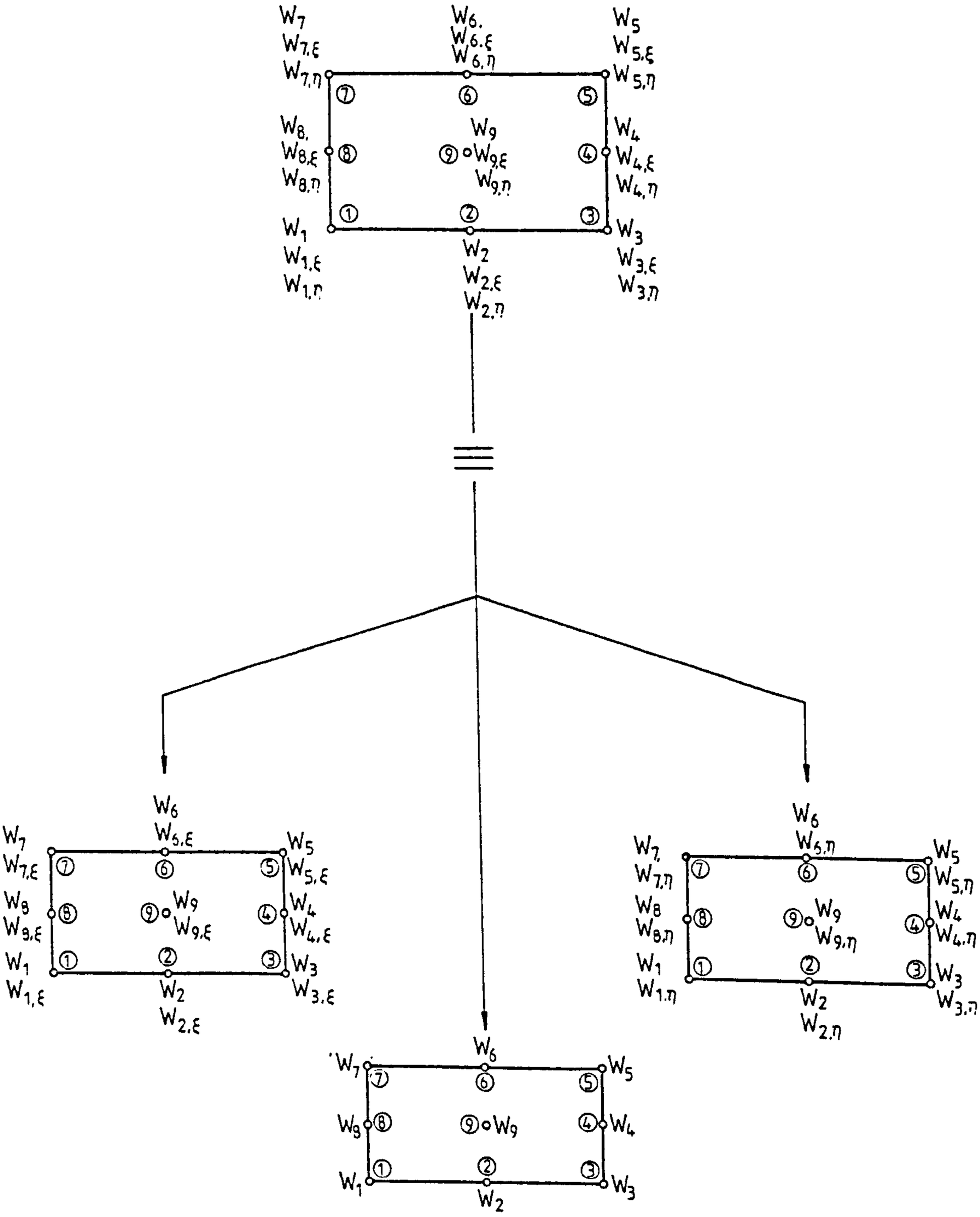

FIGURE 3·4 SUPERPOSITION PRINCIPLE FOR 9-NODE QUADRILATERAL ELEMENT.

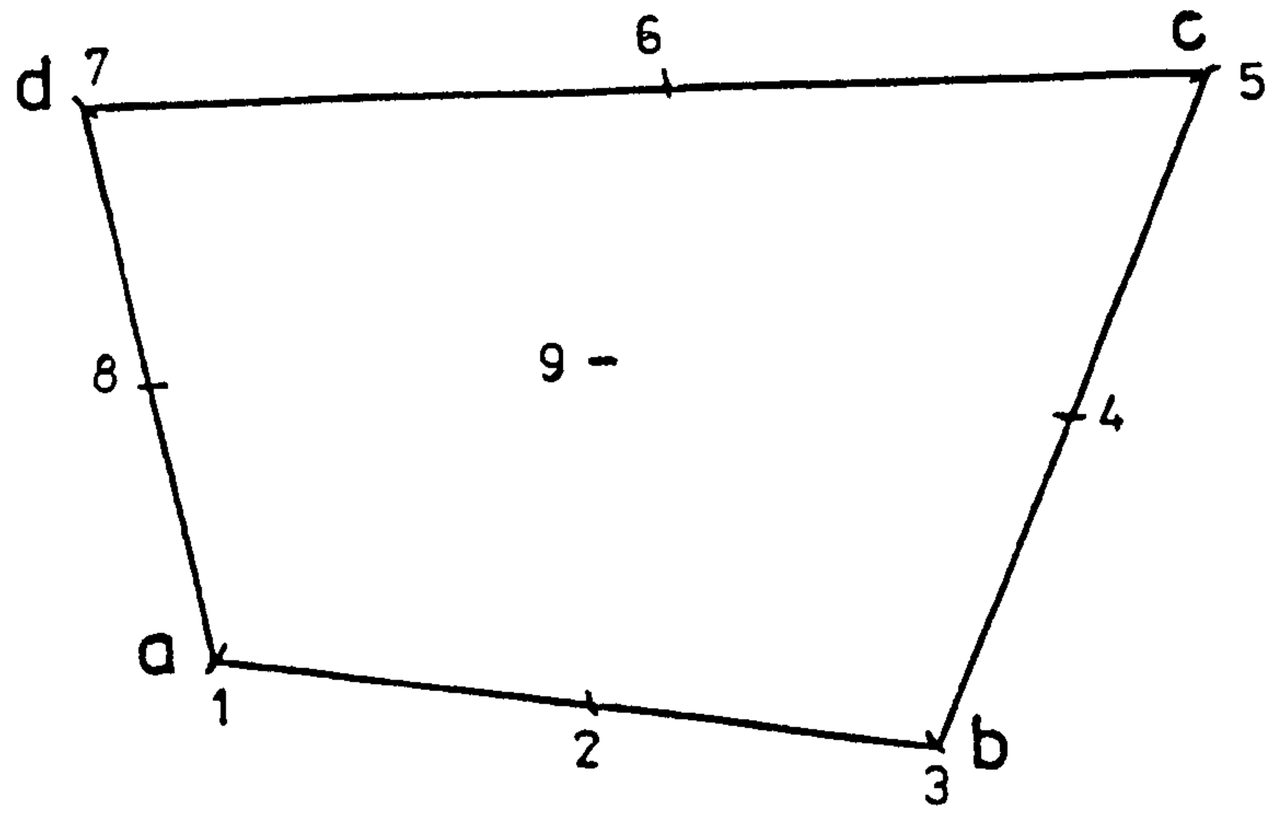

Figure 3.5 9-Node Subparametric Element

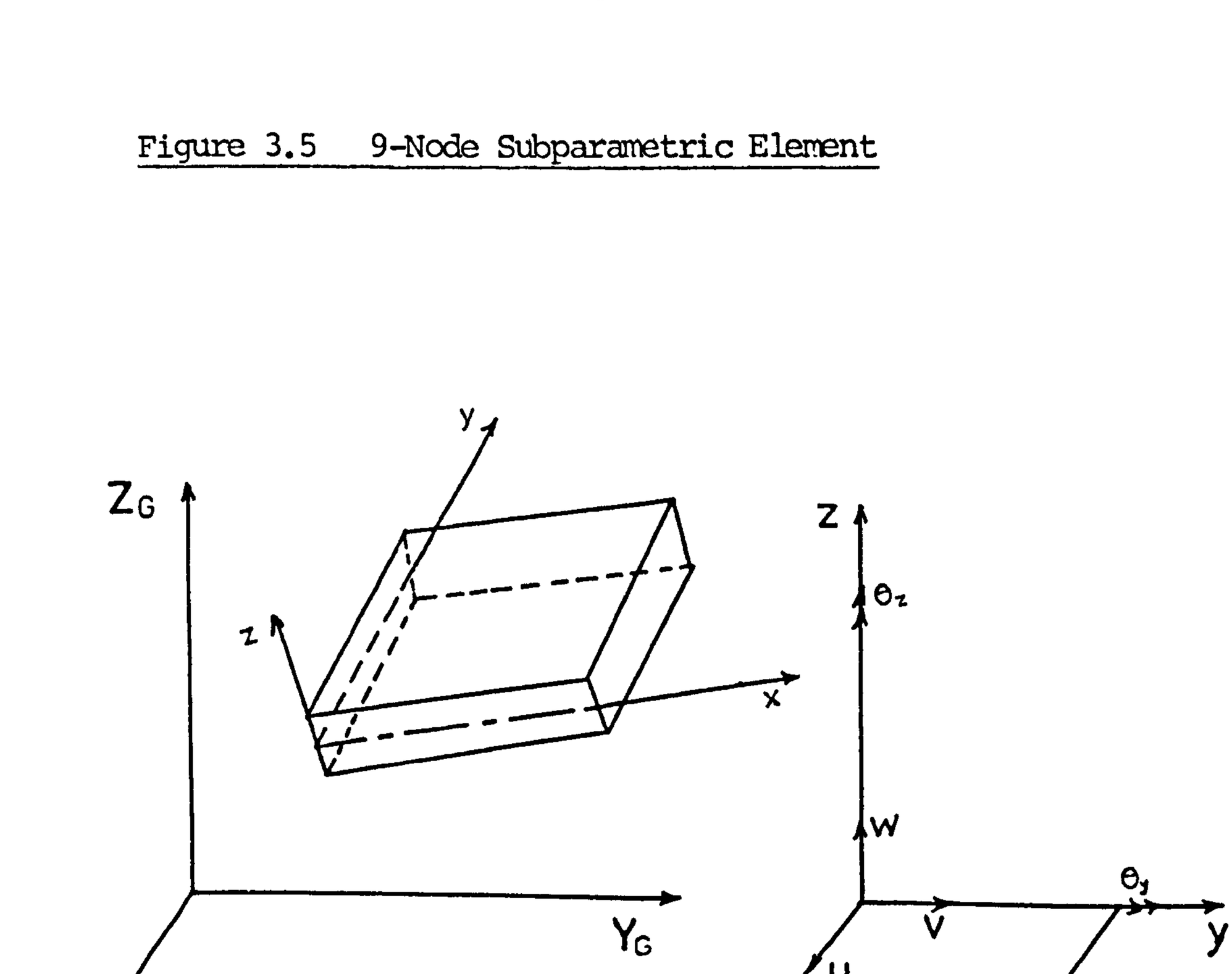

b - Local and Global System a - Displacement and Rotation Components

Figure 3.6 Facet Element Local and Global Parameters

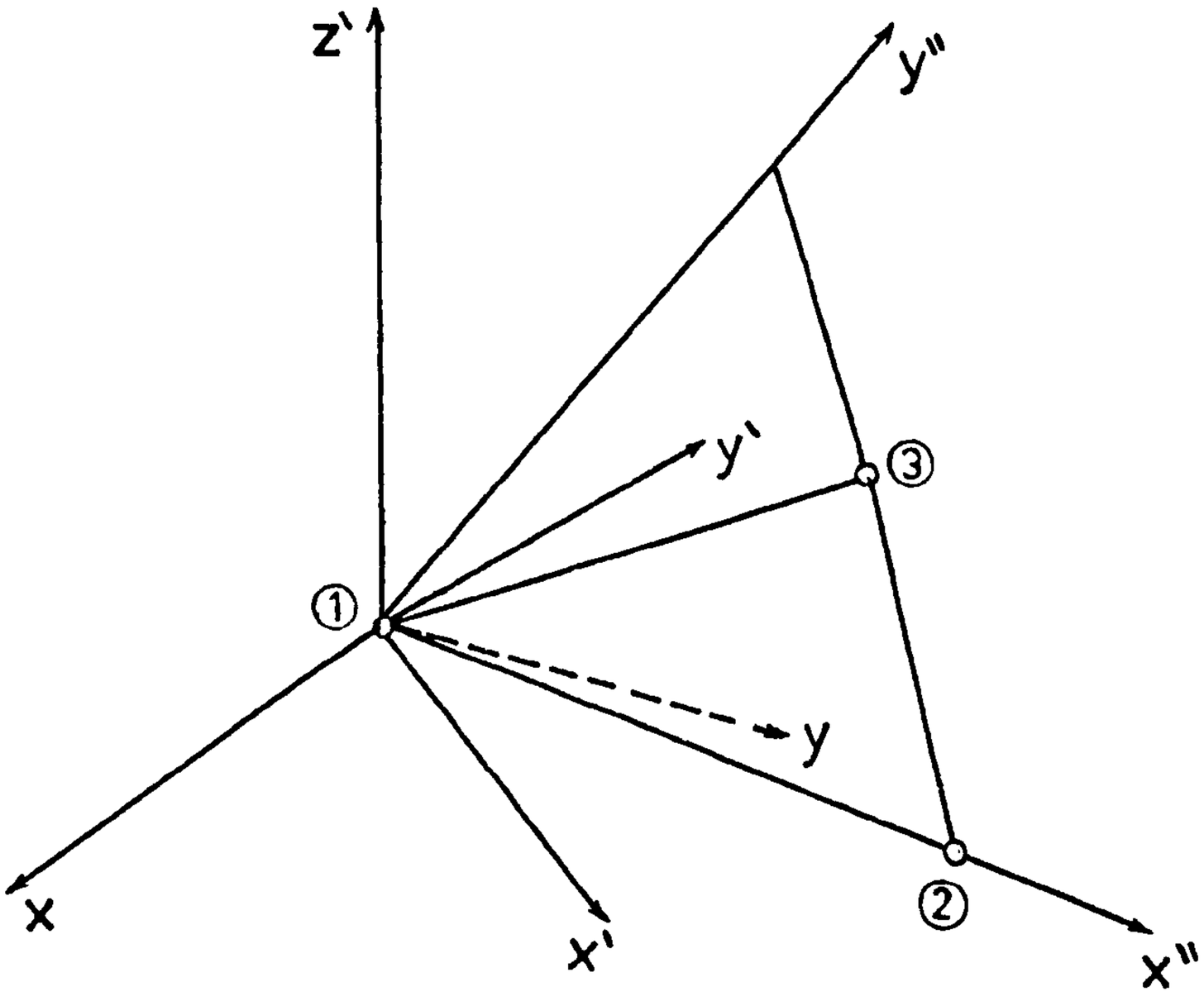

Figure 3.7 Global and Local Axes System

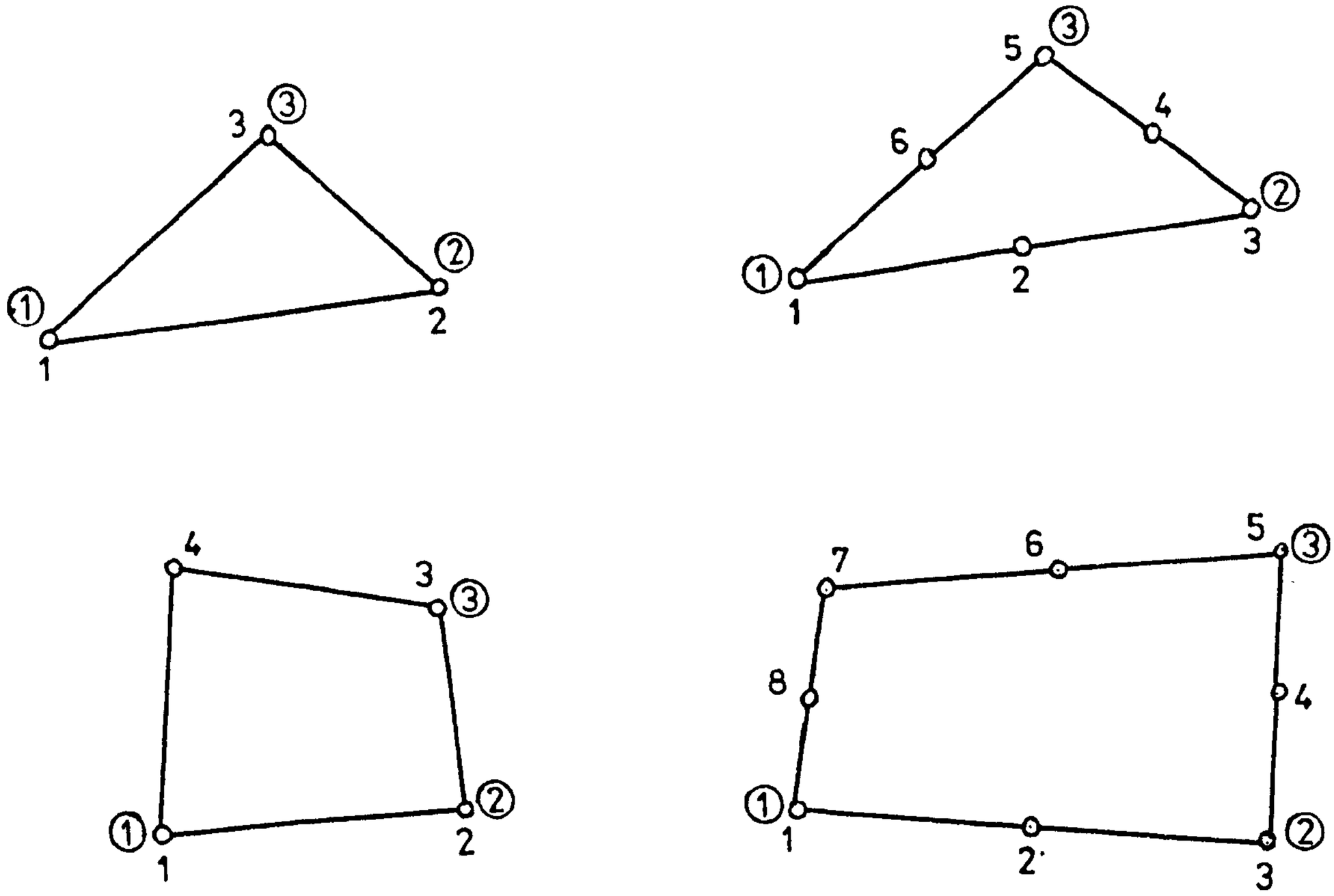

Figure 3.8 Different Types of 2-D Element

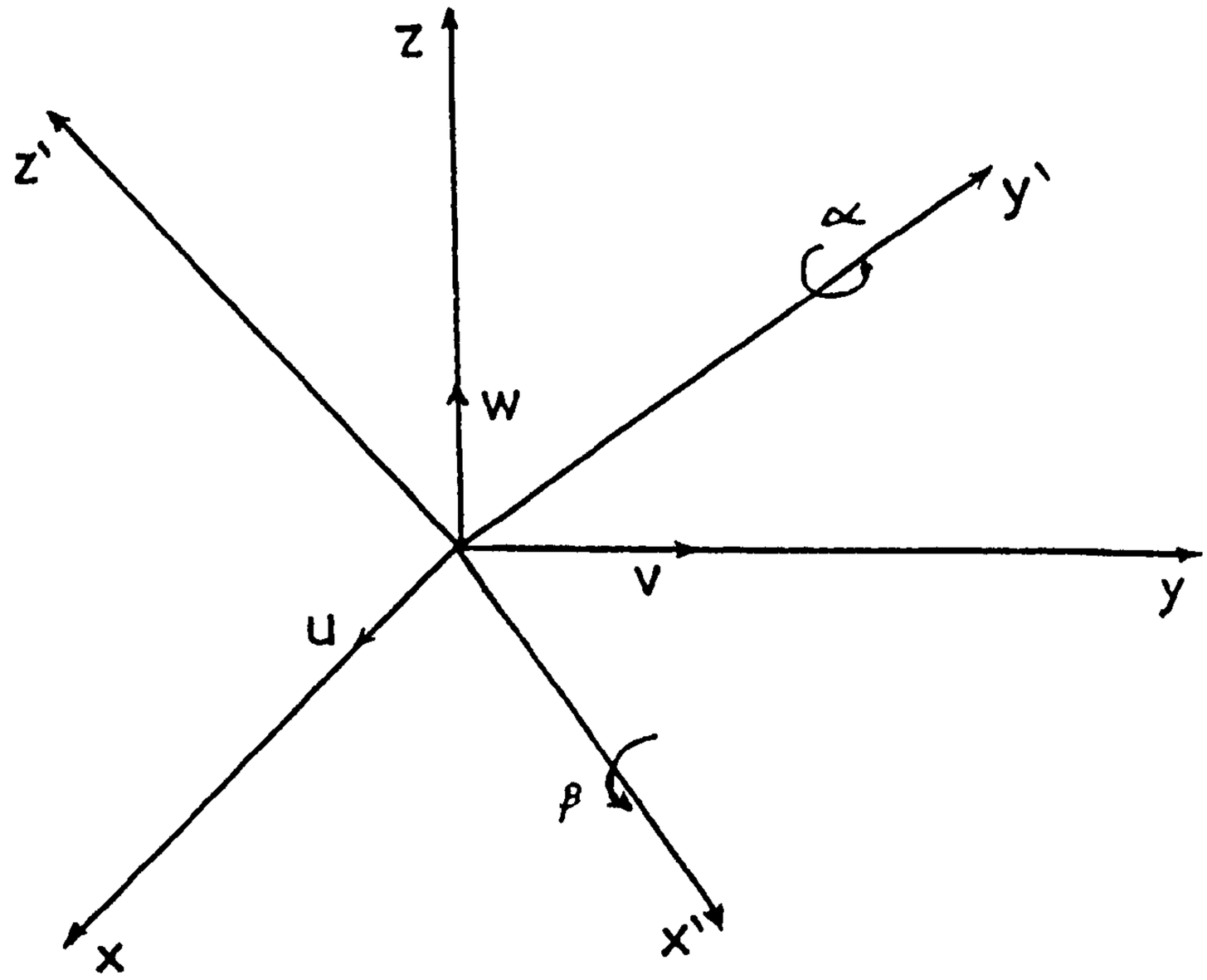

Figure 3.10 Local and Global Axis

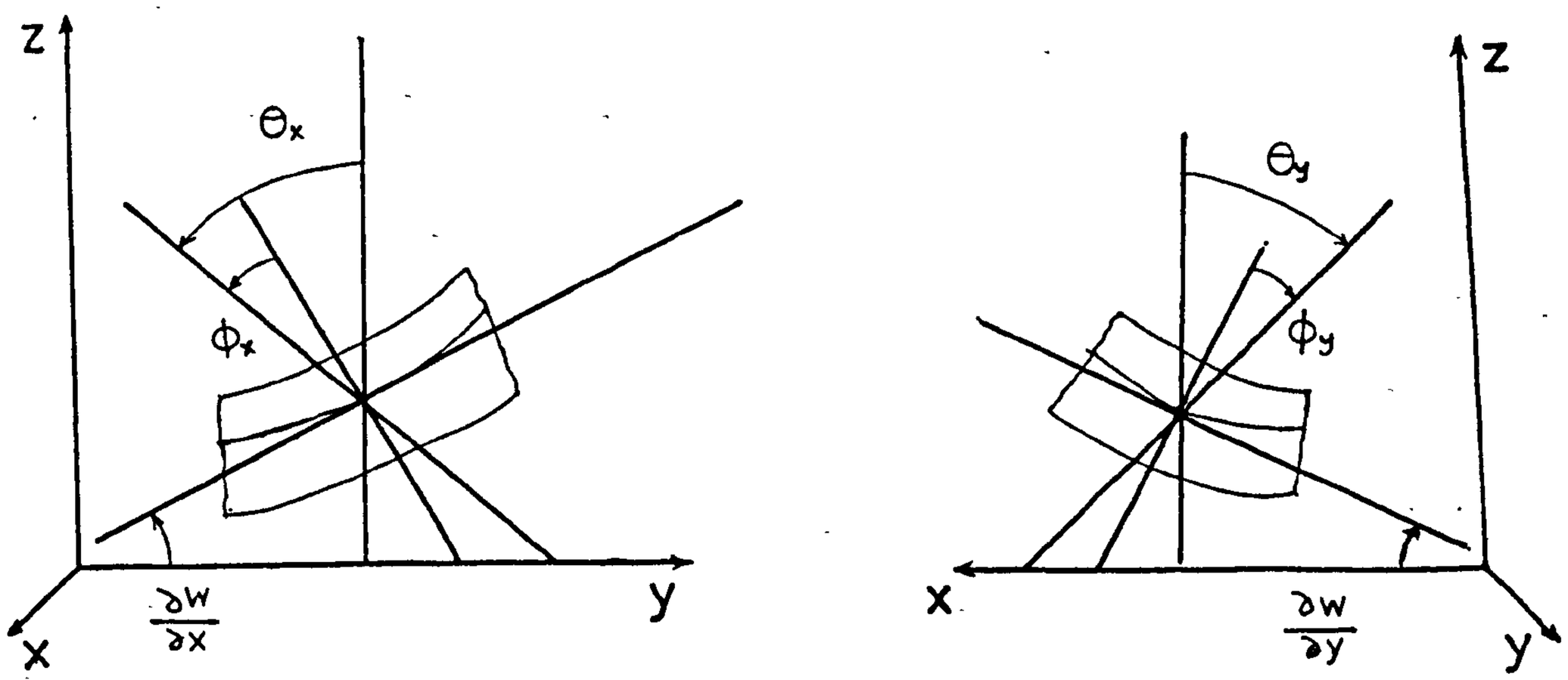

Figure 3.9 Shear Effect on Slope Angles

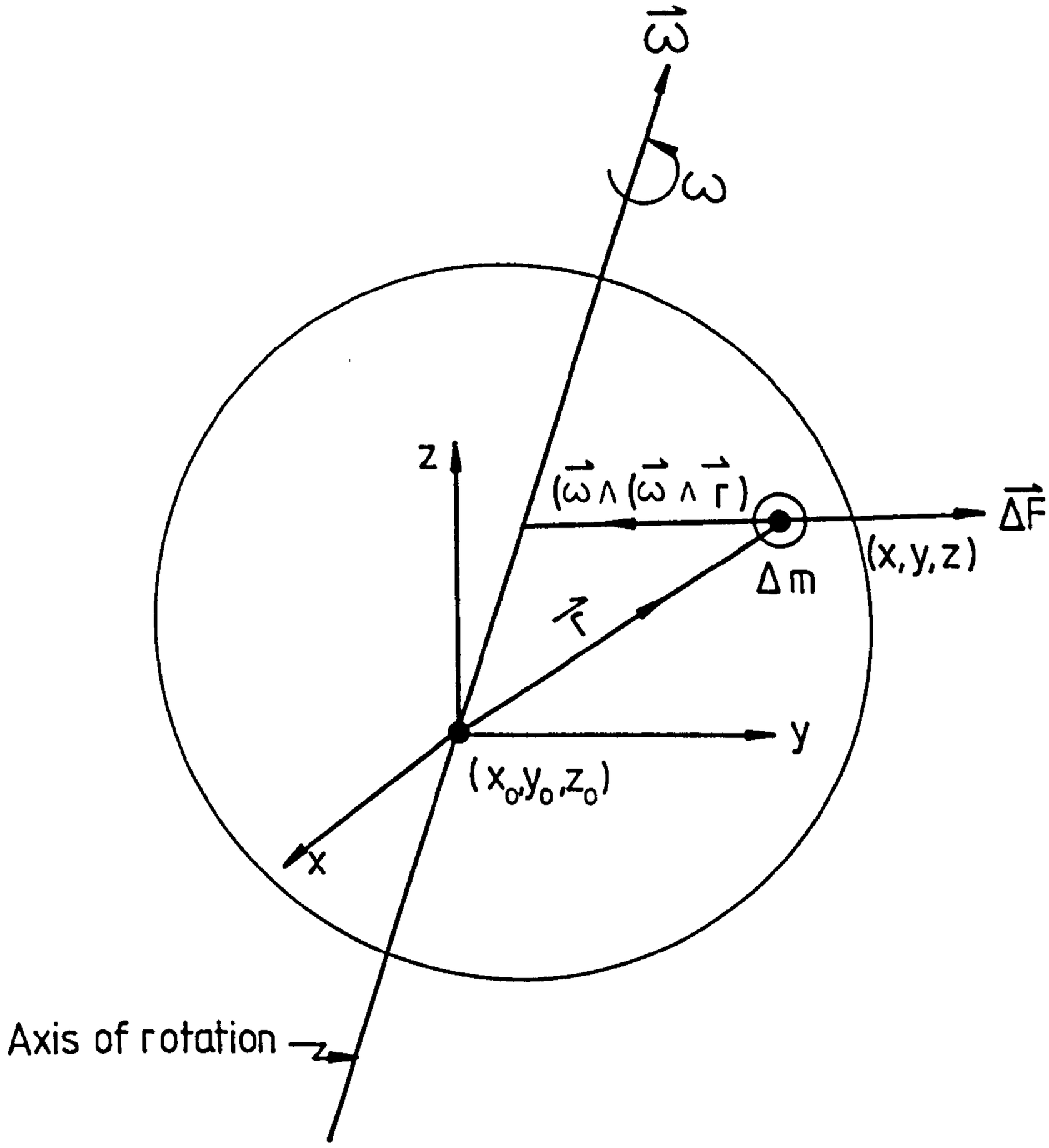

FIGURE 4·1 FORCE DUE TO ROTATIONAL INERTIA

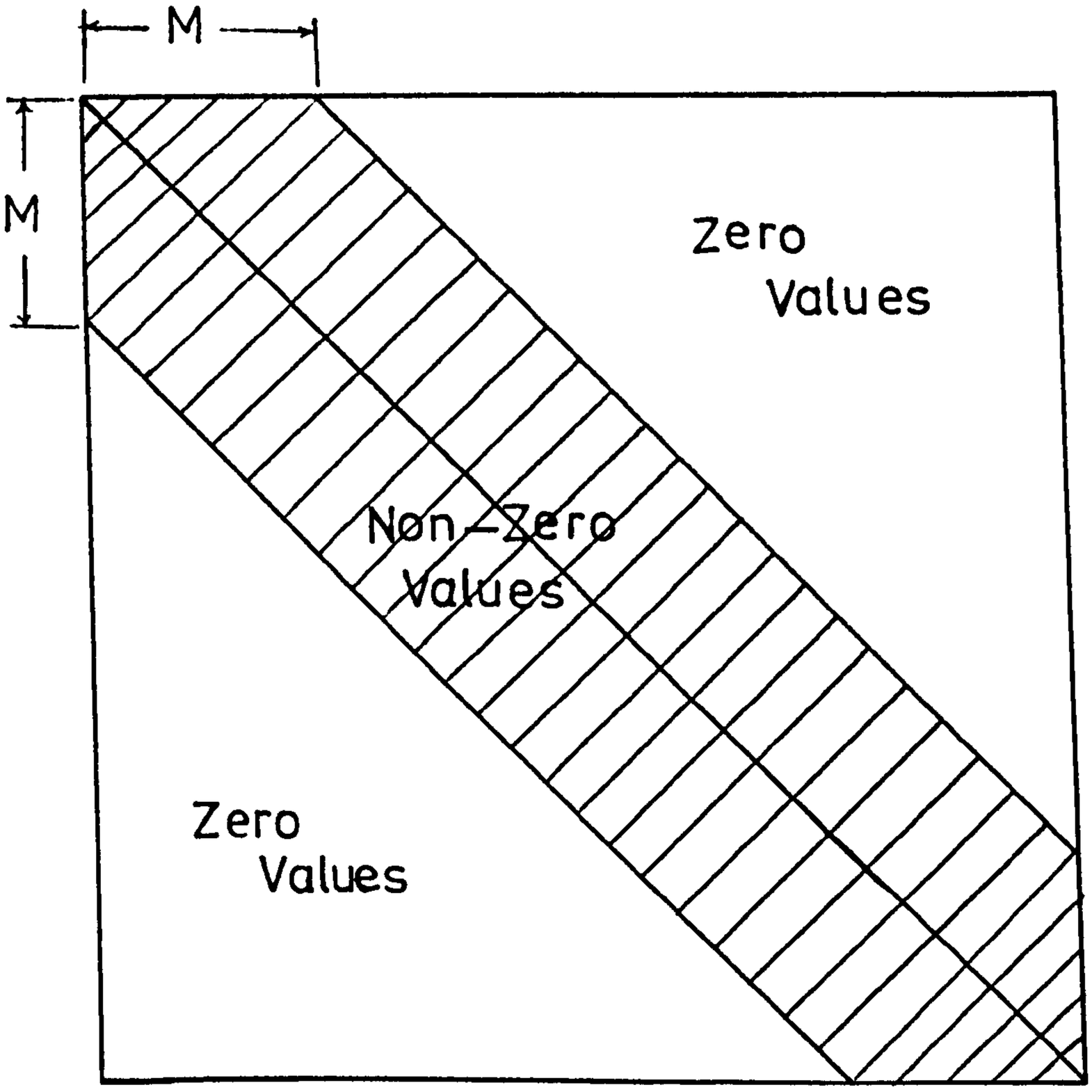

M = (D+1)* (Number of Degrees of Freedom per Node)

D : Maximum Difference Between any Two Node Numbers occurring in any Single Element in the Finite Element Mesh

Figure 4.2 A Banded Stiffness Matrix

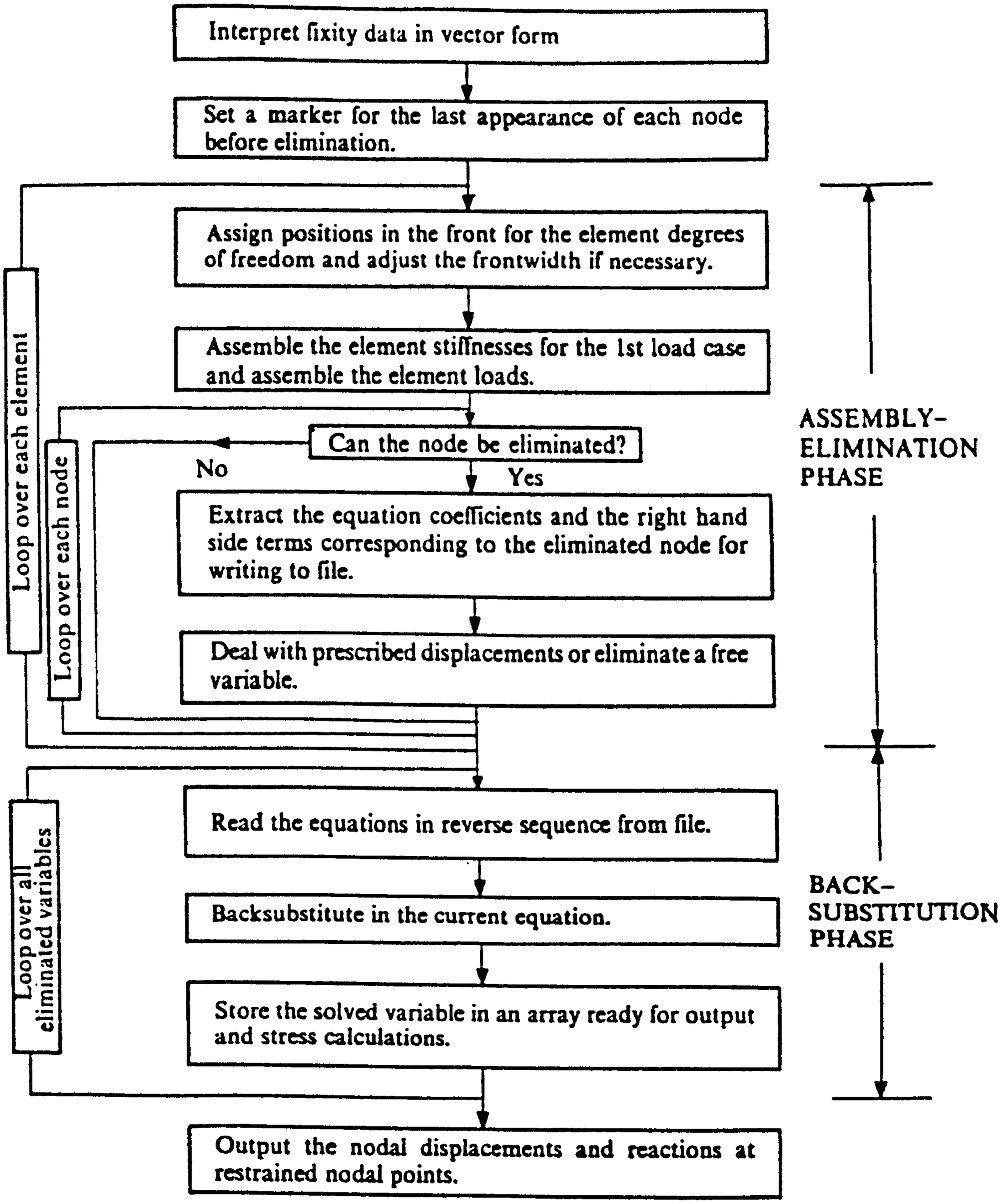

Figure 4.3 Operation sequence for frontal equation solution

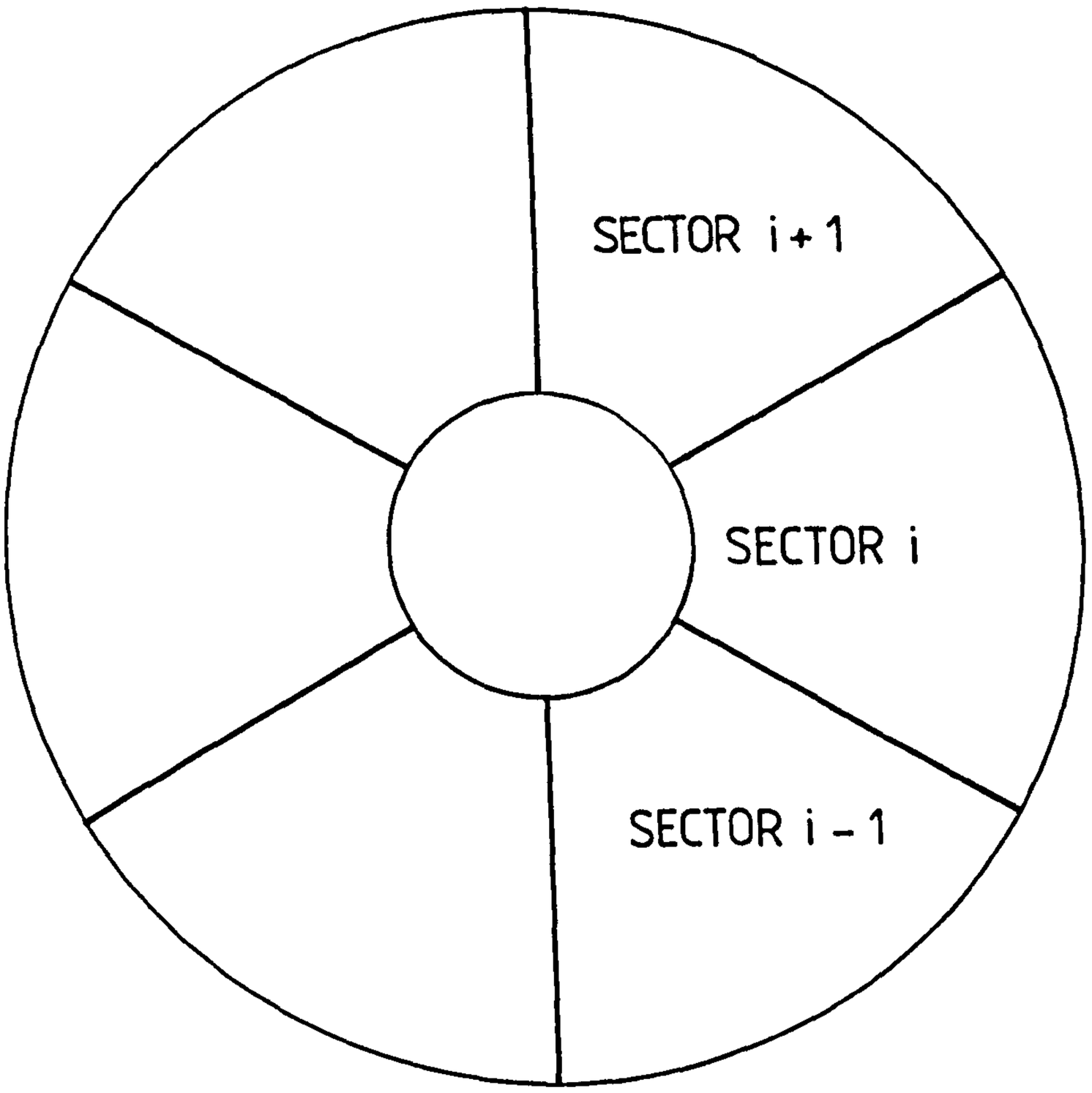

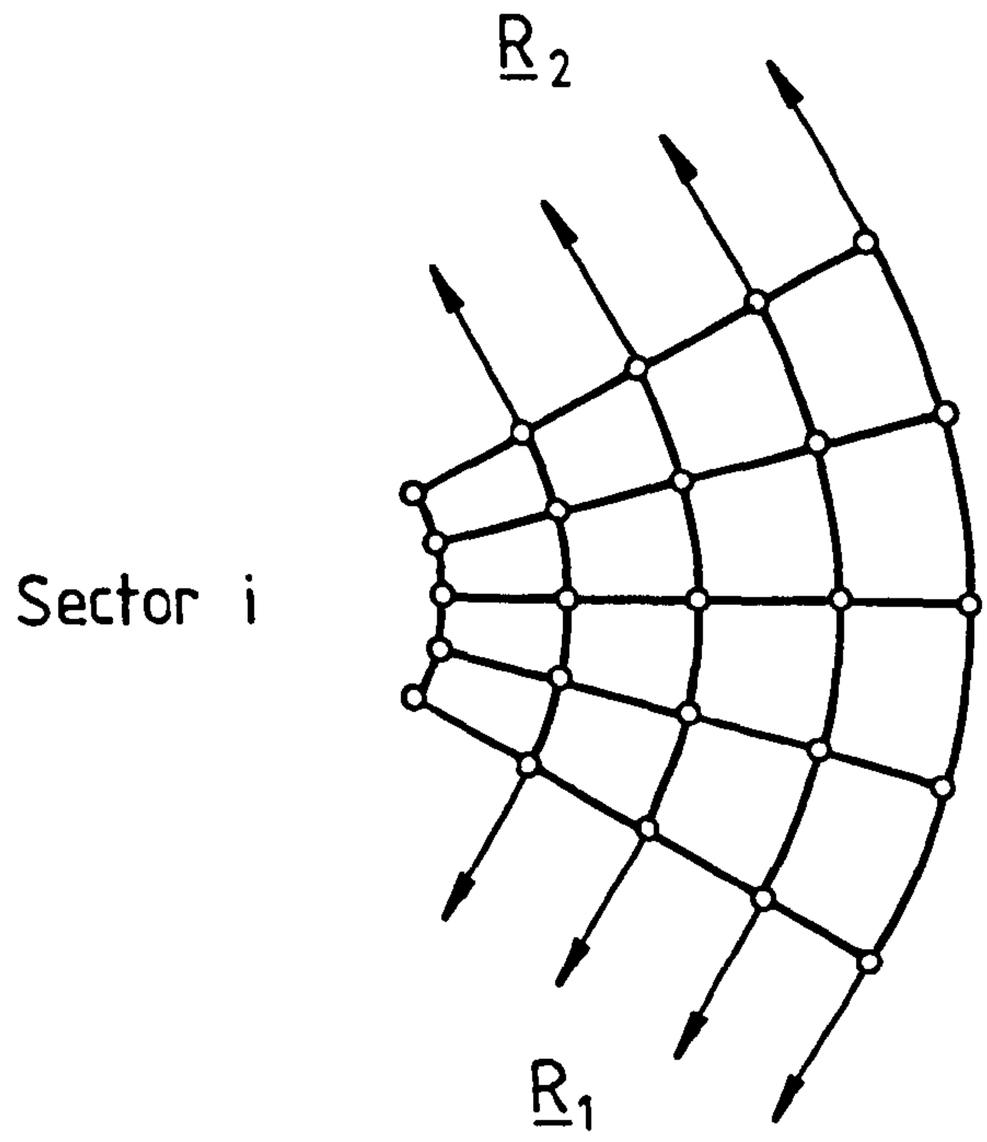

FIGURE 4·4 SECTORIALLY SYMMETRIC STRUCTURE

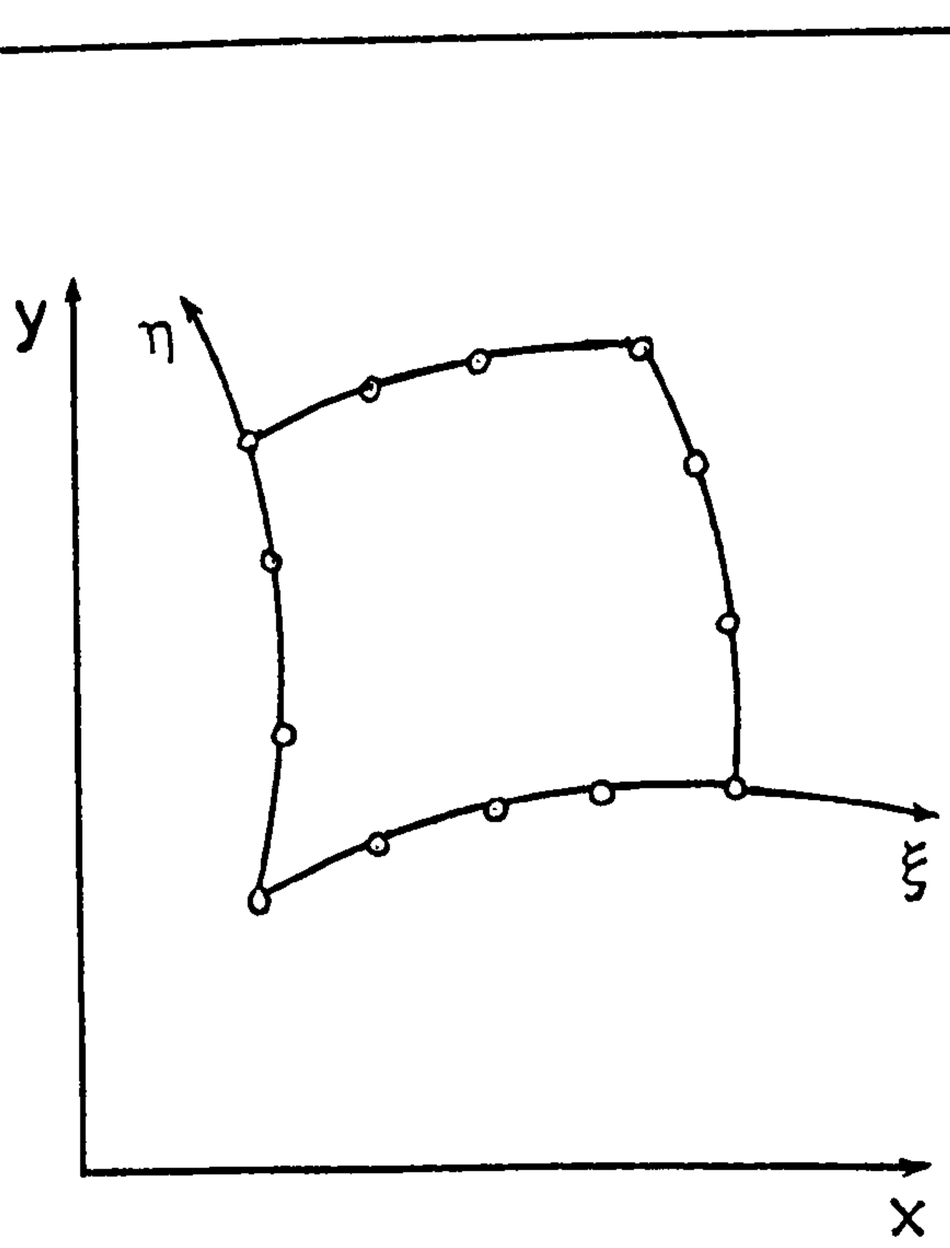

a - Quadrilateral Block in Cartesian Plane

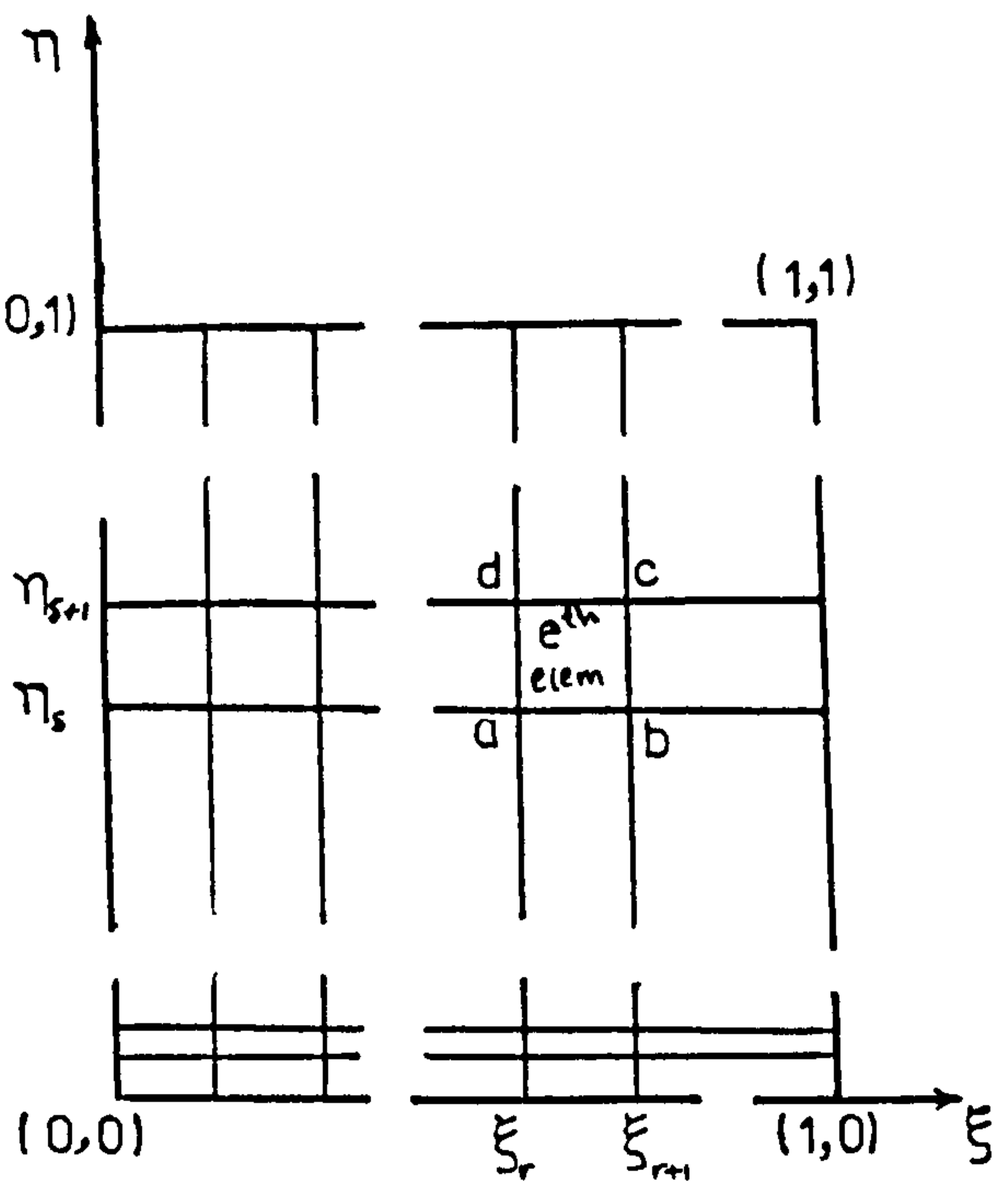

b - Divisions in ξ-η Plane

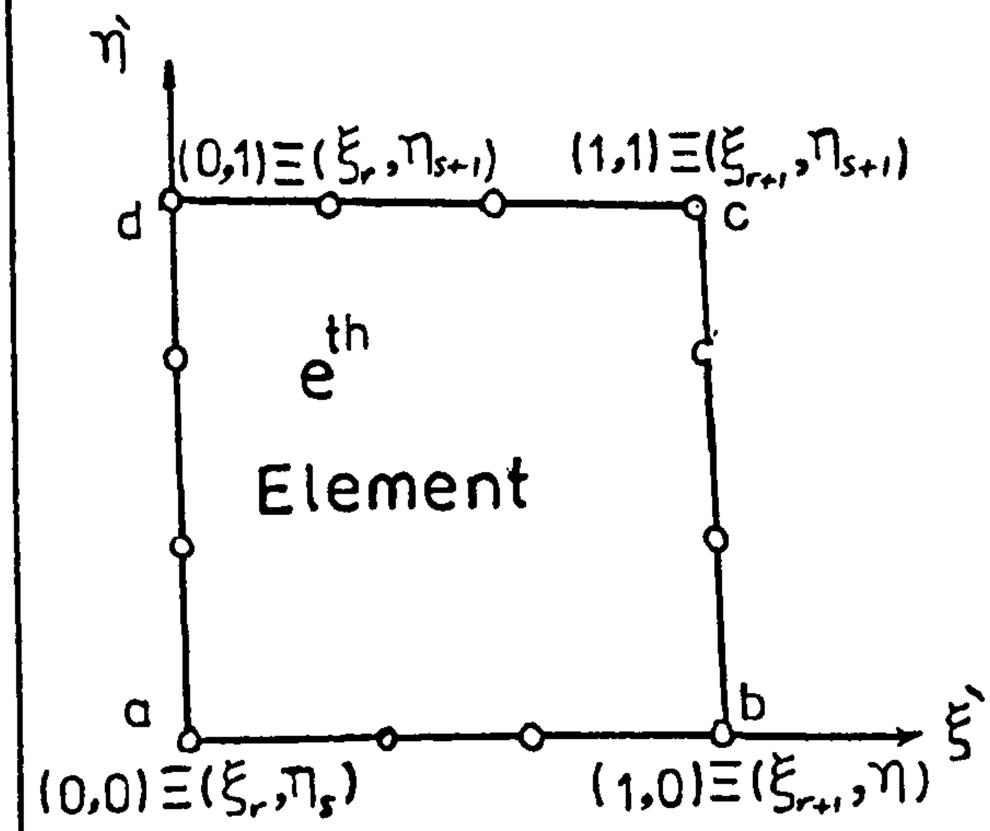

c - Element in its local ξ`-η` Plane

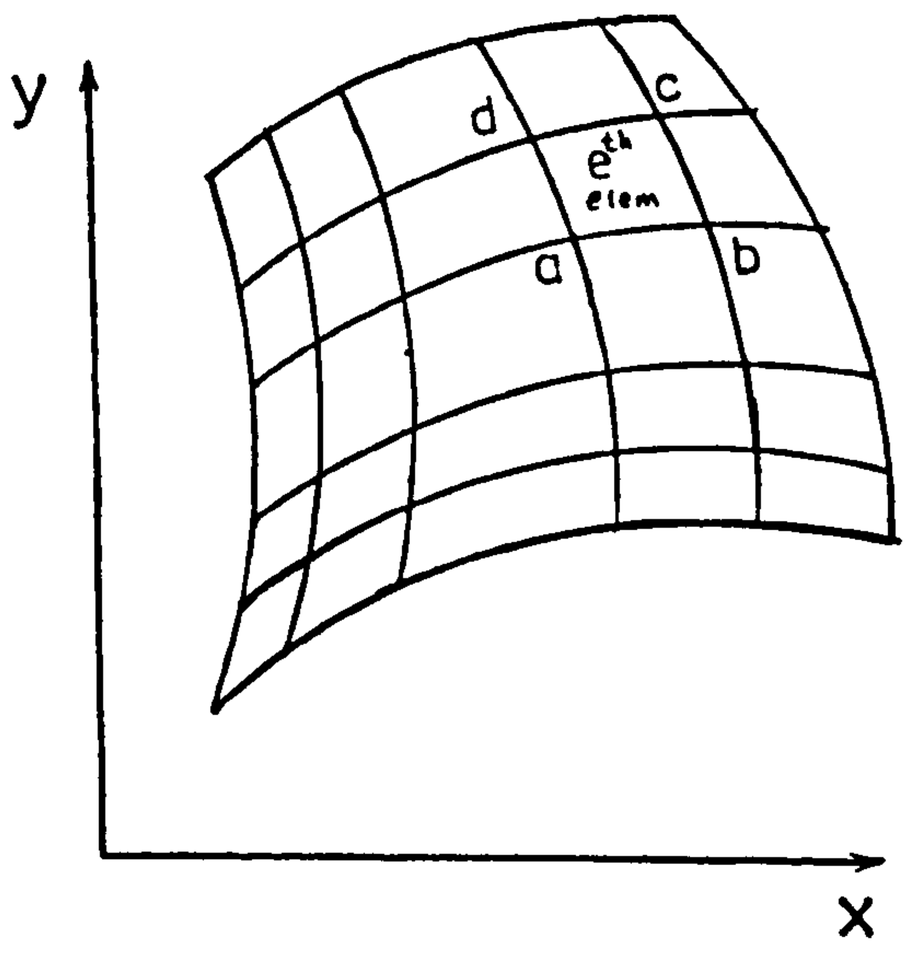

d - Block Transformed back to Cartesian Plane

Figure 6.1 Generation of Quadrilateral Elements in a Uniform Quadrilateral Block

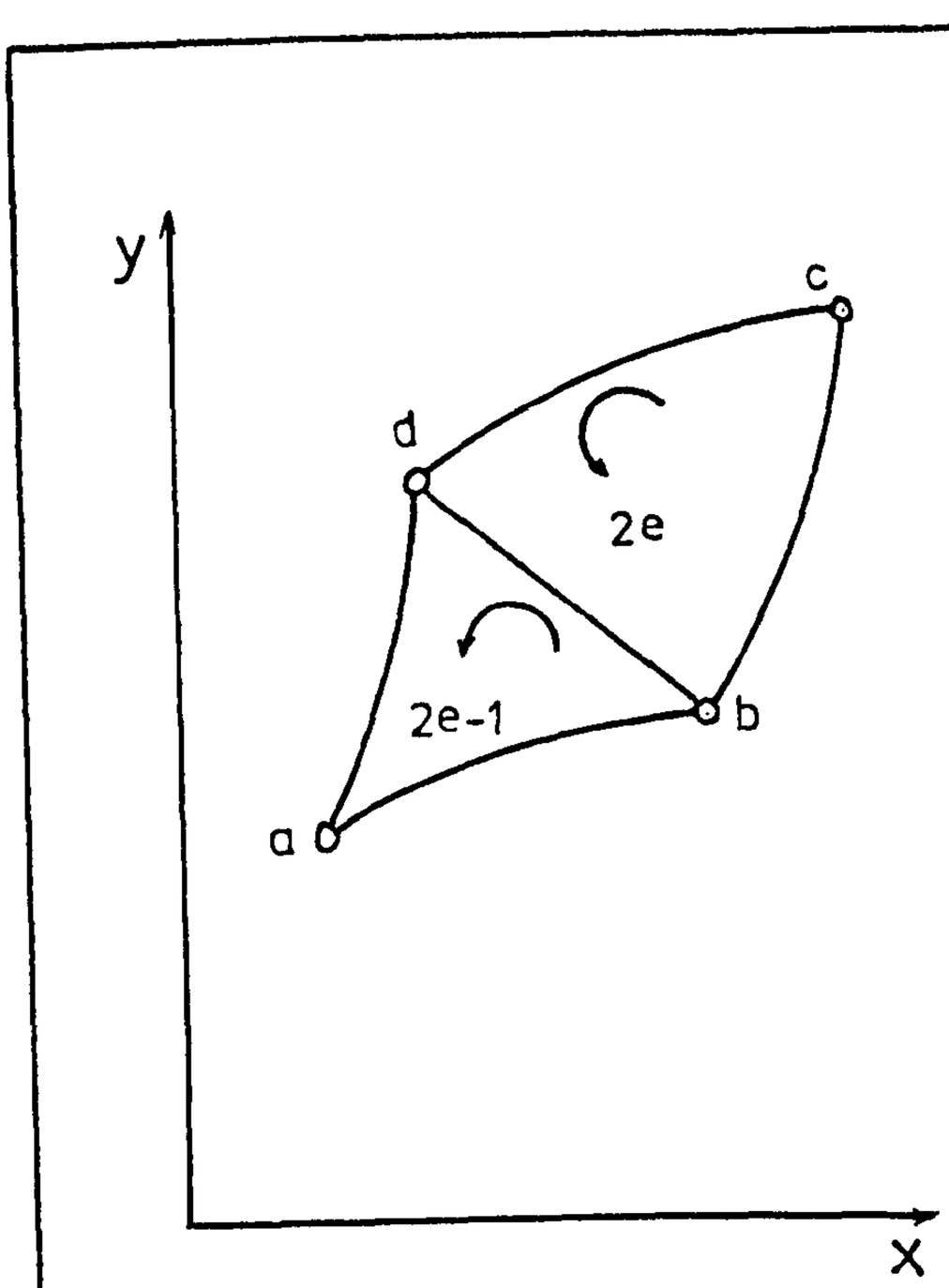

a - Case 1 of Triangulation

ac ⩾ bd

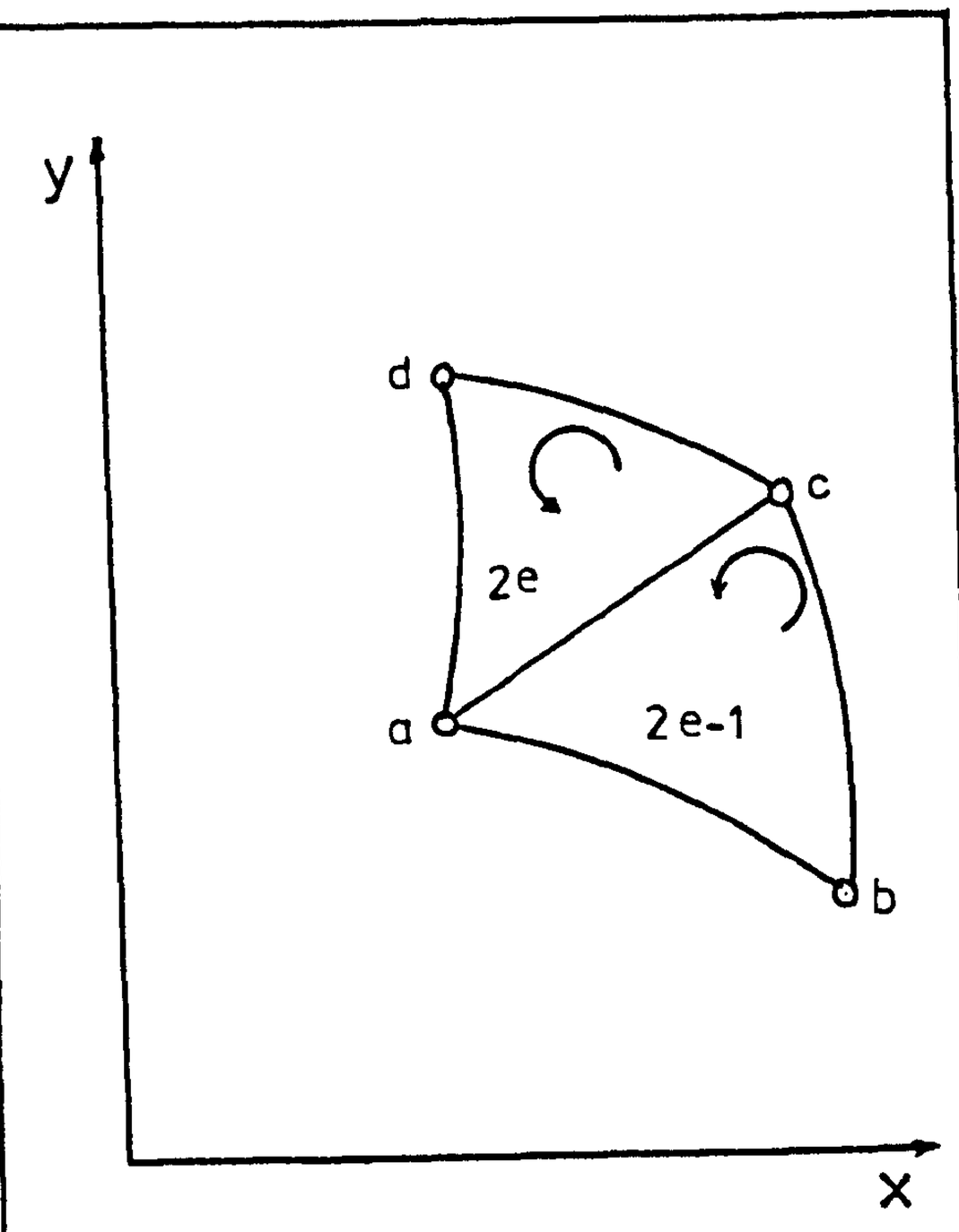

b - Case 2 of Triangulation

ac < bd

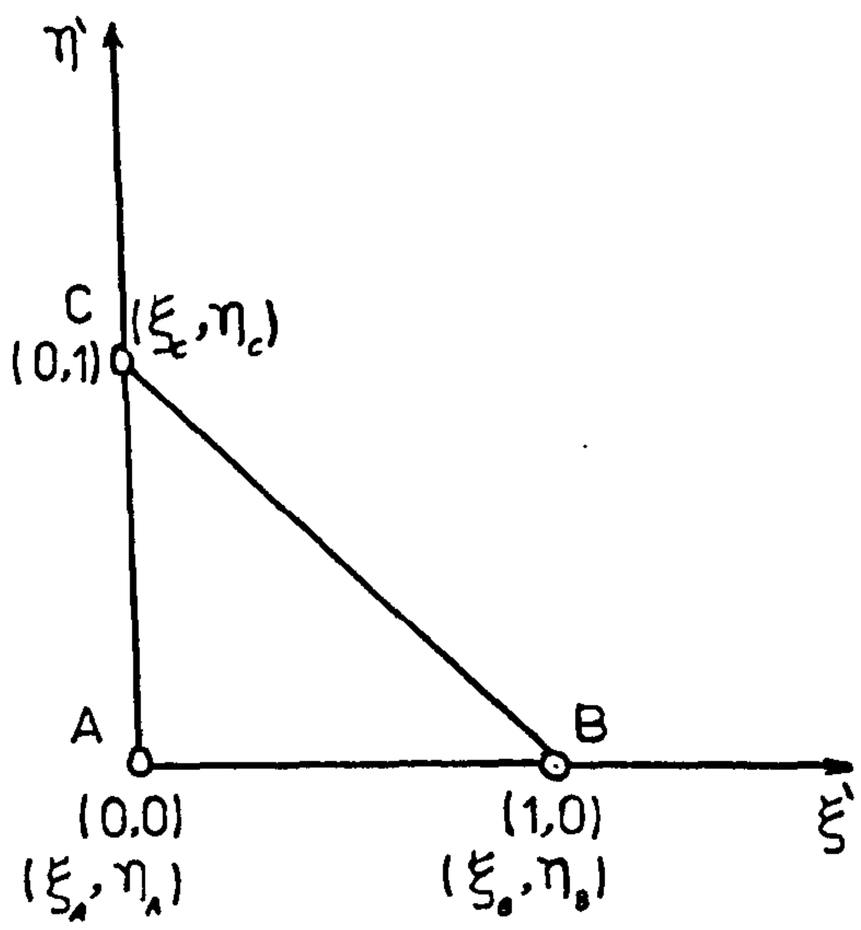

c - Element in its local

ξ'-η' system

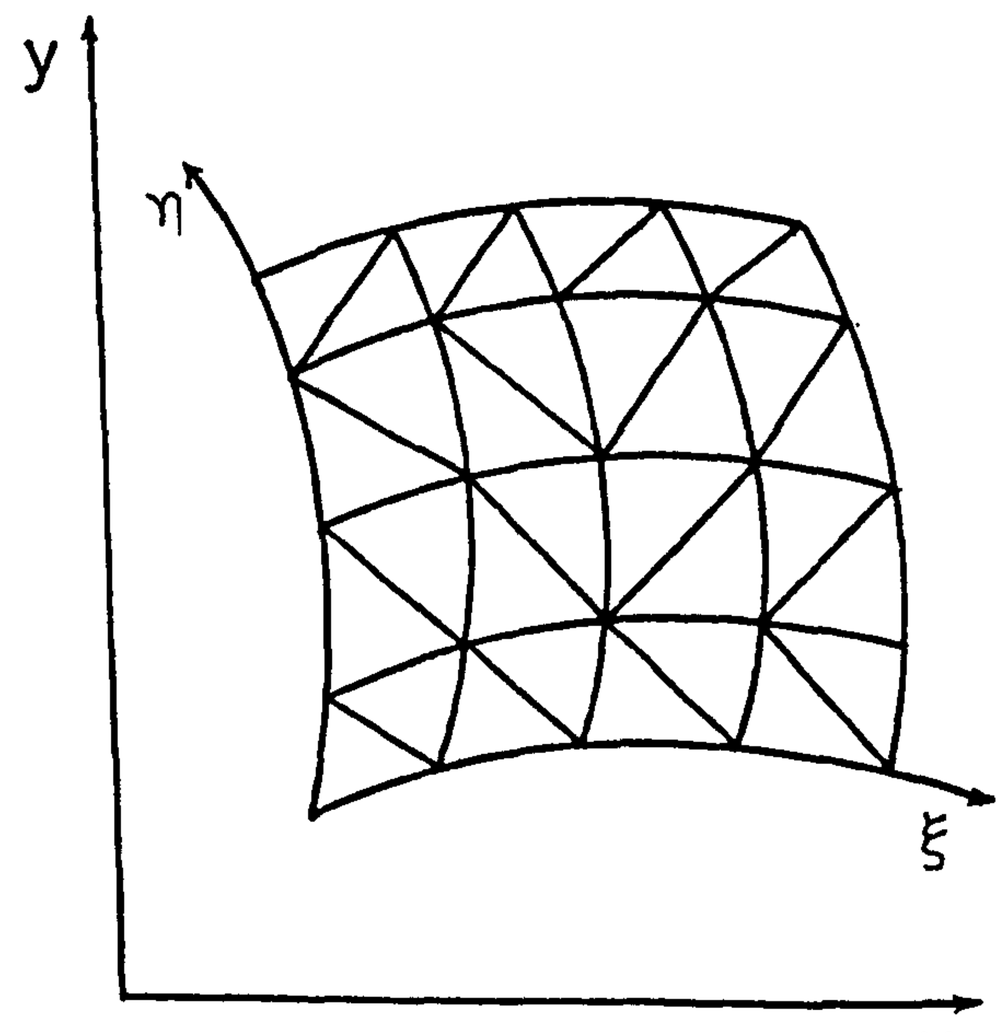

d - Block transformed back

to Cartesian plane

Figure 6.2 Generation of Triangular Elements in a Quadrilateral Block

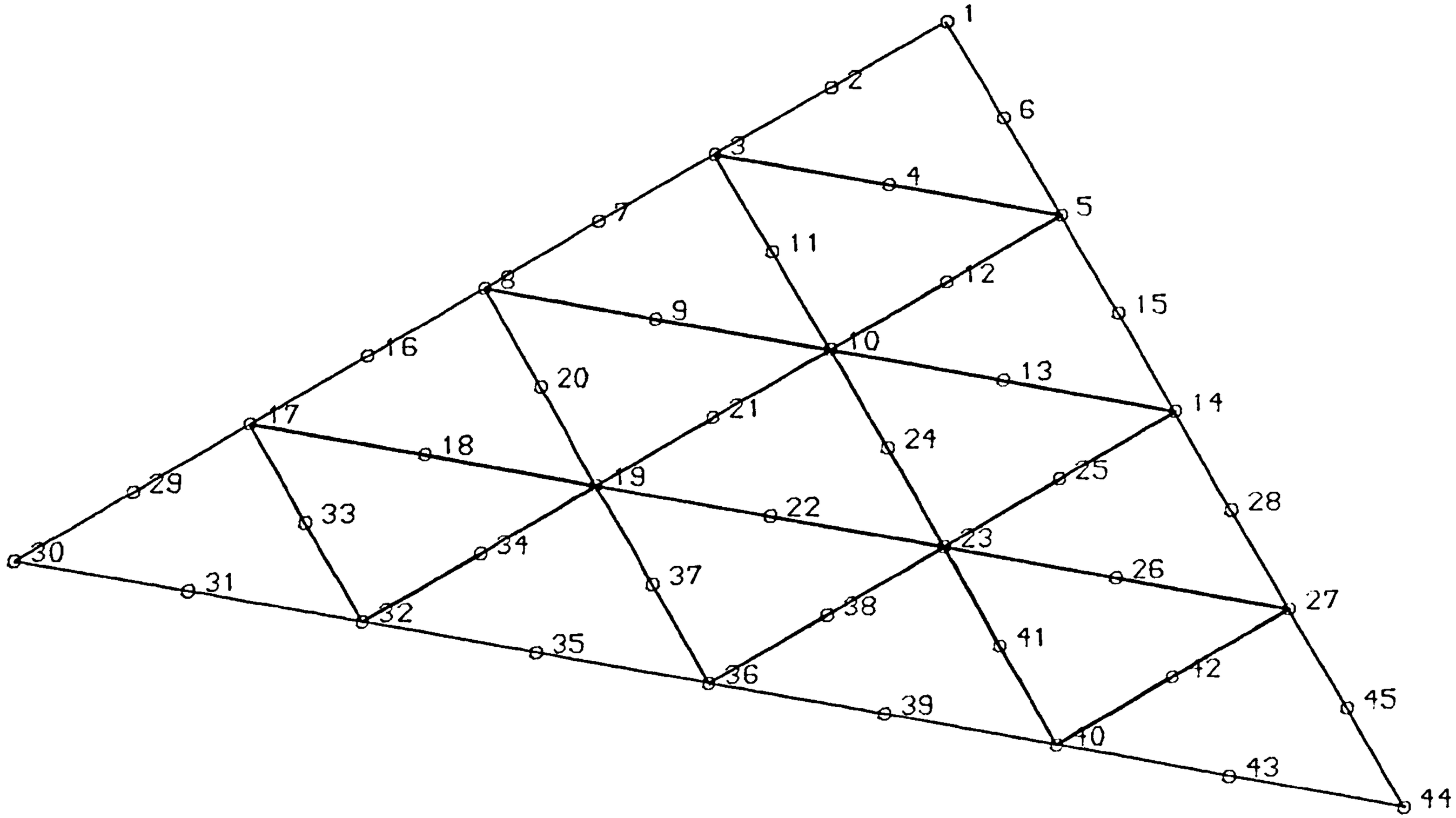

M.M.AZZAWI

Figure (6.3) Uniform Triangular Block
(Type 2)

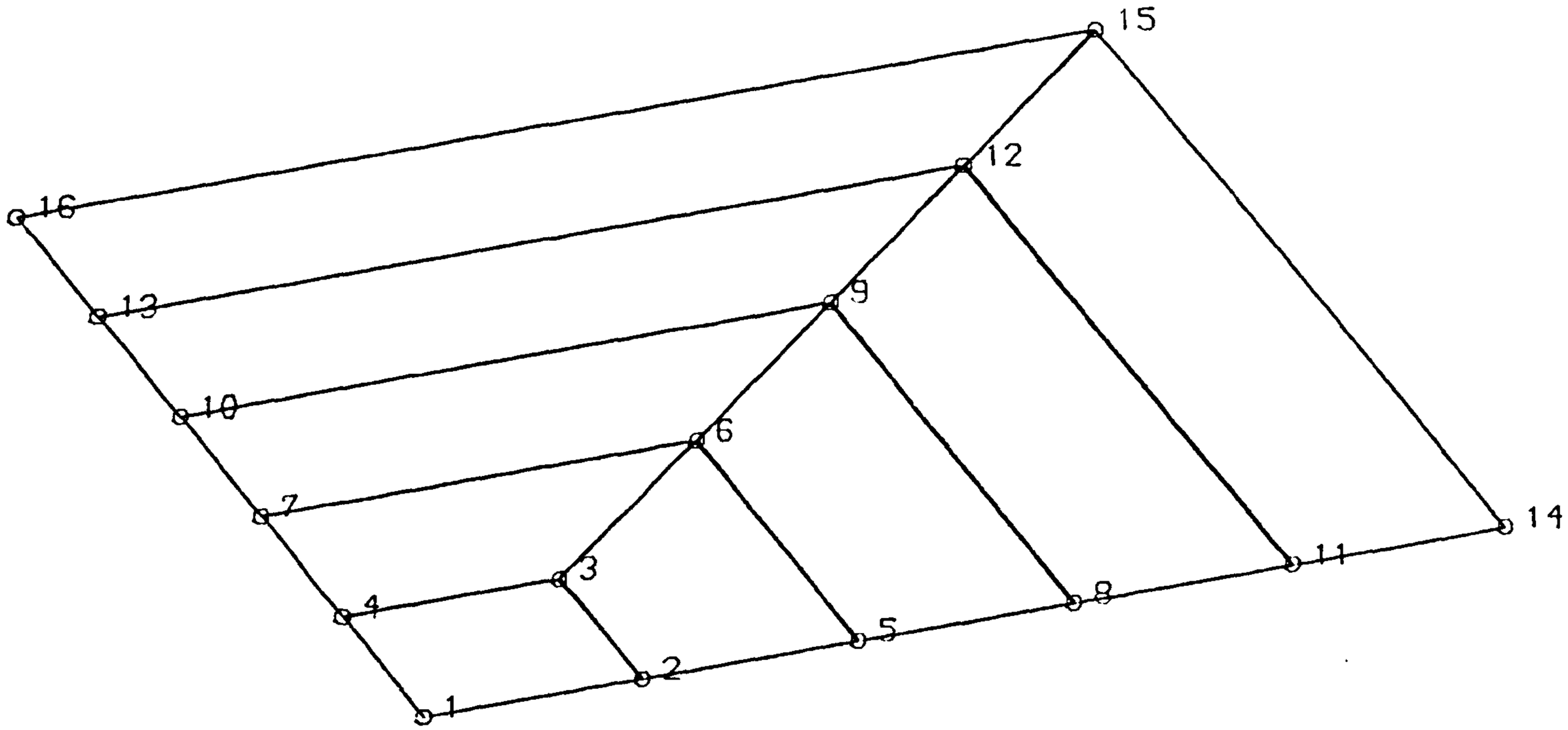

M.M.AZZAWI

Figure (6.4) Quadrilateral Zooming Block
(Type 3)

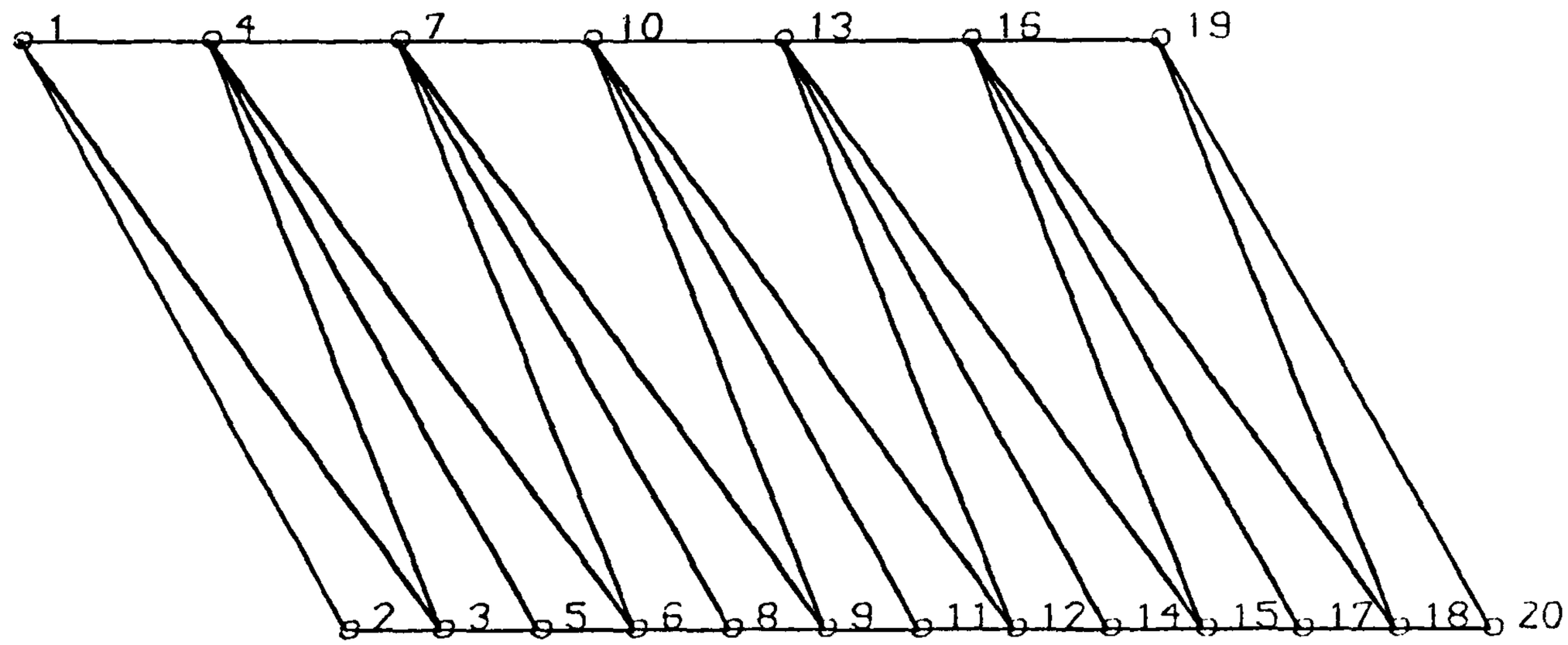

M.M.AZZAWI

Figure (6.5) Single-Layer Transition Block
(Type 4)

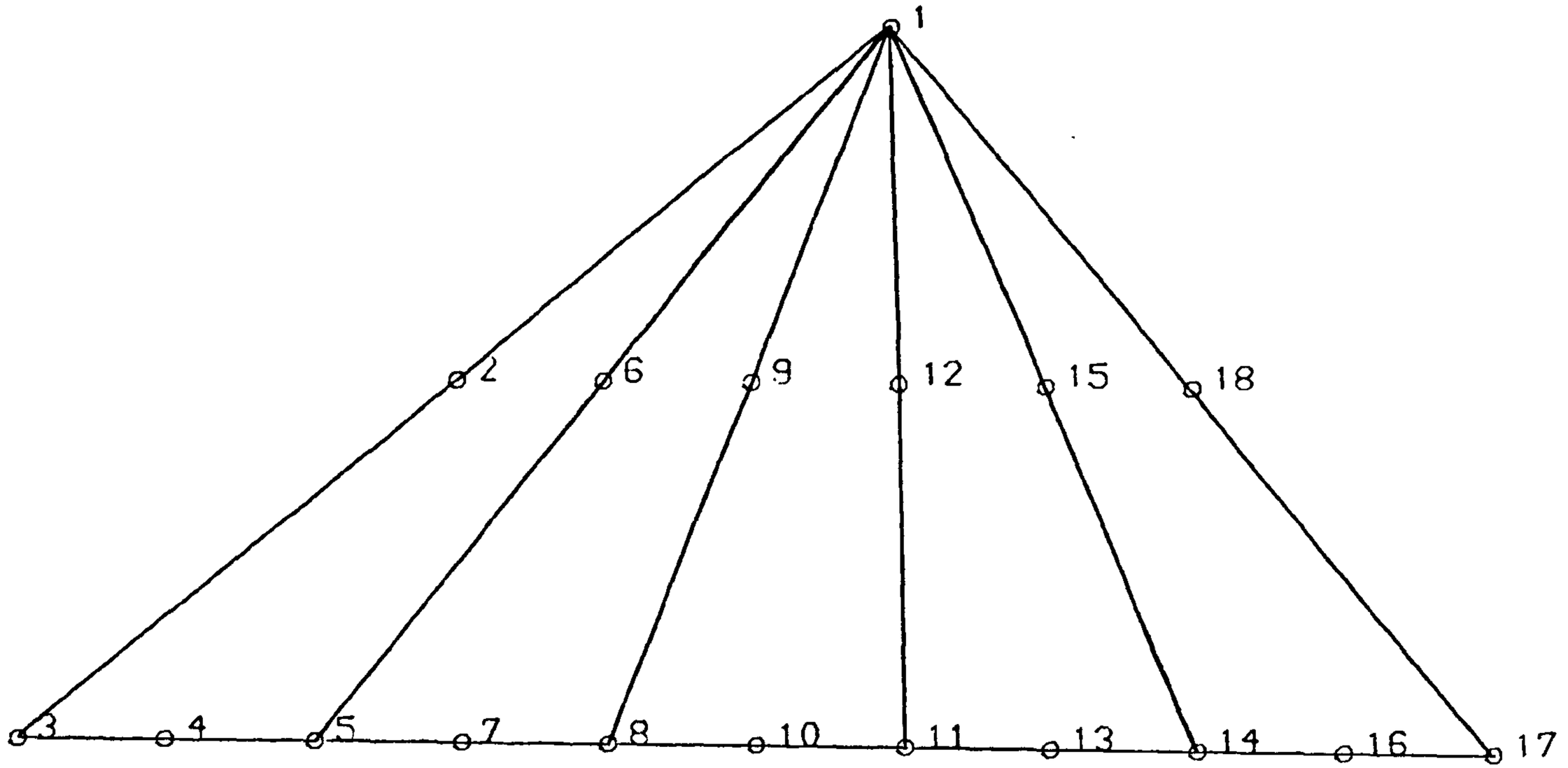

Figure (6.6) Central Triangular Block
(Type 5)

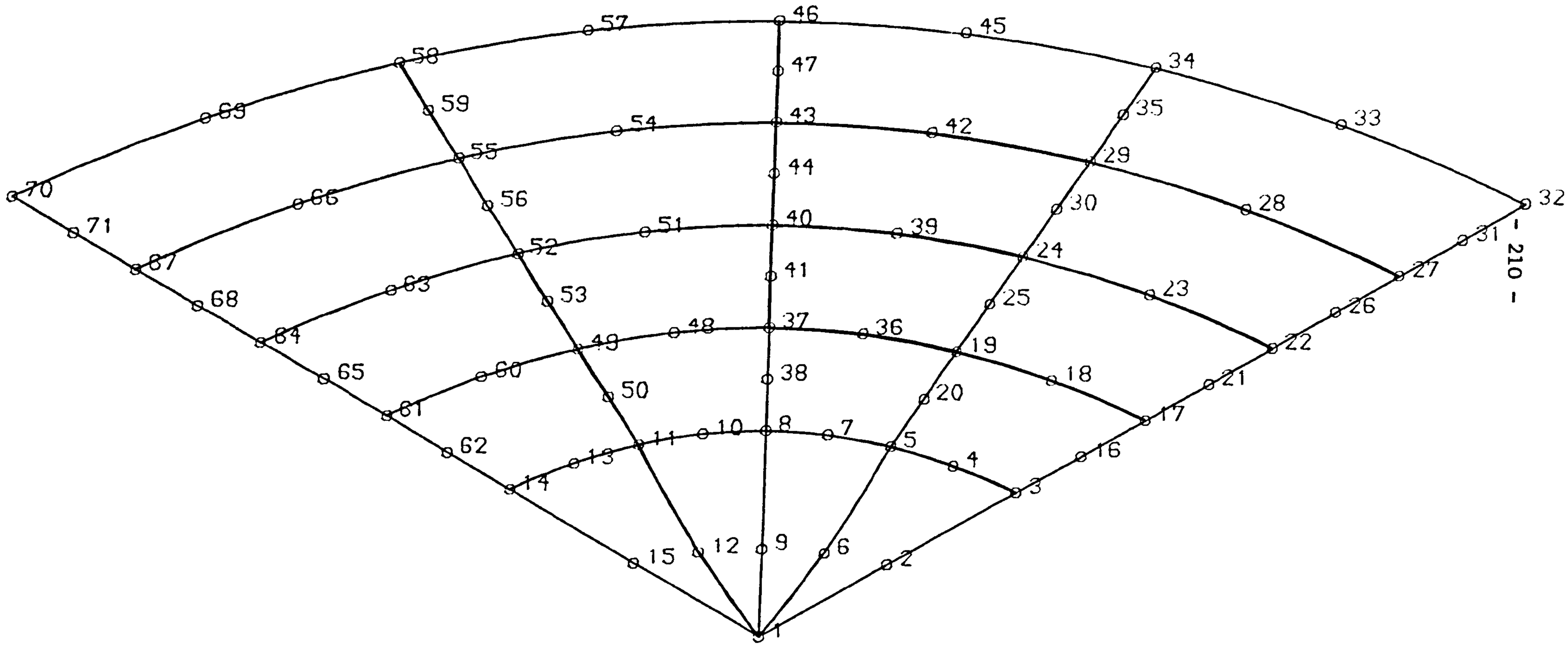

M.M.AZZAWI

Figure (6.7) Facility of the Central Triangular Block (Type 5)

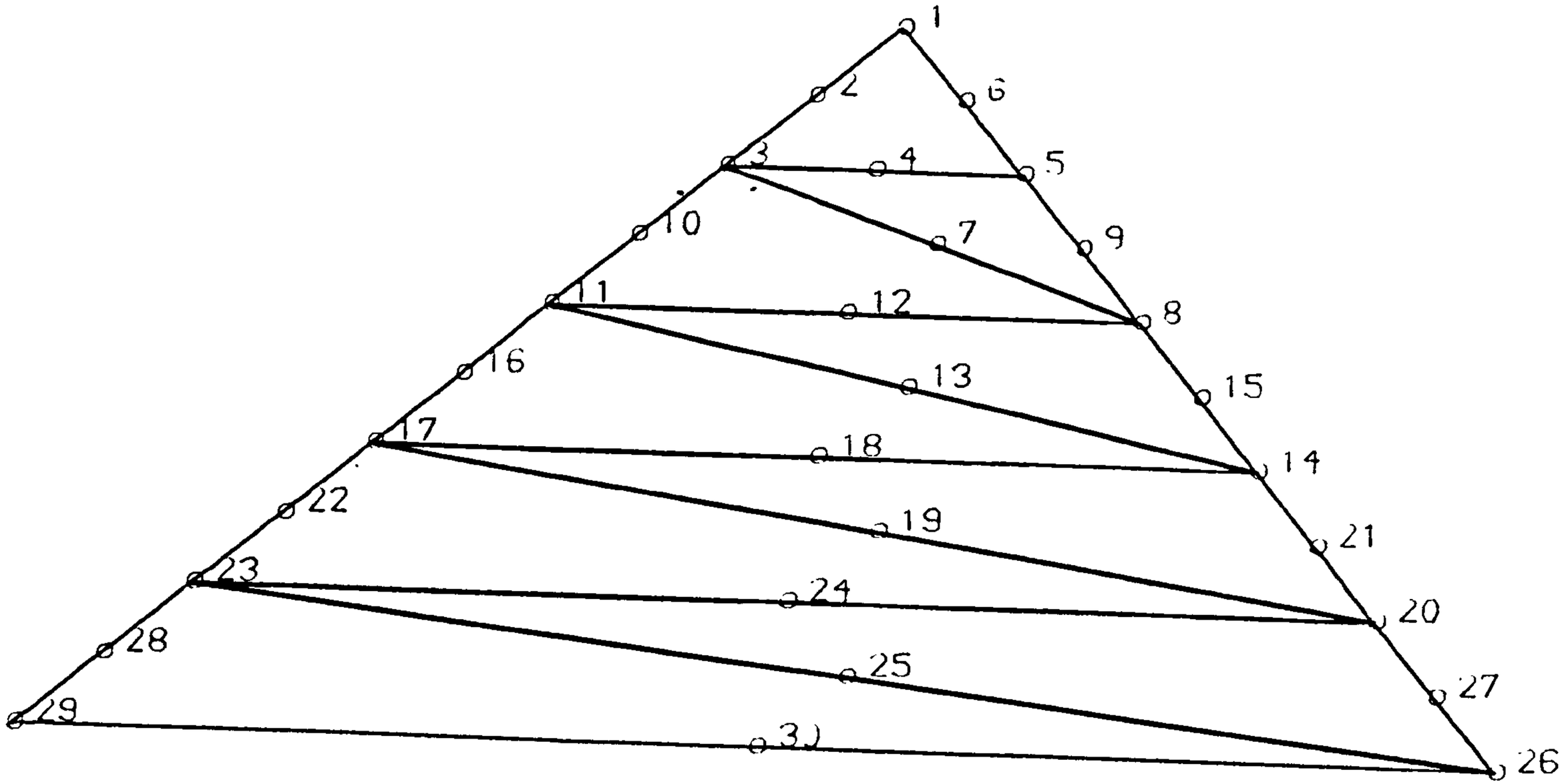

M.M.AZZAWI

Figure (6.8) Triangular Zooming Block
(Type 6)

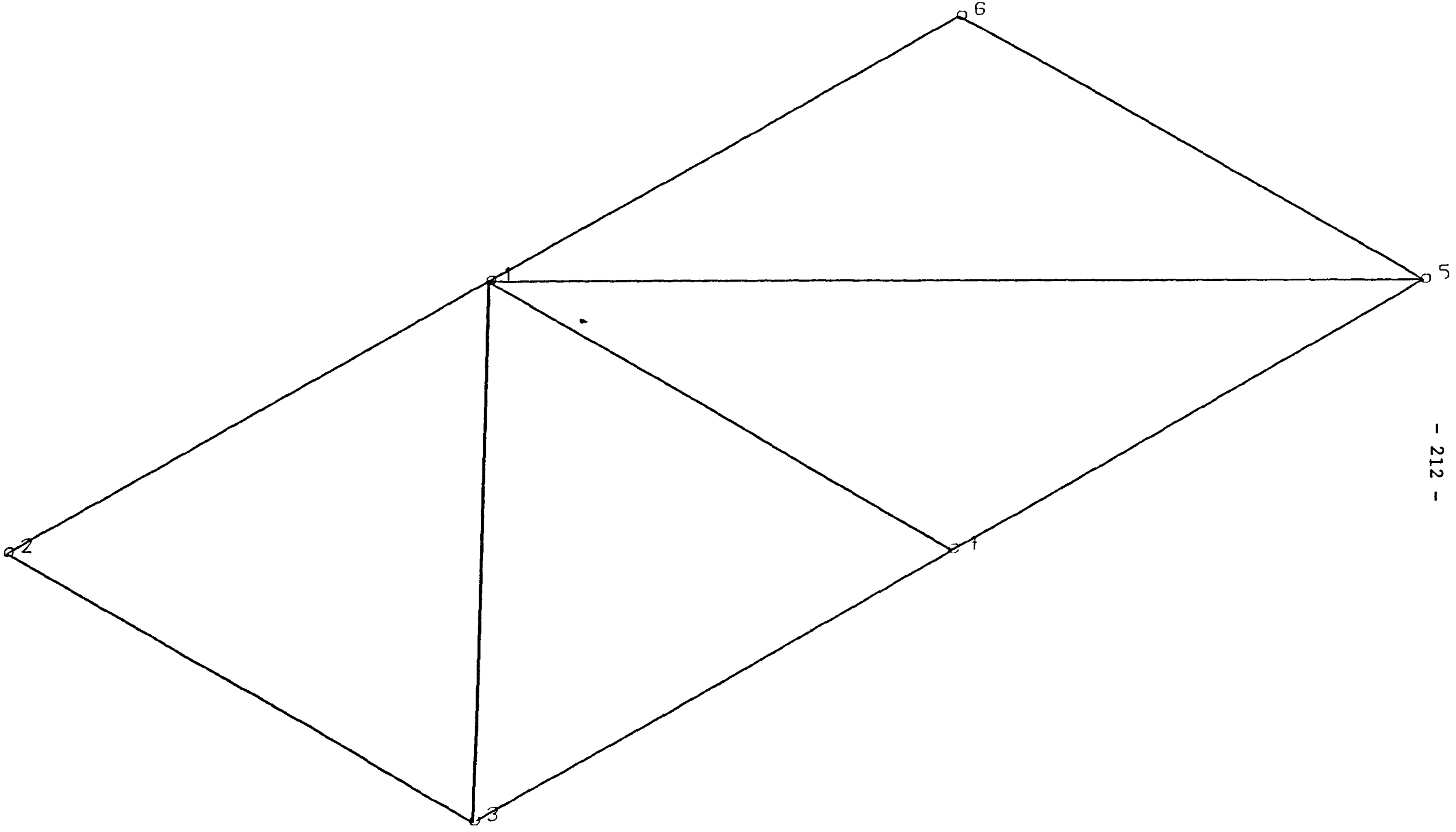

M.AZZAWI

Figure (6.9-a) Mesh Zooming By Using Block
(Type 6)

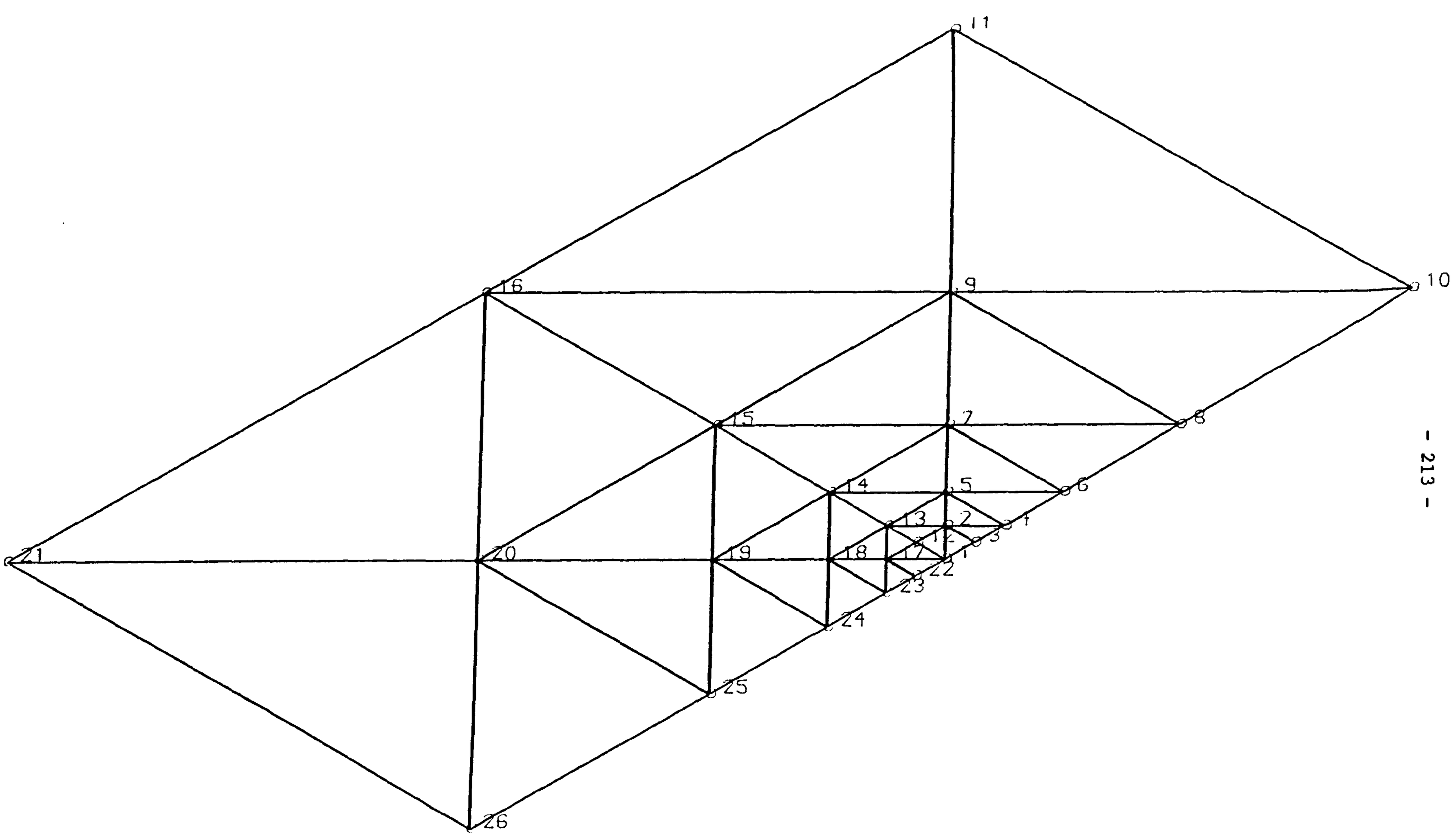

M.M.AZZAWI

Figure (6.9-b) Mesh Zooming By Using Block (Type 6)

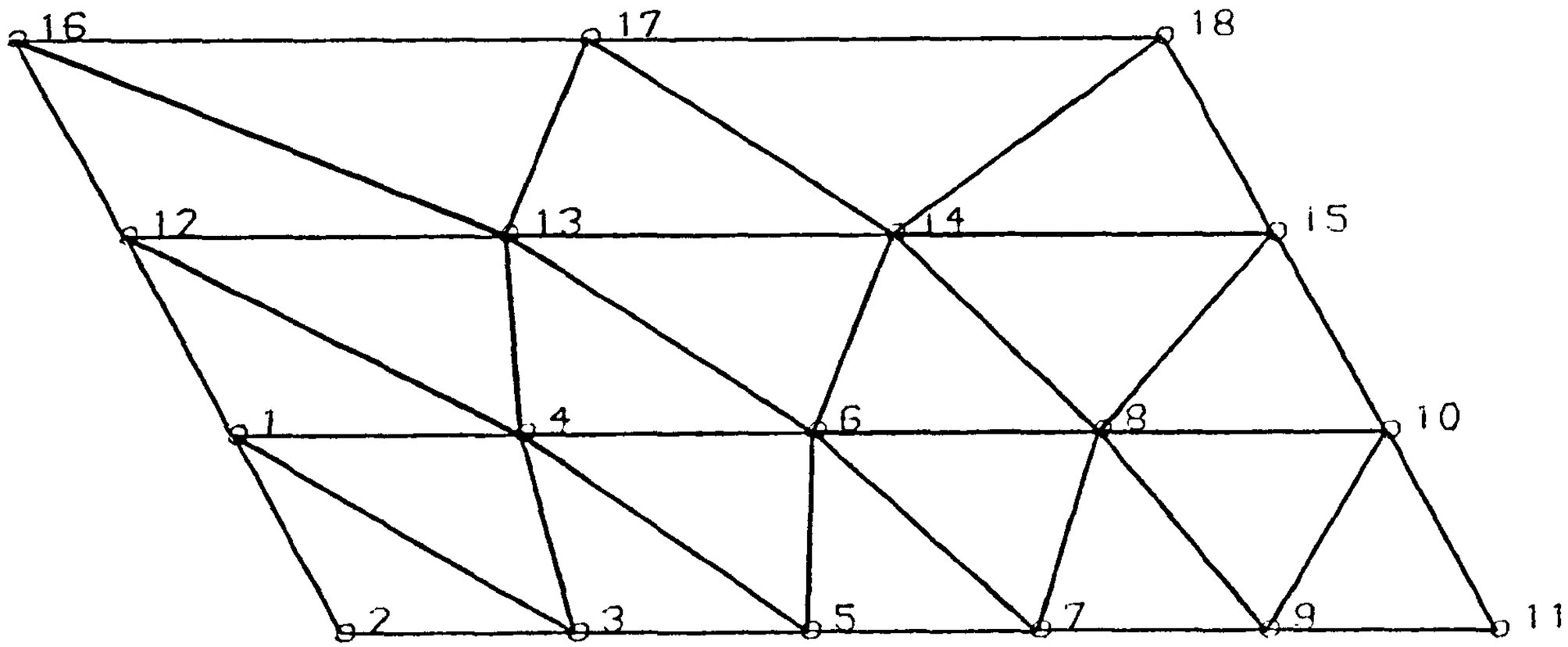

M.M.AZZAWI

Figure (6.10) Multi-Layer Transition Block
(Type 7)

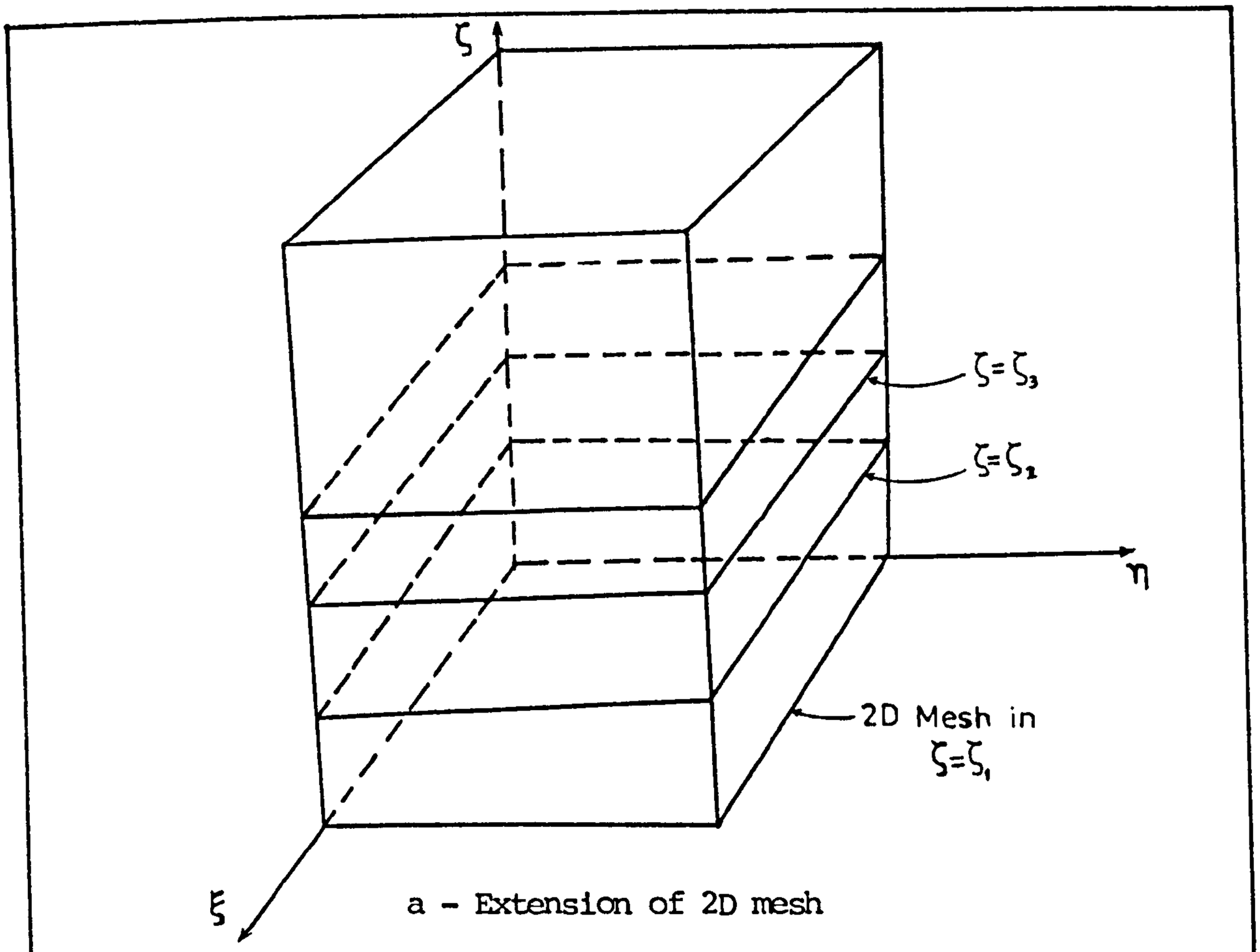

a - Extension of 2D mesh

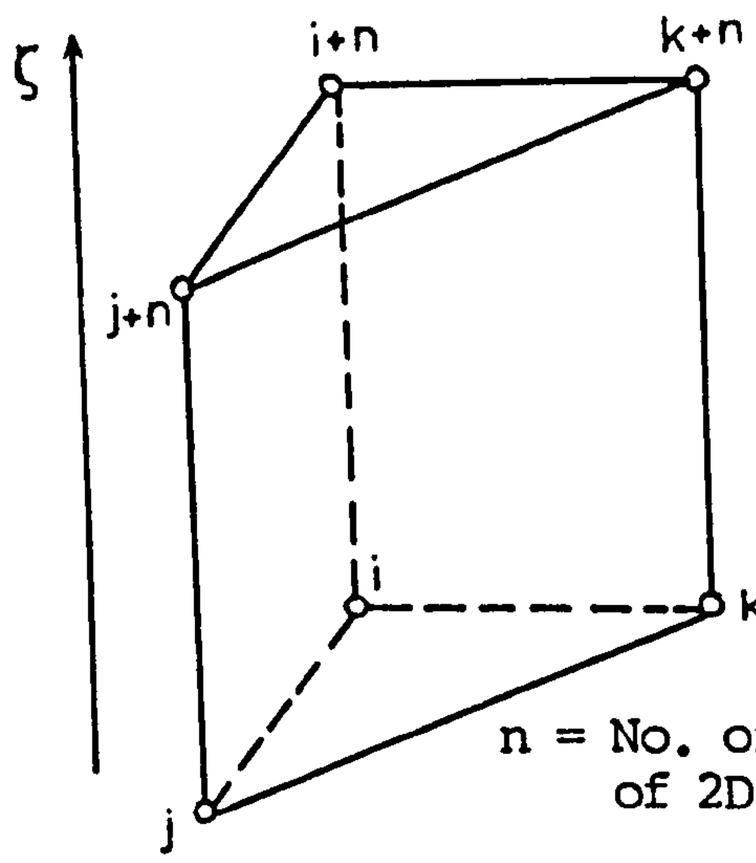

n = No. of nodes of 2D mesh

b - Extension of Triangular Element

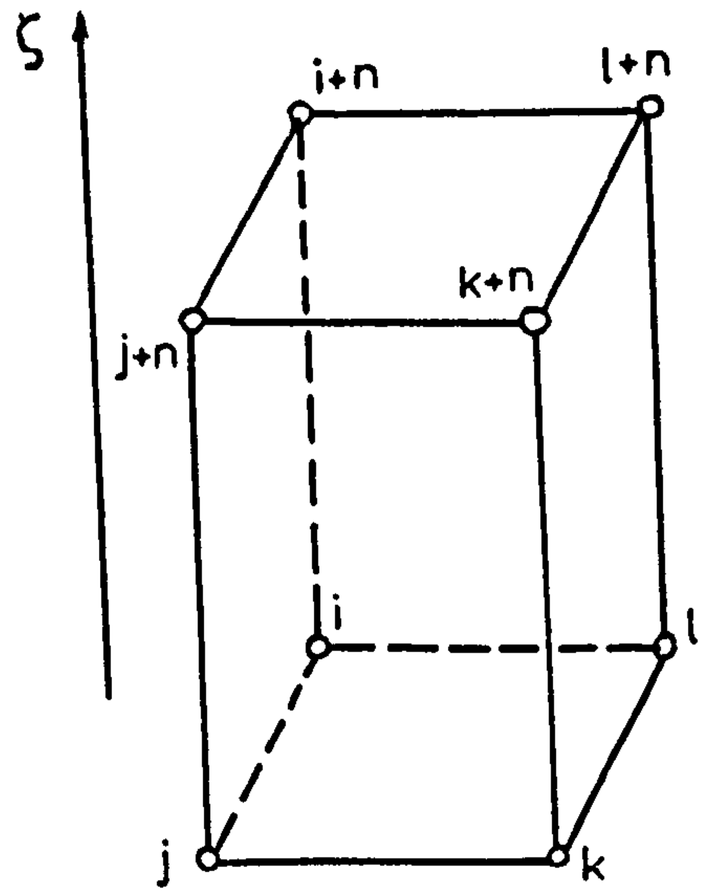

c - Extension of Quadrilateral Element

Figure 6.11 Generation of 3D Intrinsic Element from 2D Elements

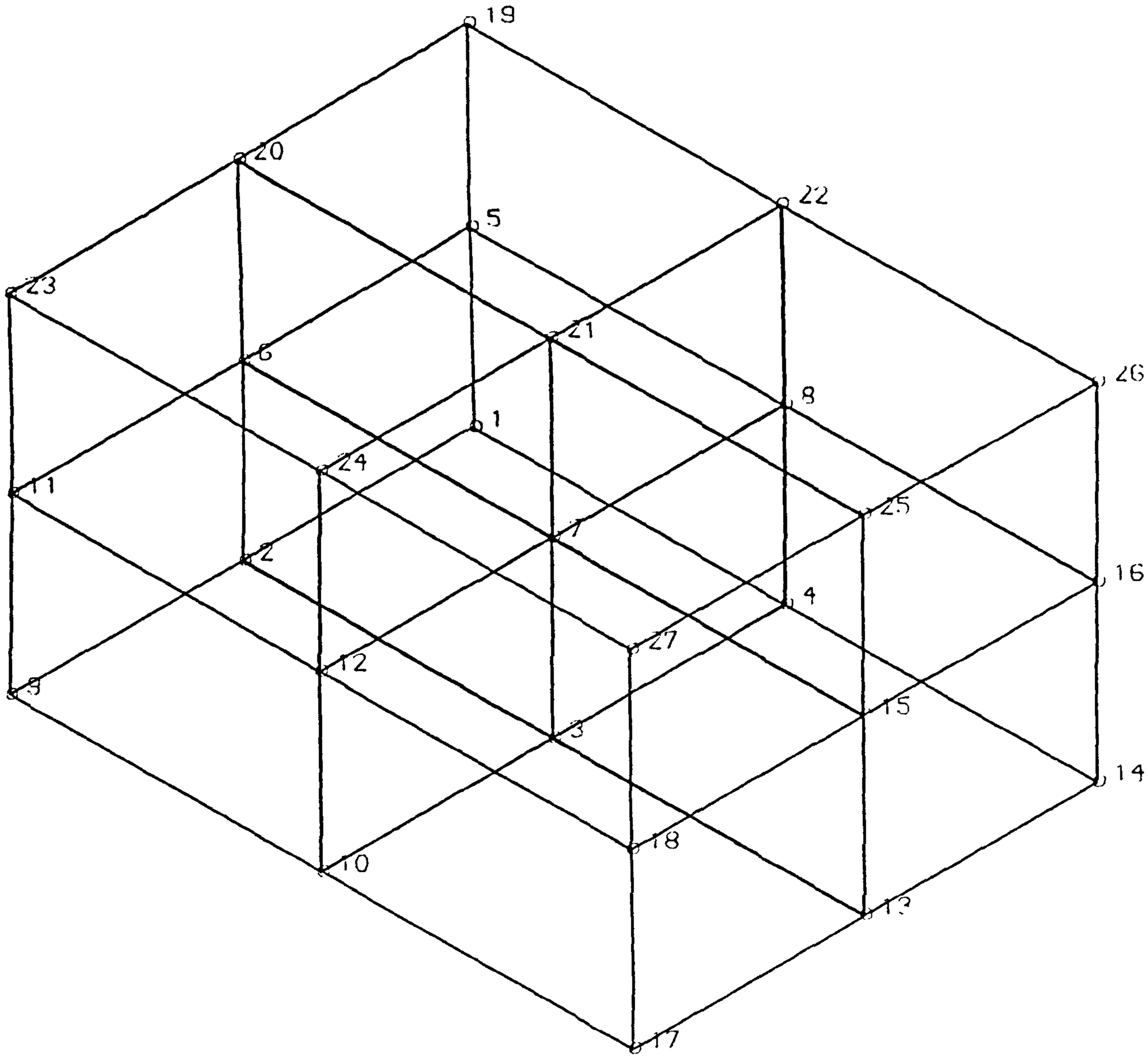

M.M.AZZAWI

Figure (6.12) Uniform Hexahedral Block
(Type 1)

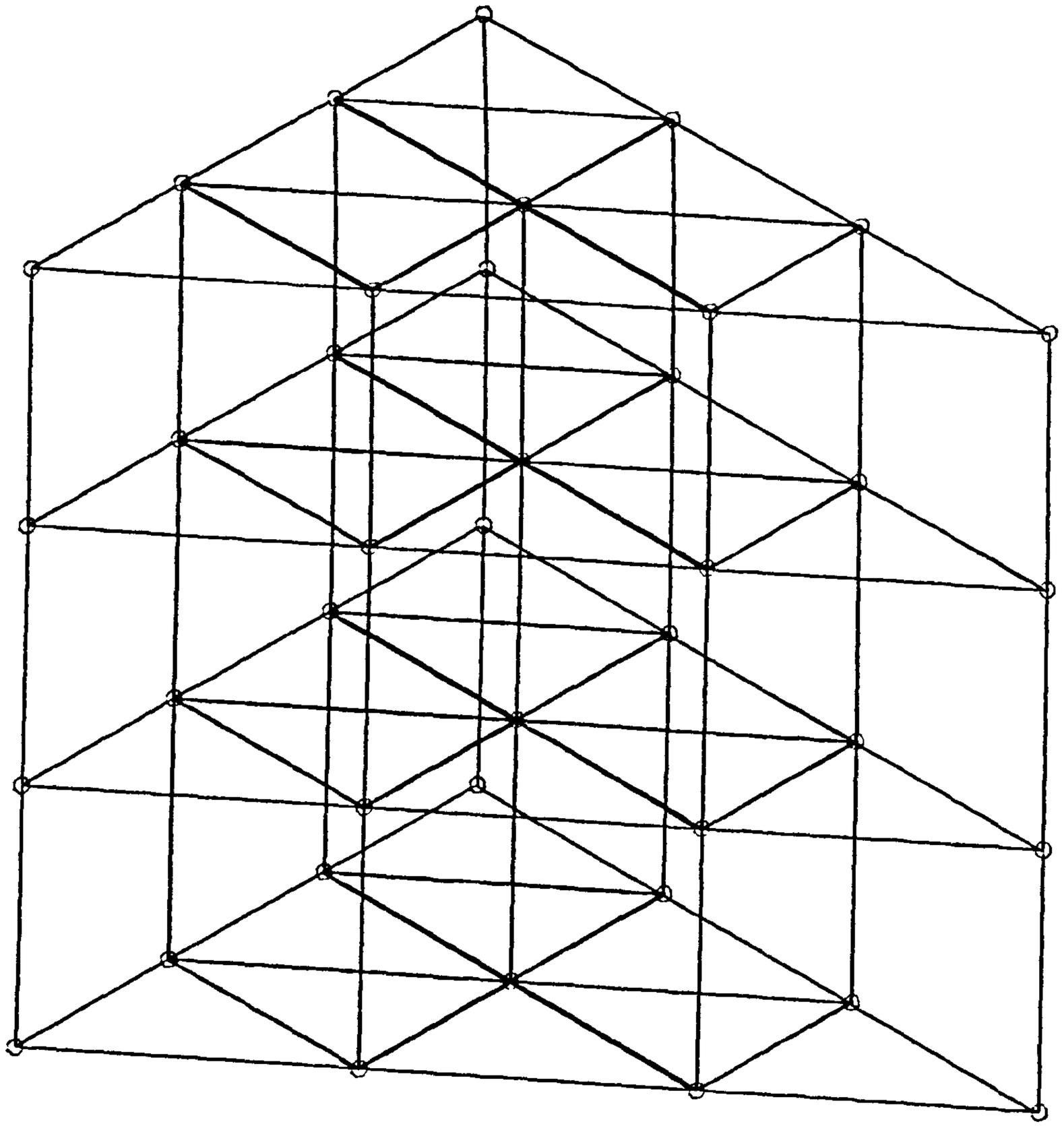

M.M.AZZAWI

Figure (6.13) Uniform Pentahedral Block
(Type 2)

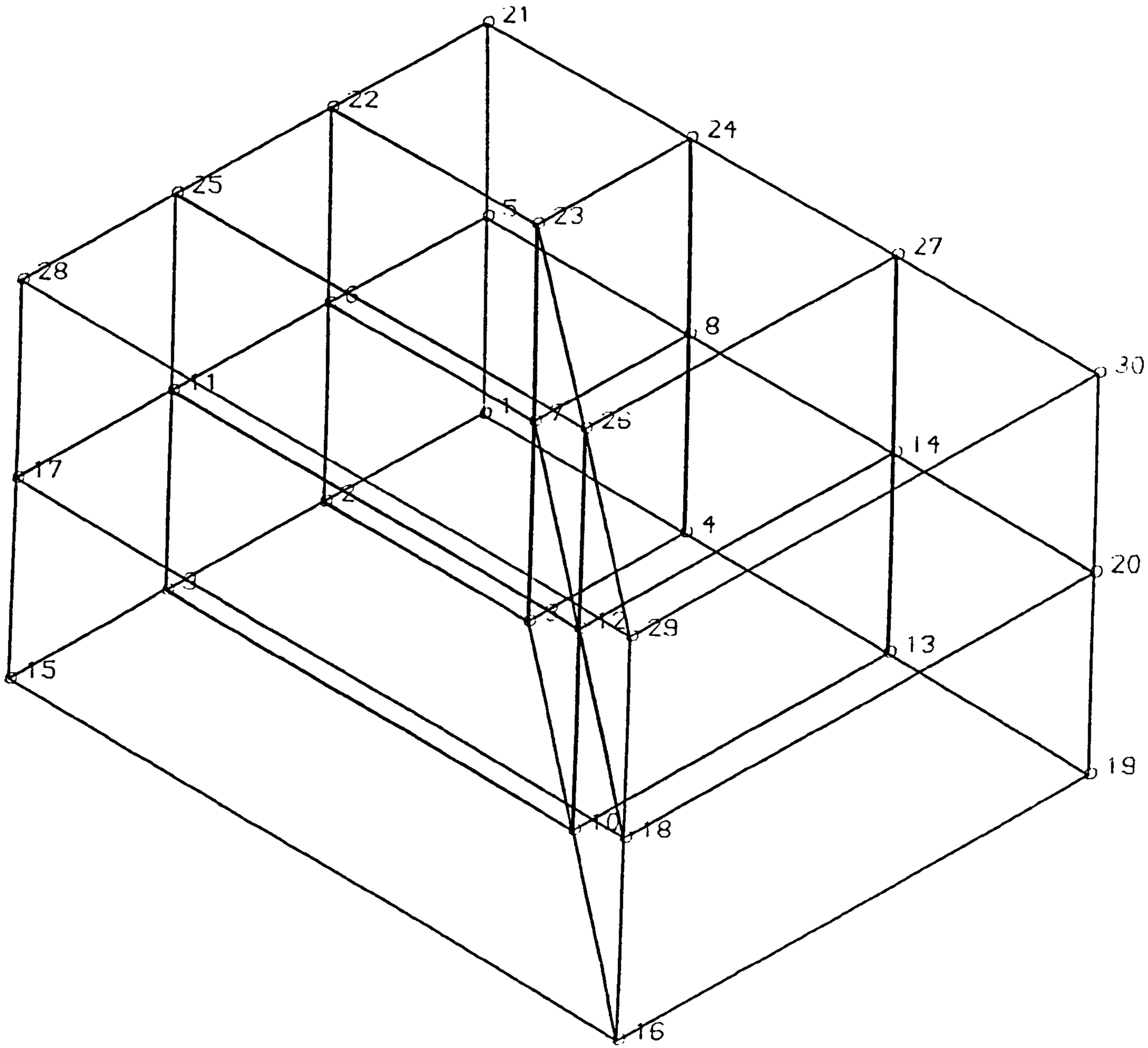

M.M.AZZAWI

Figure (6.14) Hexahedral Zooming Block
(Type 3)

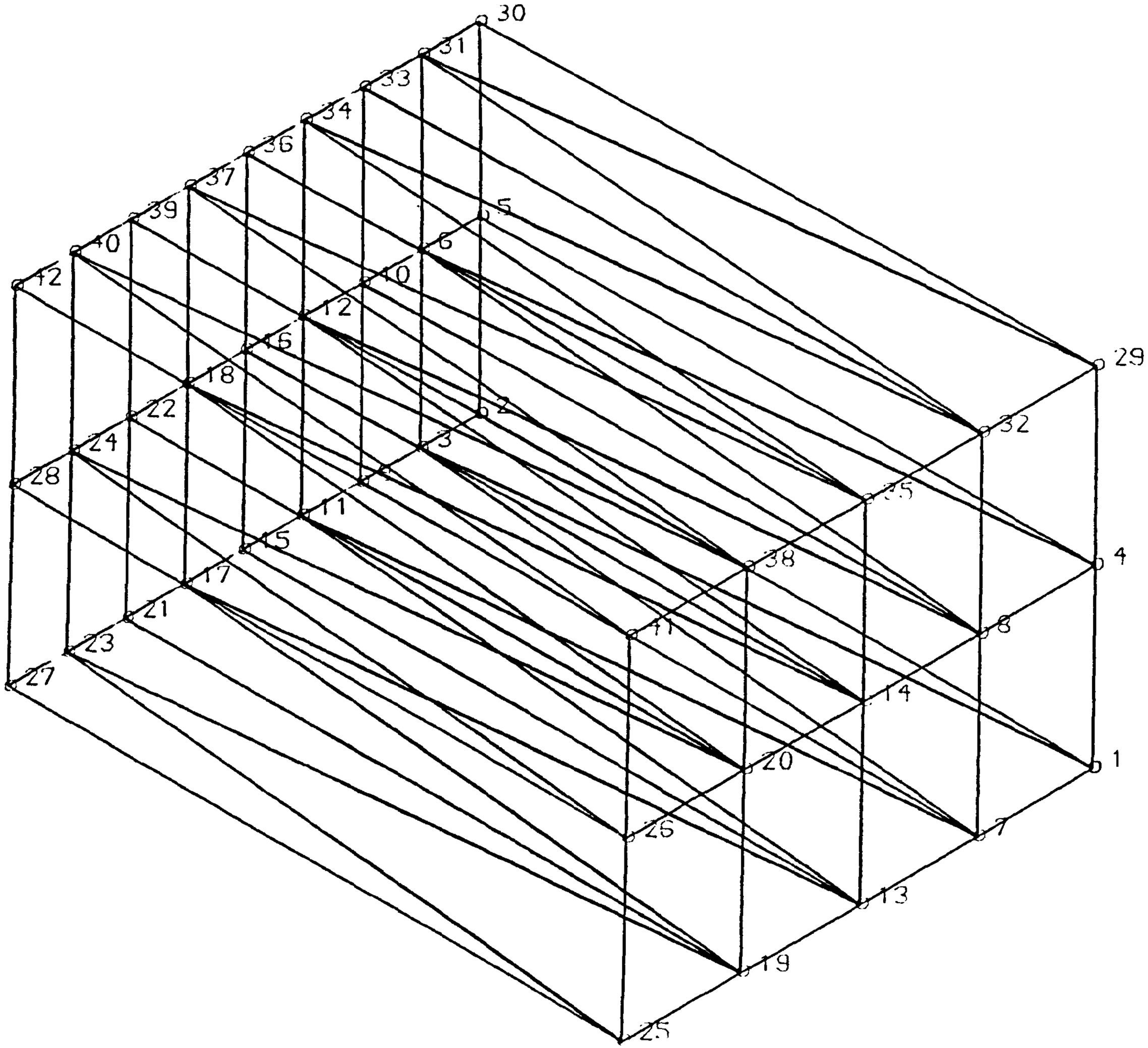

M.M.AZZAWI

Figure (6.15) Single-Layer Transition Block
(Type 4)

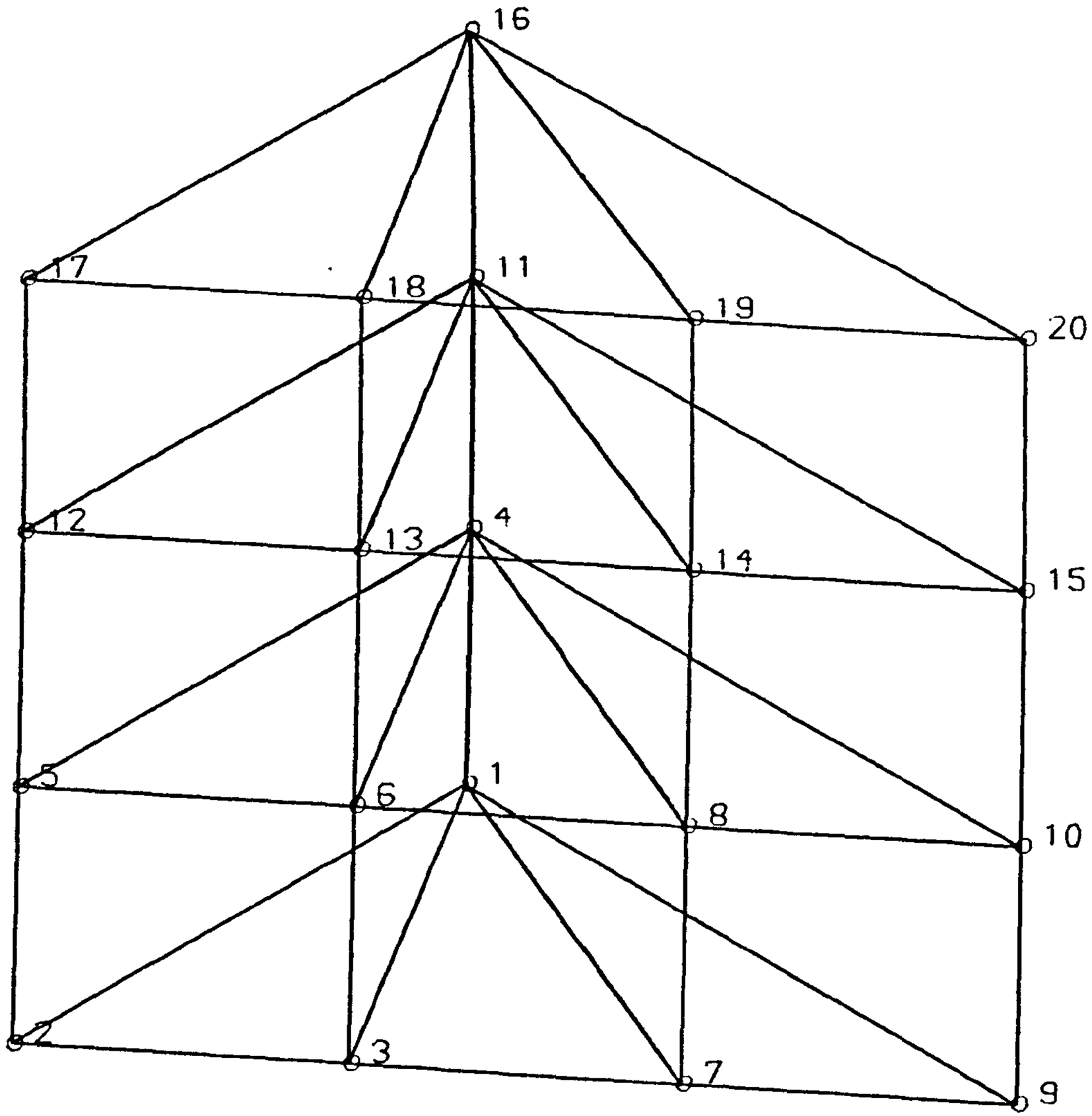

M.M.AZZAWI

Figure (6.16) Central Pentahedral Block
(Type 5)

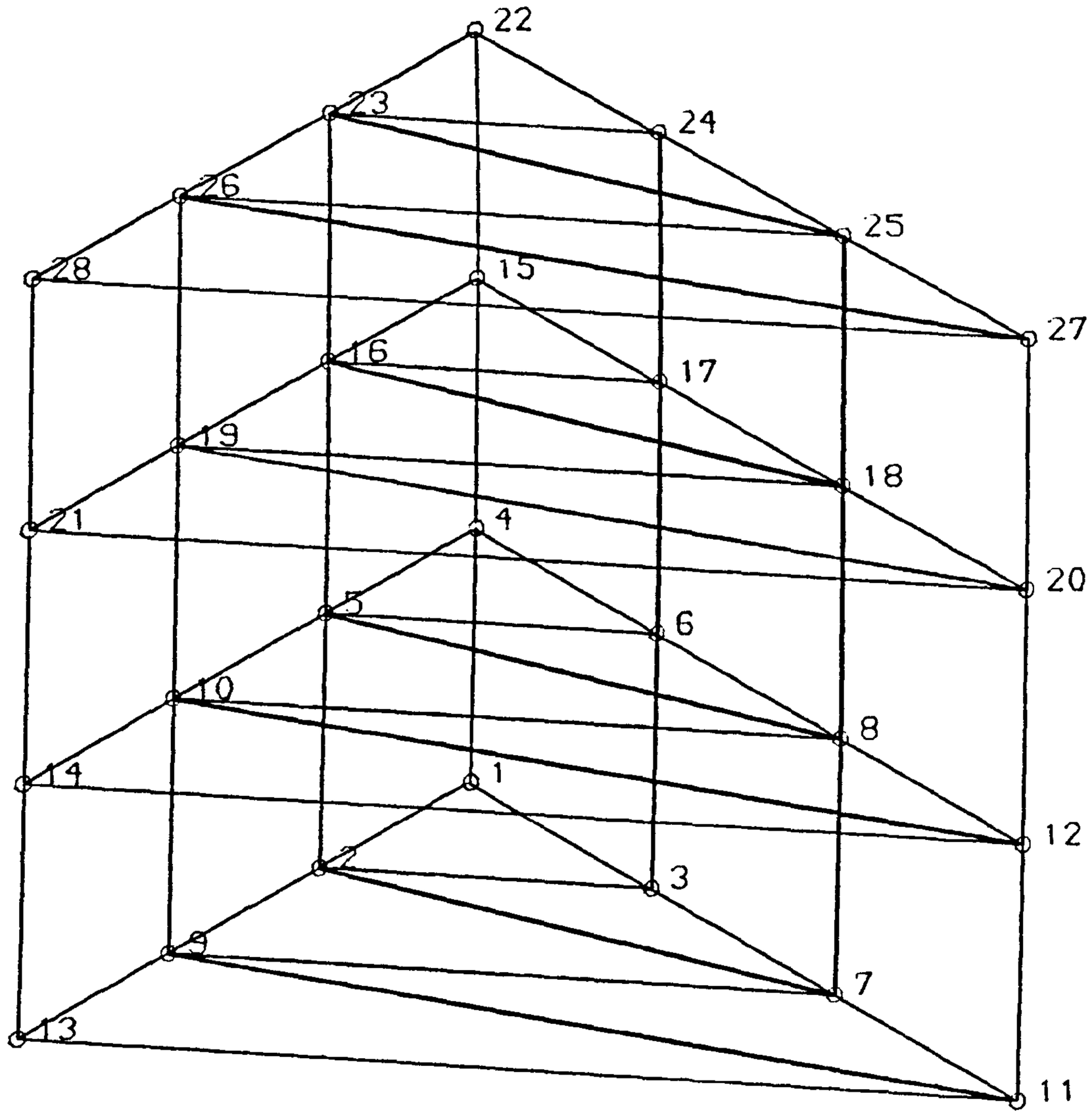

M.M.AZZAWI	Figure (6.17) Pentahedral Zooming Block (Type 6)

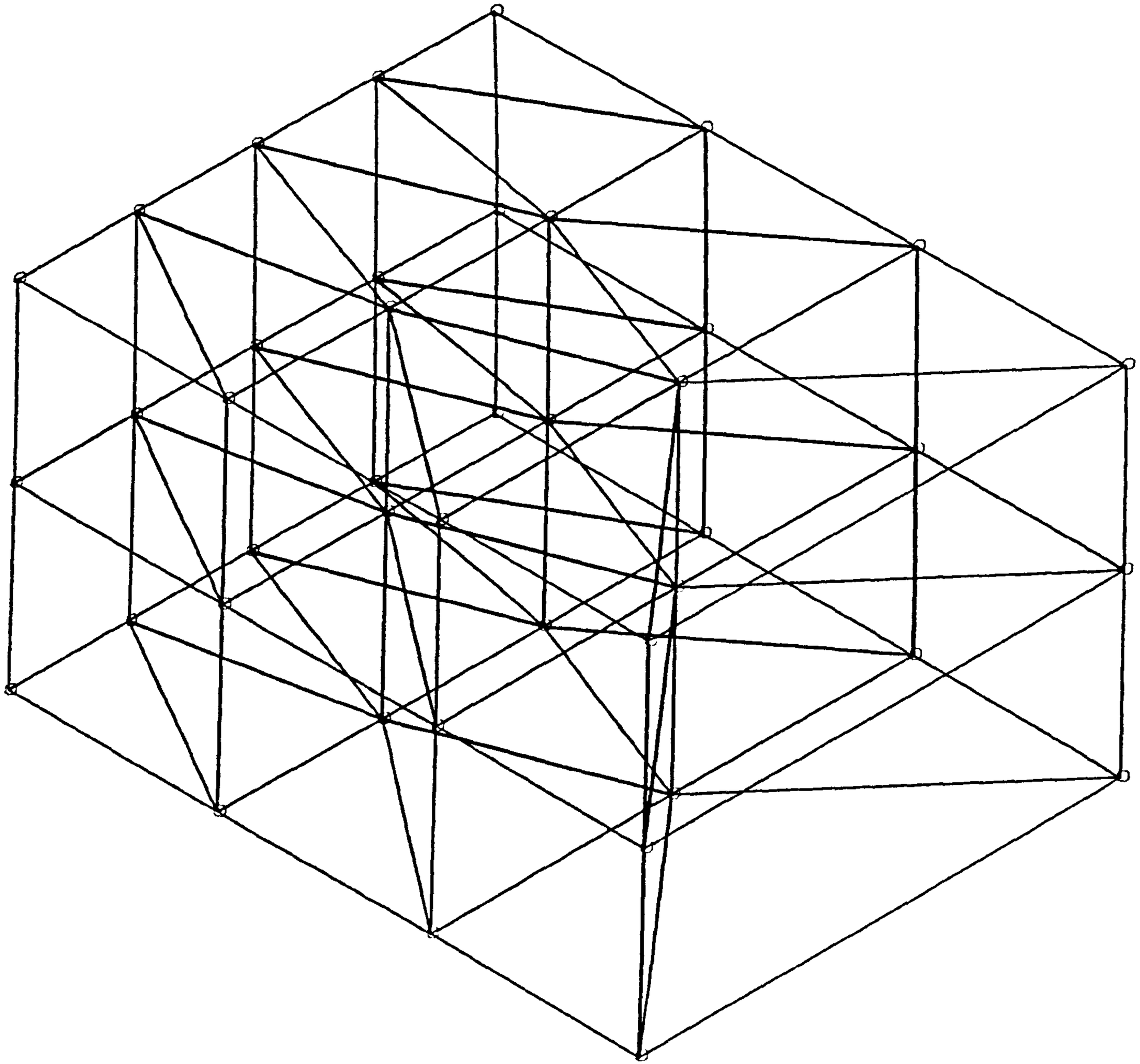

M.M.AZZAWI

Figure (6.18) Multi-Layer Transition Block
(Type 7)

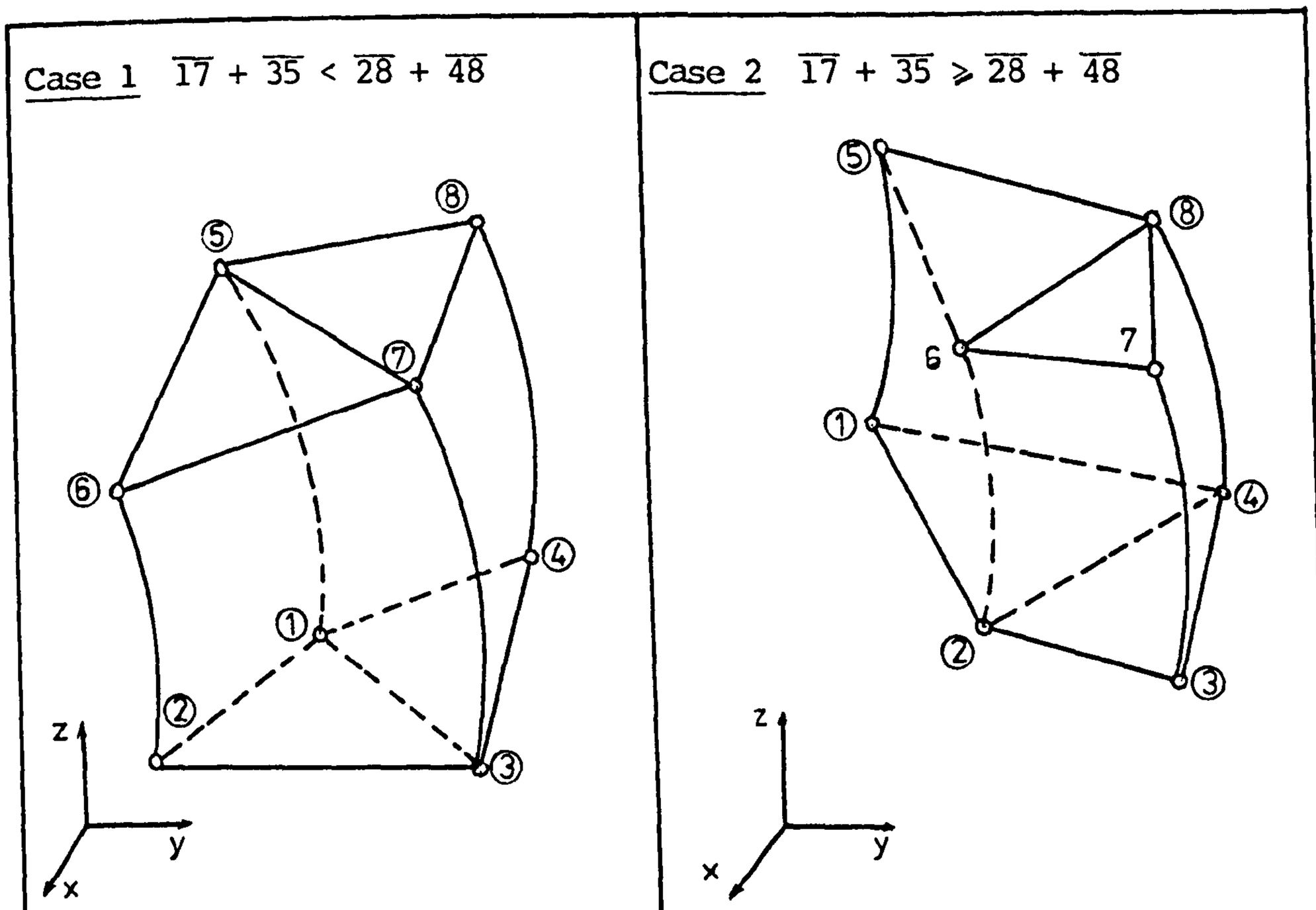

Figure 6.19 Generation of Simple Pentahedra in a Hexahedral Element

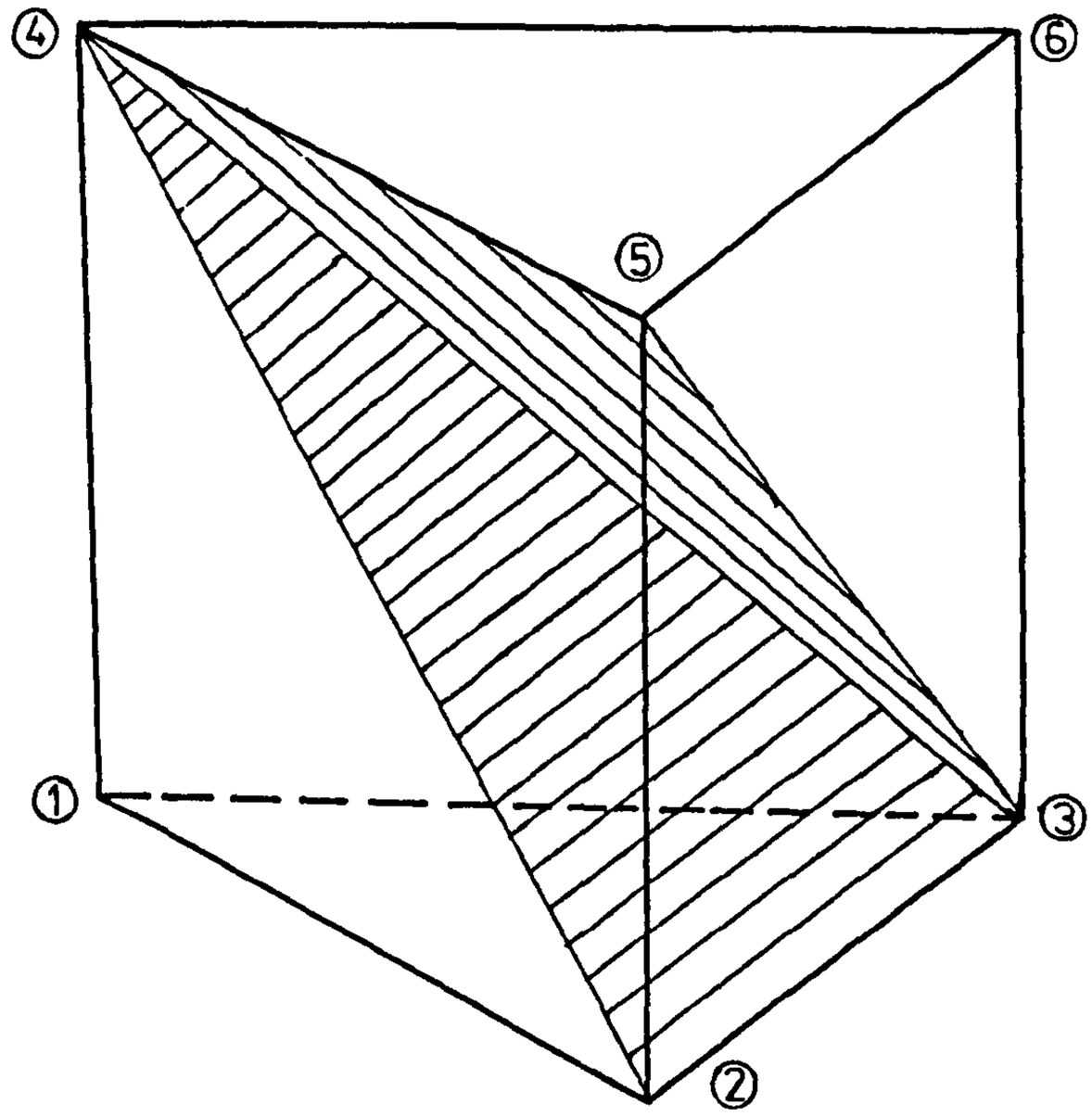

Figure 6.20 Generation of Simple Tetrahedra in a Pentahedral Element

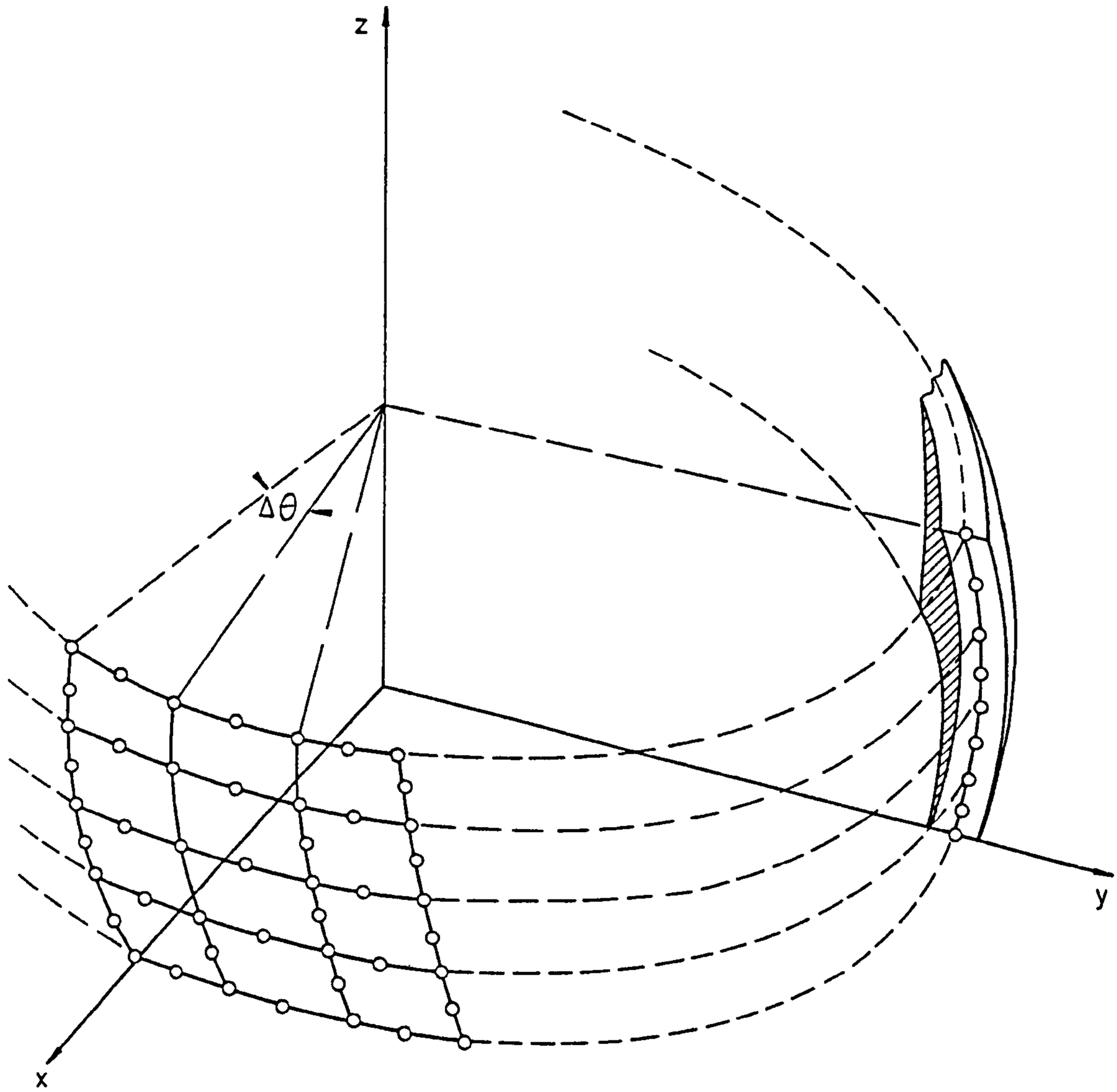

FIGURE 6·21 GENERATION OF FULL MESH FOR AXISYMMETRIC SHELL STRUCTURE.

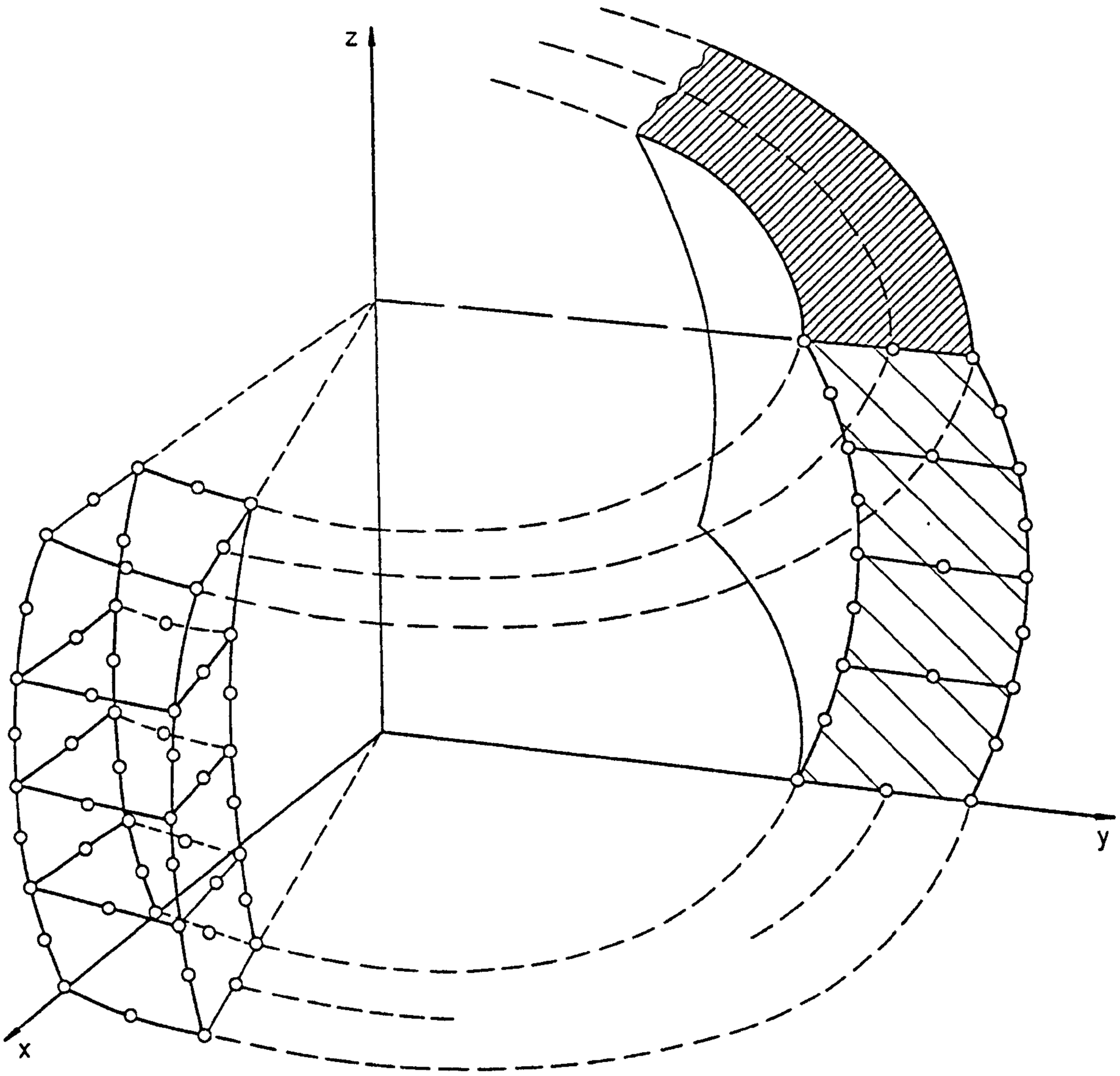

FIGURE 6·22 GENERATION OF FULL 3D MESH FROM 2D AXISYMMETRIC MESH.

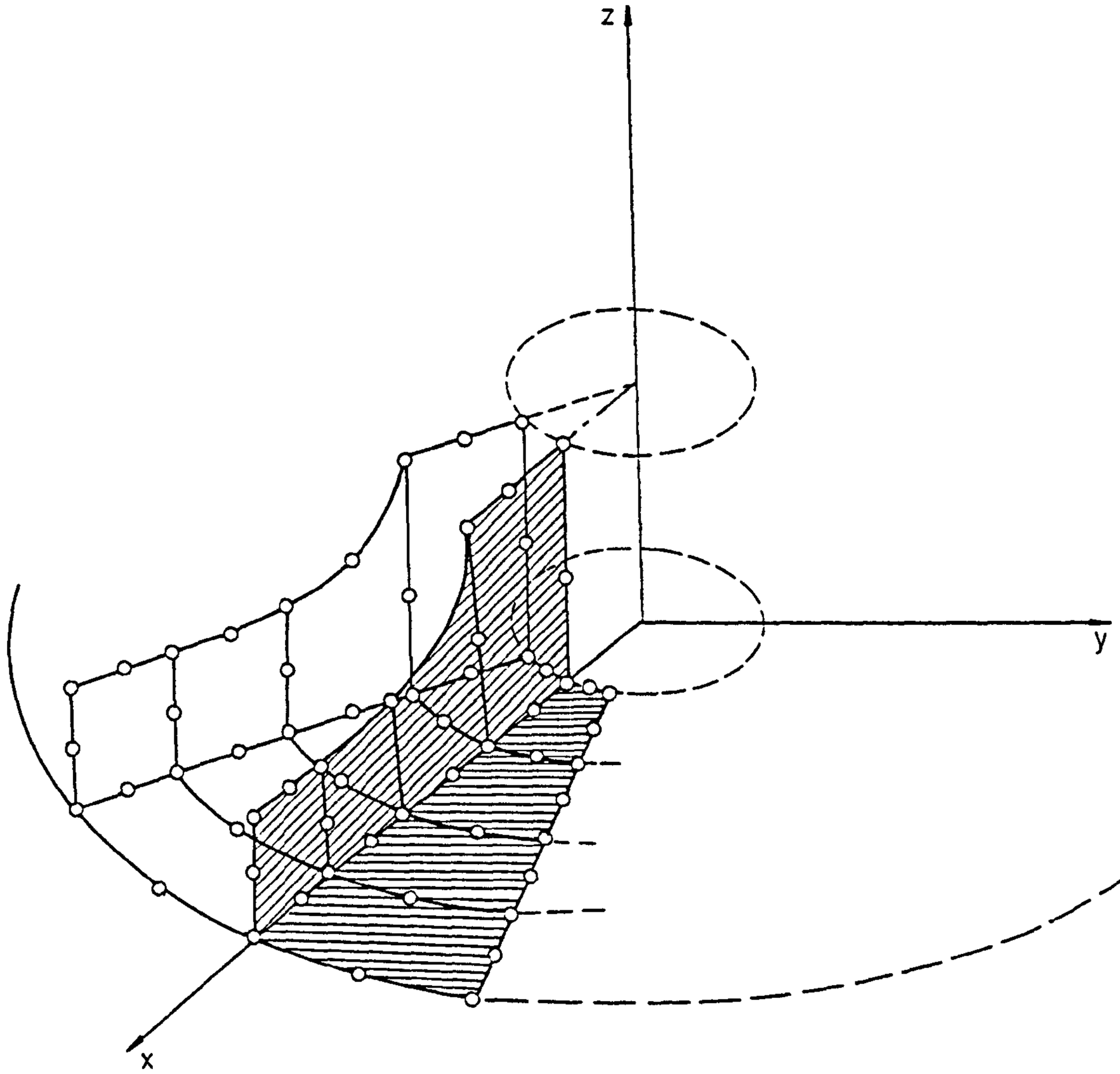

FIGURE 6·23 GENERATION OF FULL MESH FOR SECTORIALLY SYMMETRIC STRUCTURE.

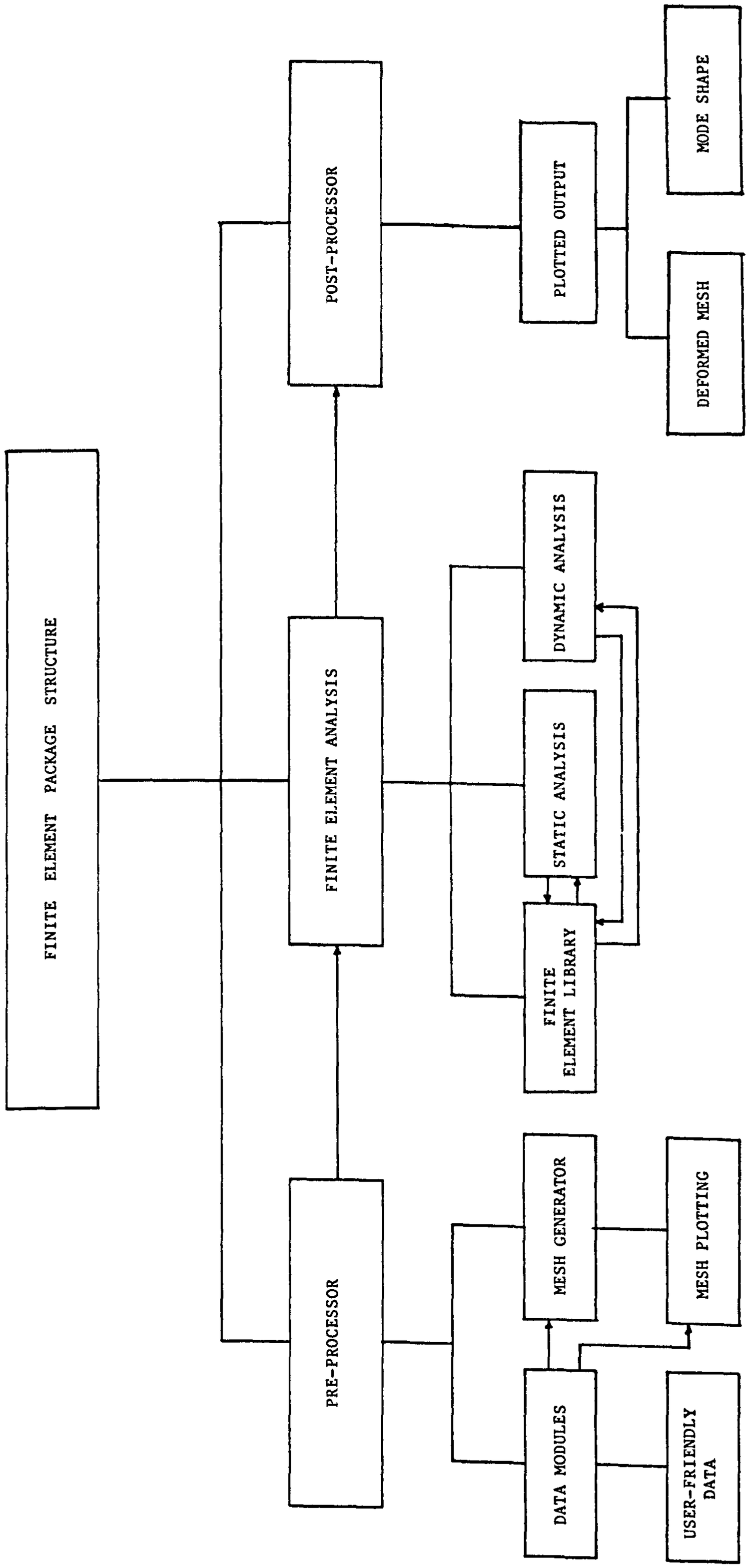

PACKAGE STRUCTURE

FIGURE 7.1

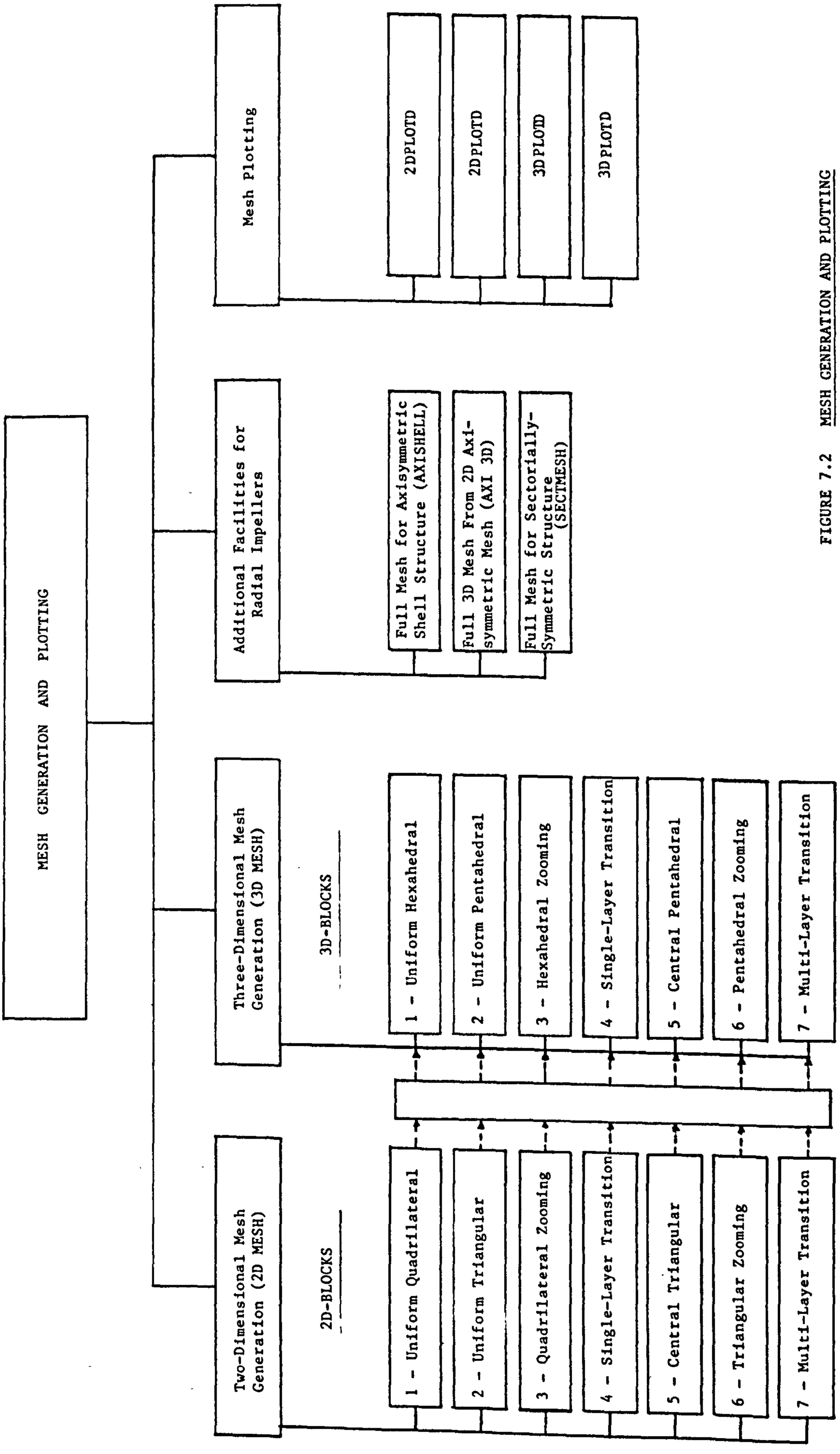

FIGURE 7.2 MESH GENERATION AND PLOTTING

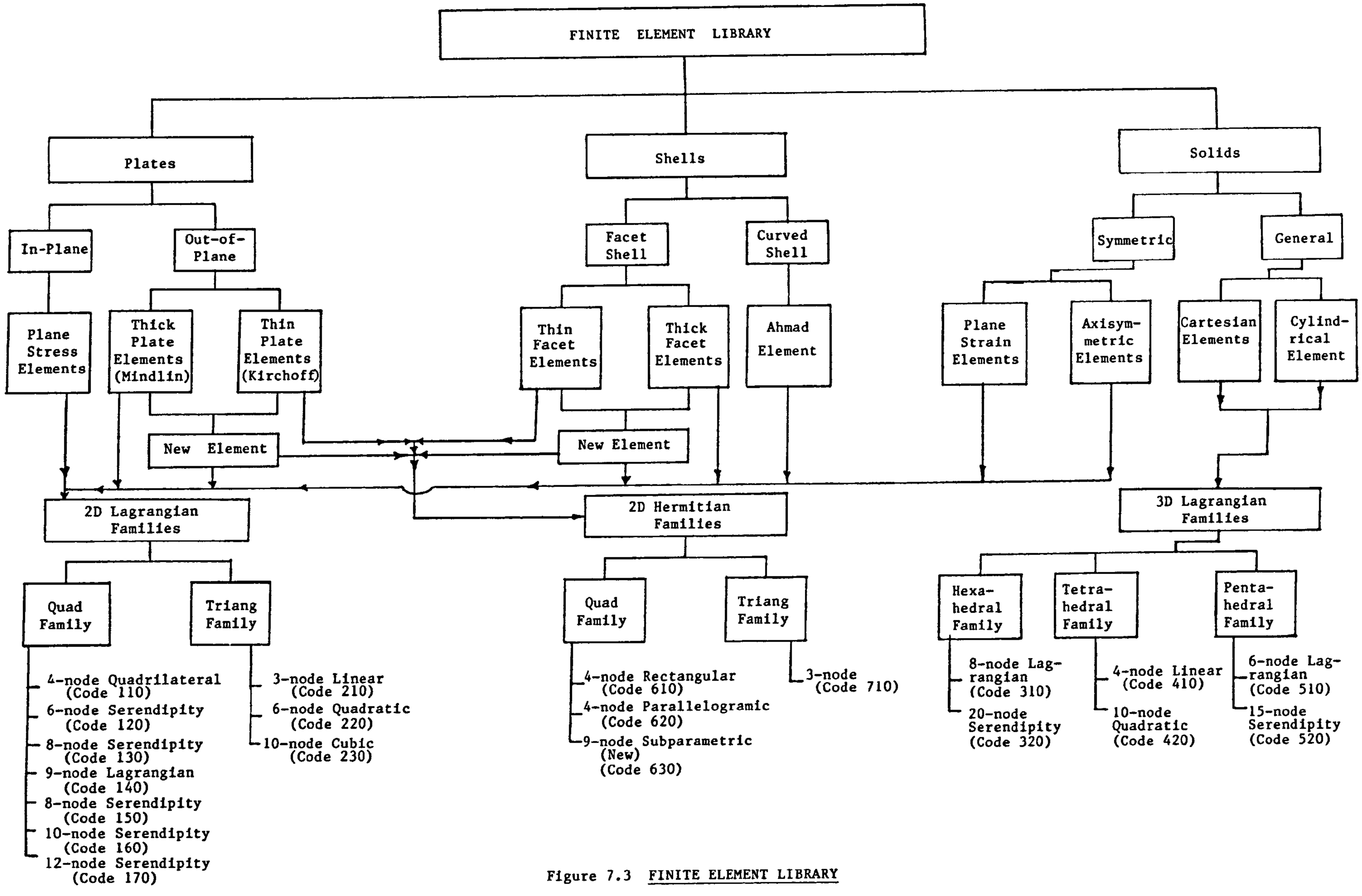

Figure 7.3 FINITE ELEMENT LIBRARY

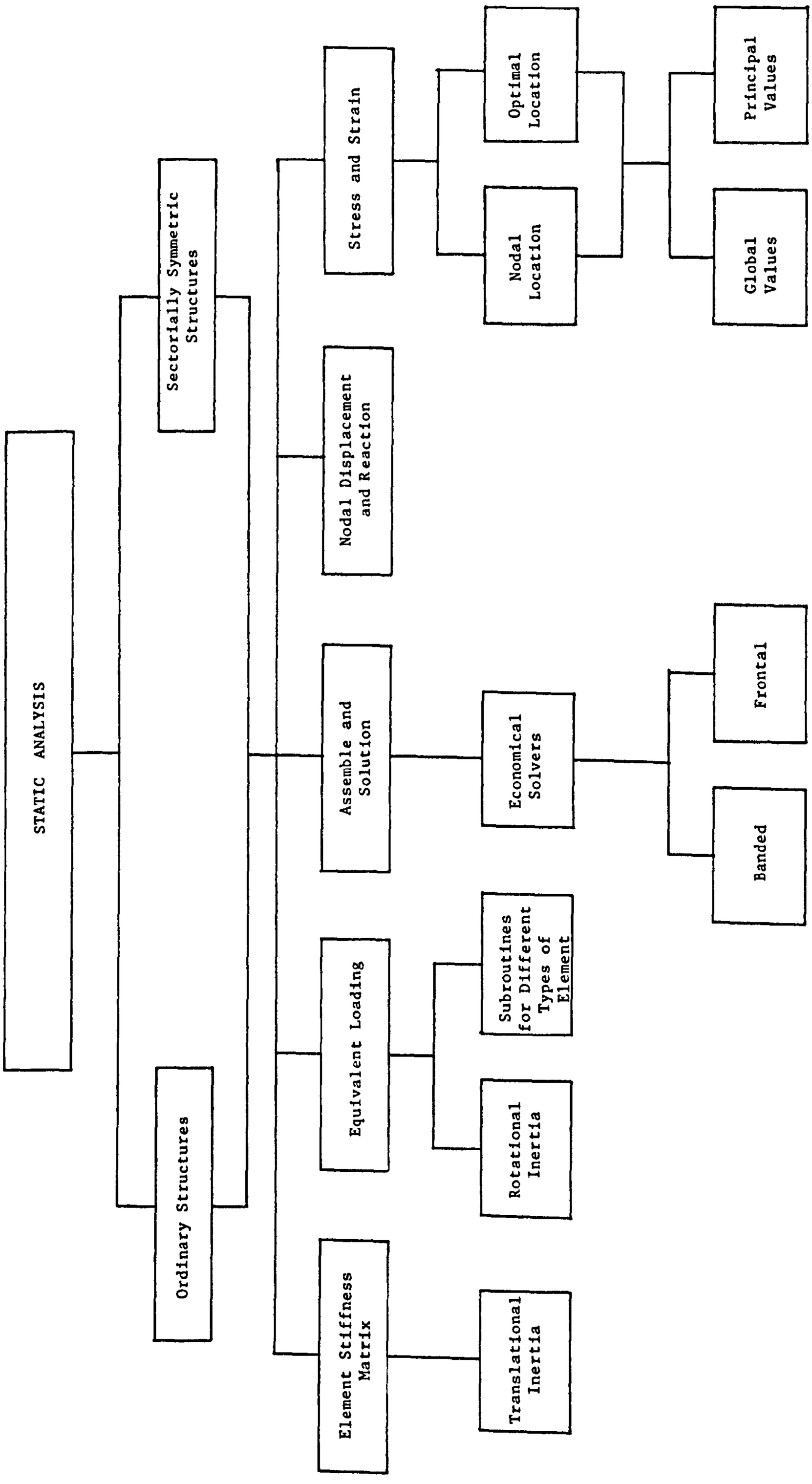

Figure 7.4 STATIC ANALYSIS MODULES

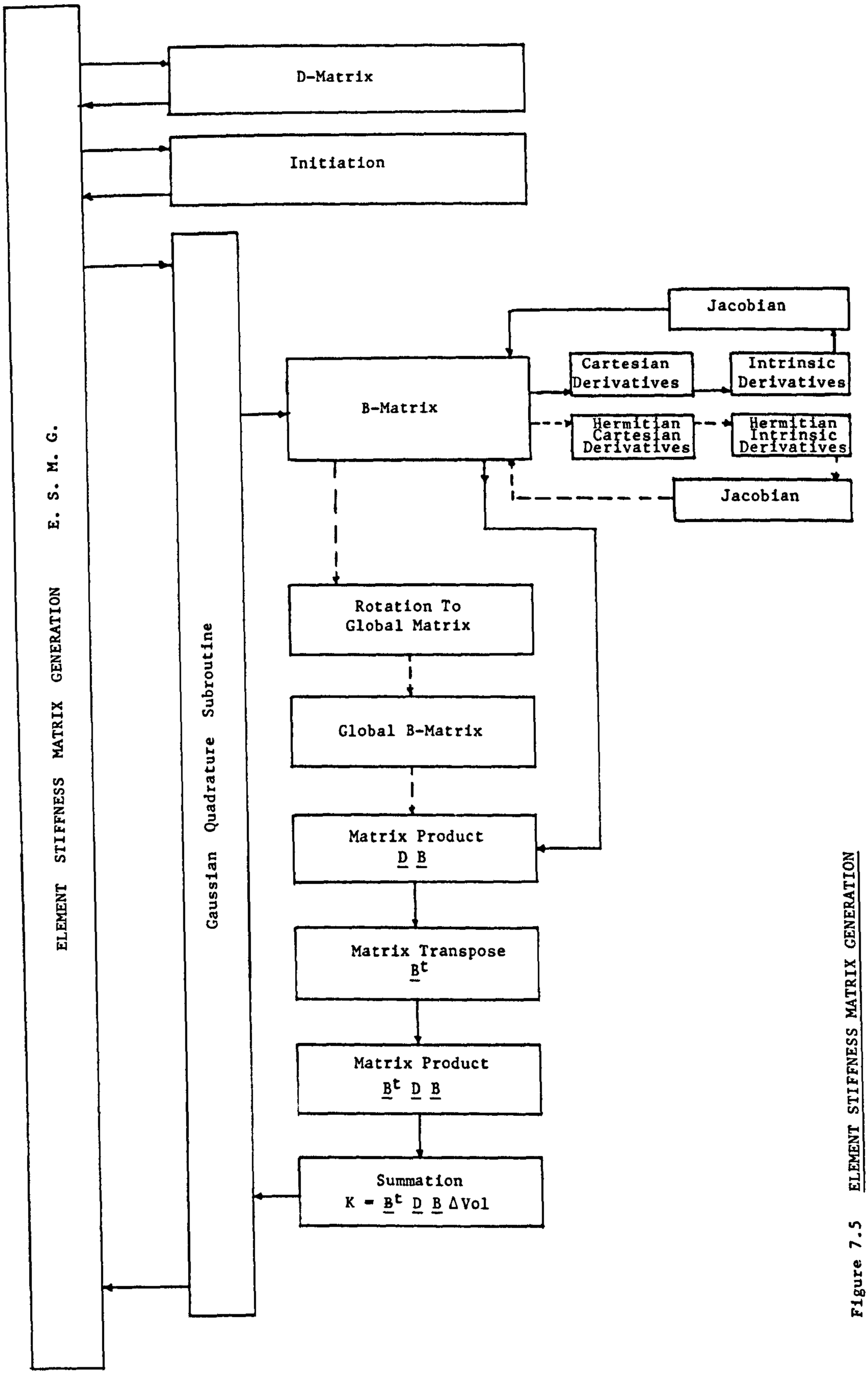

Figure 7.5 ELEMENT STIFFNESS MATRIX GENERATION

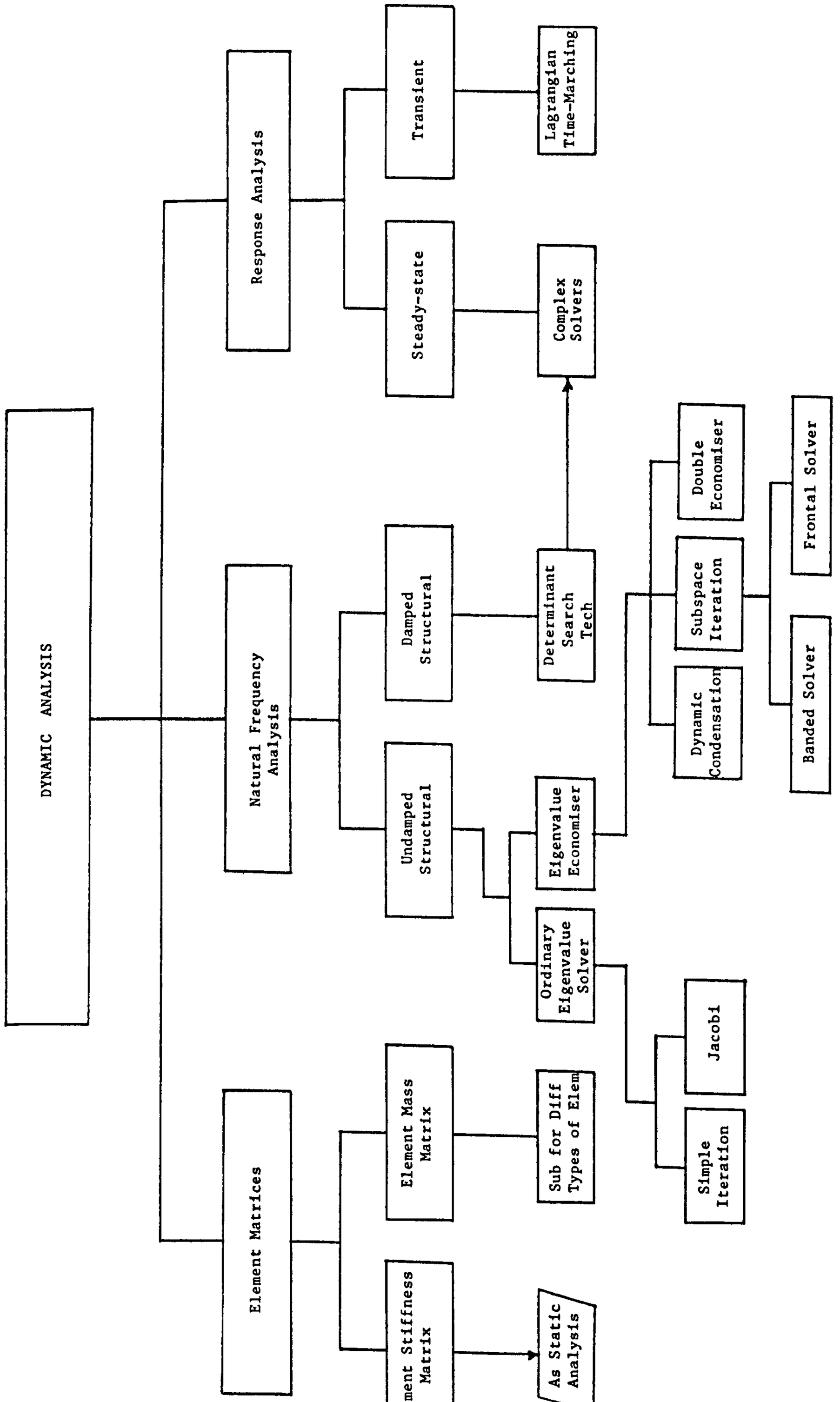

Figure 7.6 DYNAMIC ANALYSIS MODULES

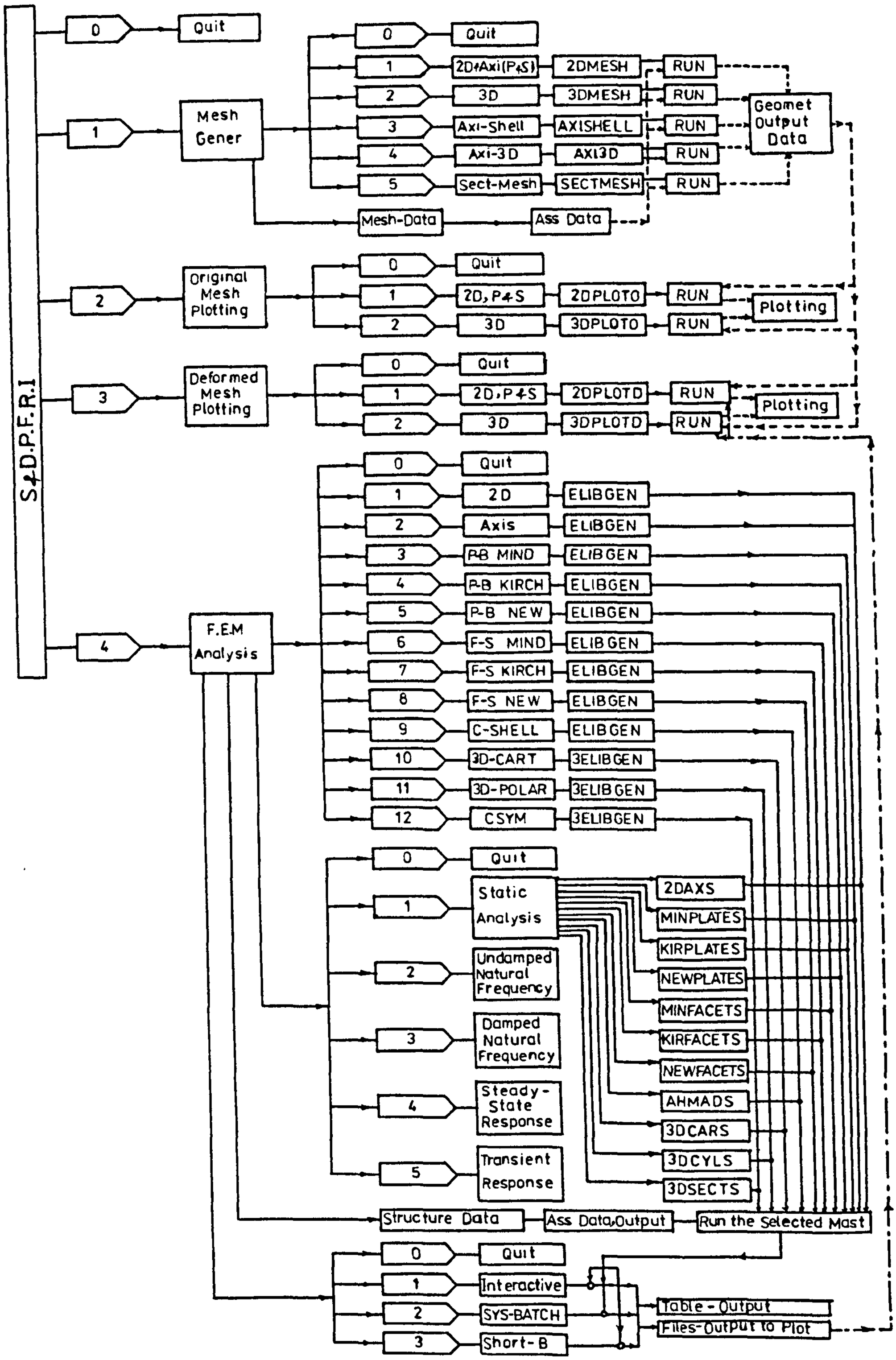

Figure 7.7 VAX Command Procedure

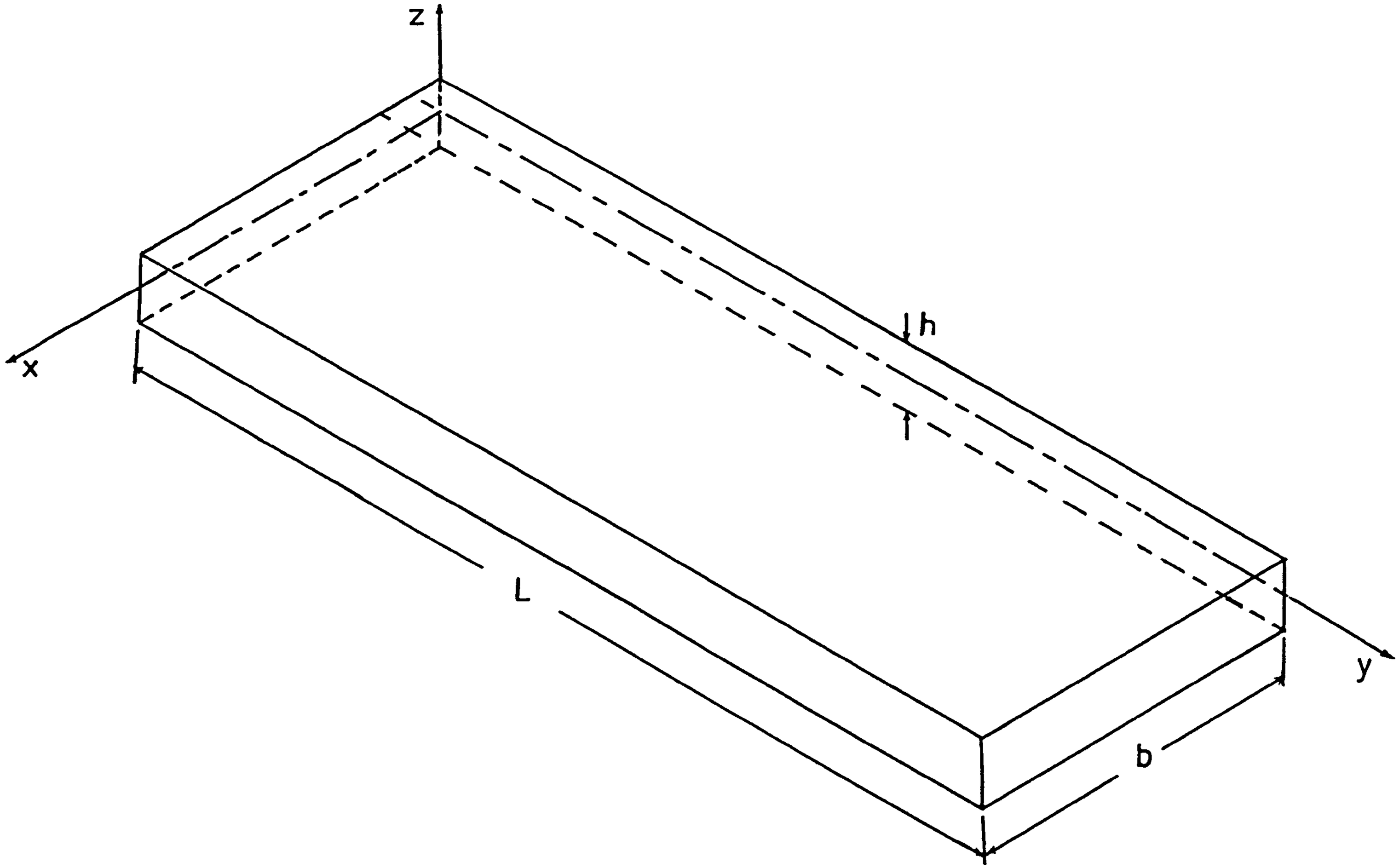

Figure (8.1) Cantilever Plate Used For Plate-Bending Element Verification.

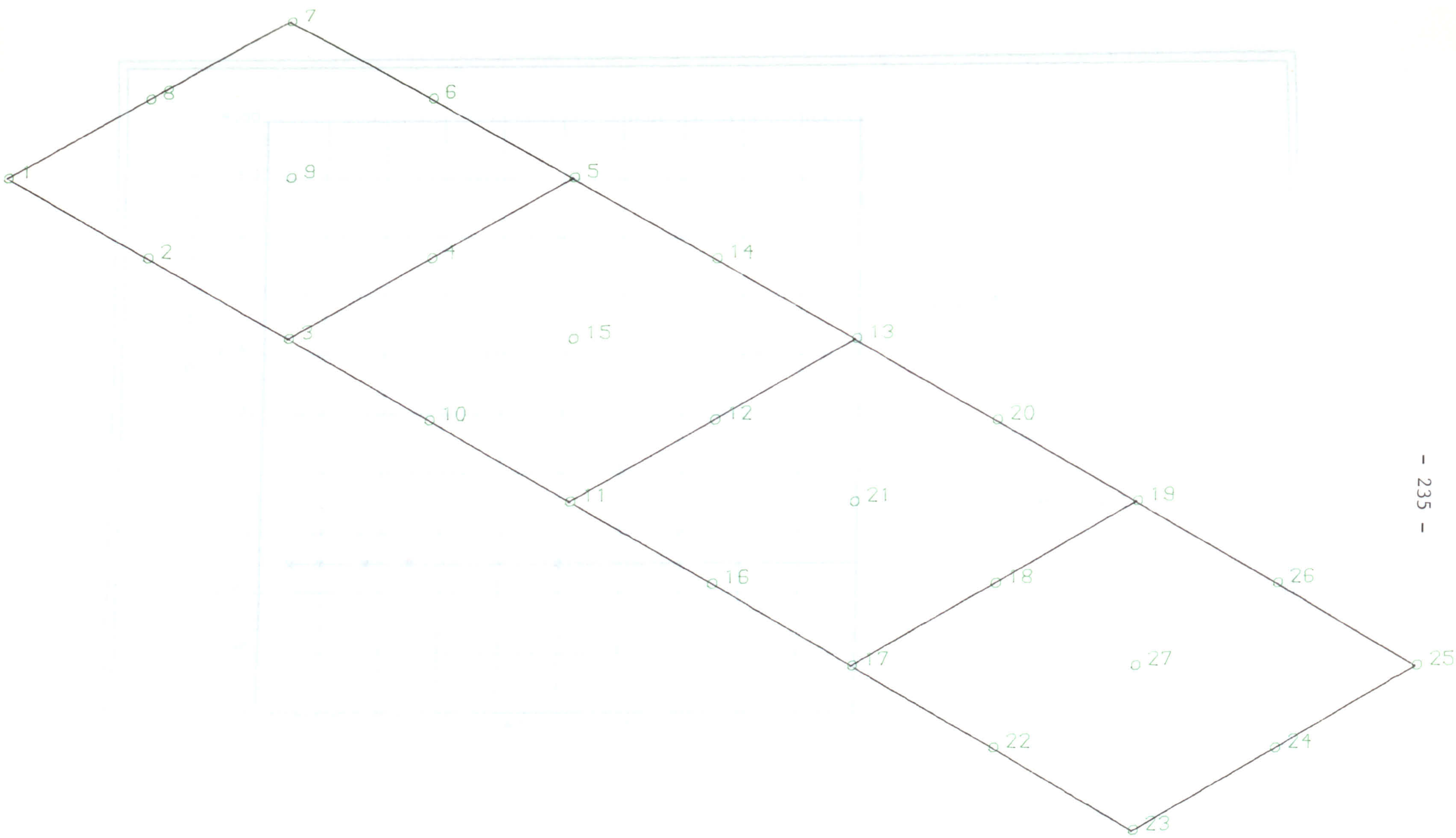

M.AZZAWI

Figure (8.2) Plate-Bending Case-Study
Using 9-Node Element.

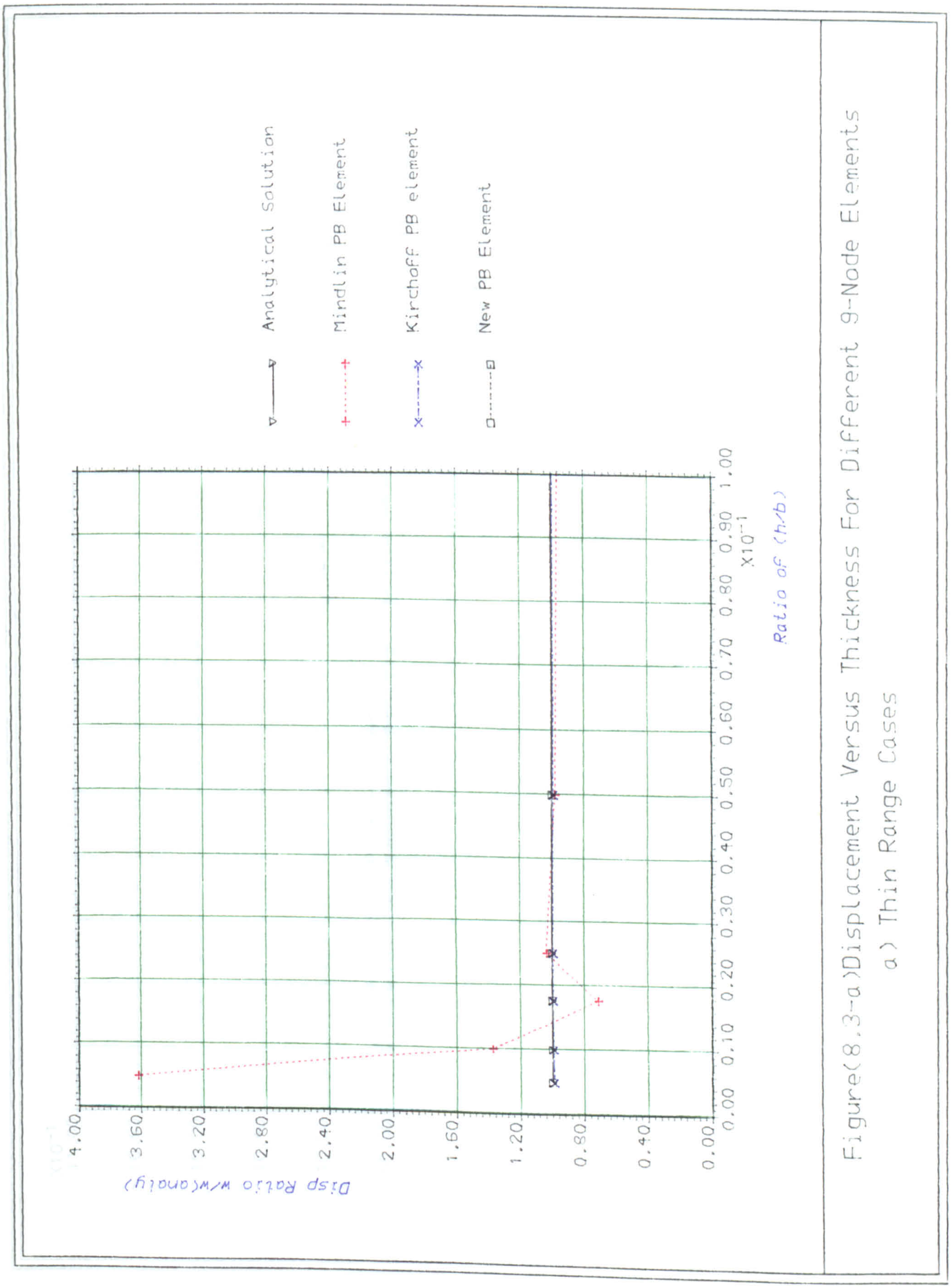

Figure(8.3-a)Displacement Versus Thickness For Different 9-Node Elements

a) Thin Range Cases

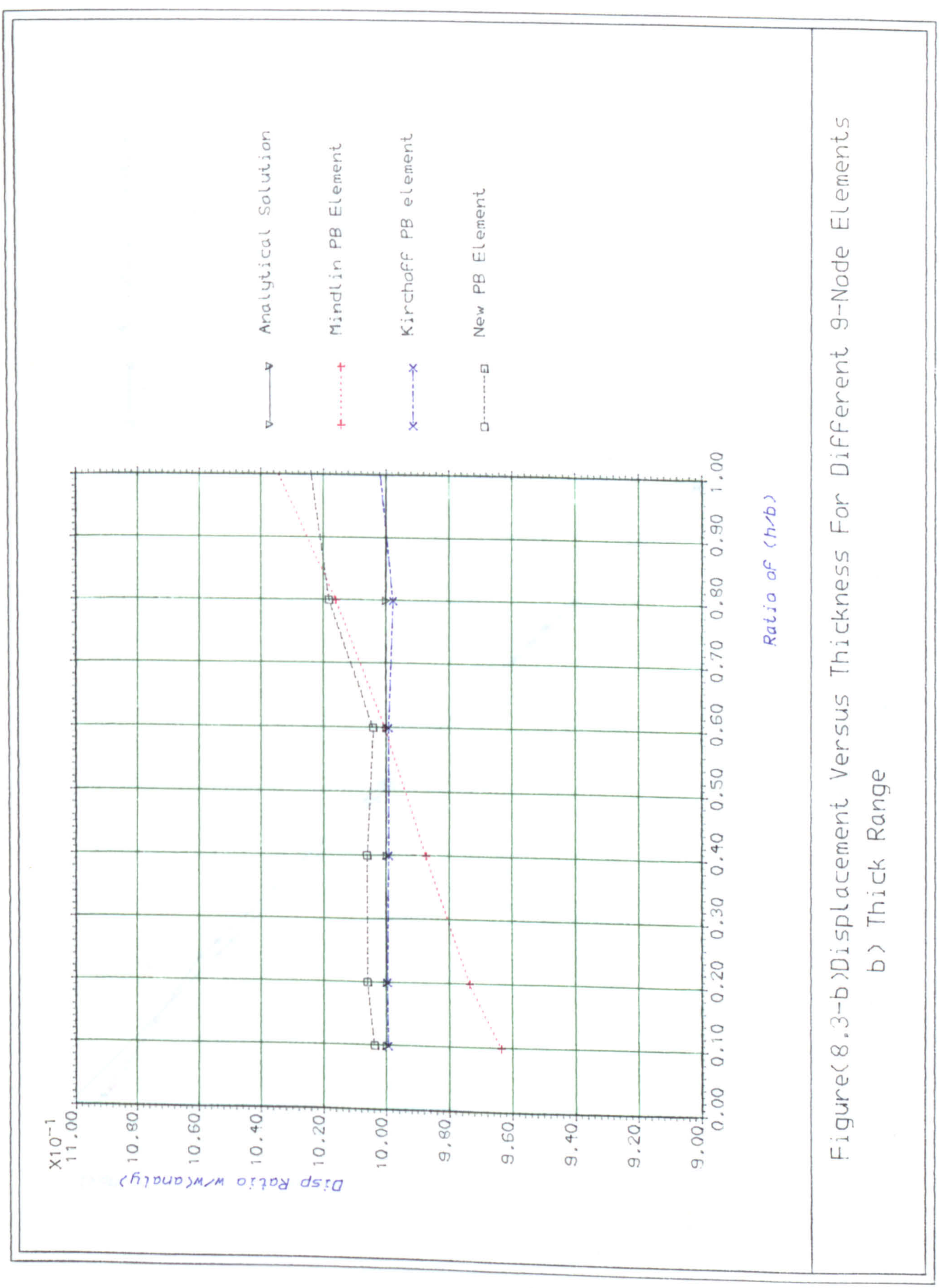

Figure(8.3-b)Displacement Versus Thickness For Different 9-Node Elements
b) Thick Range

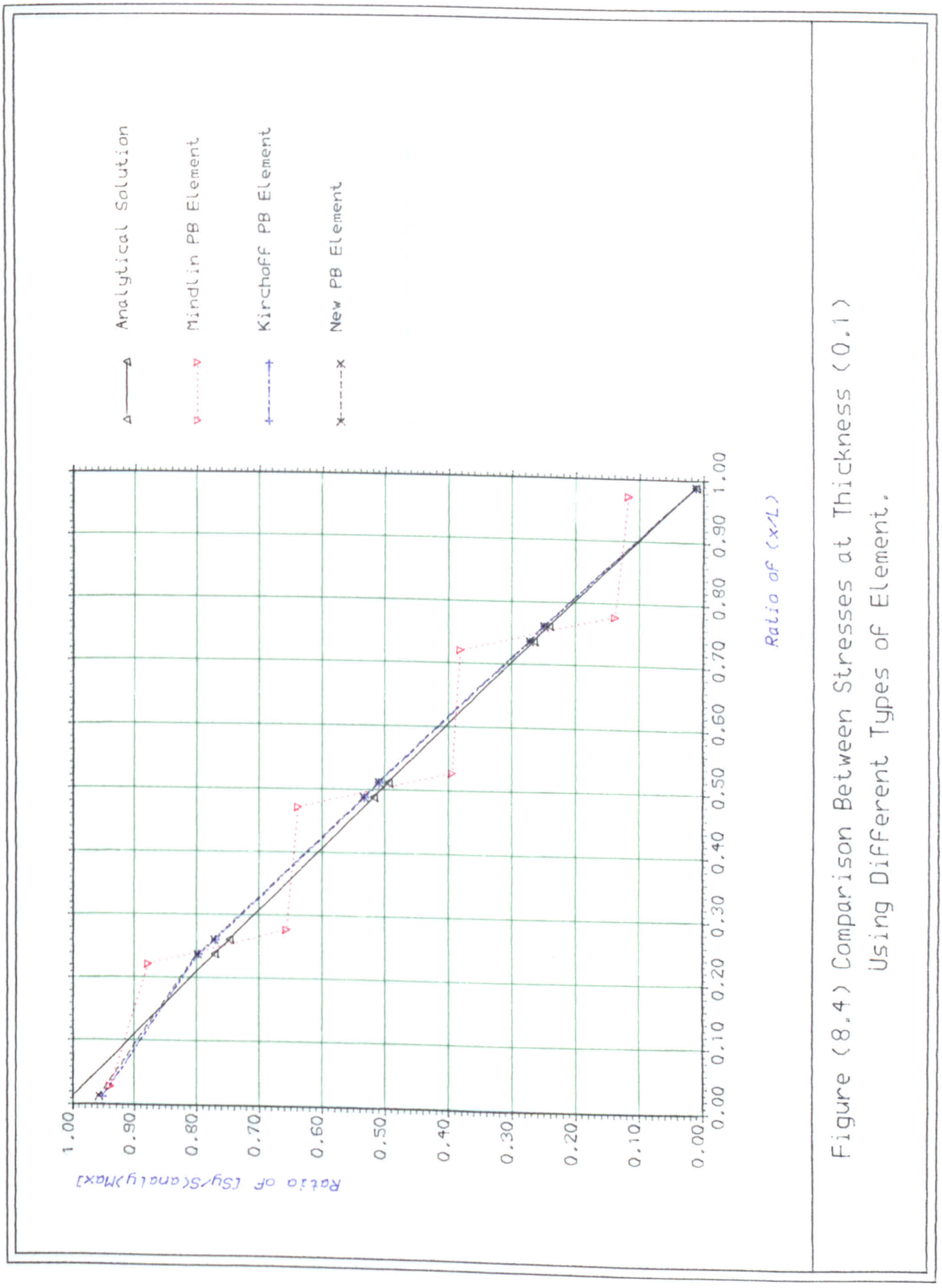

Figure (8.4) Comparison Between Stresses at Thickness (0.1) Using Different Types of Element.

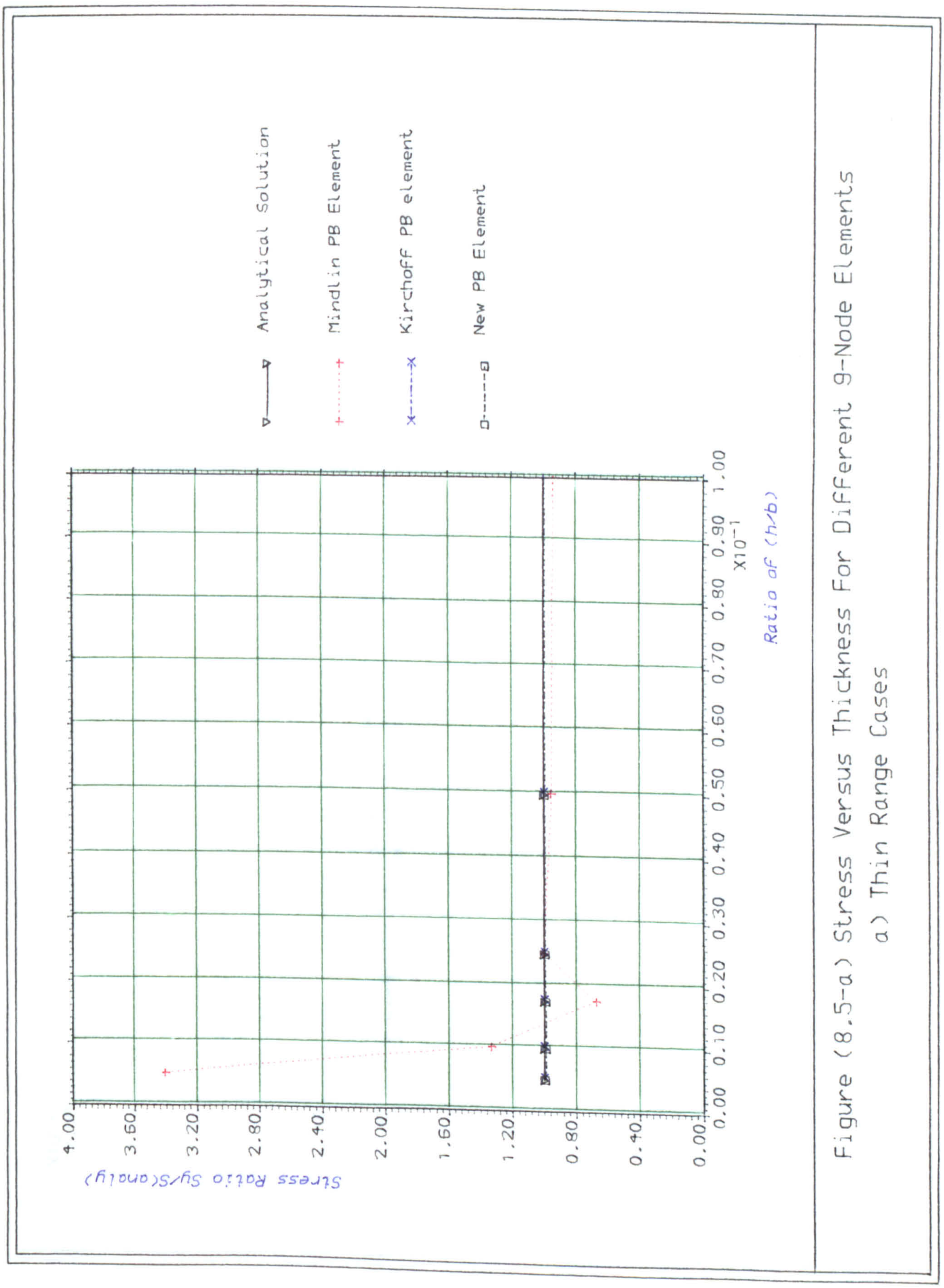

Figure (8.5-a) Stress Versus Thickness For Different 9-Node Elements

a) Thin Range Cases

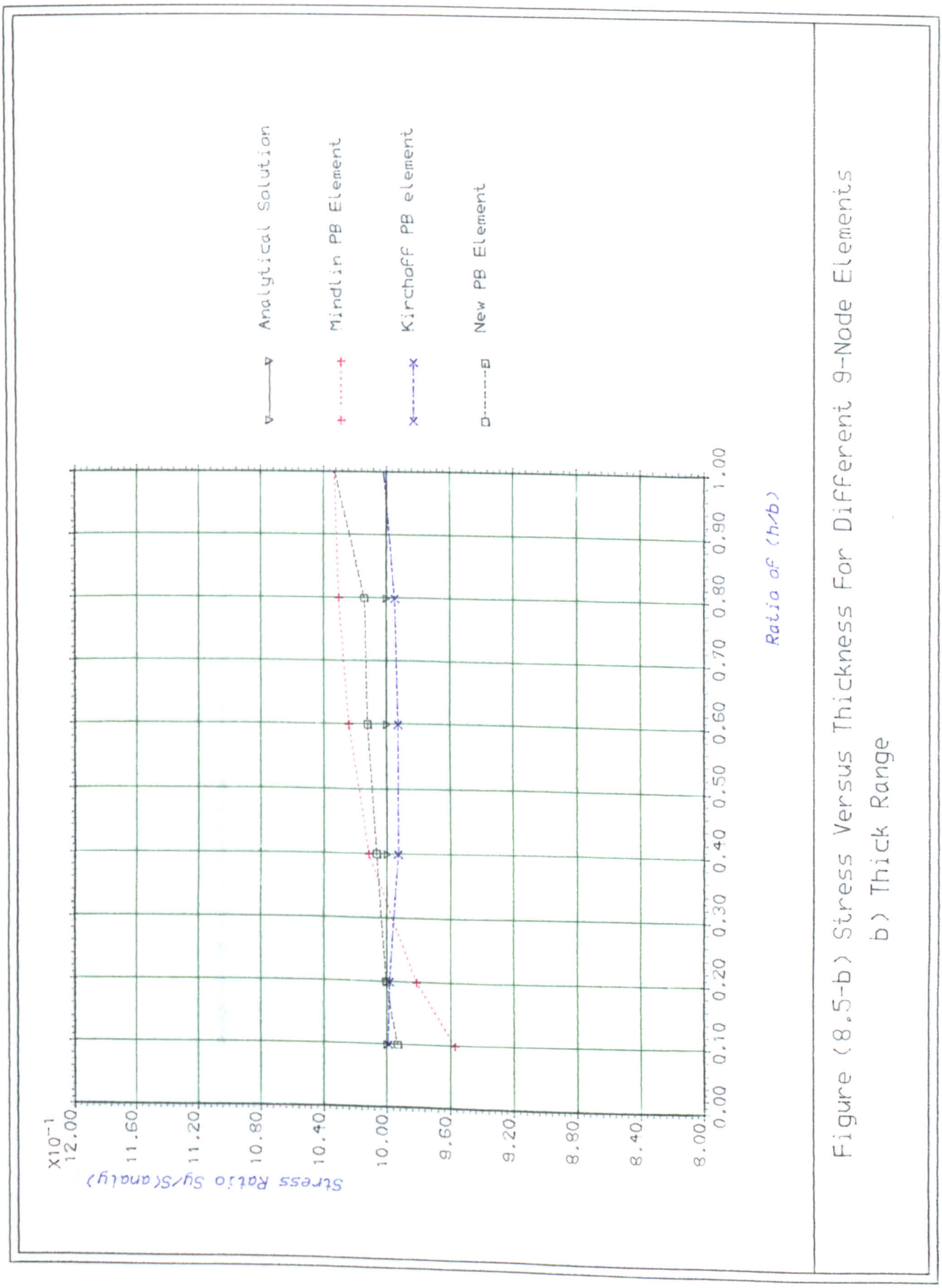

Figure (8.5-b) Stress Versus Thickness For Different 9-Node Elements

b) Thick Range

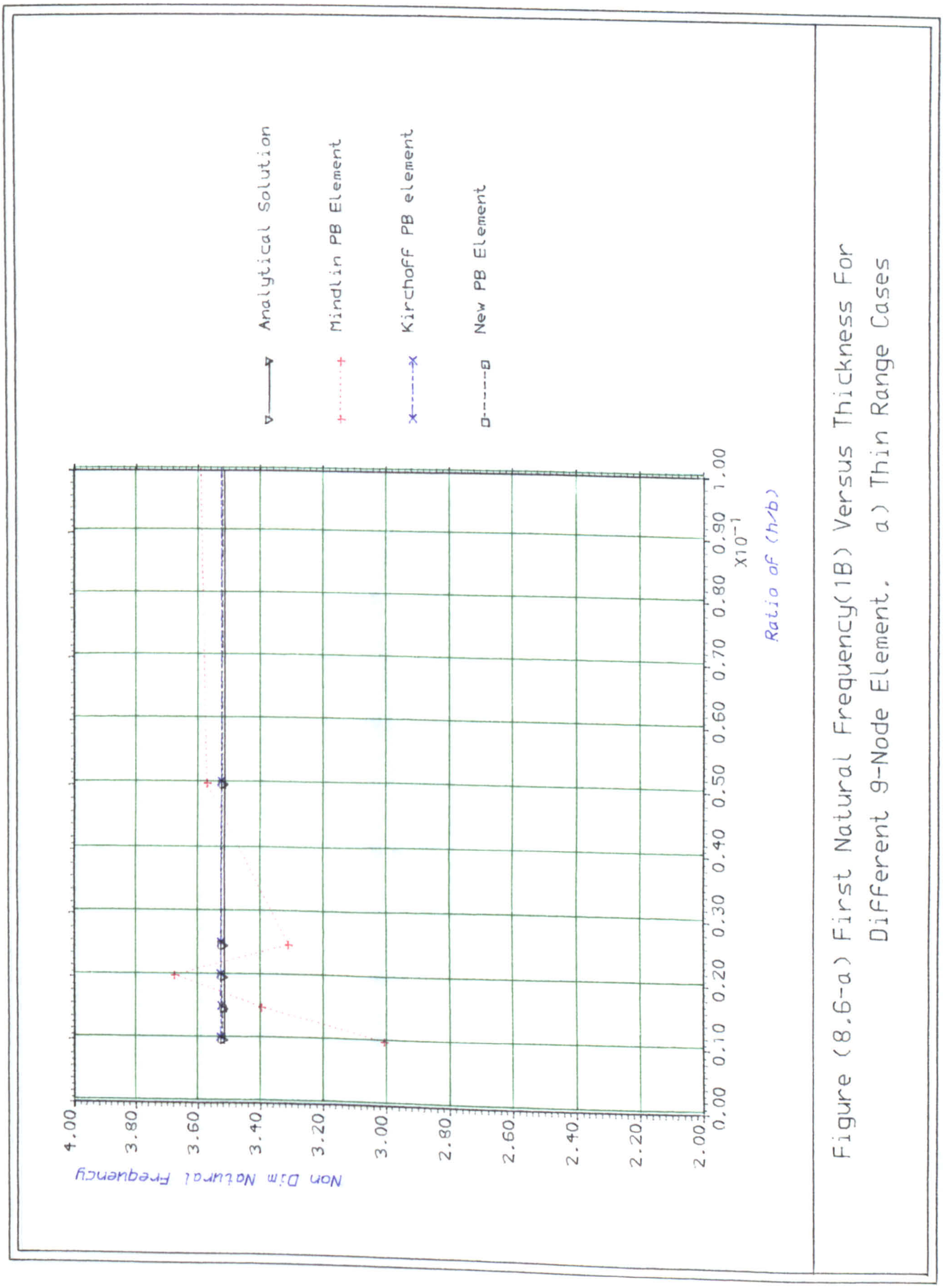

Figure (8.6-a) First Natural Frequency(1B) Versus Thickness For Different 9-Node Element. a) Thin Range Cases

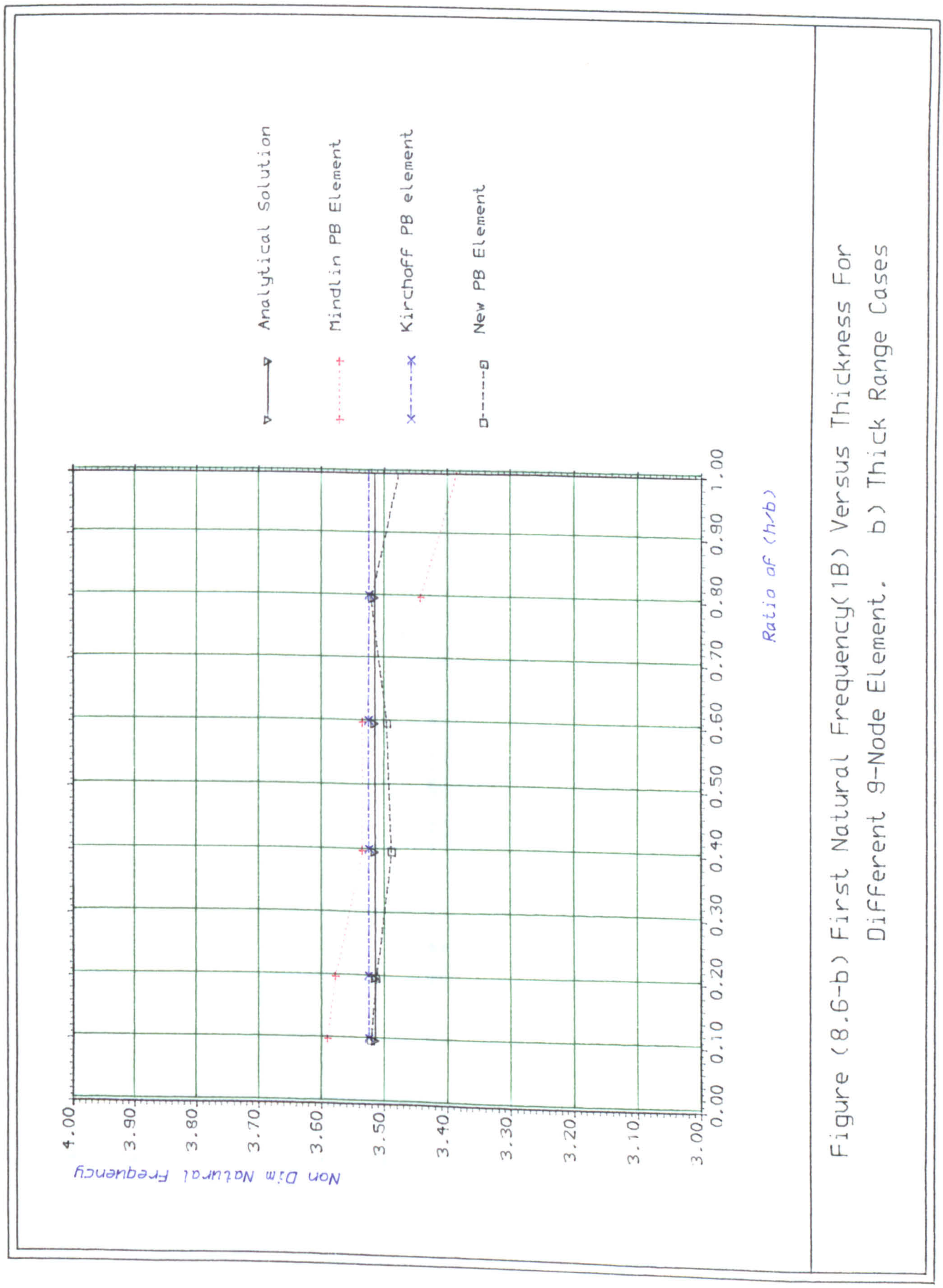

Figure (8.6-b) First Natural Frequency(1B) Versus Thickness For Different 9-Node Element. a) Thick Range Cases b) Thick Range Cases

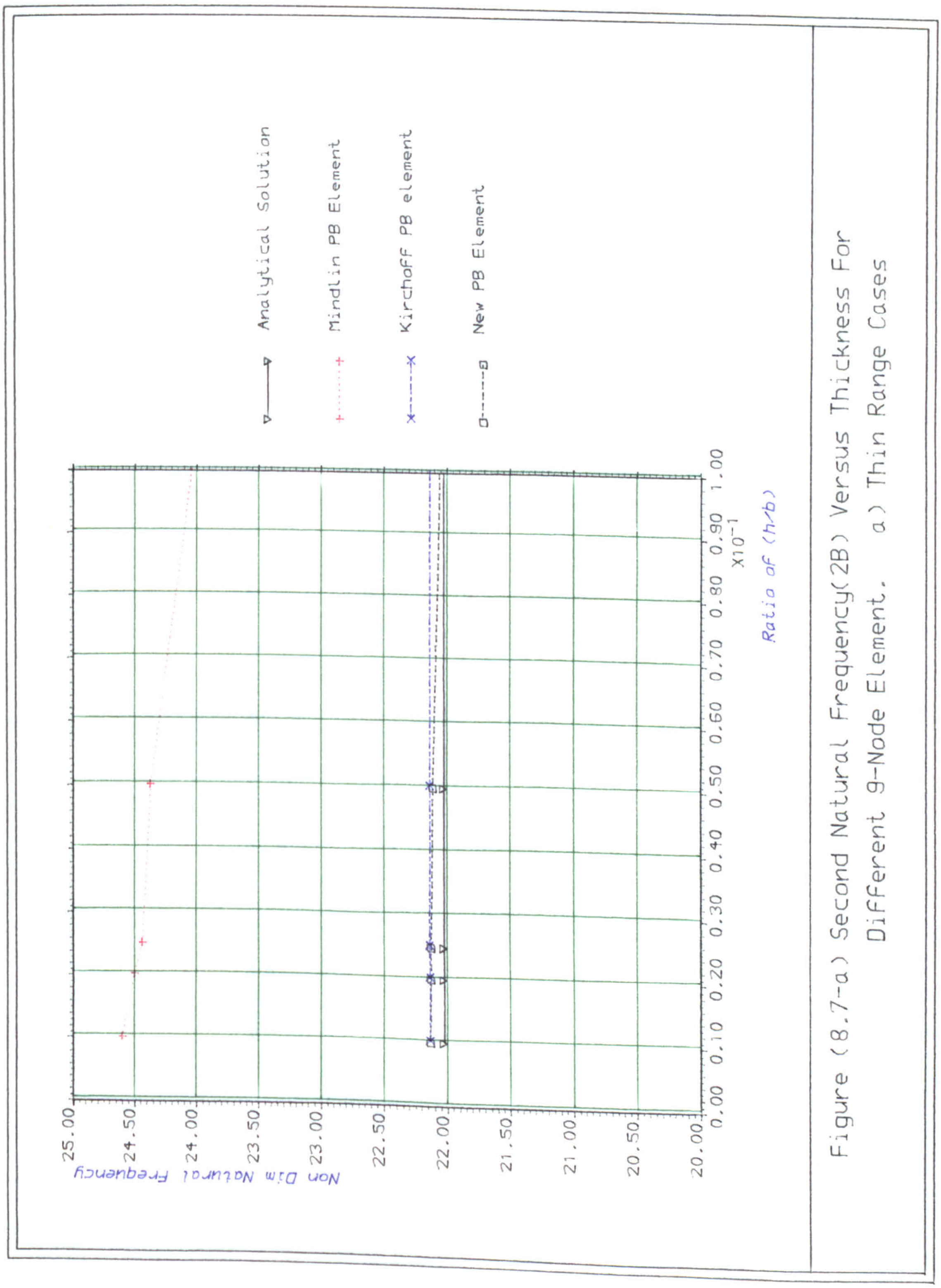

Figure (8.7-a) Second Natural Frequency(2B) Versus Thickness For Different 9-Node Element. a) Thin Range Cases

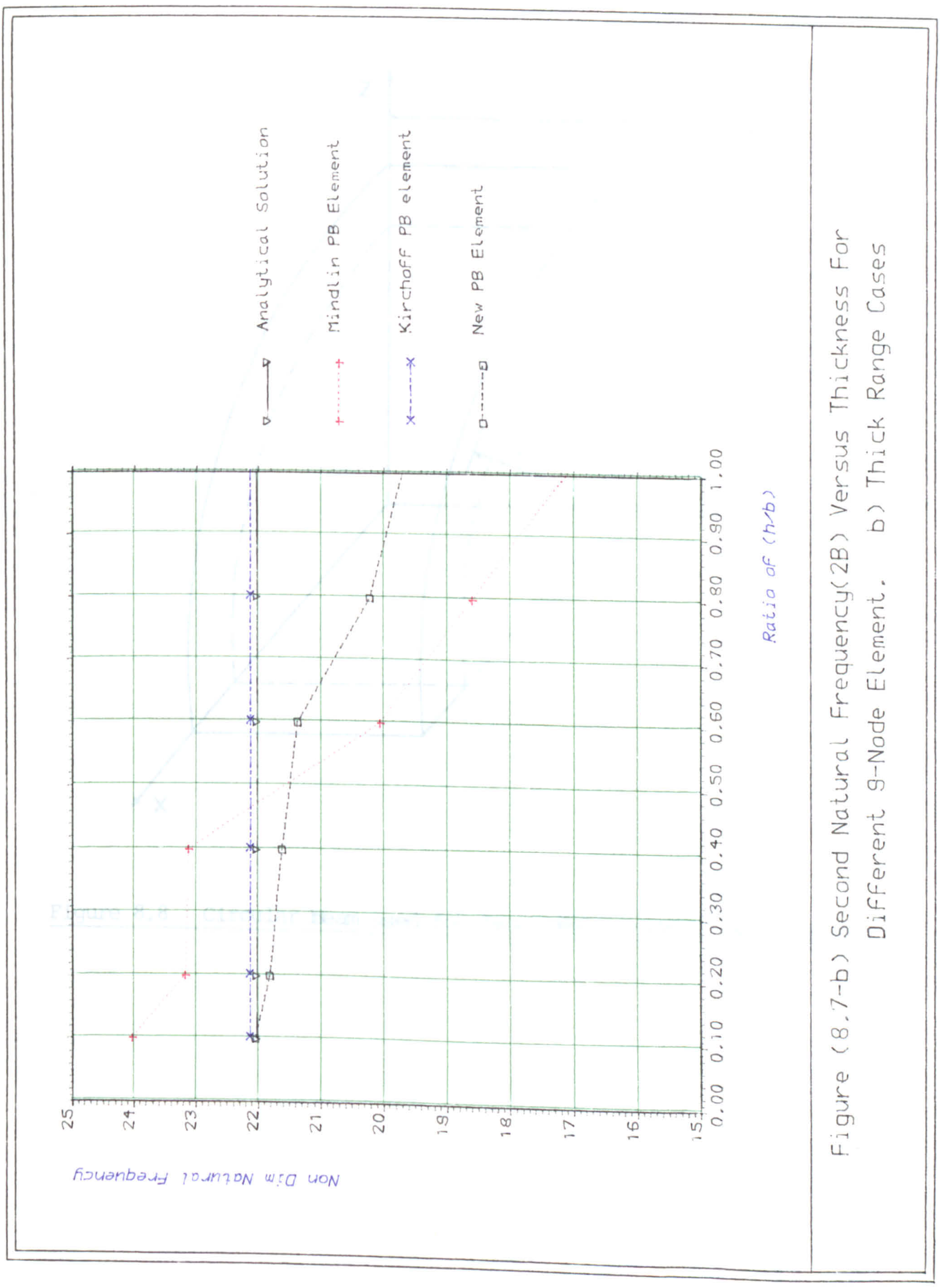

Figure (8.7-b) Second Natural Frequency(2B) Versus Thickness For Different 9-Node Element. b) Thick Range Cases

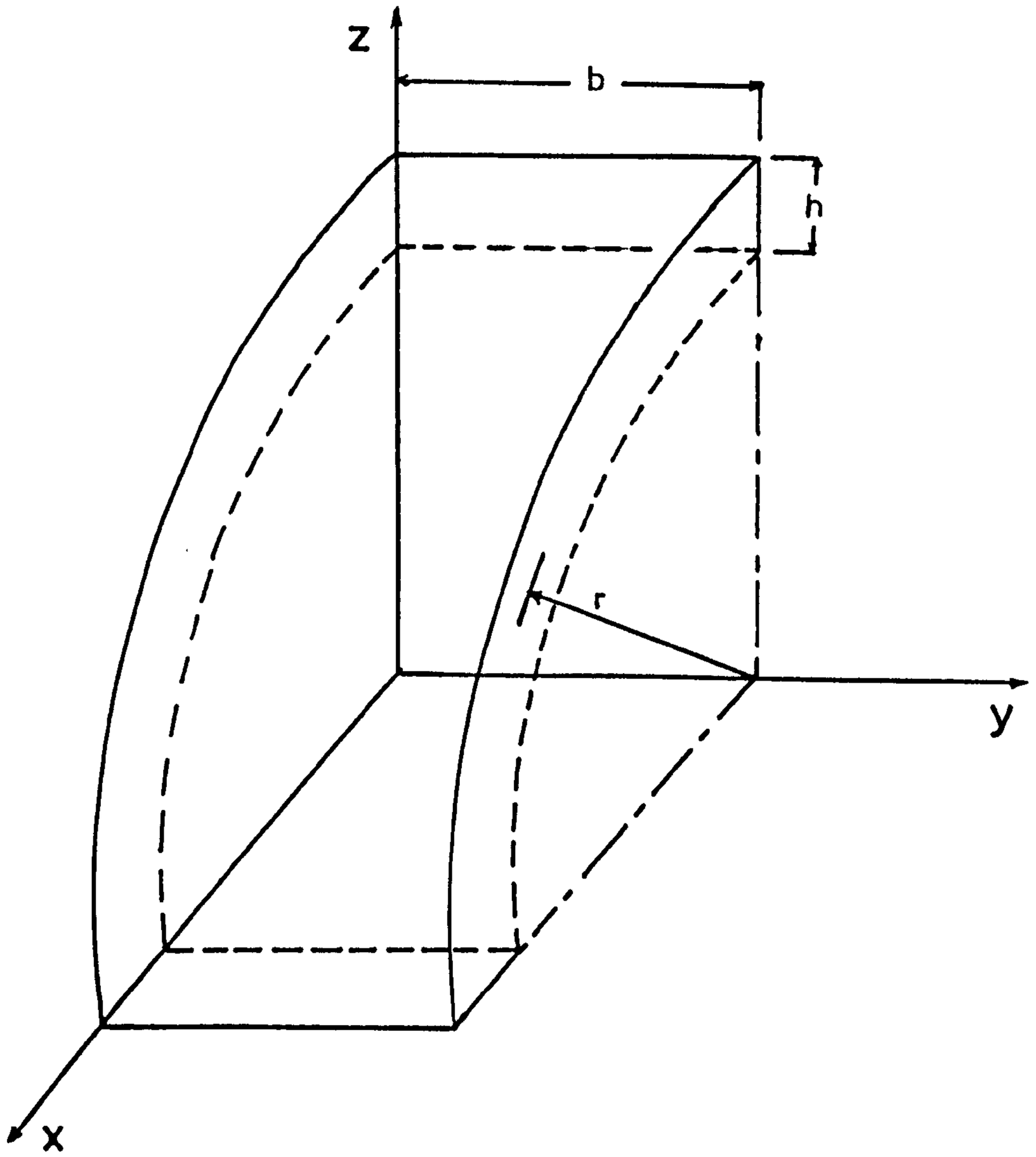

Figure 8.8 Circular beam used for facet-shell element verification

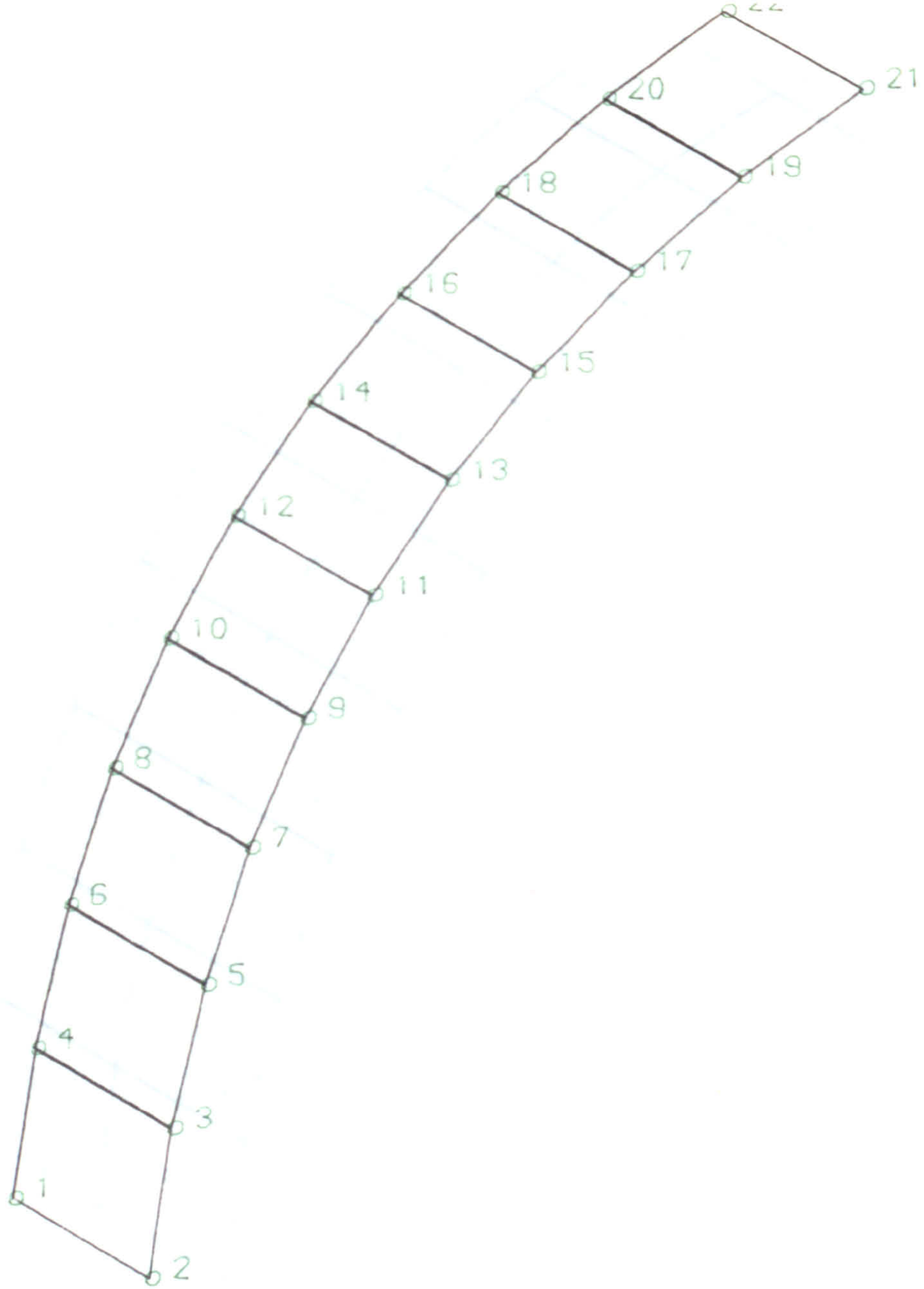

M.AZZAWI

Figure (8.9) Circular Beam Case-Study
Using 4-Node Element.

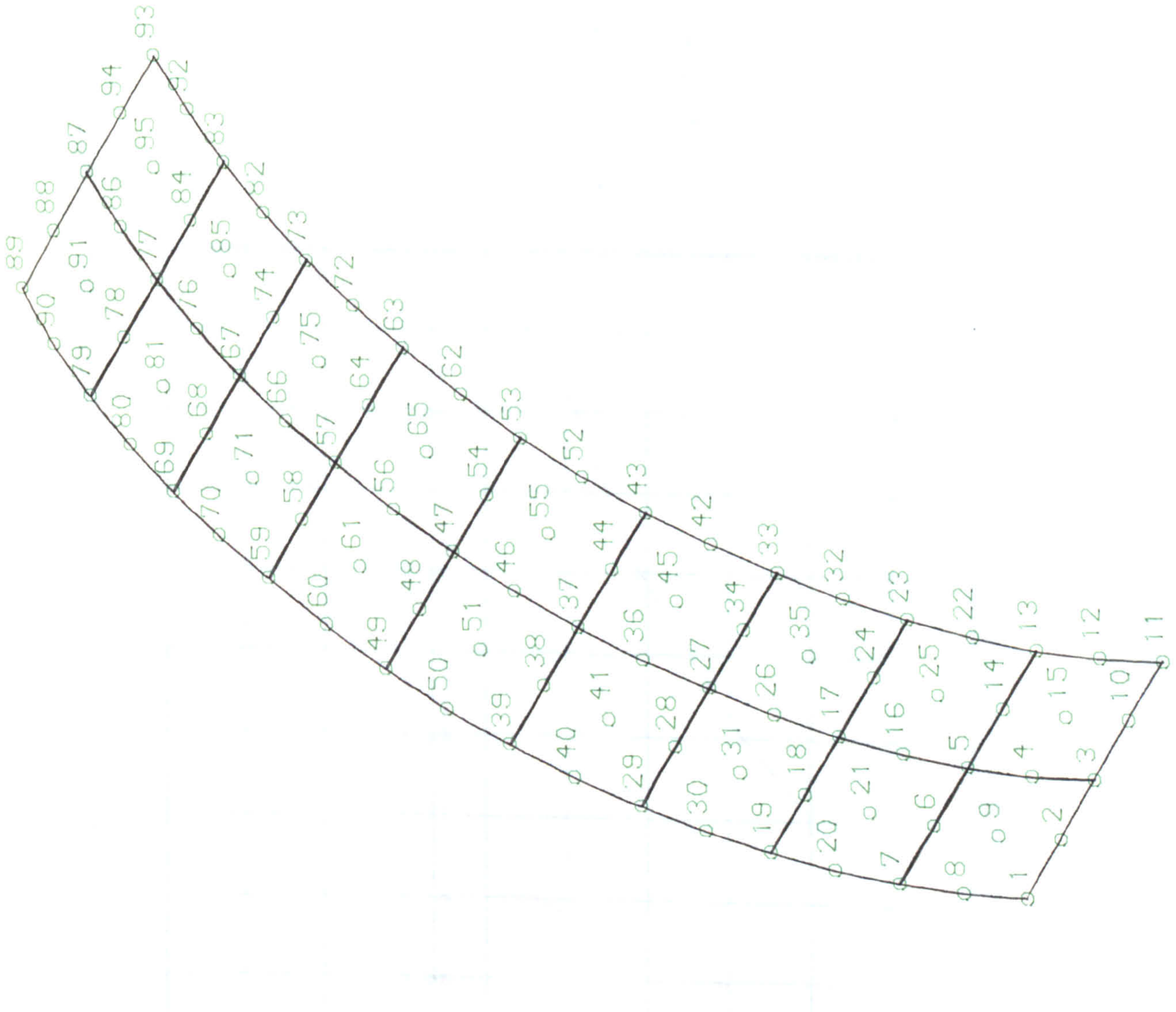

Figure (8.10) Circular Beam Case-Study
Using 9-Node Element.

M.AZZAM

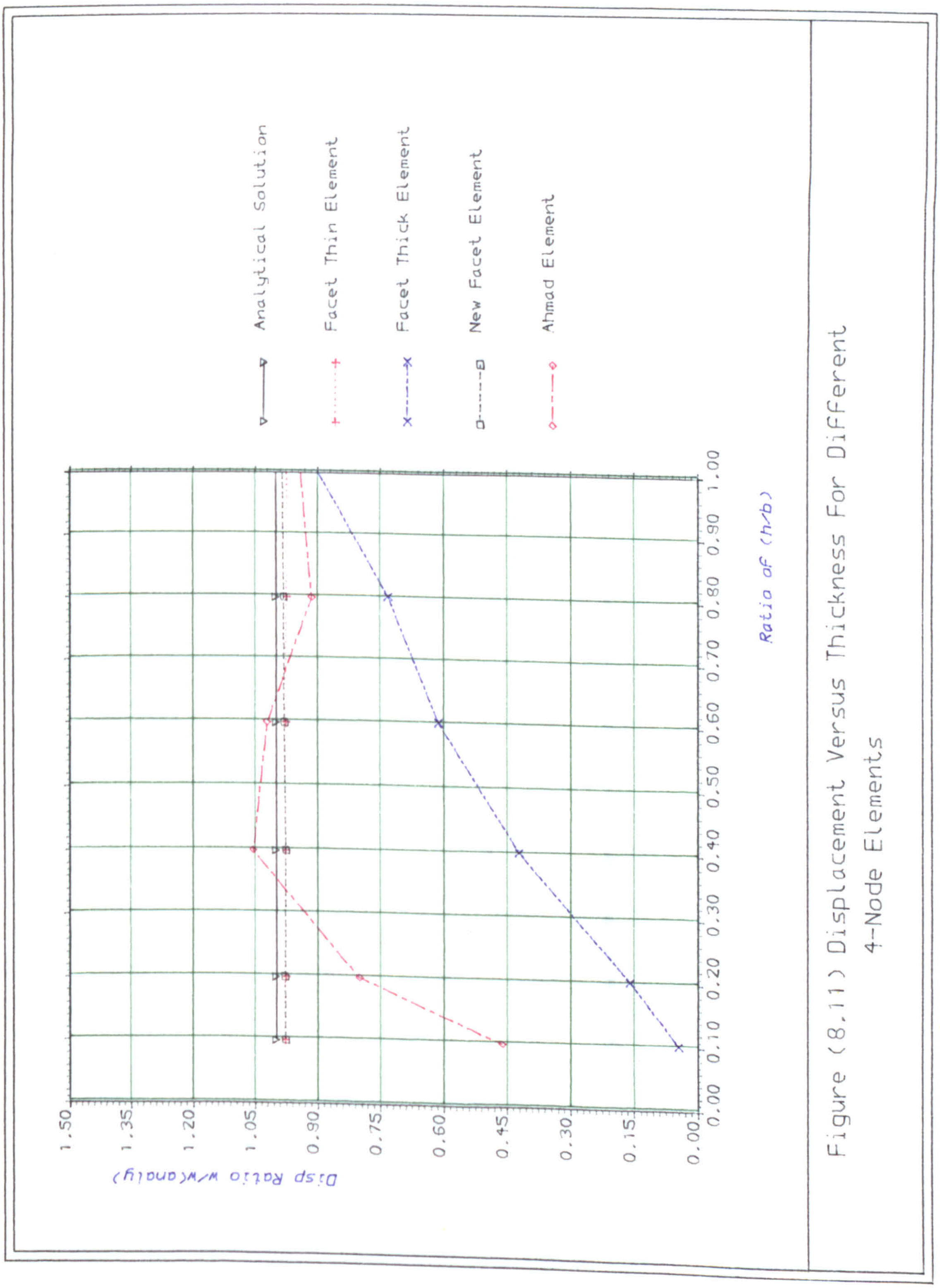

Figure (8.11) Displacement Versus Thickness For Different 4-Node Elements

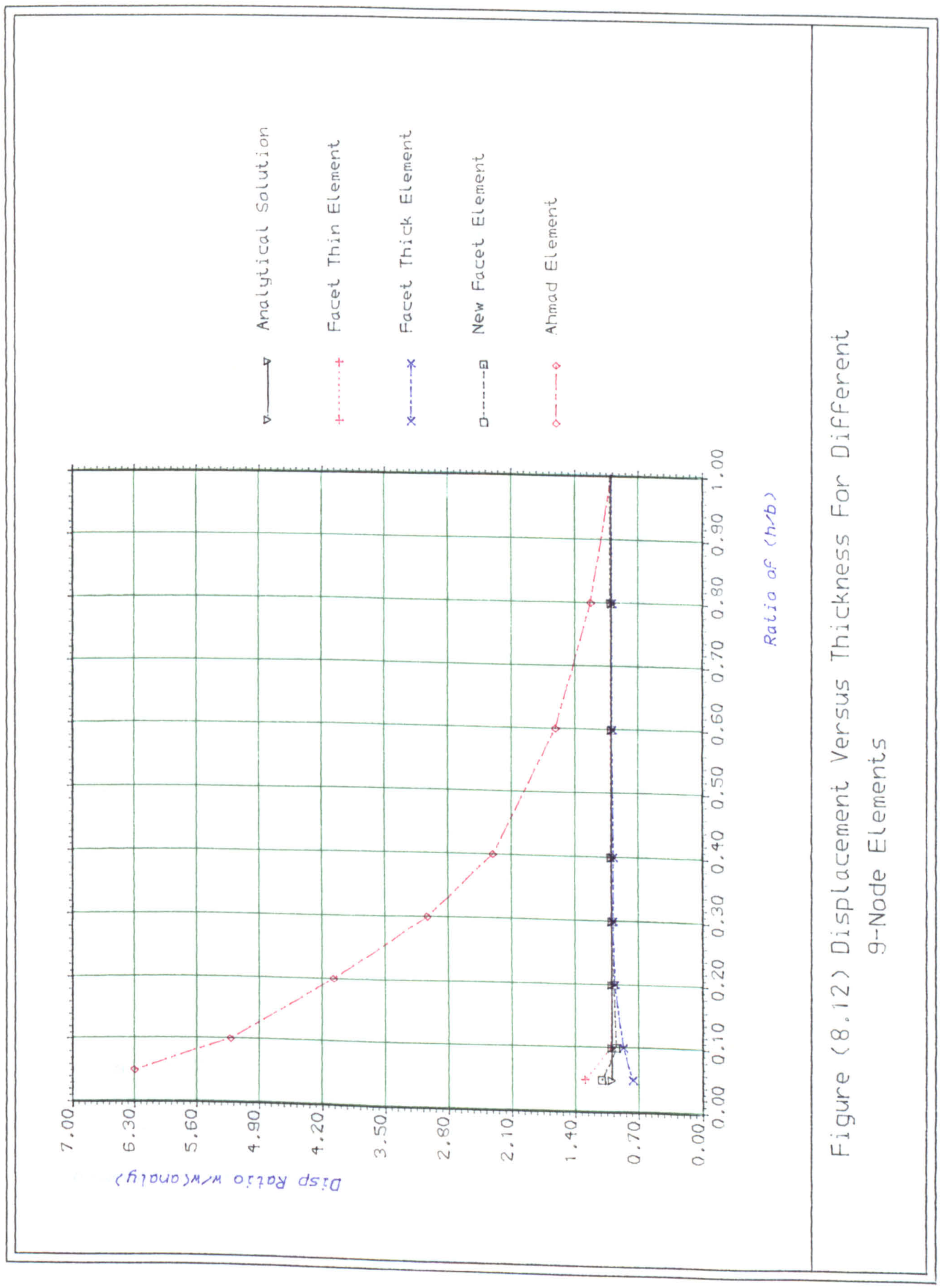

Figure (8.12) Displacement Versus Thickness For Different 9-Node Elements

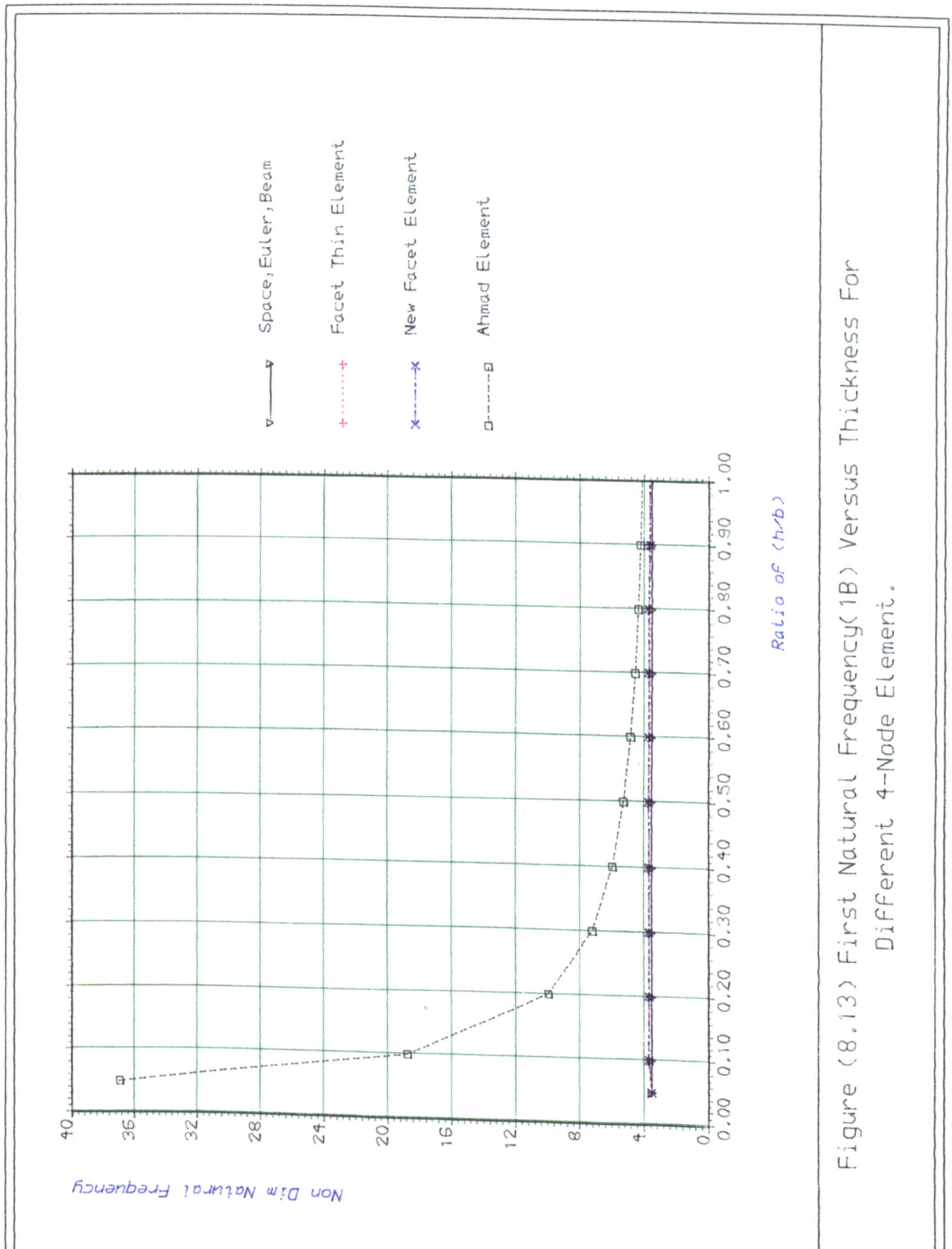

Figure (8.13) First Natural Frequency(1B) Versus Thickness For Different 4-Node Element.

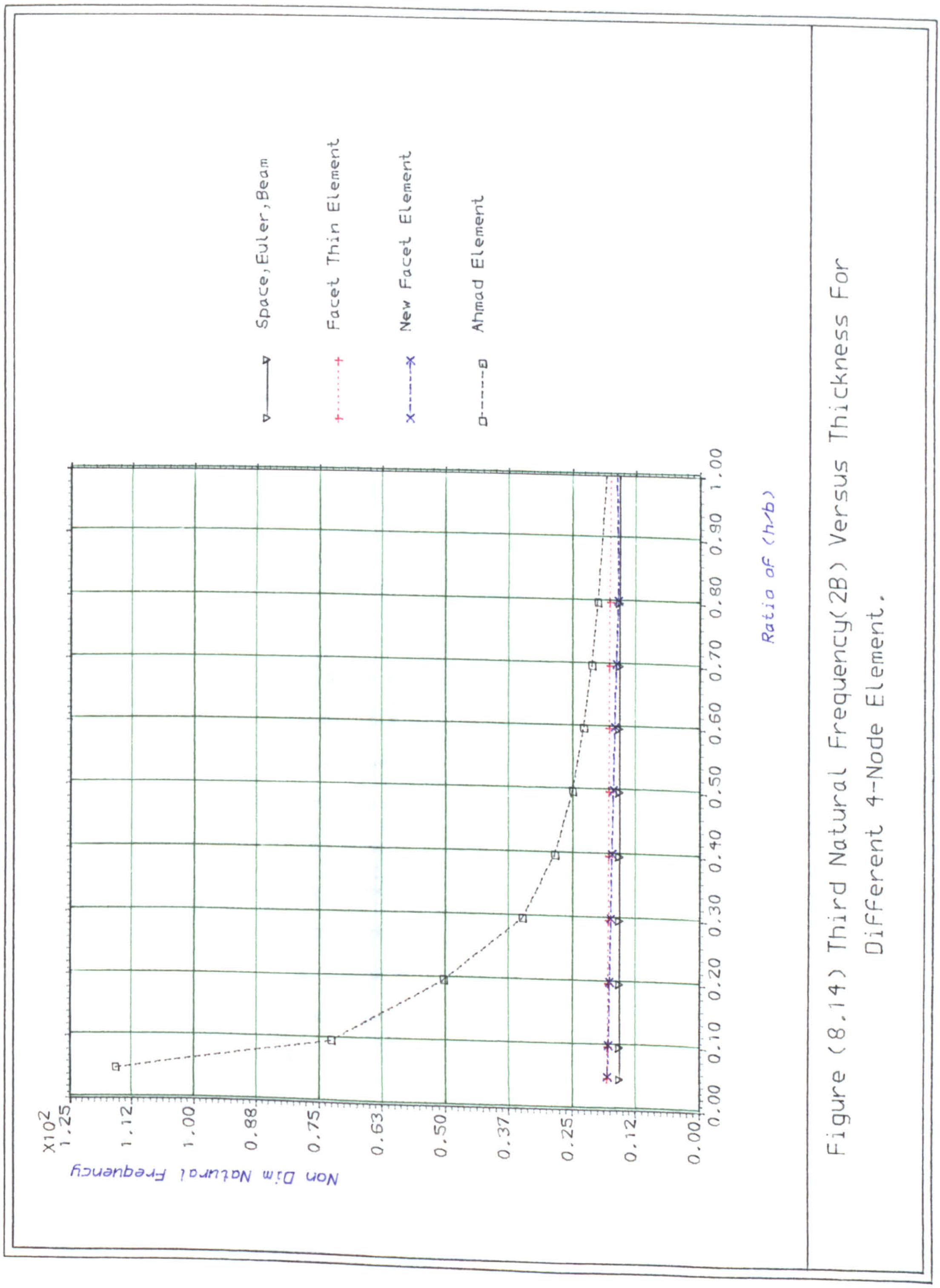

Figure (8.14) Third Natural Frequency(2B) Versus Thickness For Different 4-Node Element.

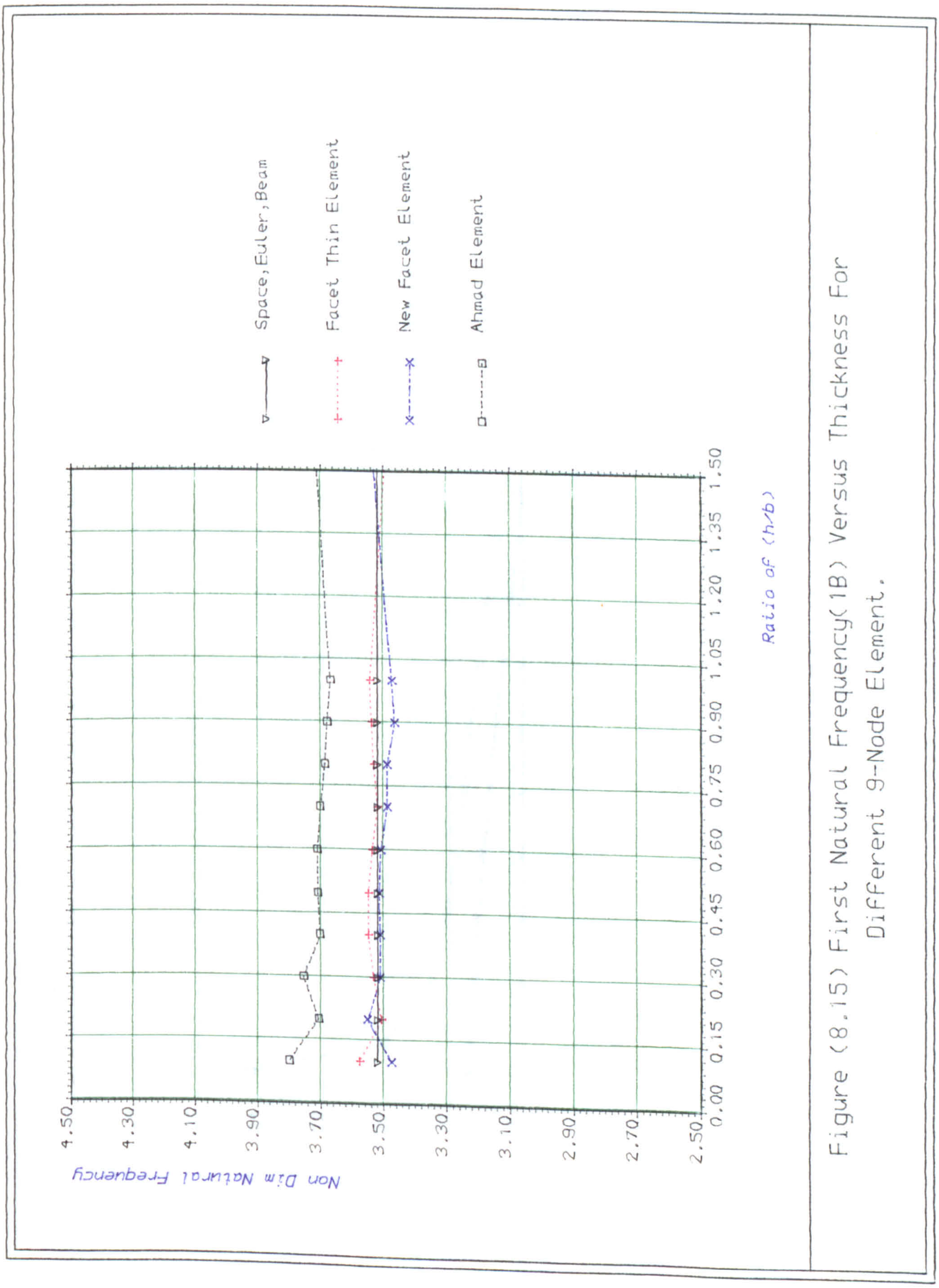

Figure (8.15) First Natural Frequency(1B) Versus Thickness For Different 9-Node Element.

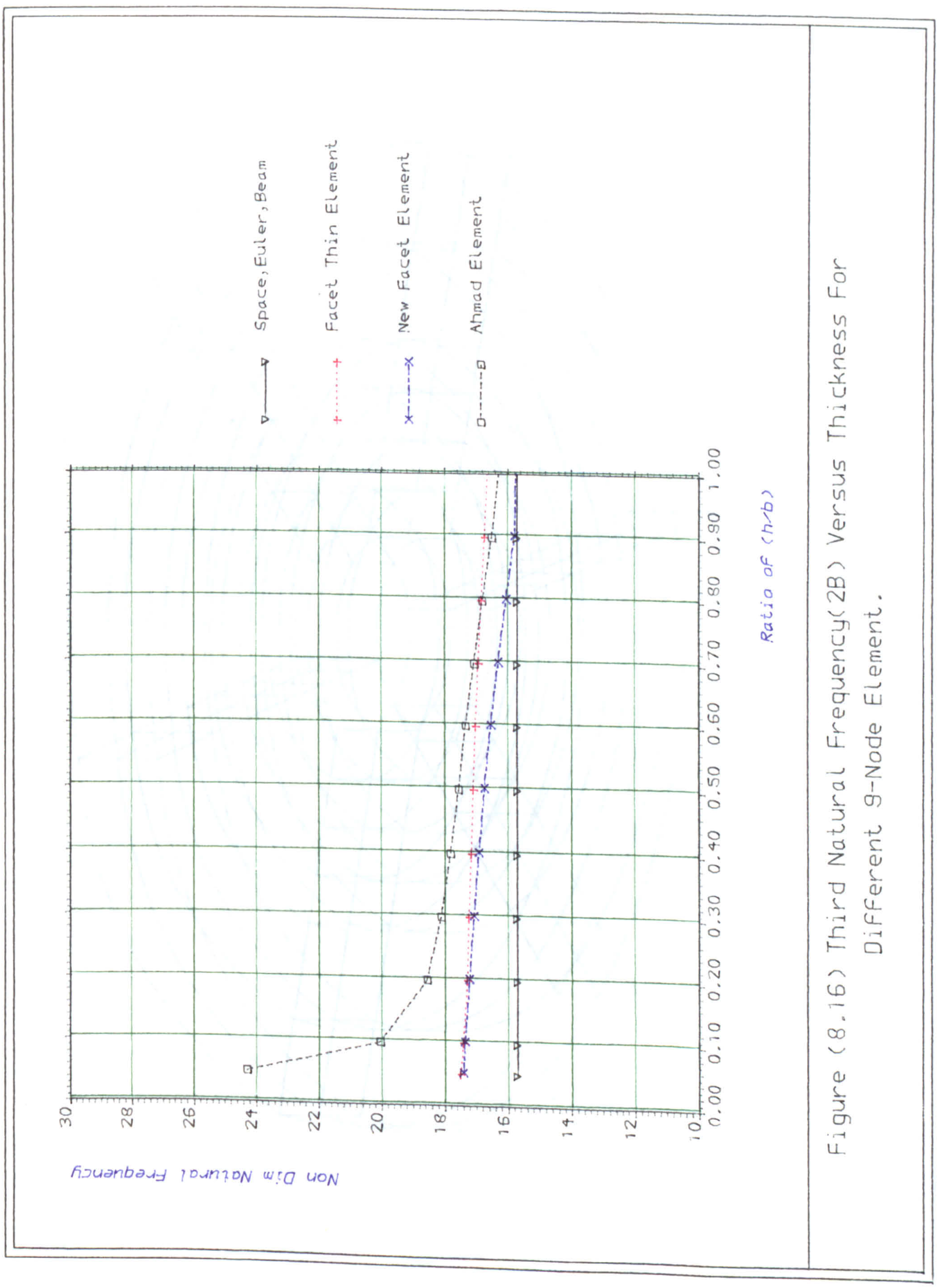

Figure (8.16) Third Natural Frequency(2B) Versus Thickness For Different 9-Node Element.

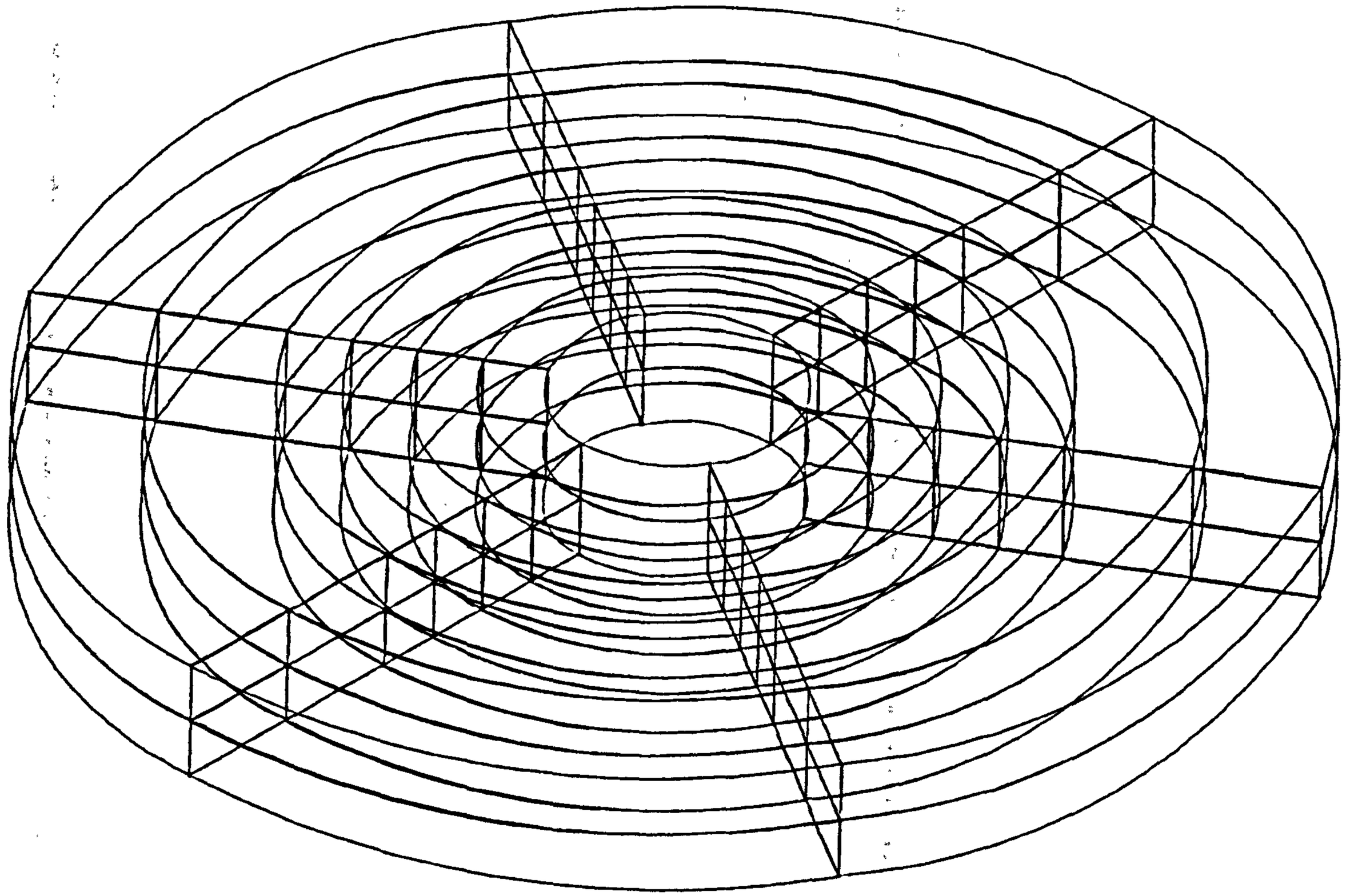

M.AZZAWI

Figure (8.17) Three-Dimensional Mesh For Disc
Using 20-Node Brick Elements.

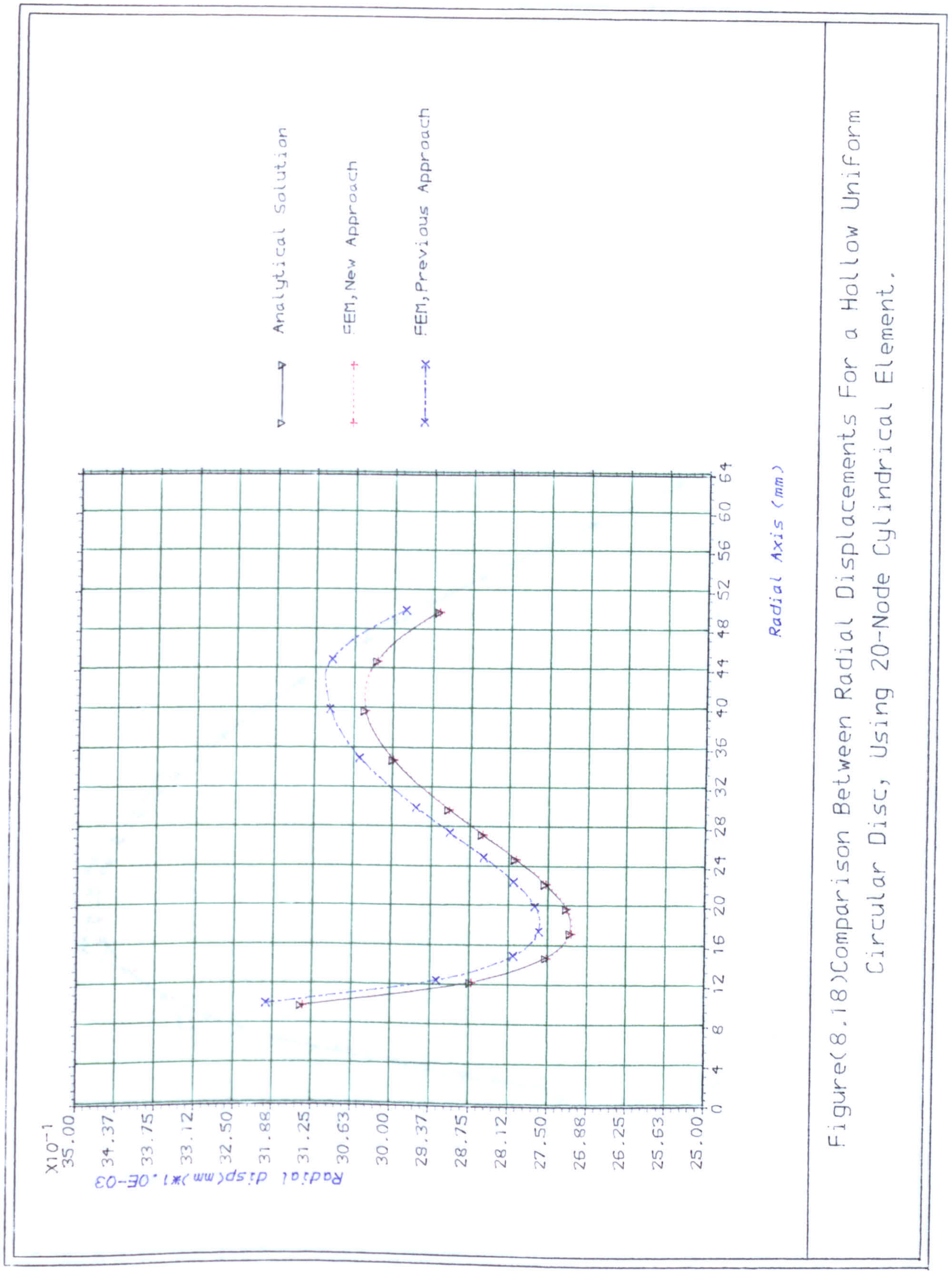

Figure(8.18)Comparison Between Radial Displacements For a Hollow Circular Disc, Using 20-Node Cylindrical Element.

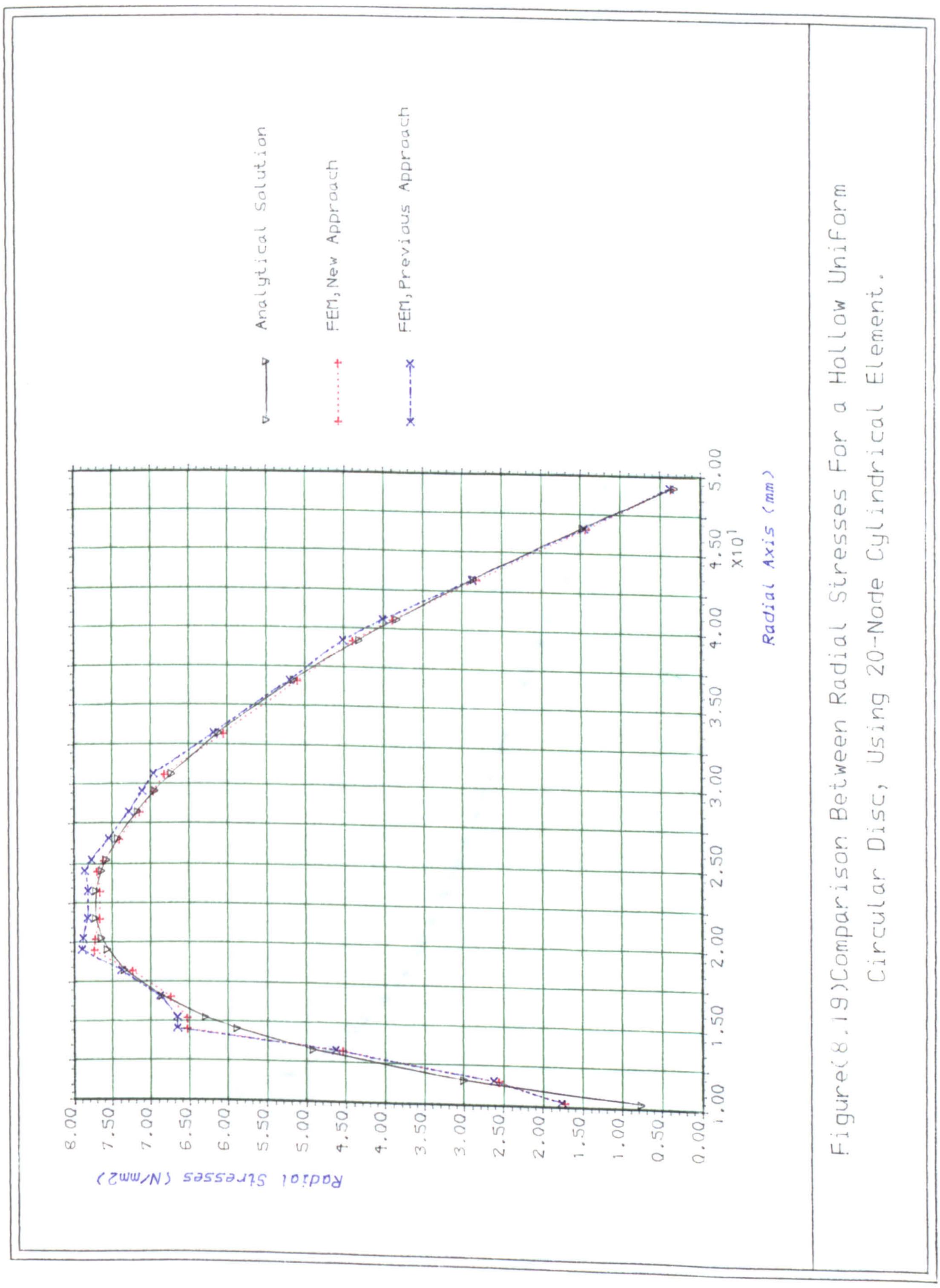

Figure(8.19)Comparison Between Radial Stresses For a Hollow Uniform Circular Disc, Using 20-Node Cylindrical Element.

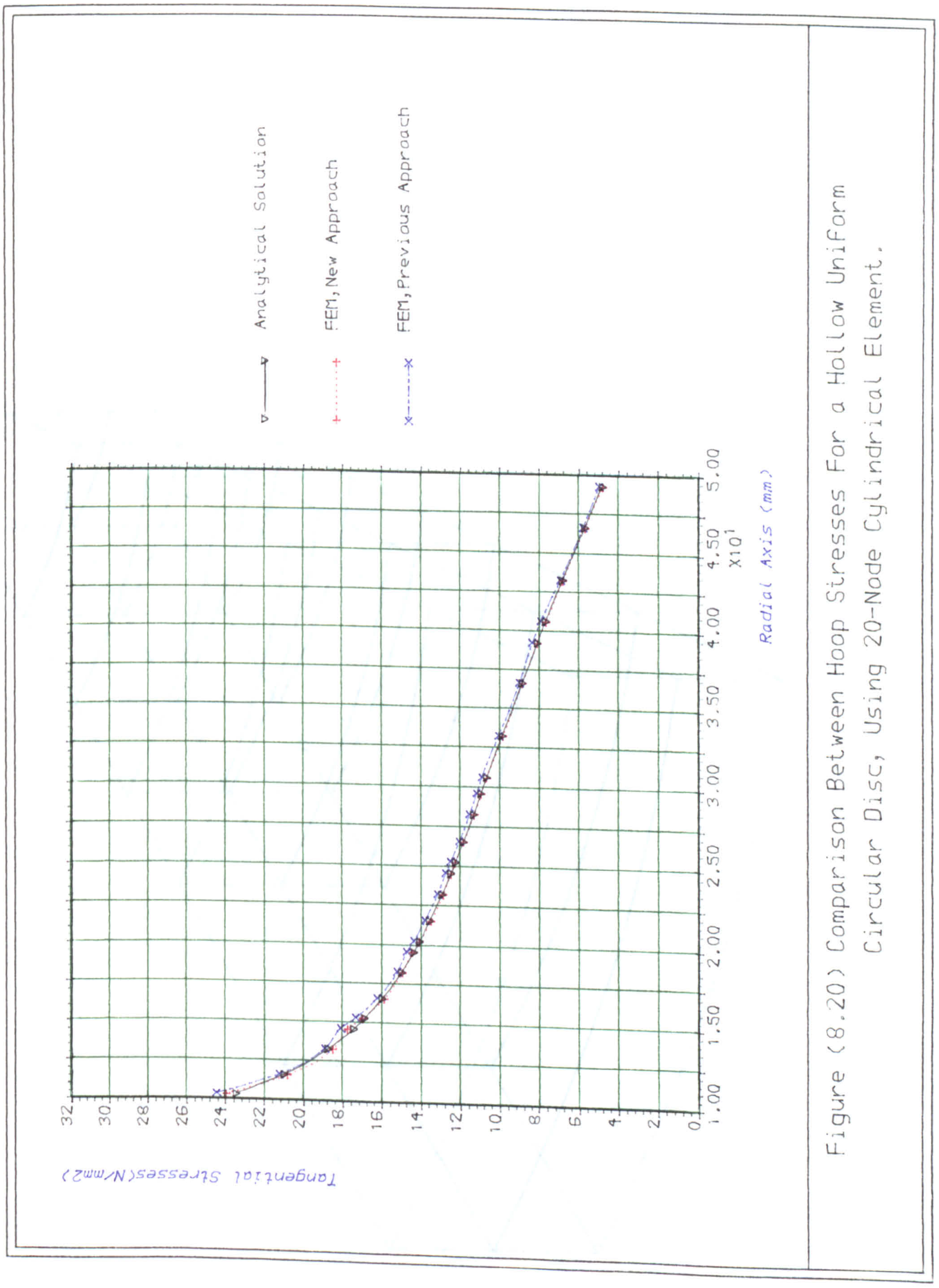

Figure (8.20) Comparison Between Hoop Stresses For a Hollow Uniform Circular Disc, Using 20-Node Cylindrical Element.

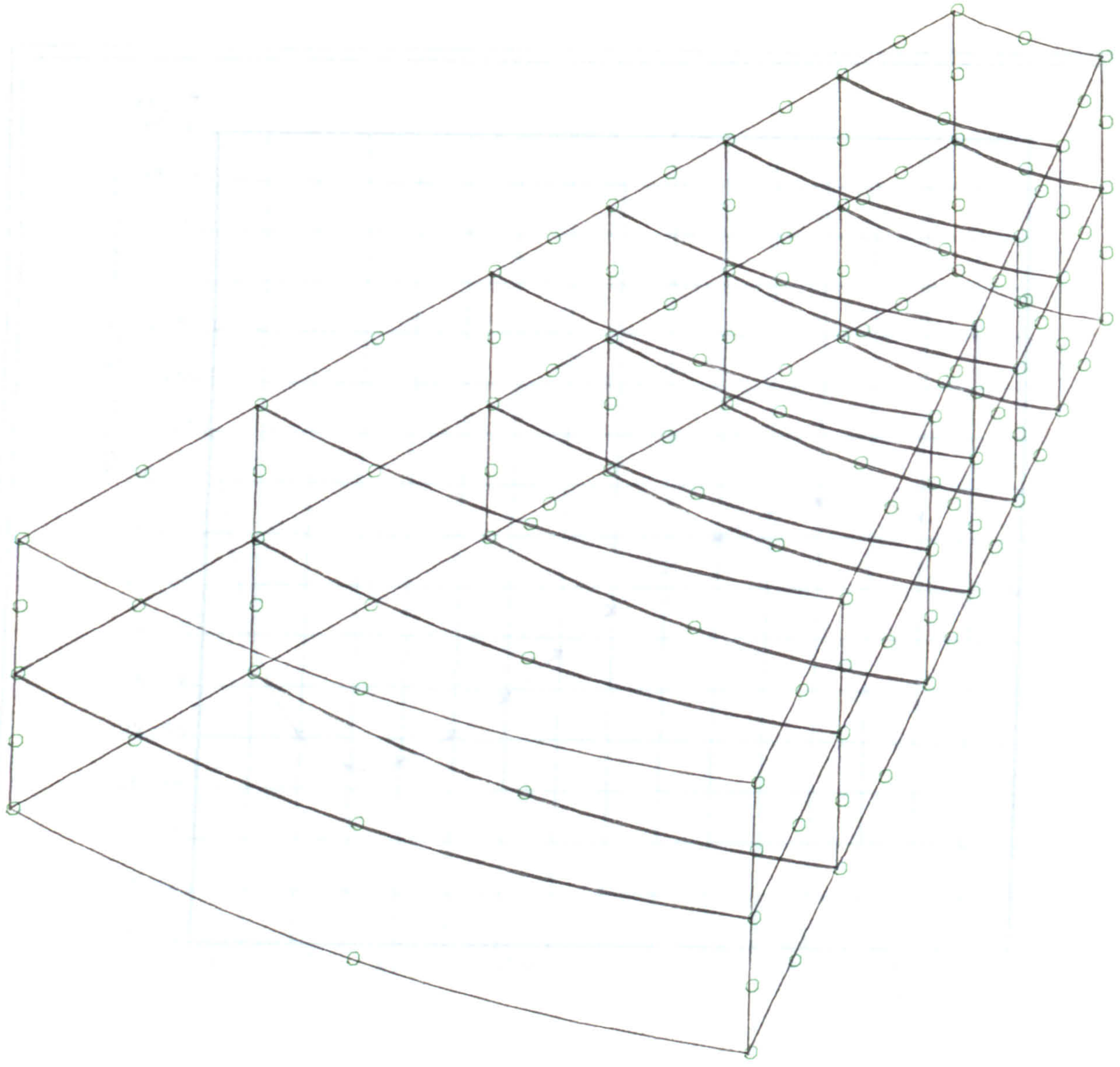

Figure (8.21) Three-Dimensional Mesh For a Single Sector of Disc Using 20-Node Brick Elements.

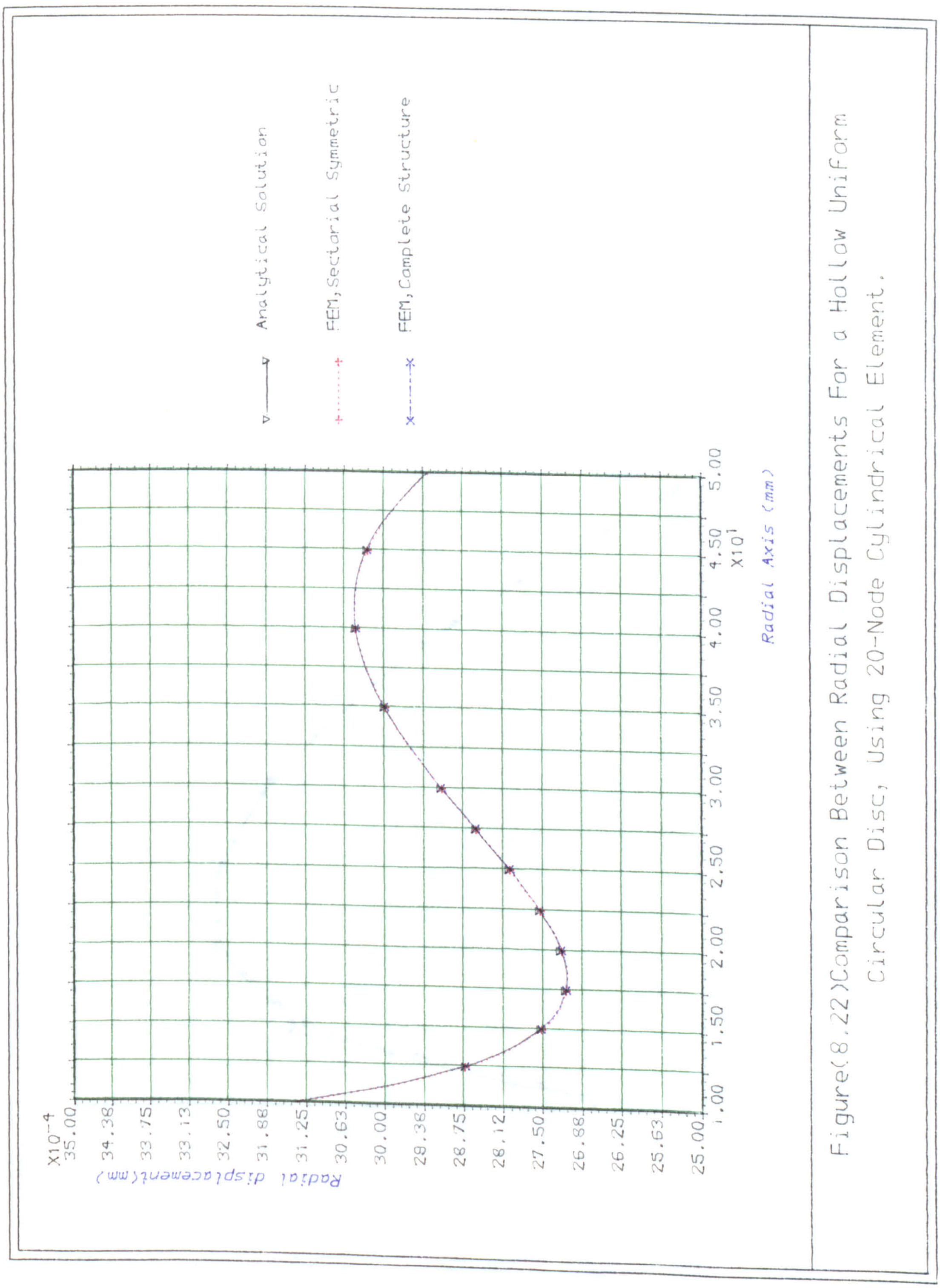

Figure(8.22)Comparison Between Radial Displacements For a Hollow Uniform Circular Disc, Using 20-Node Cylindrical Element.

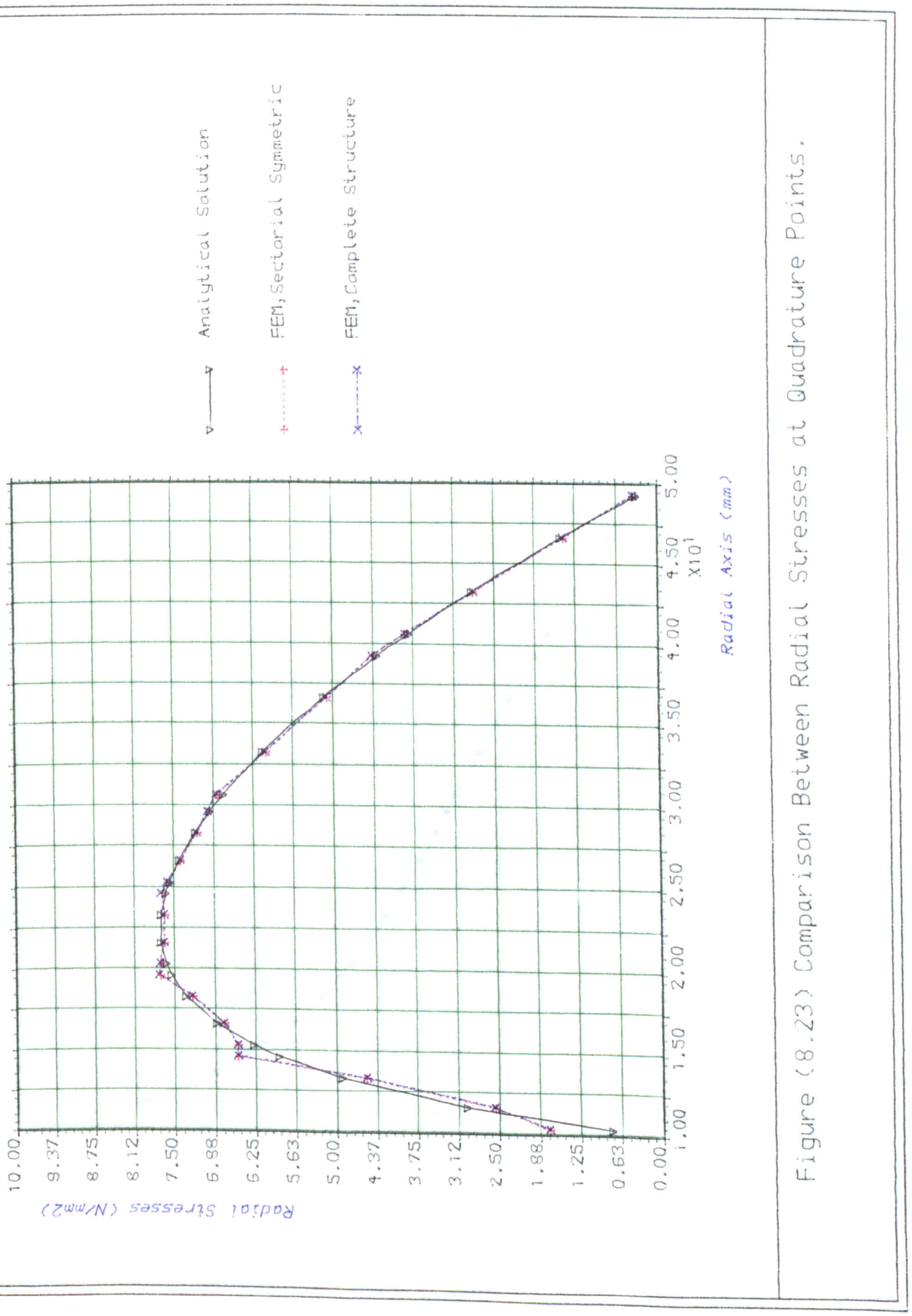

Figure (8.23) Comparison Between Radial Stresses at Quadrature Points.

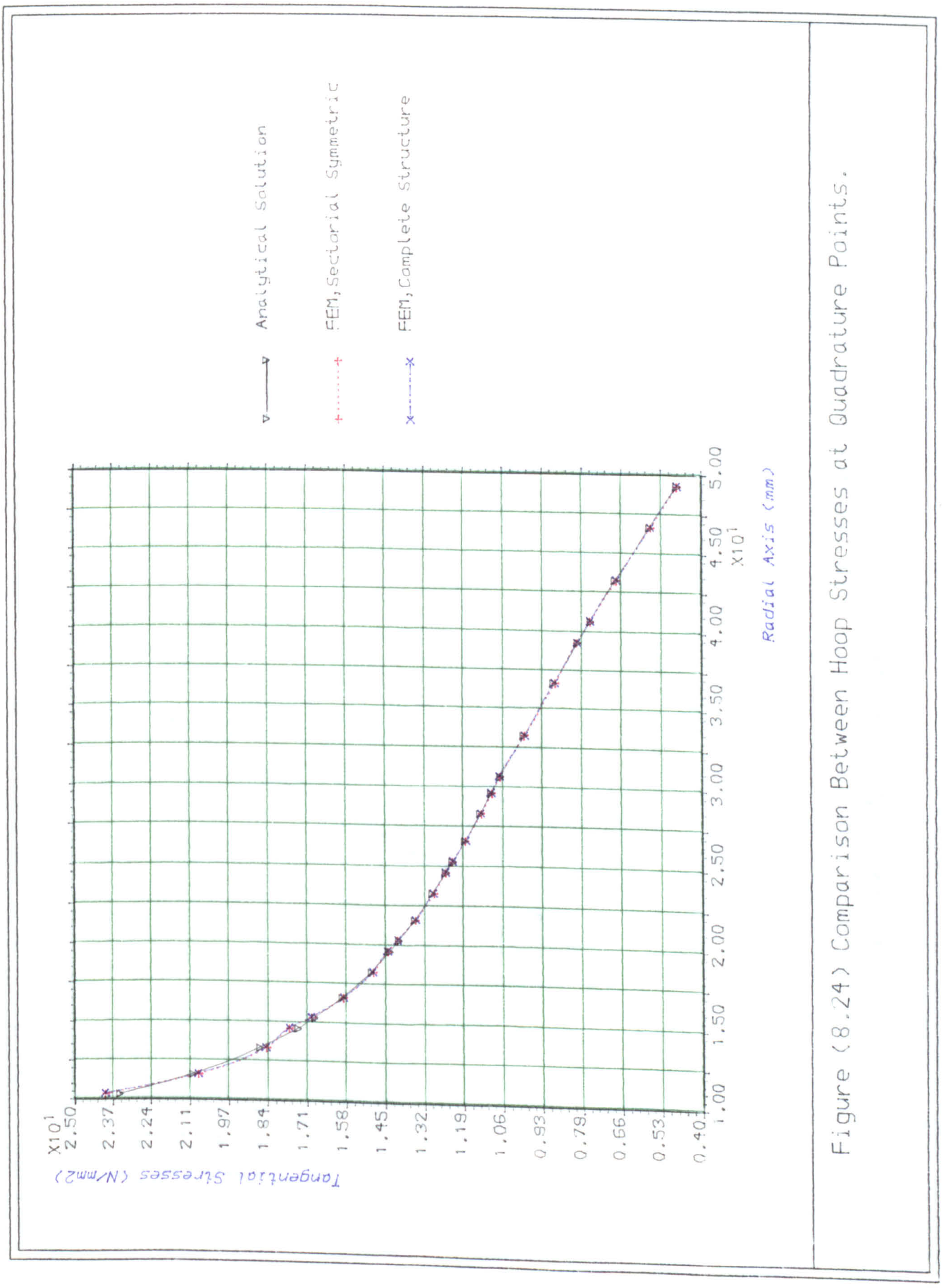

Figure (8.24) Comparison Between Hoop Stresses at Quadrature Points.

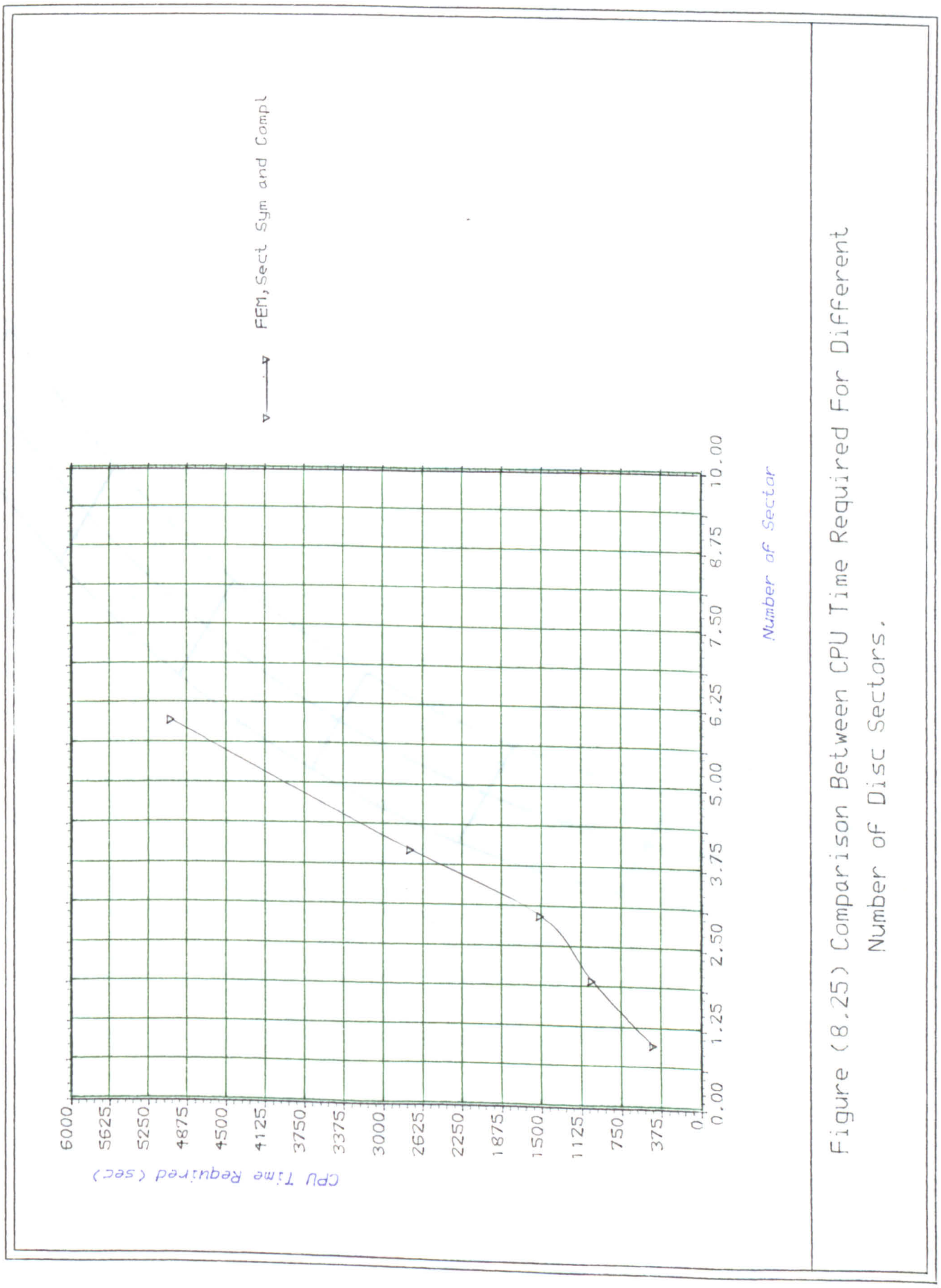

Figure (8.25) Comparison Between CPU Time Required For Different Number of Disc Sectors.

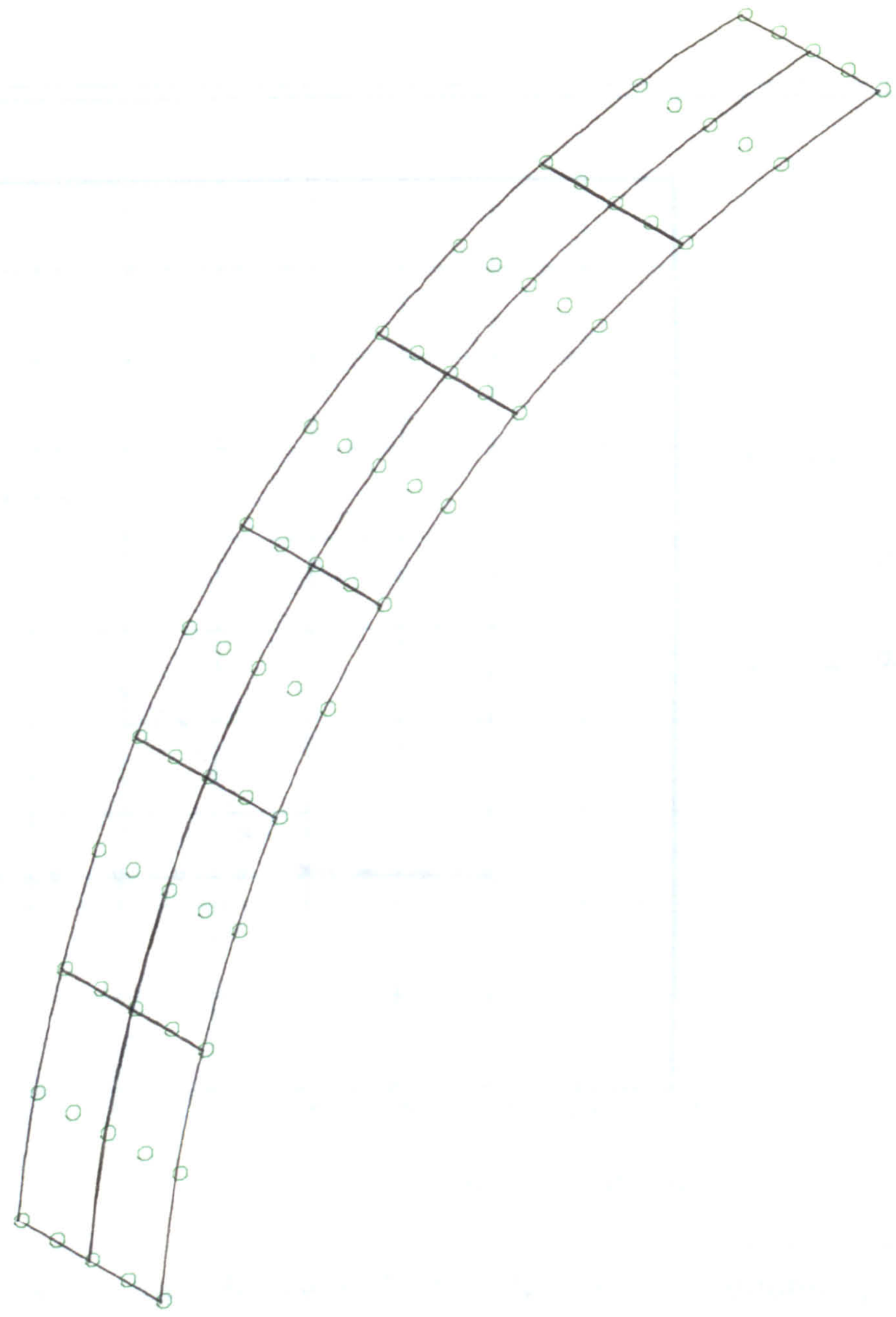

M.M.AZZAWI

Figure (8.26) Circular Beam Case-Study
Using 9-Node Element.

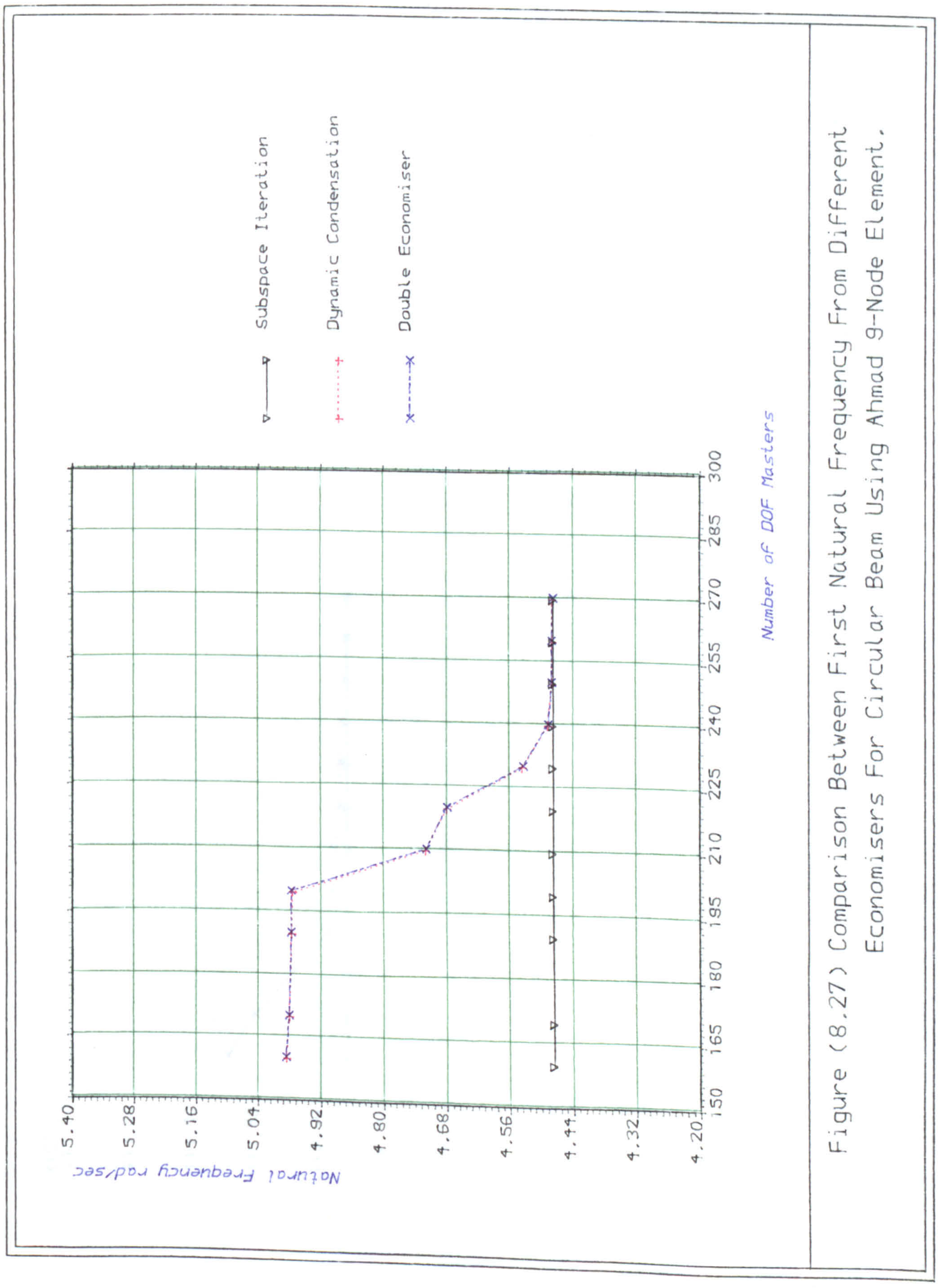

Figure (8.27) Comparison Between First Natural Frequency From Different Economisers For Circular Beam Using Ahmad 9-Node Element.

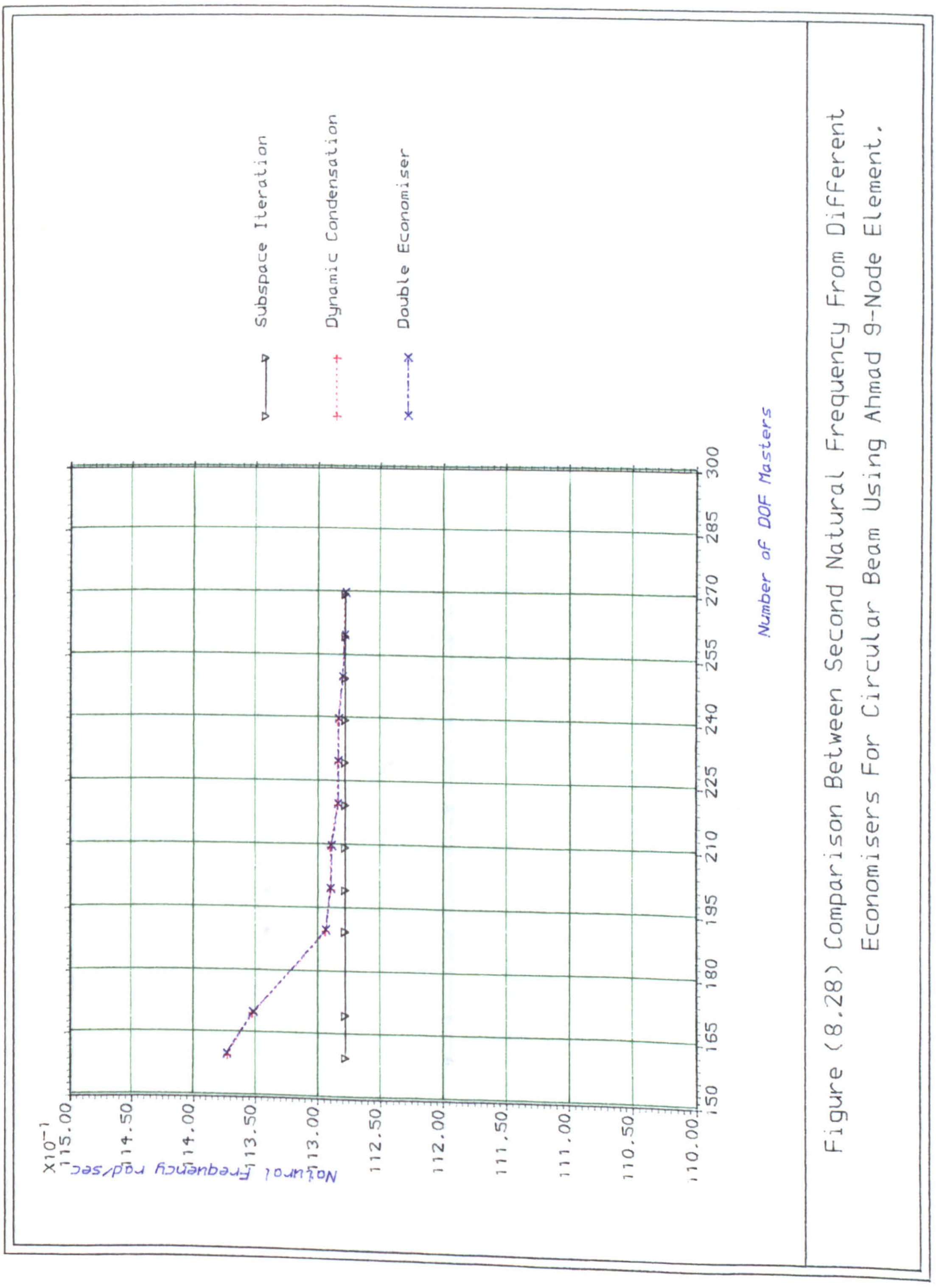

Figure (8.28) Comparison Between Second Natural Frequency From Different Economisers For Circular Beam Using Ahmad 9-Node Element.

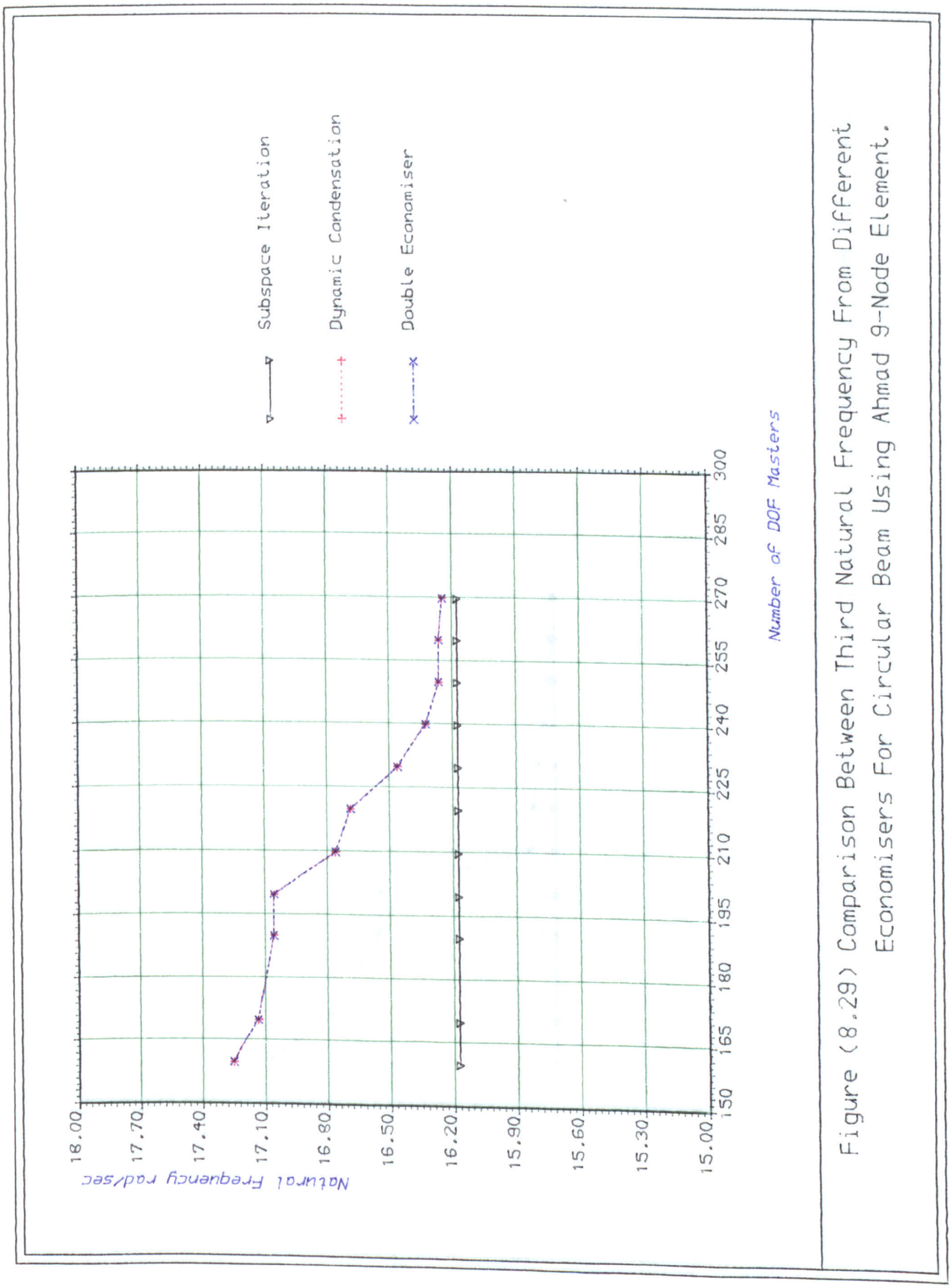

Figure (8.29) Comparison Between Third Natural Frequency From Different Economisers For Circular Beam Using Ahmad 9-Node Element.

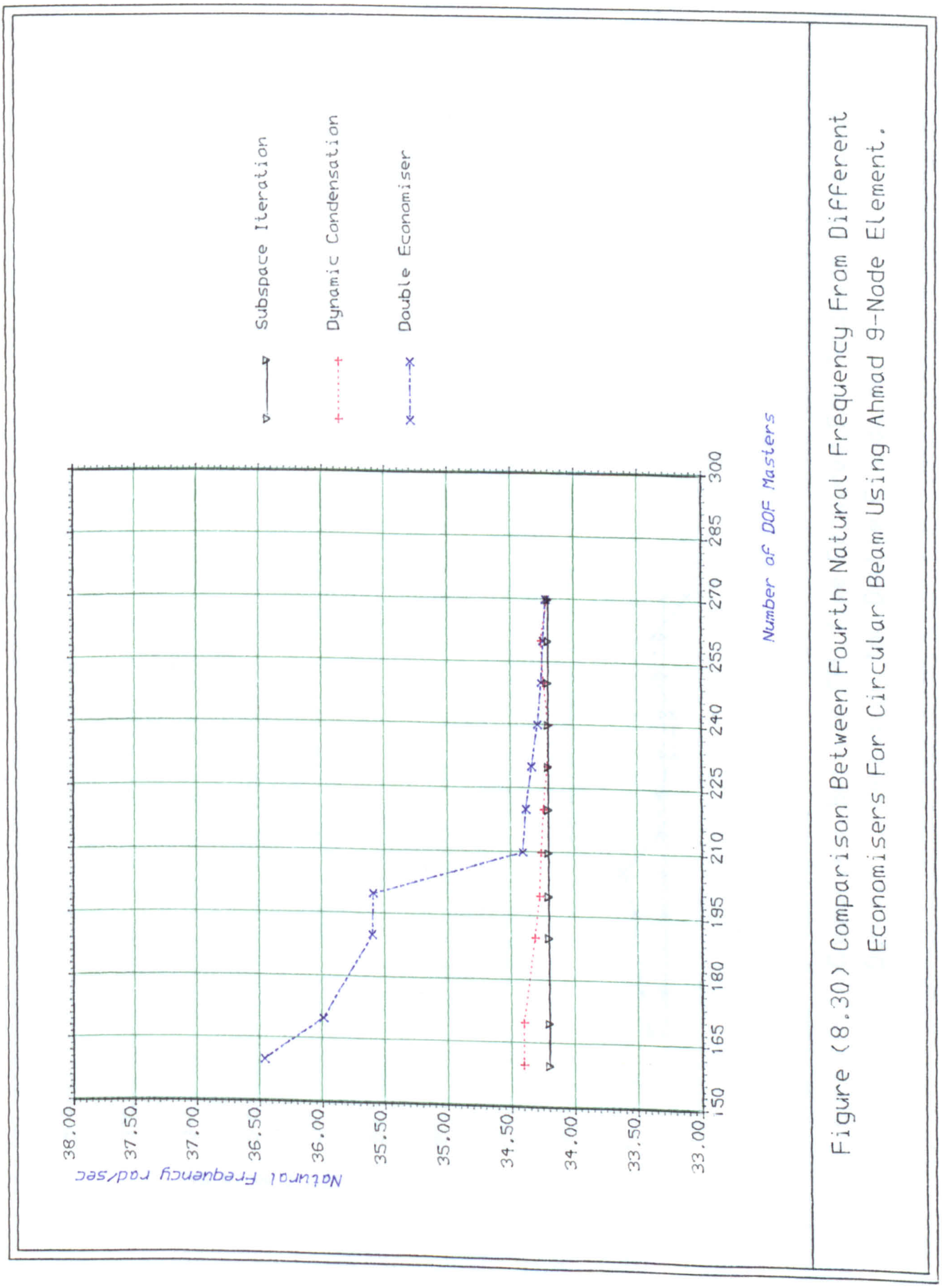

Figure (8.30) Comparison Between Fourth Natural Frequency From Different Economisers For Circular Beam Using Ahmad 9-Node Element.

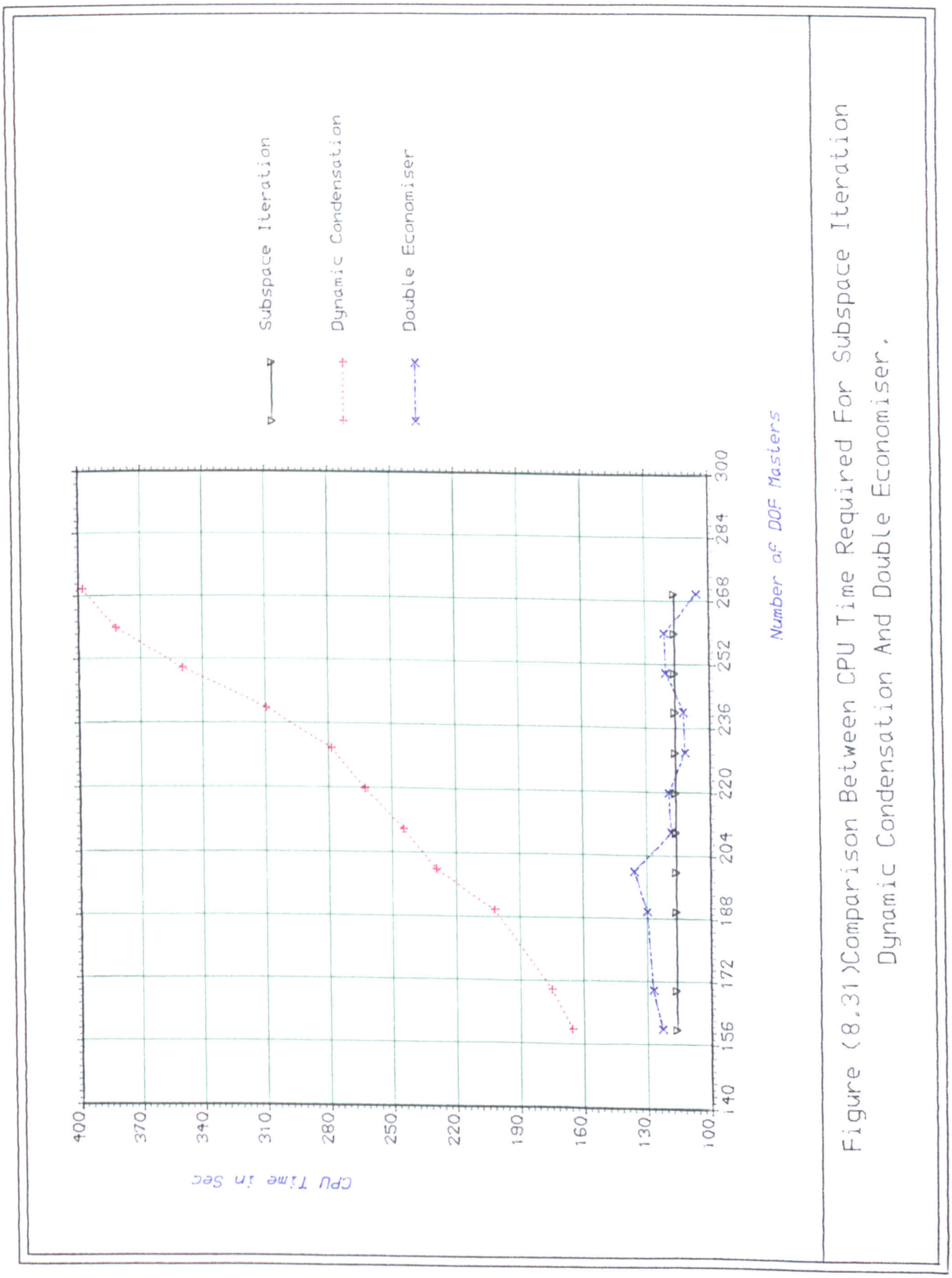

Figure (8.31)Comparison Between CPU Time Required For Subspace Iteration, Dynamic Condensation And Double Economiser.

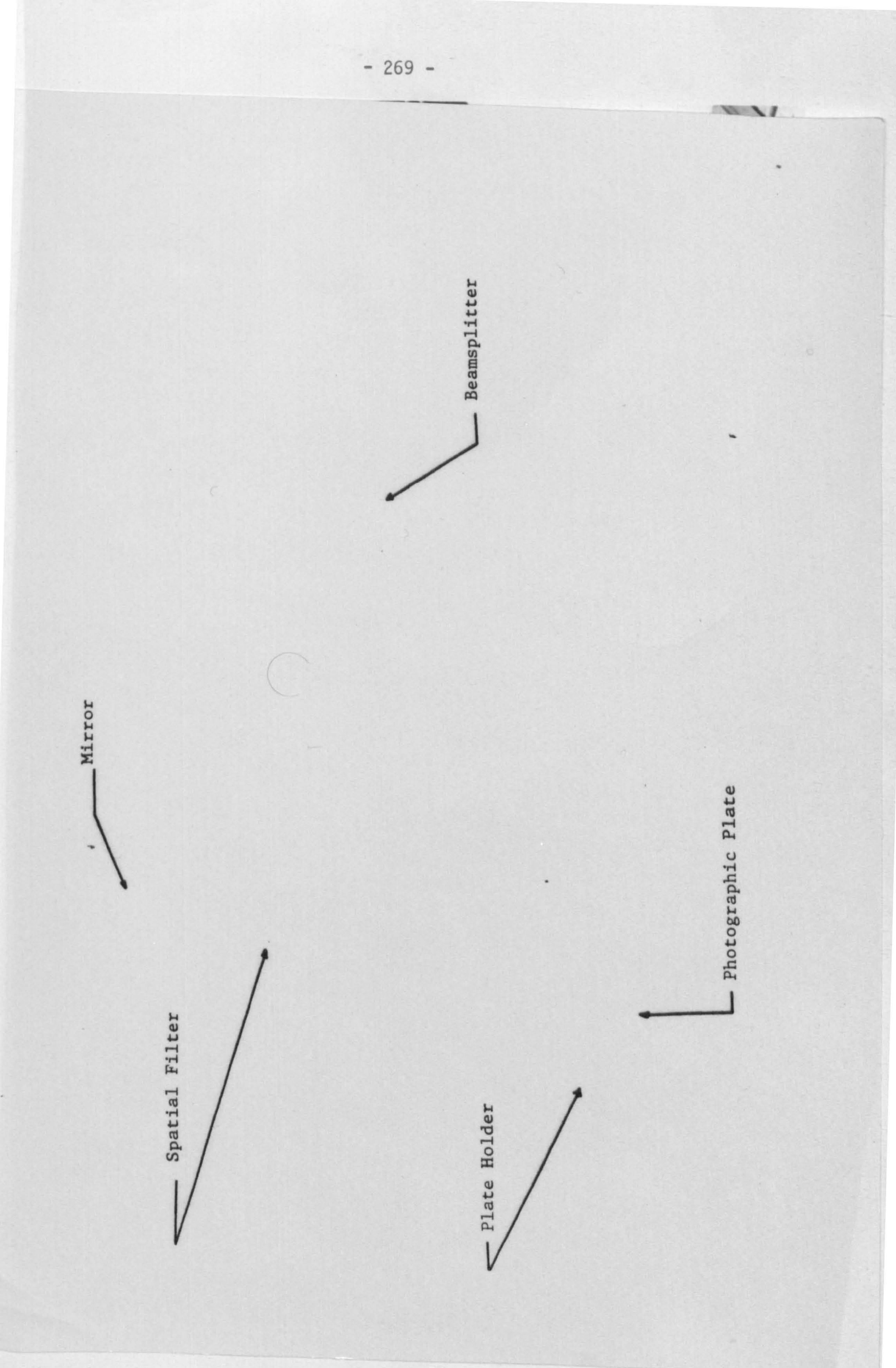
Beamsplitter
Mirror
Spatial Filter
Photographic Plate
Plate Holder

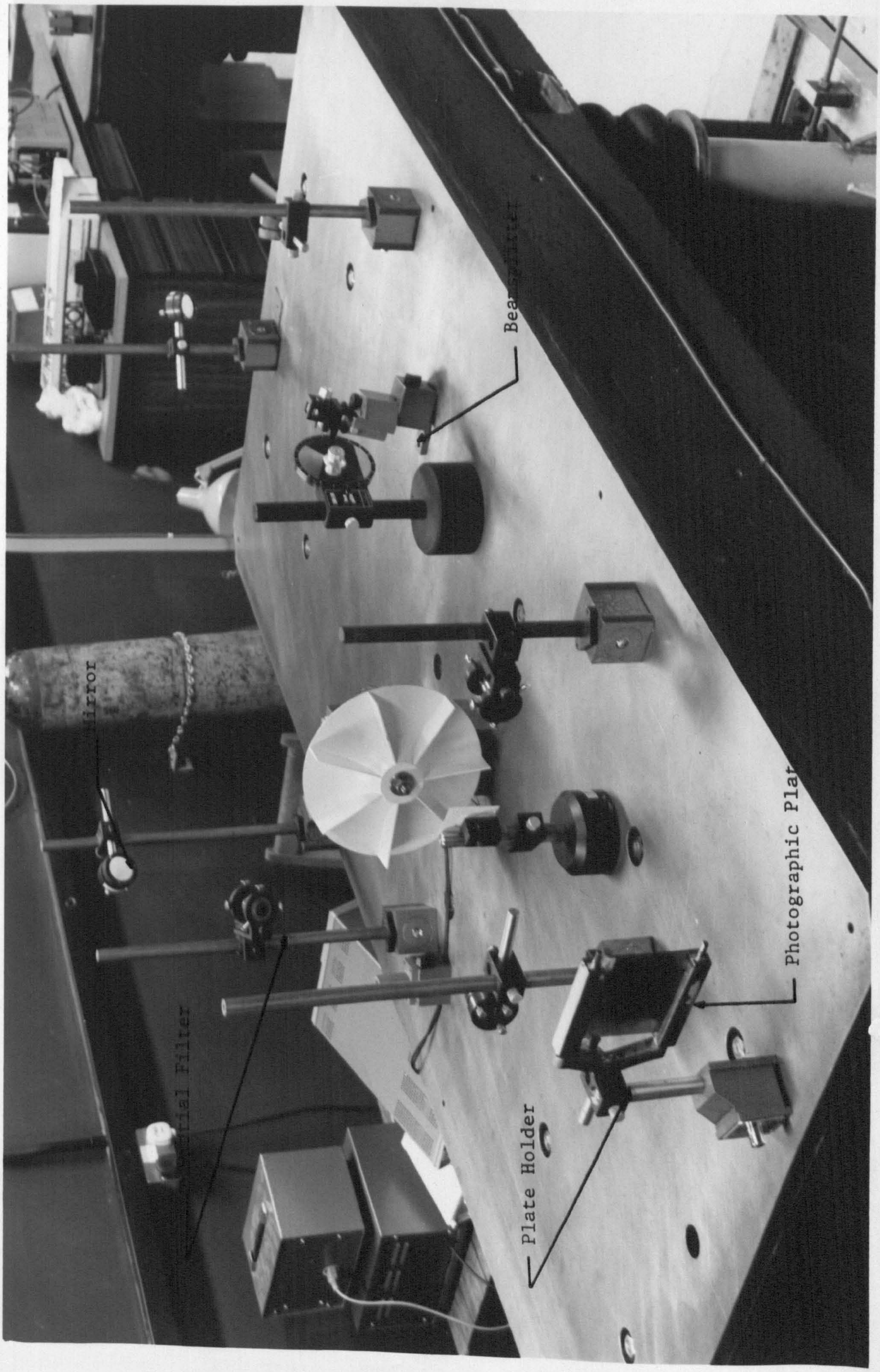

Figure 8.32 General View of the Holography Test Rig

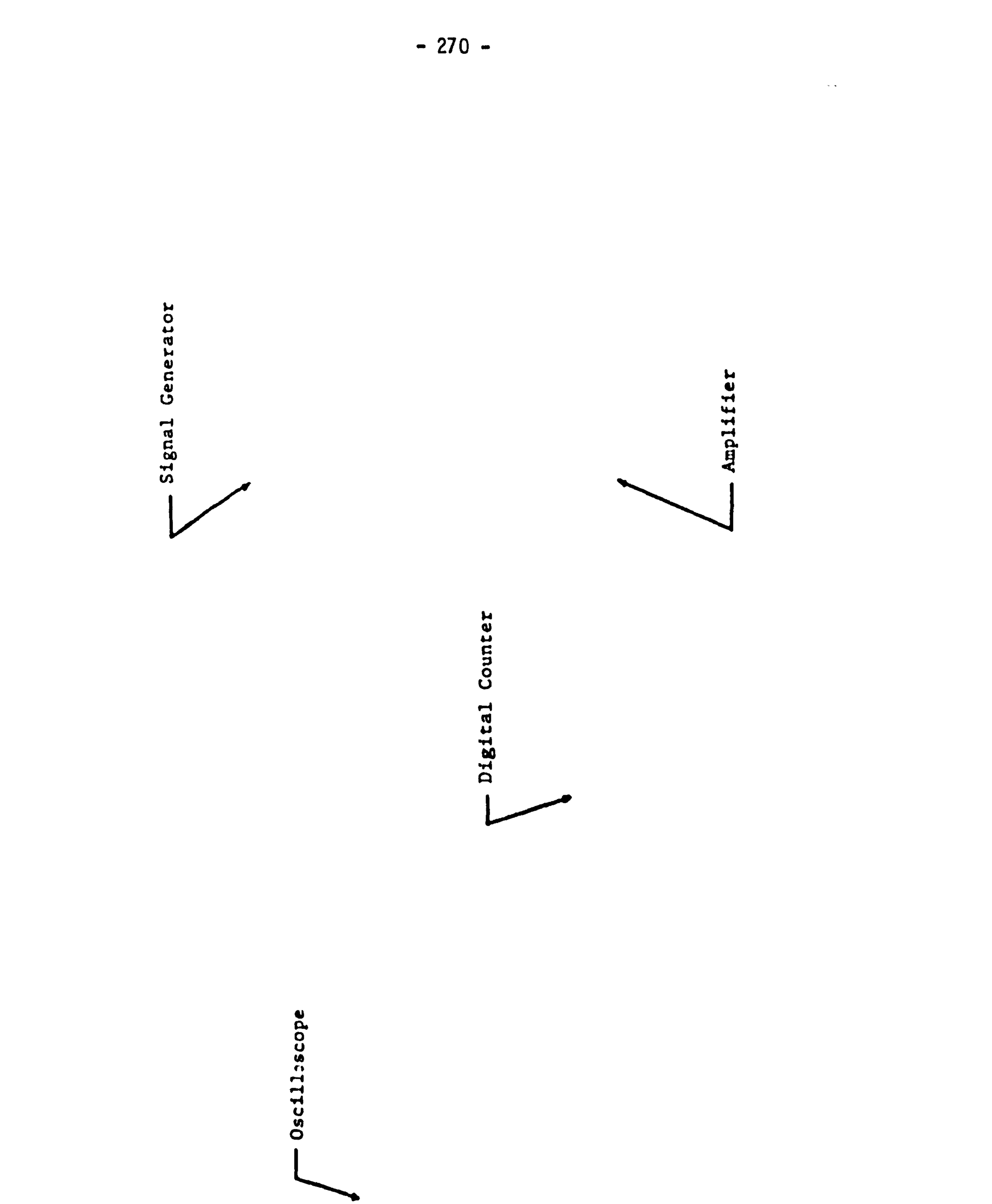
Signal Generator
Amplifier
Digital Counter
Oscilloscope

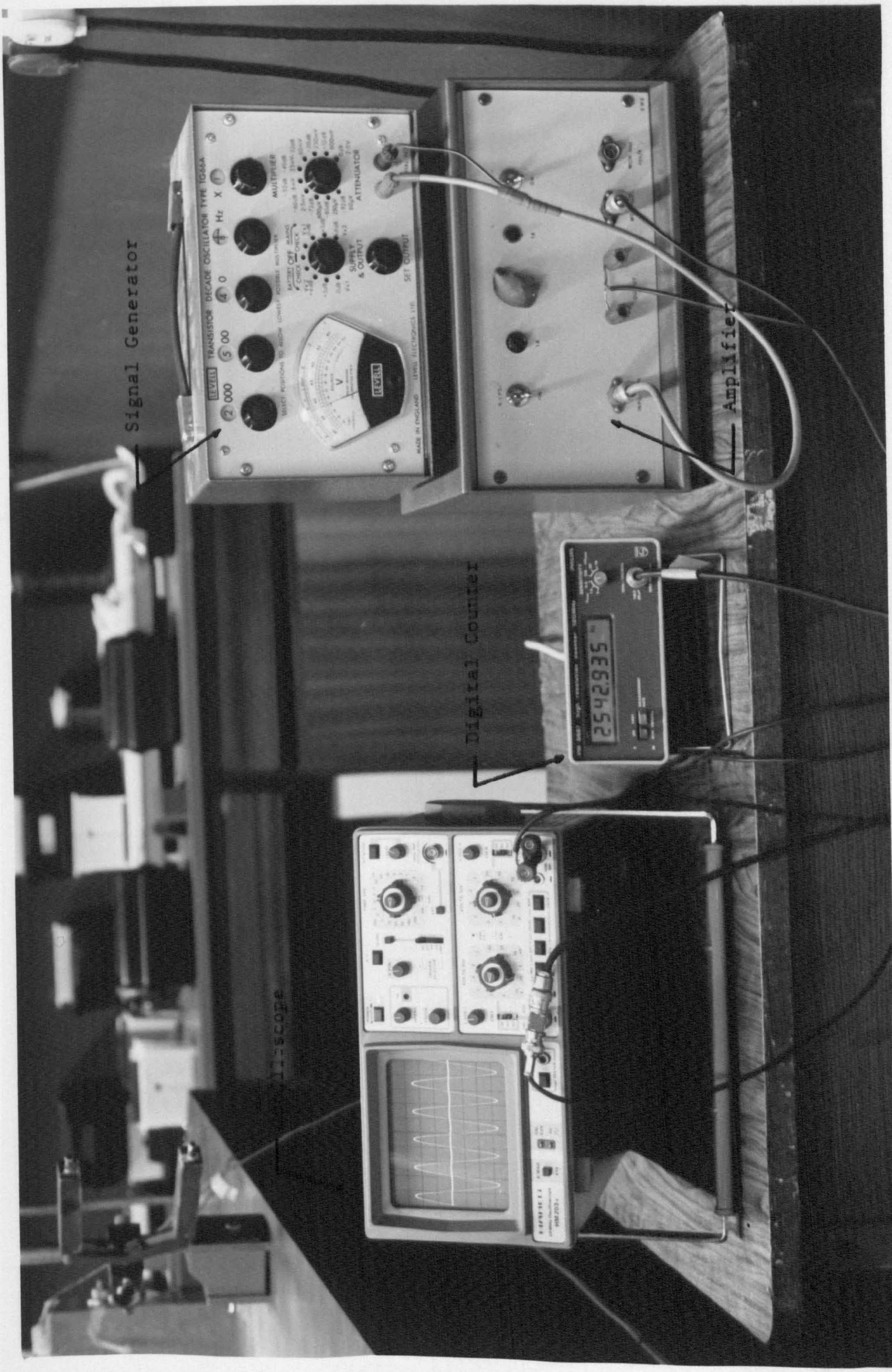

Figure 8.33 Instrumentation of the Holography Rig

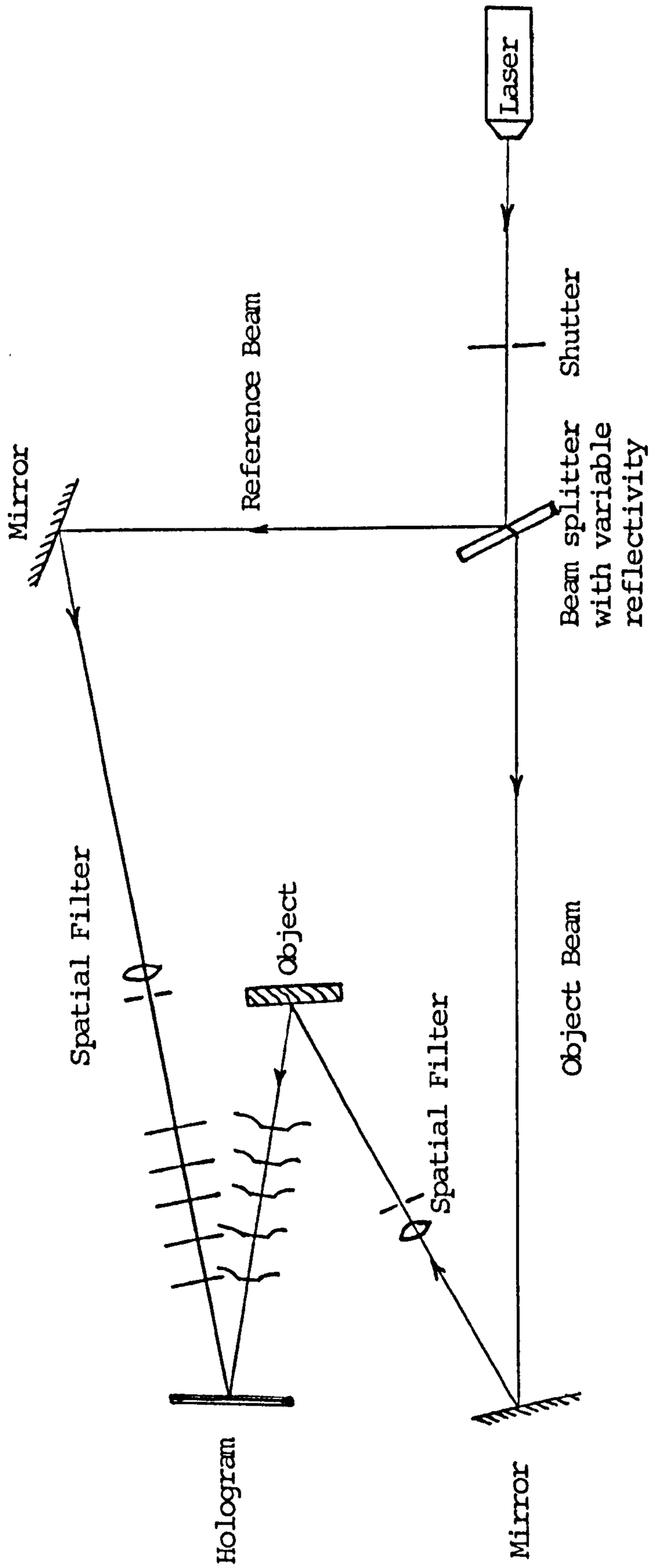

Figure 8.34 Set Up of Hologram Recording System

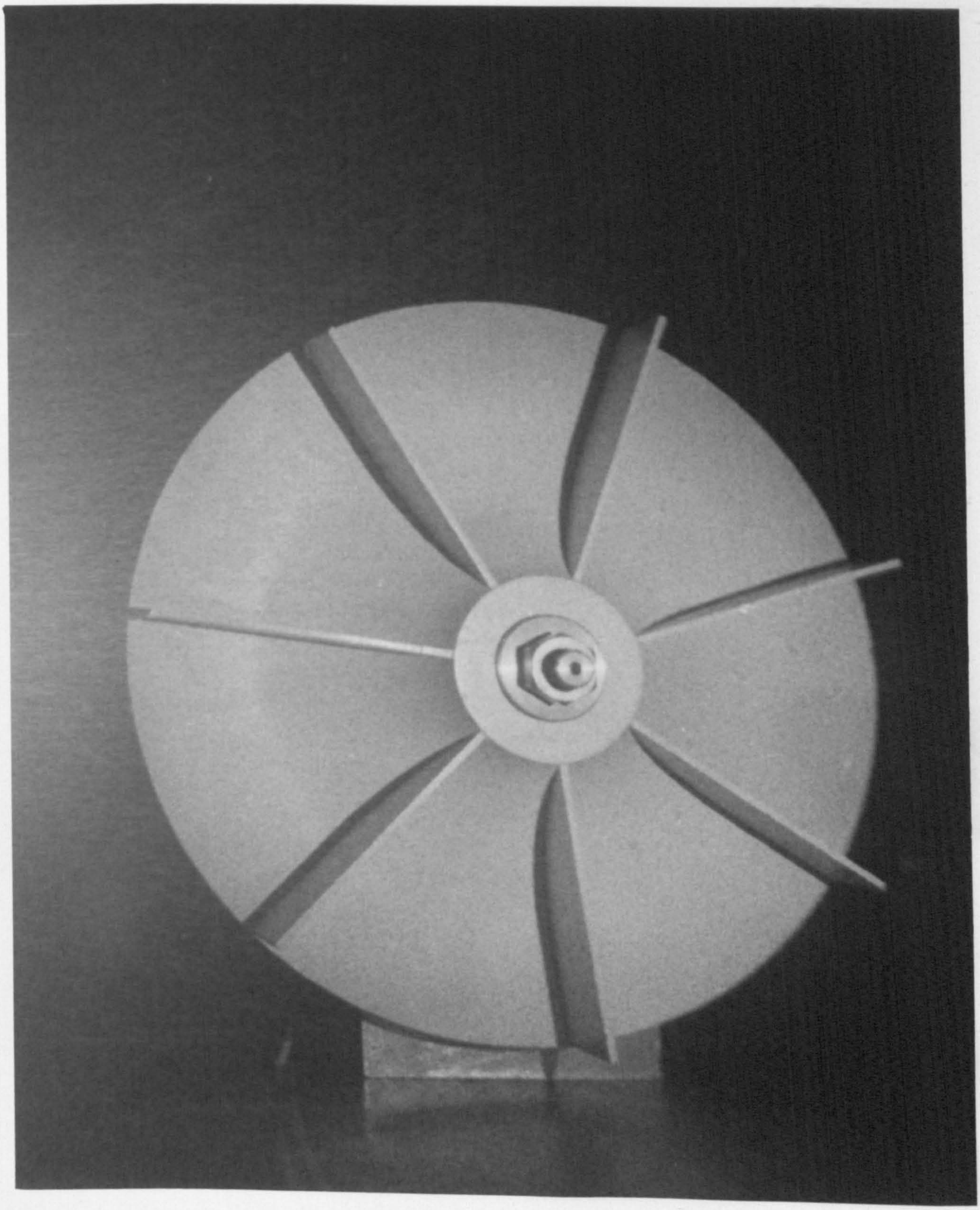

Figure 8.35 Radial Impeller of Case One

Figure 8.36 Mode Shape of the Impeller
Vibrating at 2418.2 Hz

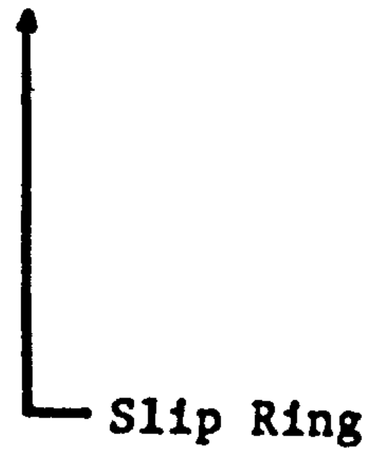
Slip Ring

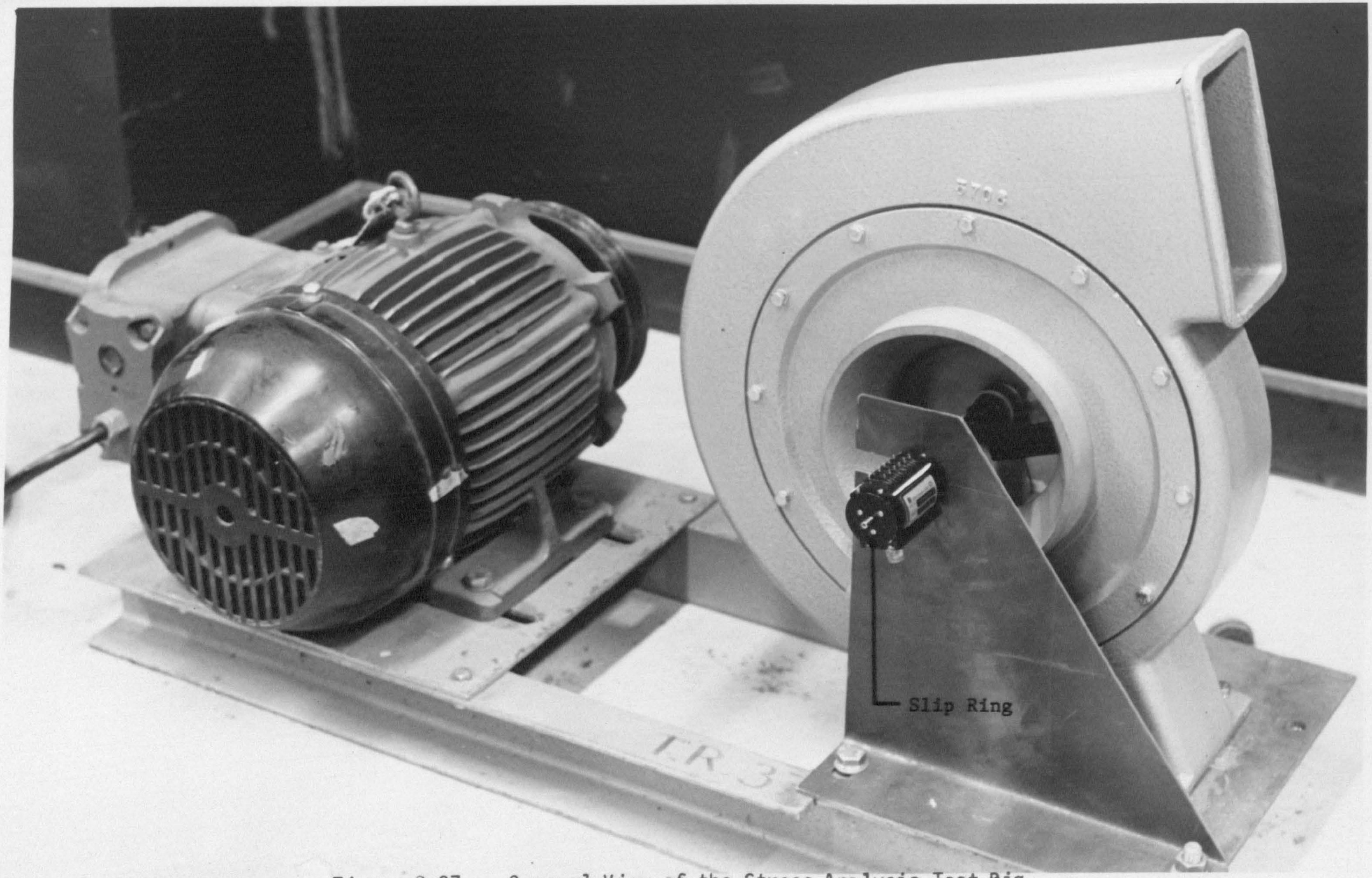

Figure 8.37-a General View of the Stress Analysis Test Rig

D.C. Power Supply

Microprocessor Voltmeter

Resistance Box for Strain Gauge Bridge

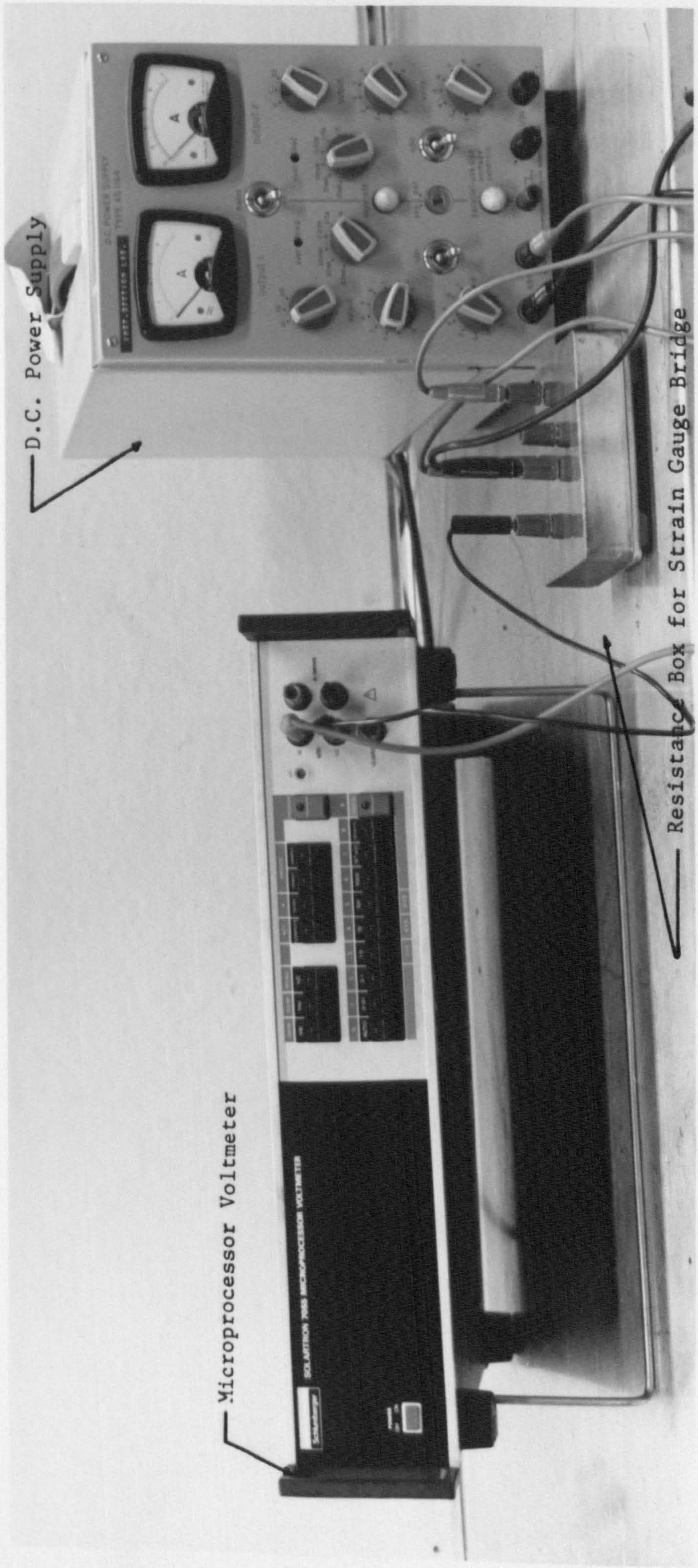

Figure 8.37-b Instrumentation of the Stress Analysis Rig

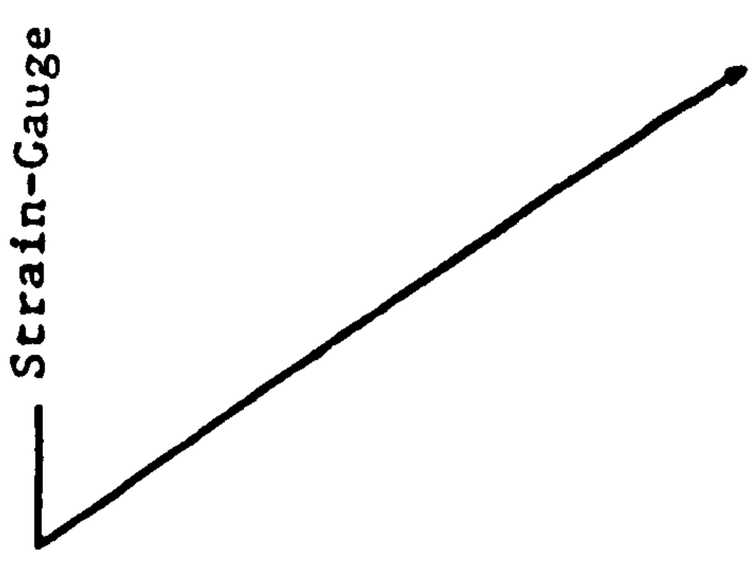
Strain-Gauge

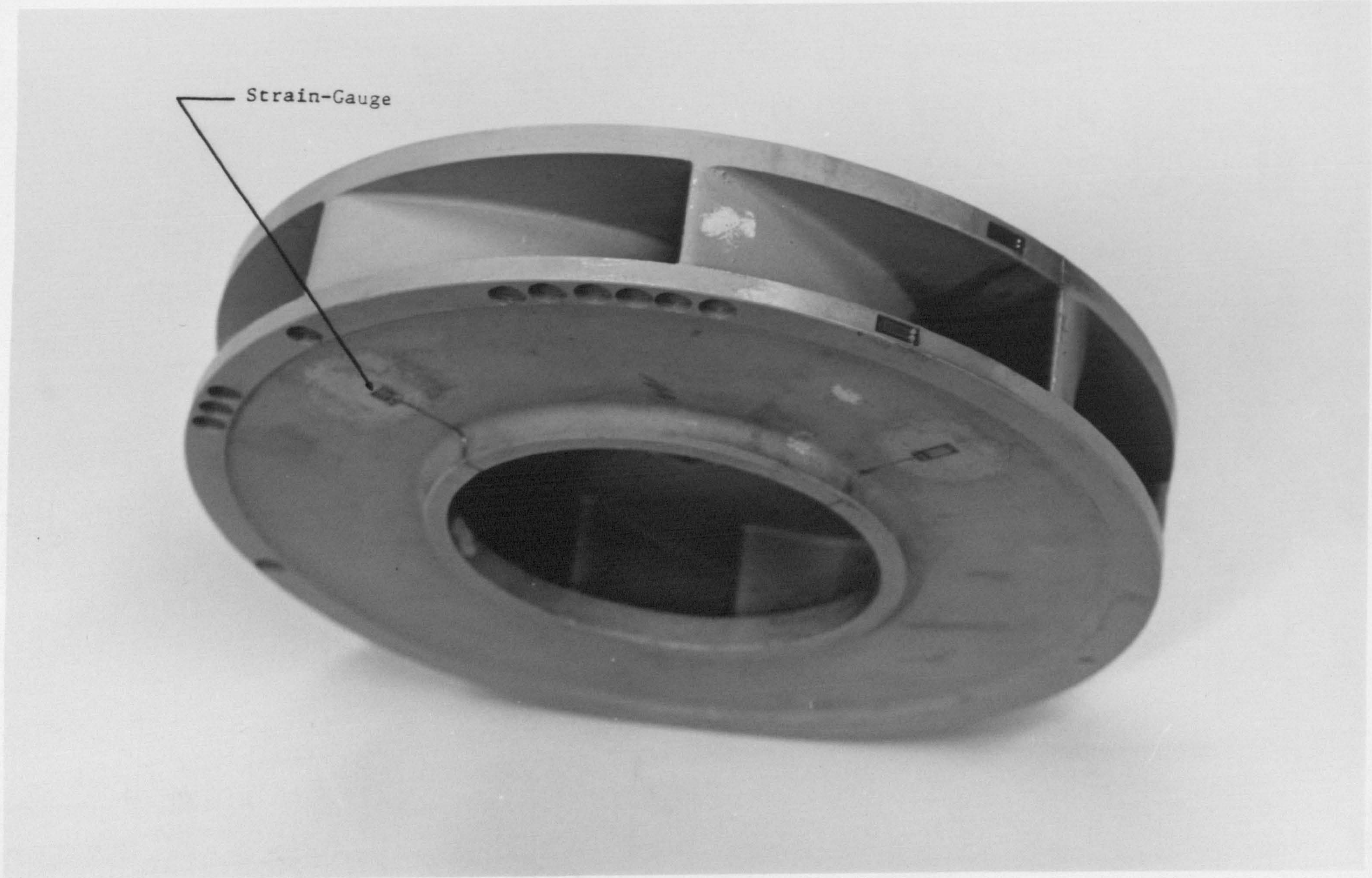

Figure 8.38-a Radial Impeller of Case Two (Side View)

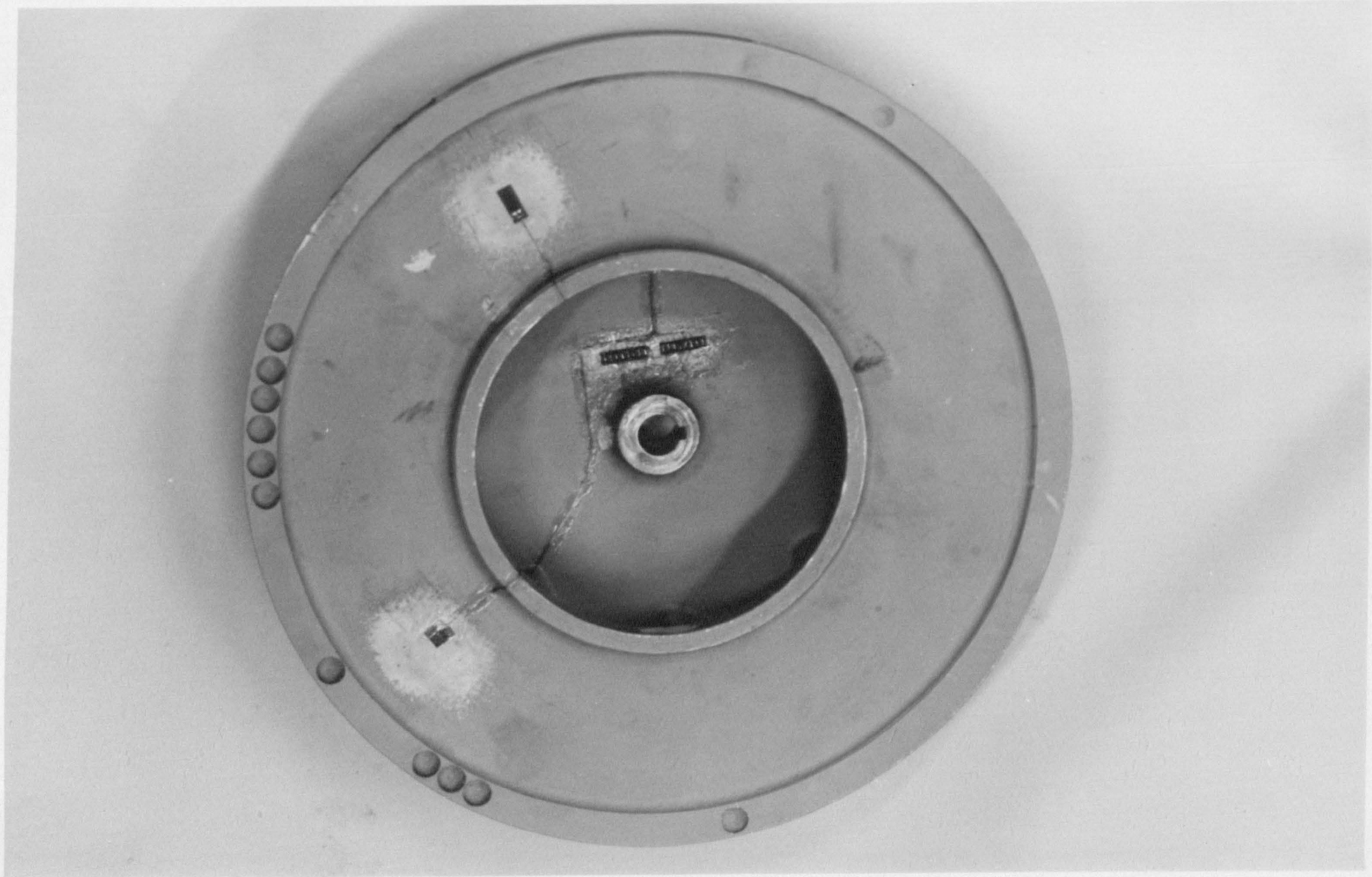

Figure 8.38-b Radial Impeller of Case Two (Top View)

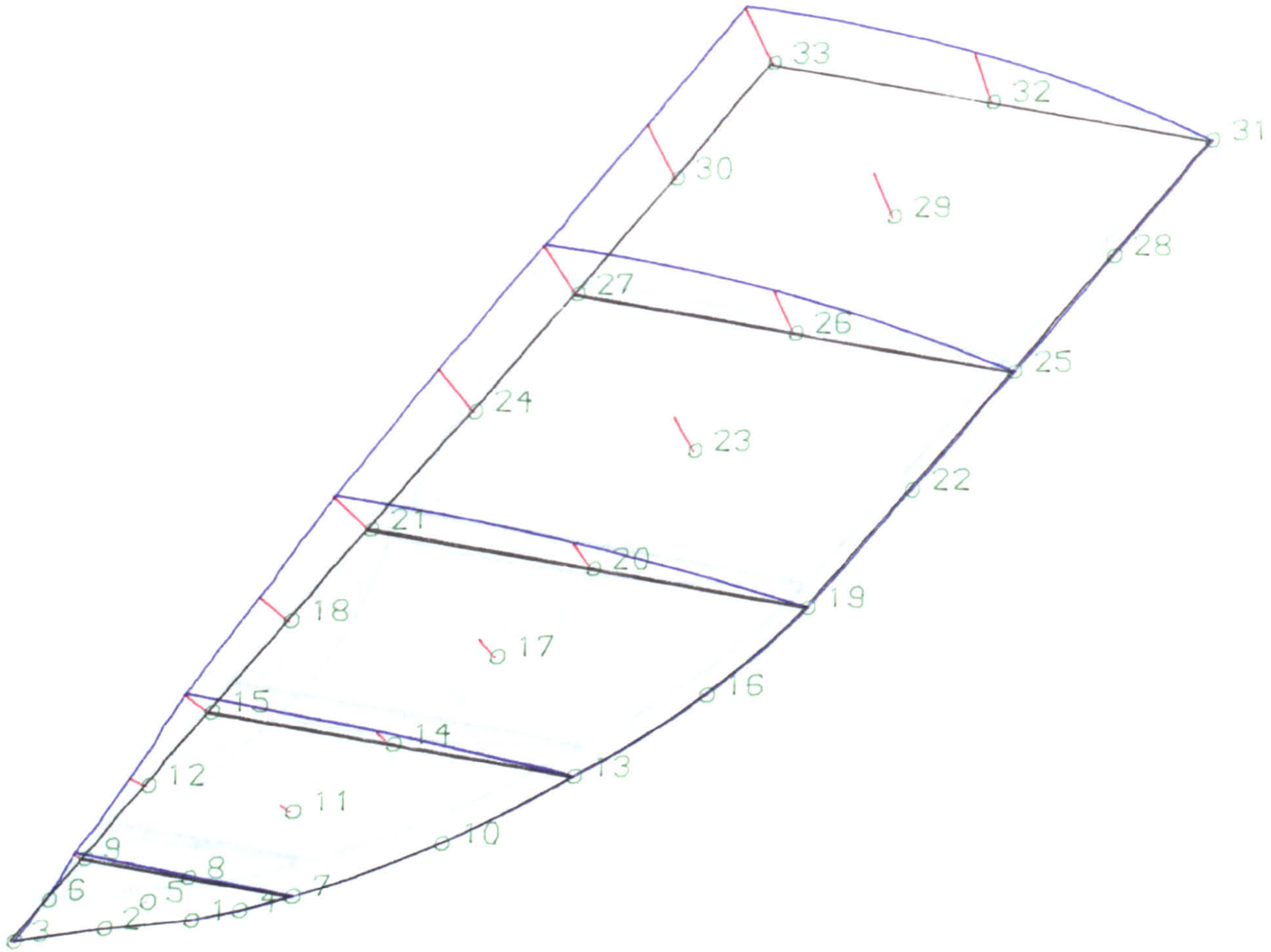

M.AZZAWI

Figure (8.39-a) First Mode-Shape of Blade, Using 9-Node Element Mesh Number (1)

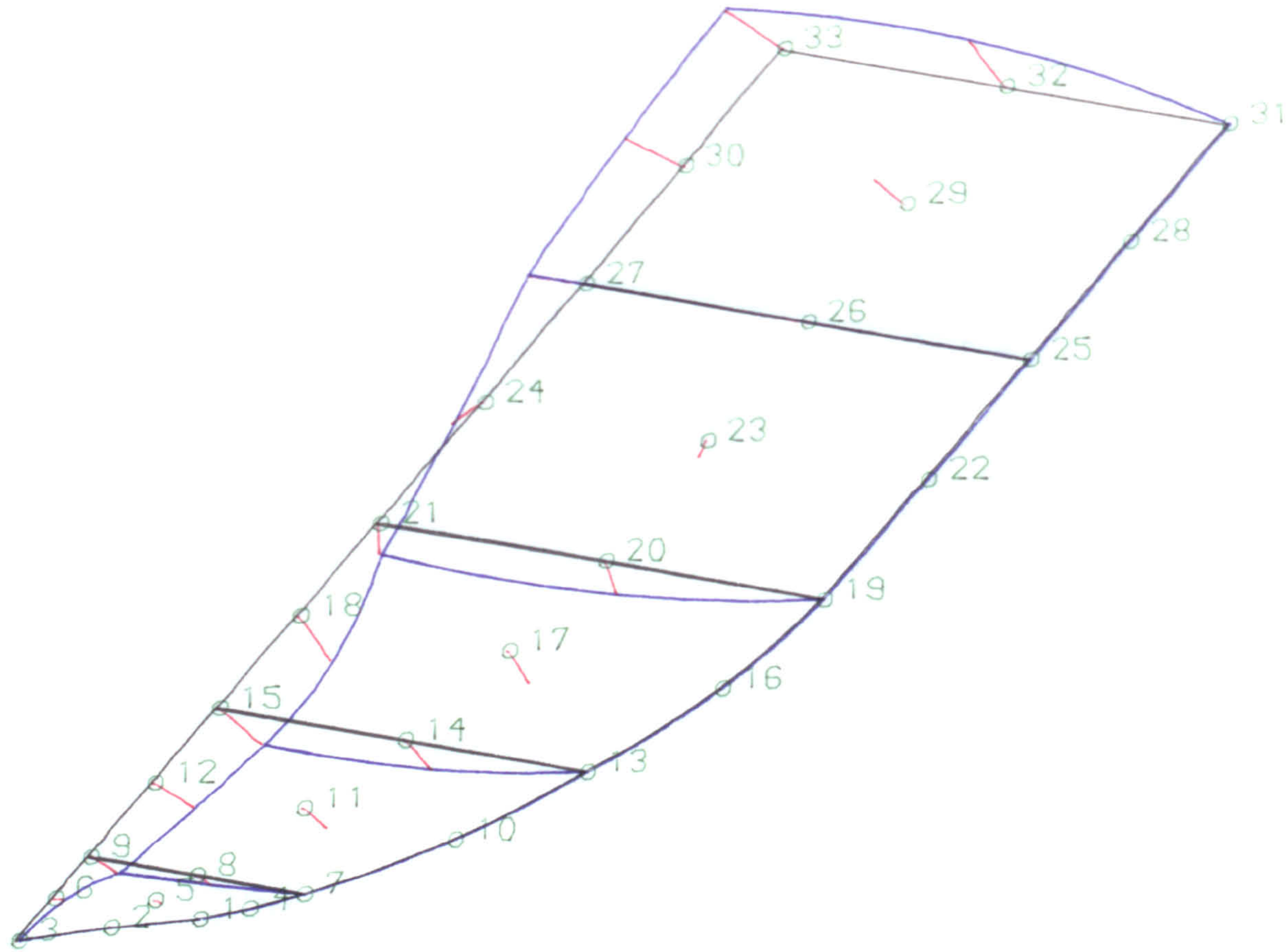

M.AZZAWI

Figure (8.39-b) Second Mode-Shape of Blade, Using 9-Node Element
Mesh Number (1)

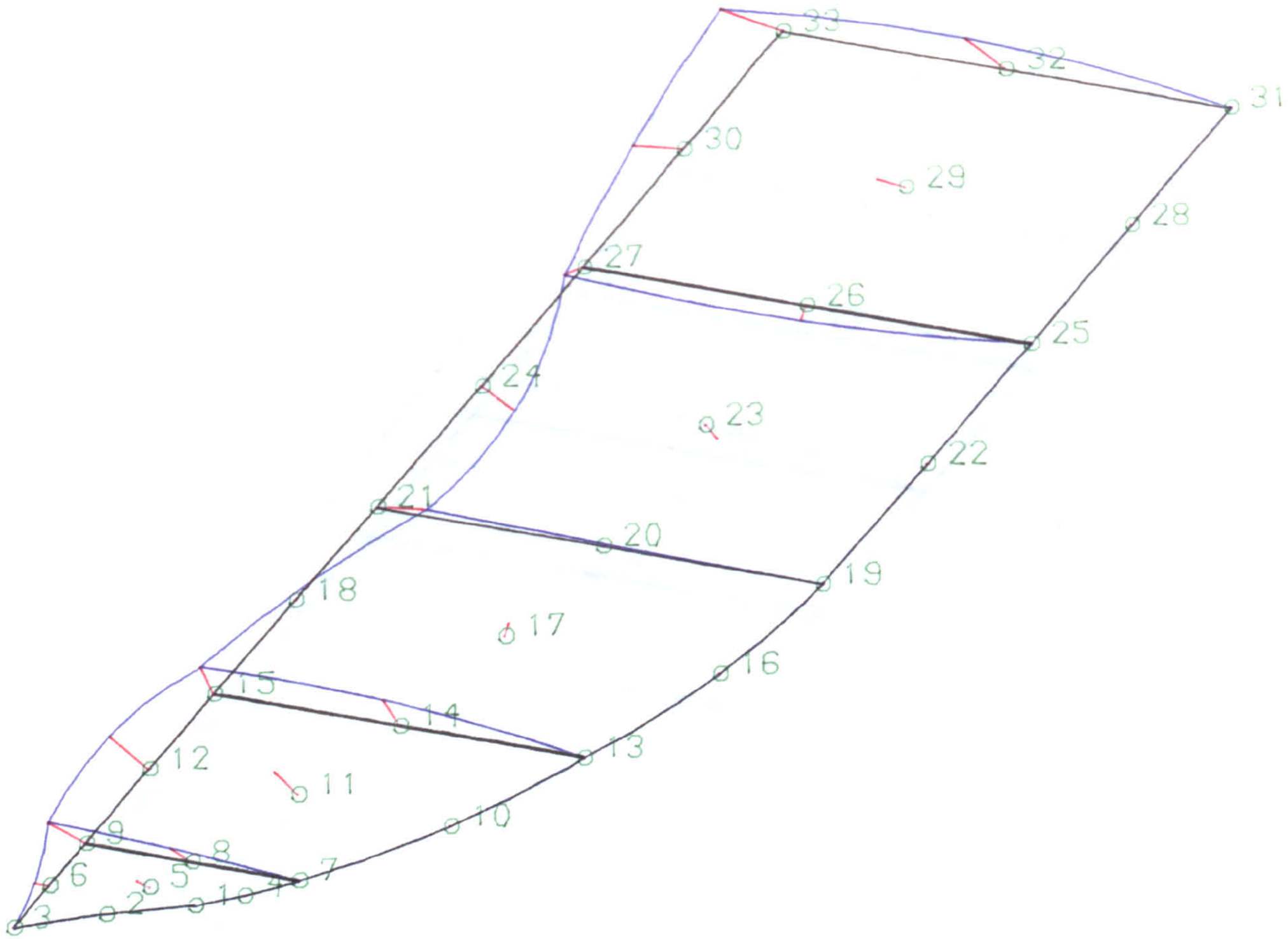

M.AZZAWI

Figure (8.39-c) Third Mode-Shape of Blade, Using 9-Node Element
Mesh Number (1)

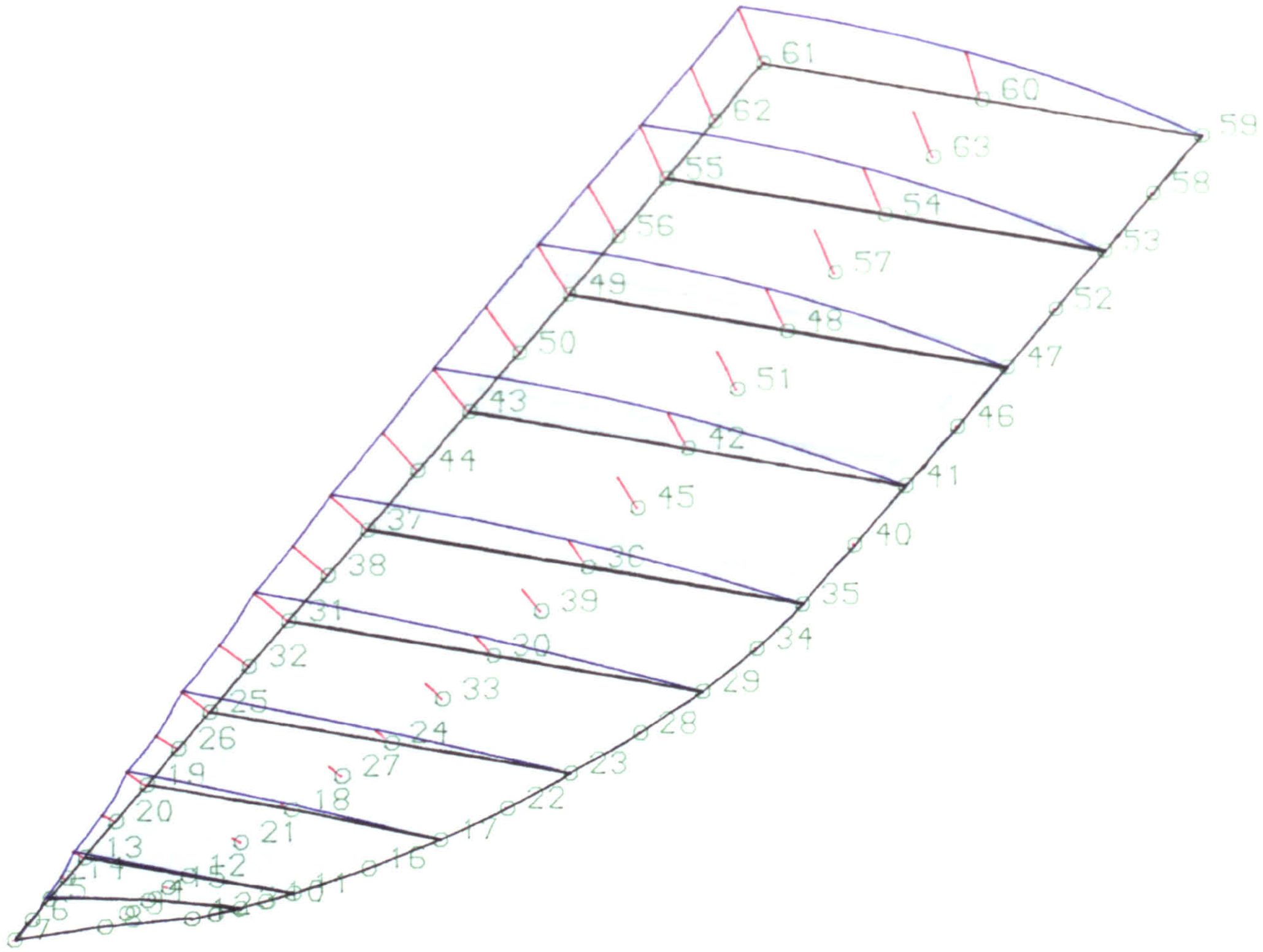

M.M.AZZAWI

Figure (8.40-a) First Mode-Shape of Blade, Using 9-Node Element
Mesh Number (2)

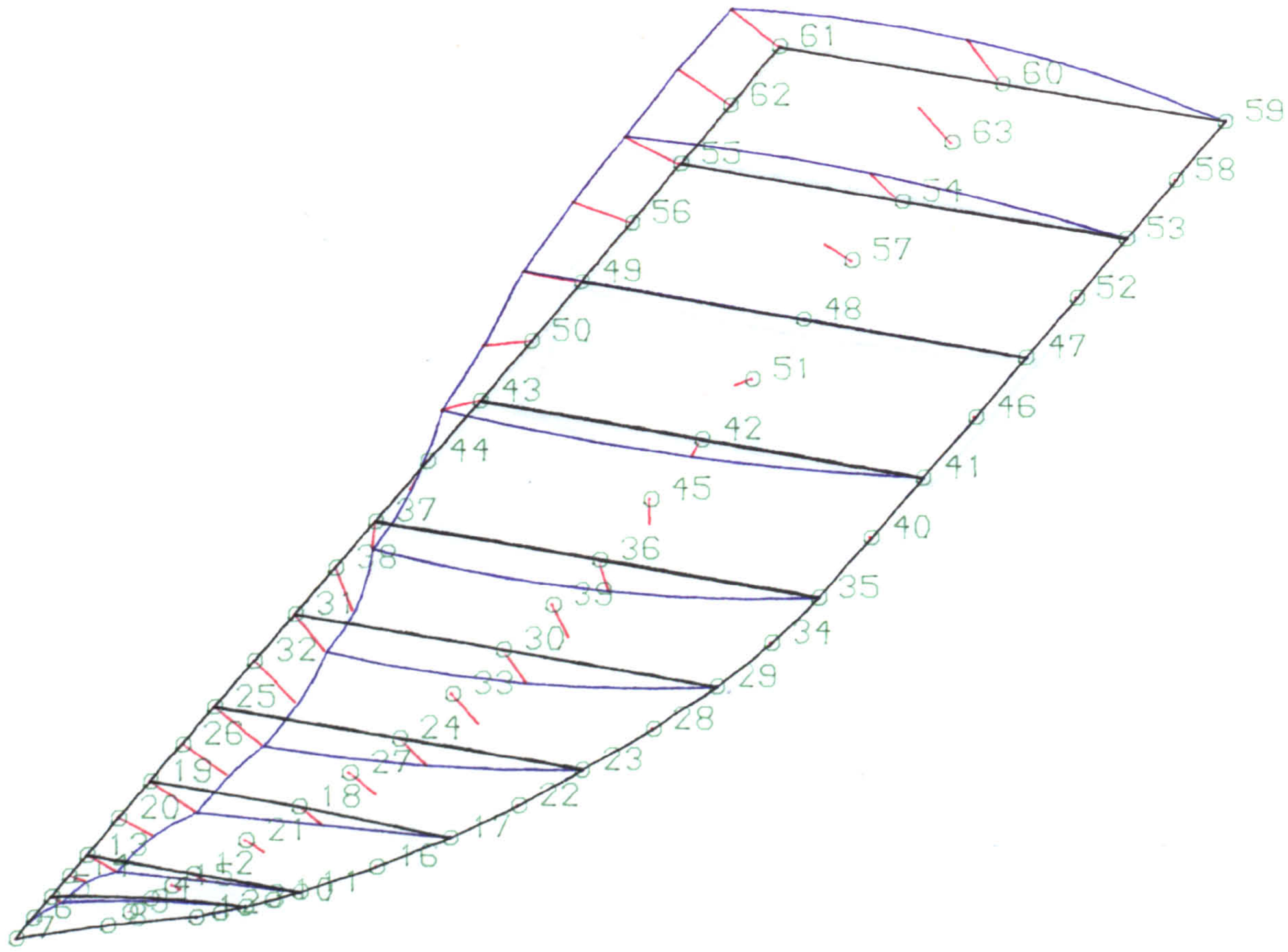

M.M.AZZAWI

Figure (8.40-b) Second Mode-Shape of Blade, Using 9-Node Element Mesh Number (2)

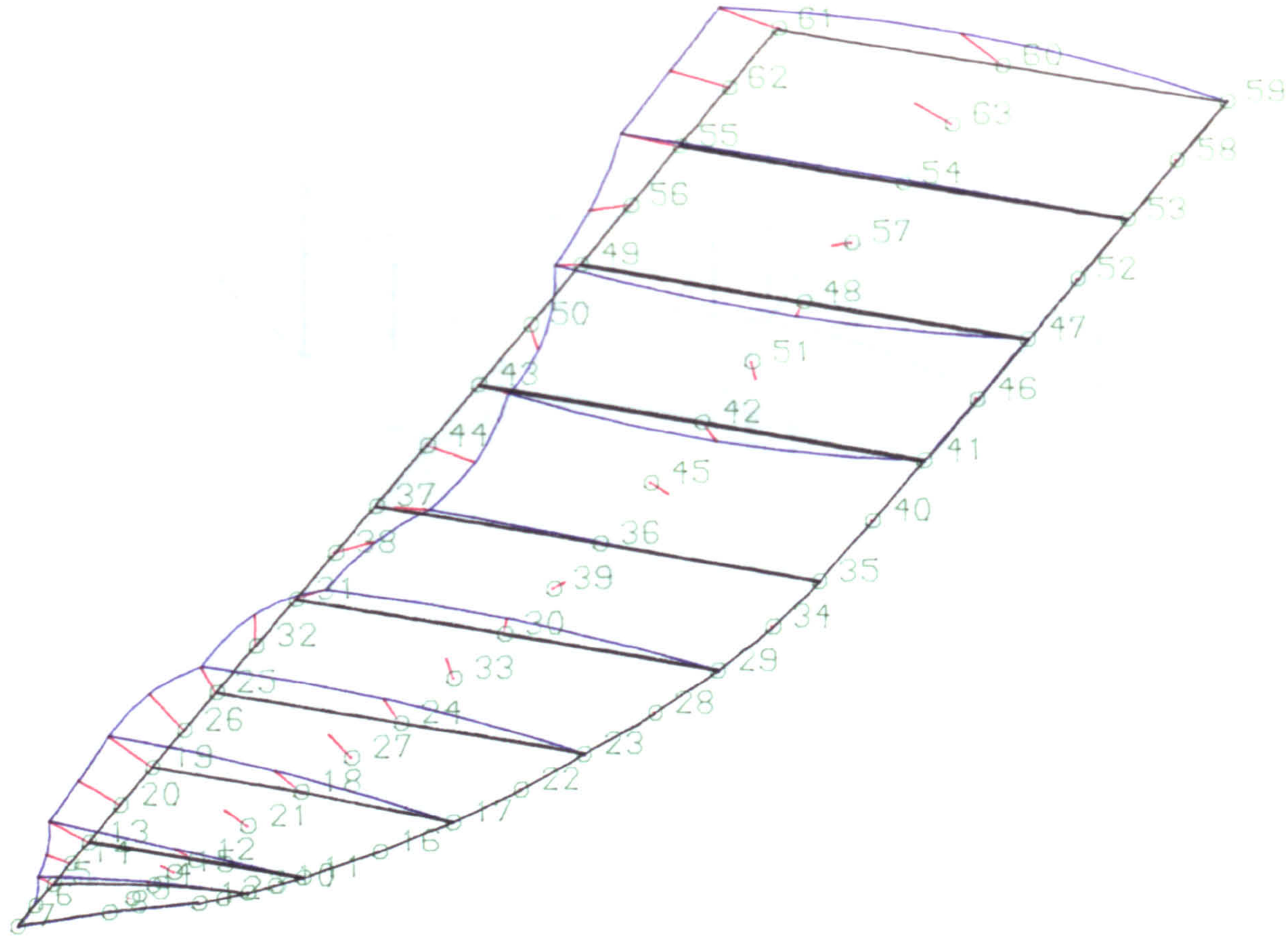

M.M.AZZAWI

Figure (8.40-c) Third Mode-Shape of Blade, Using 9-Node Element Mesh Number (2)

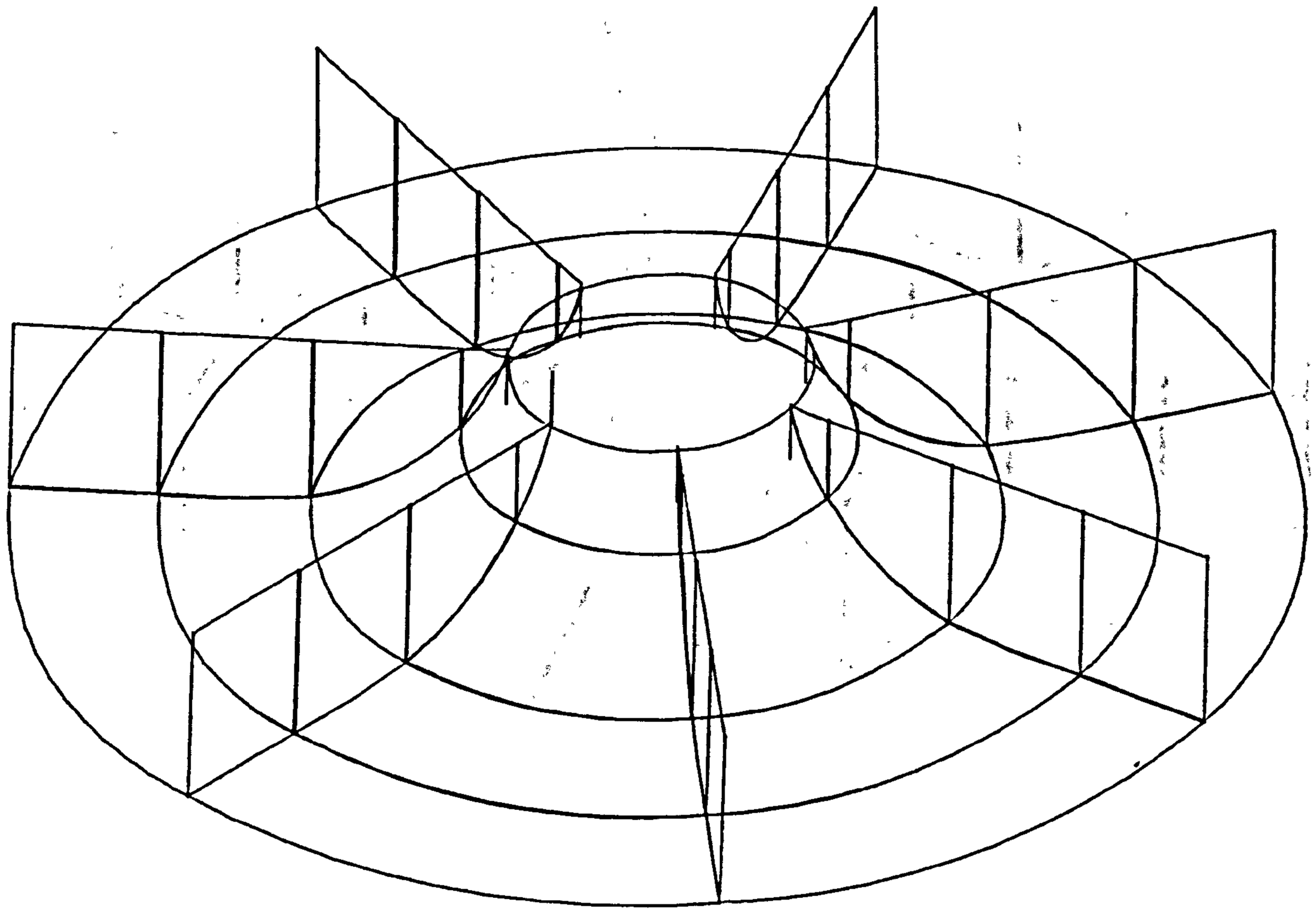

M.M.AZZAWI

Figure (8.41-a) Finite Element Mesh of Radial Impeller
Mesh of 56 (9-Node) Element, 256 Nodes.

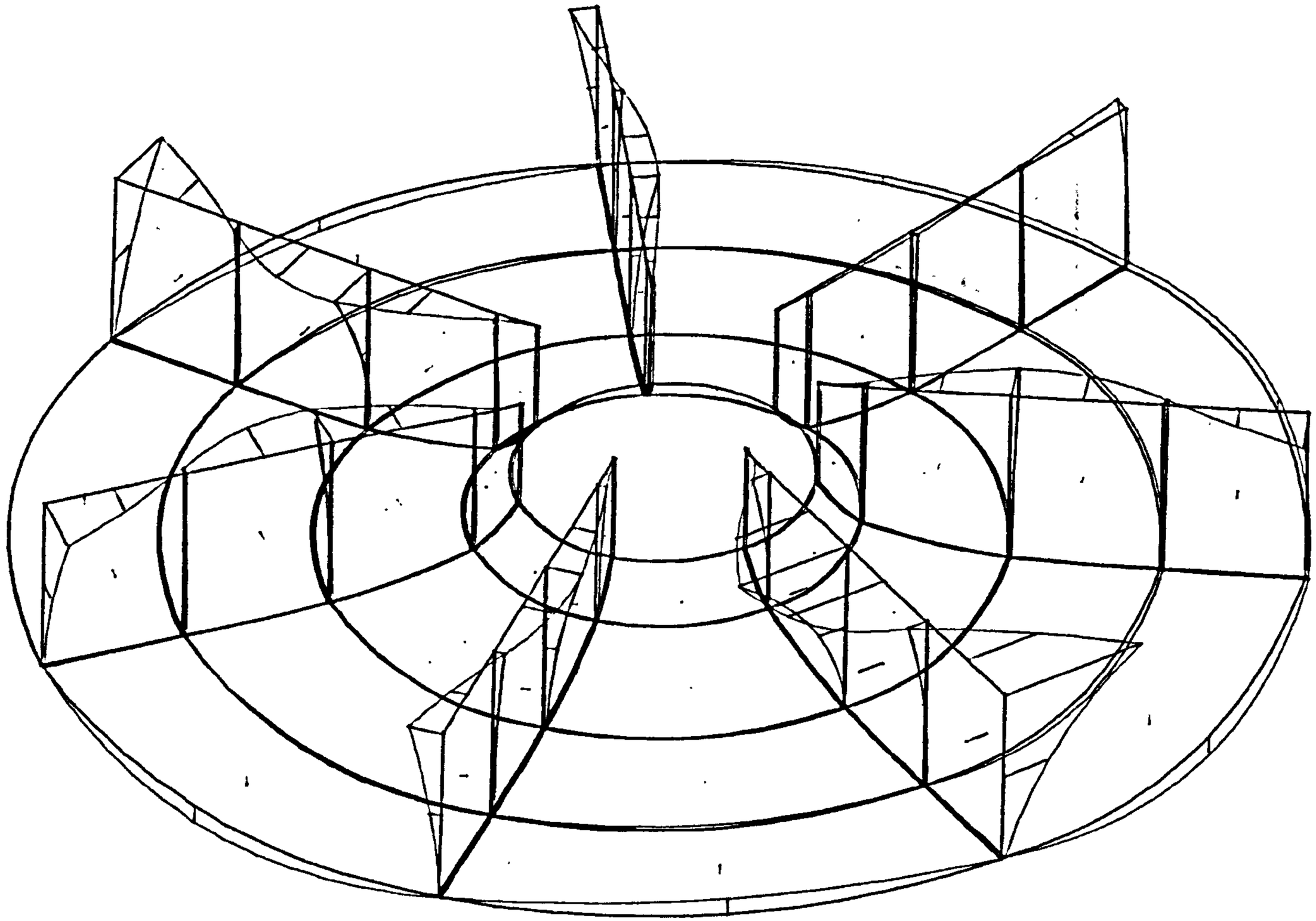

OMEGA11 = 16804.00000000

M.M.AZZAWI

Figure (8.41-b) Mode Shape of Radial Impeller, Using 9-Node Element Mesh Number (1), of 56 Elements, 256 Nodes.

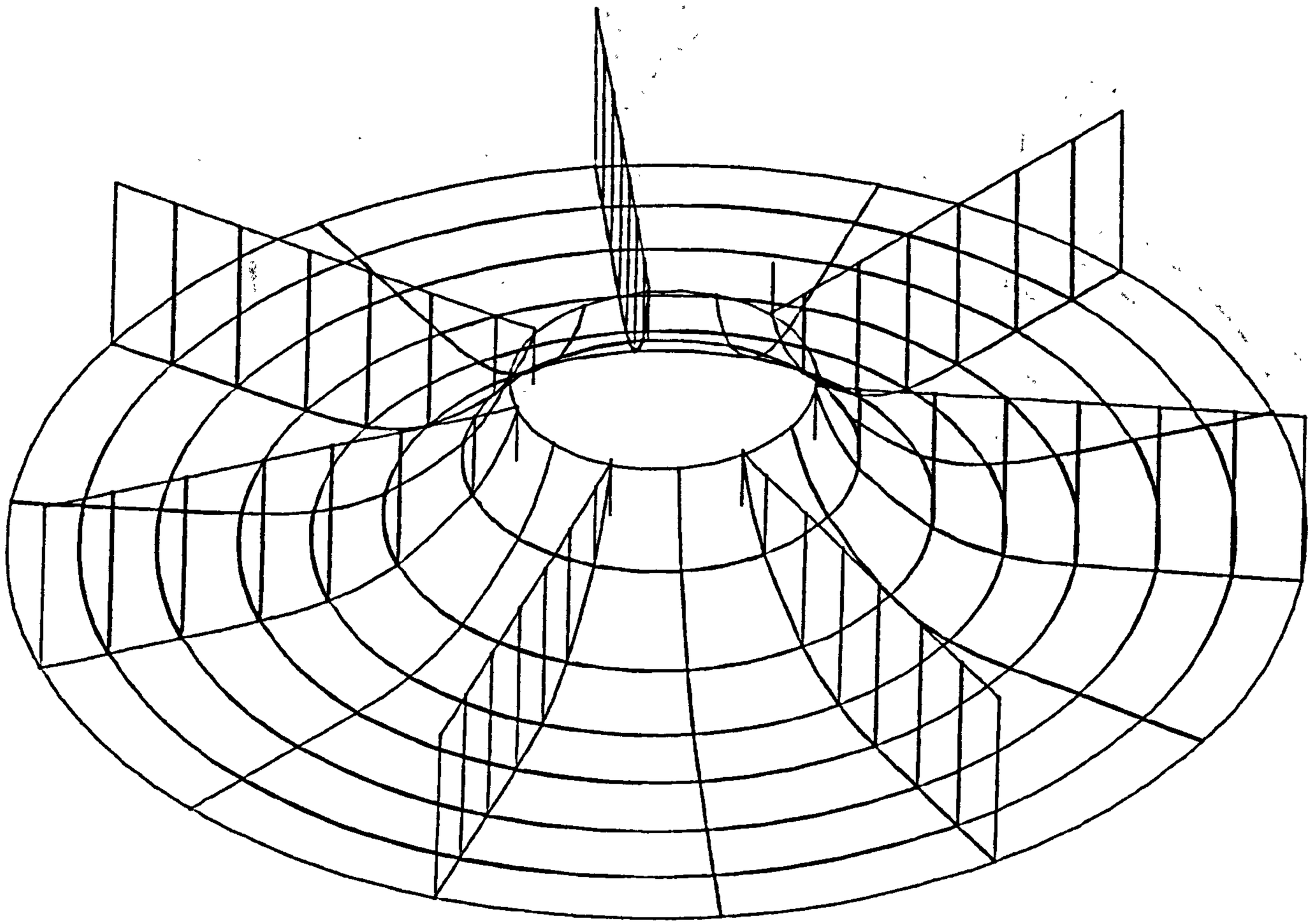

Figure (8.42-a) Finite Element Mesh of Radial Impeller
Mesh of 147 (9-Node) Element, 630 Nodes

M.M.AZZAWI

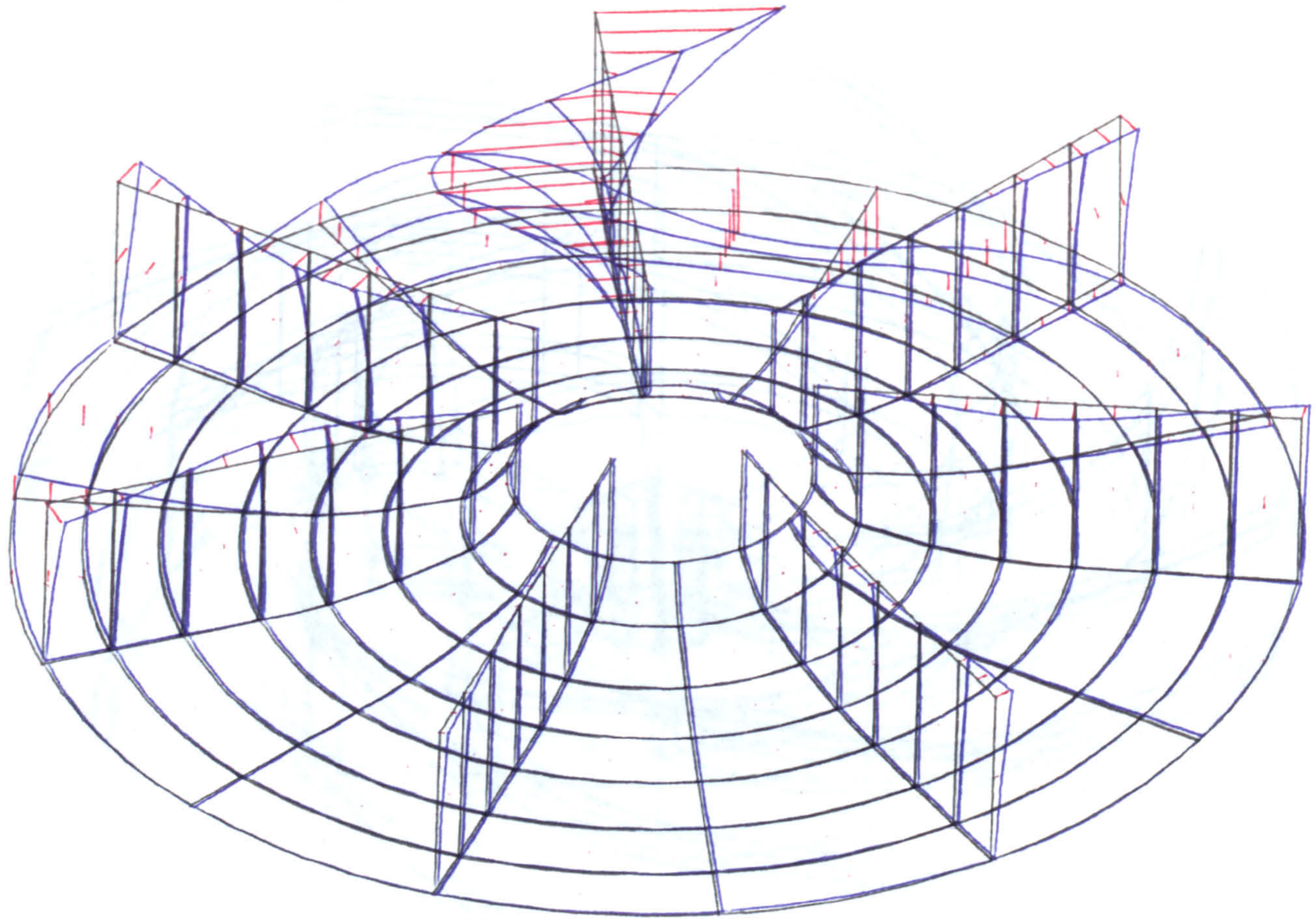

OMEGA11 = 16024.59960937

M.M.AZZAWI

Figure (8.42-b) Mode Shape of Radial Impeller, Using 9-Node Element
Mesh Number (1) of 147 Element, 630 Nodes.

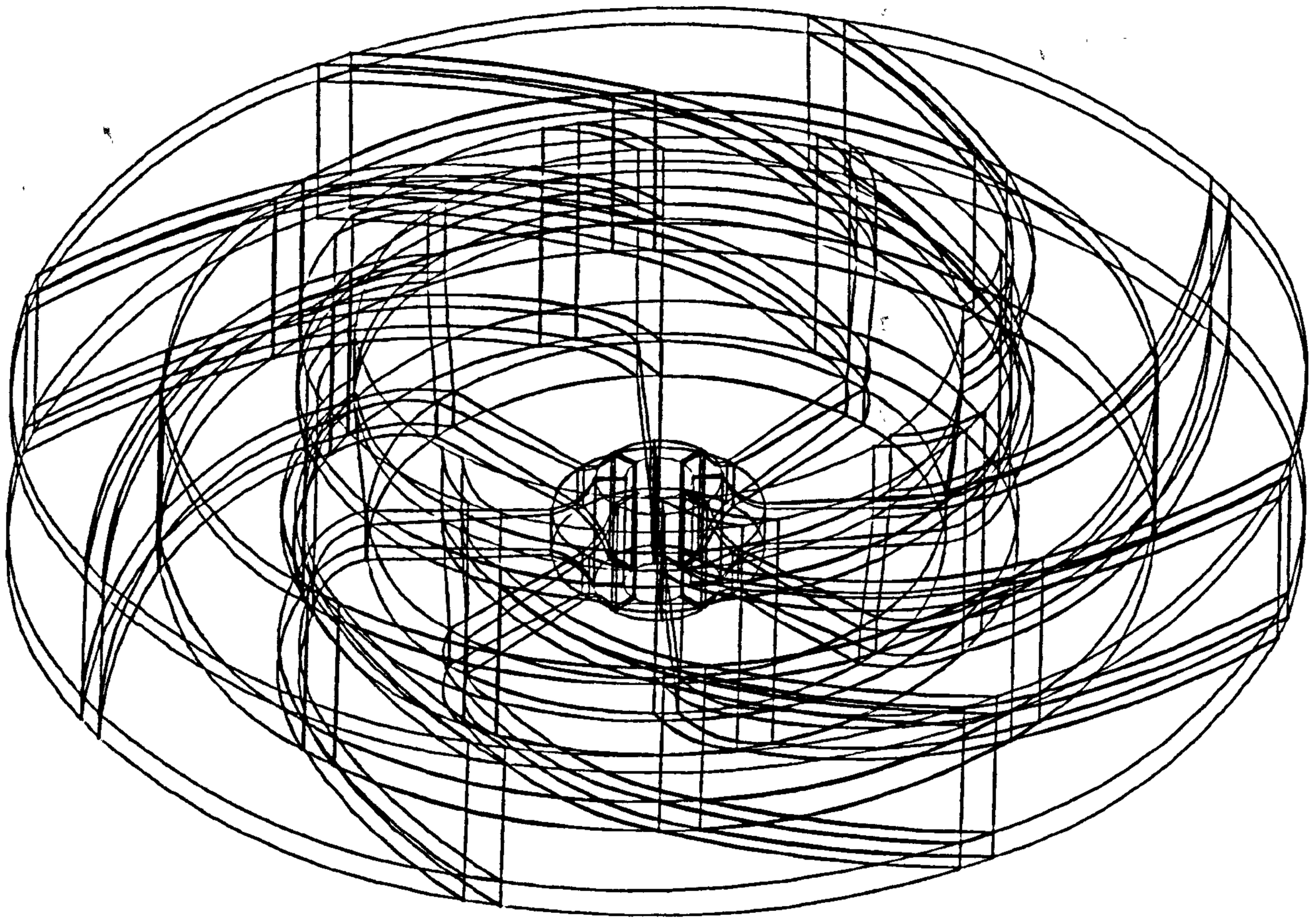

M.M.AZZAWI

Figure (8.43) Finite-Element Mesh of Radial Impeller, Case (2)
Mesh of 184 (20-Node) Element, 1400 Nodes.

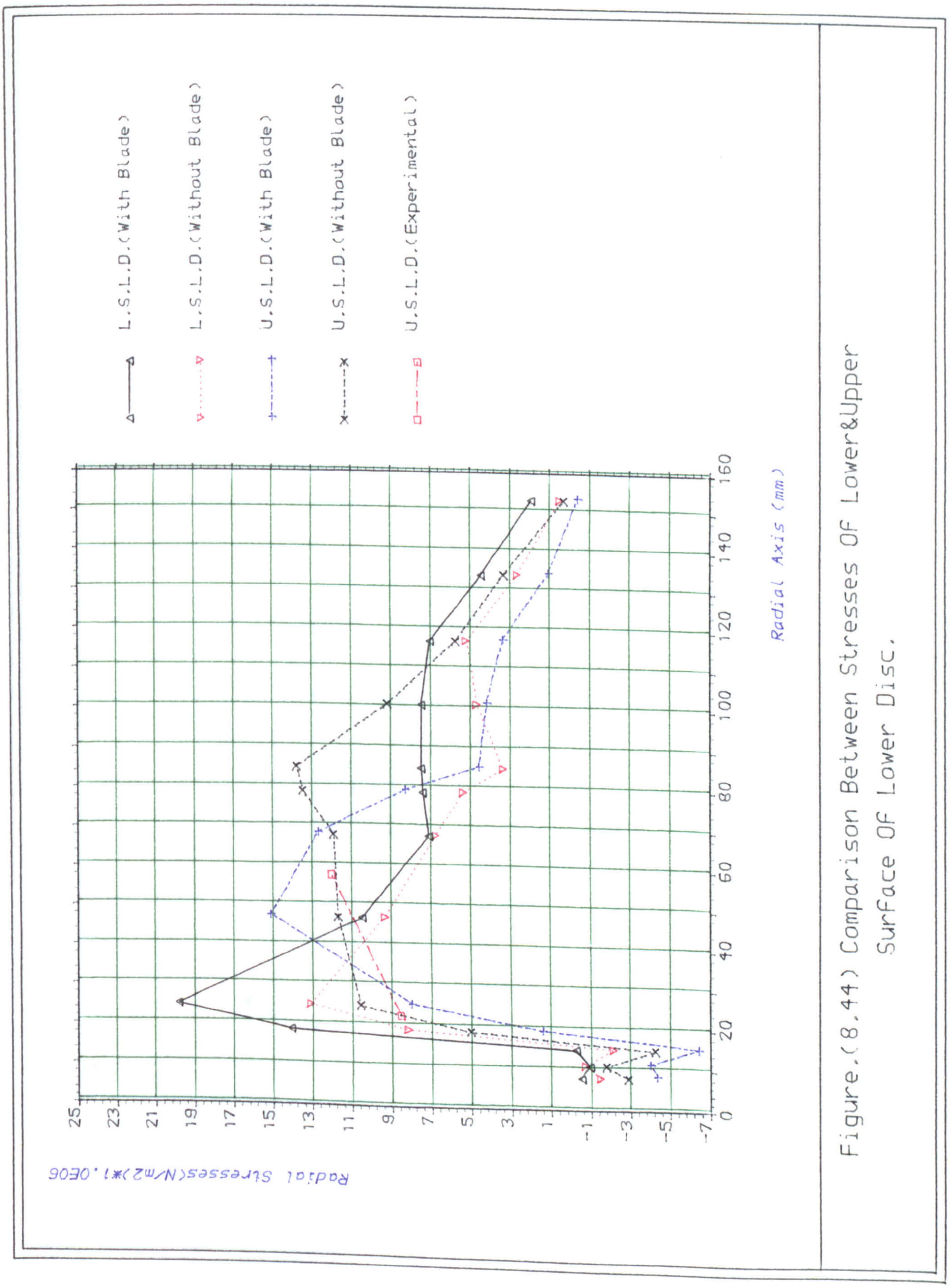

Figure.(8.44) Comparison Between Stresses OF Lower&Upper Surface Of Lower Disc.

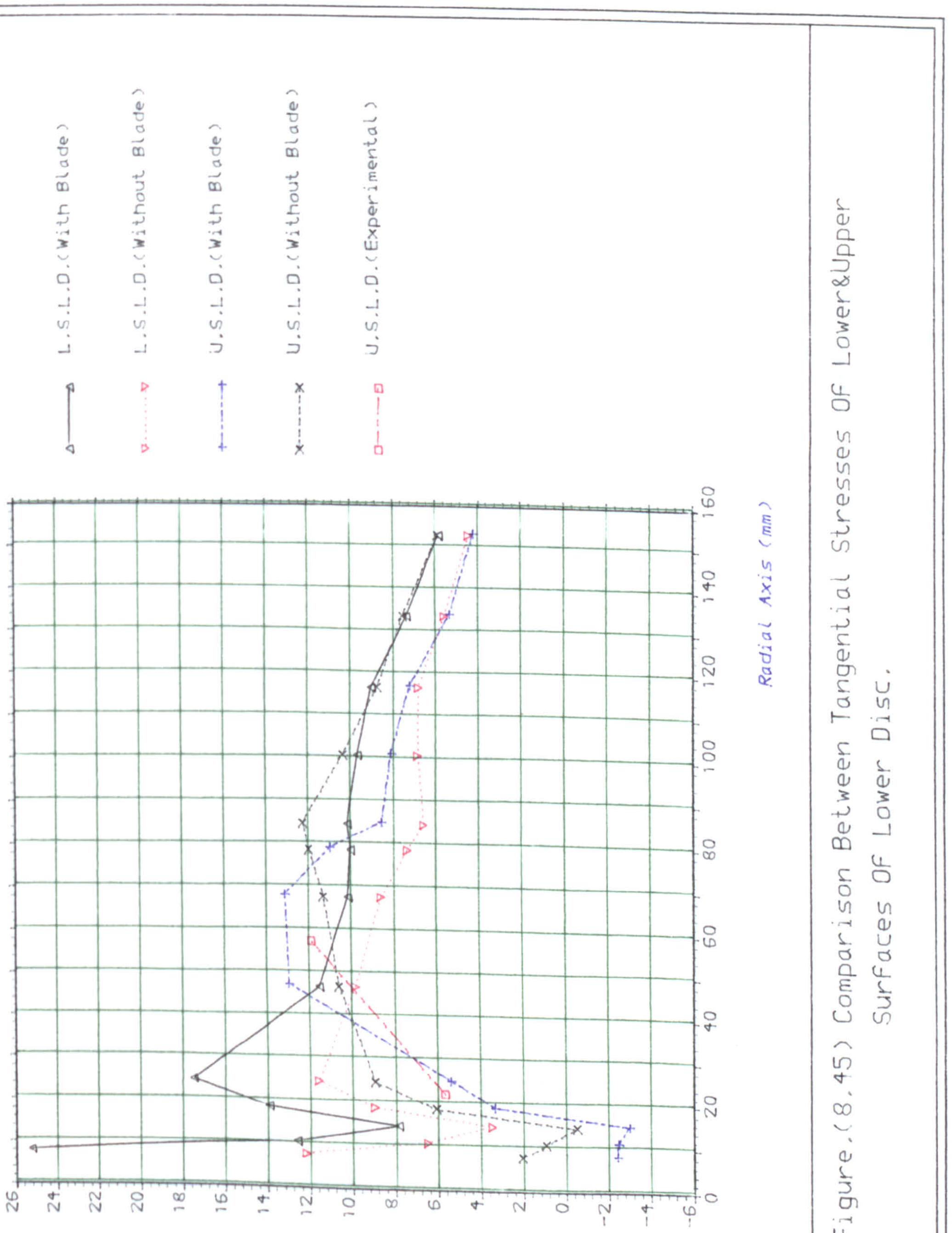

Figure.(8.45) Comparison Between Tangential Stresses Of Lower&Upper Surfaces Of Lower Disc.

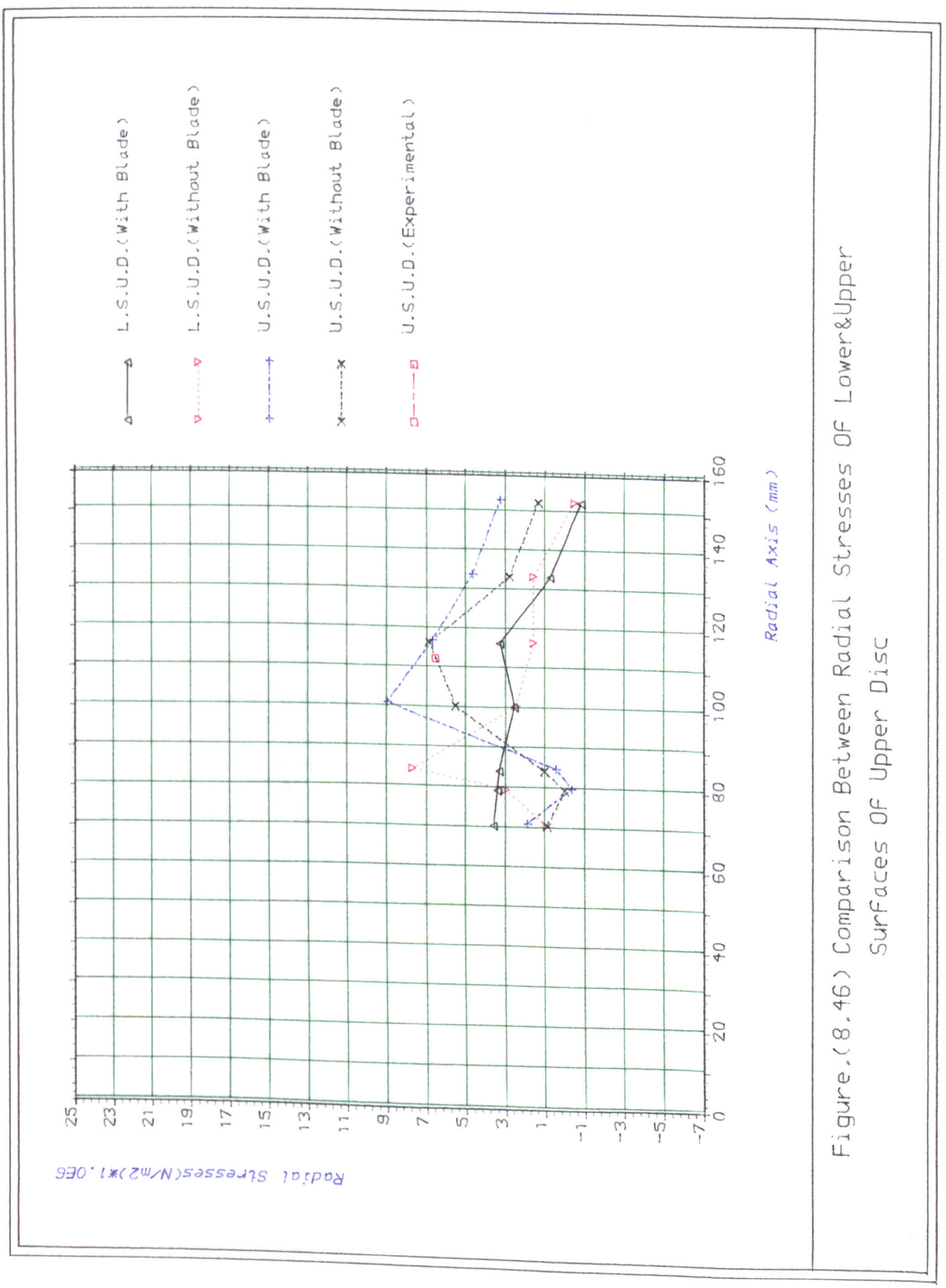

Figure.(8.46) Comparison Between Radial Stresses OF Lower&Upper Surfaces Of Upper Disc

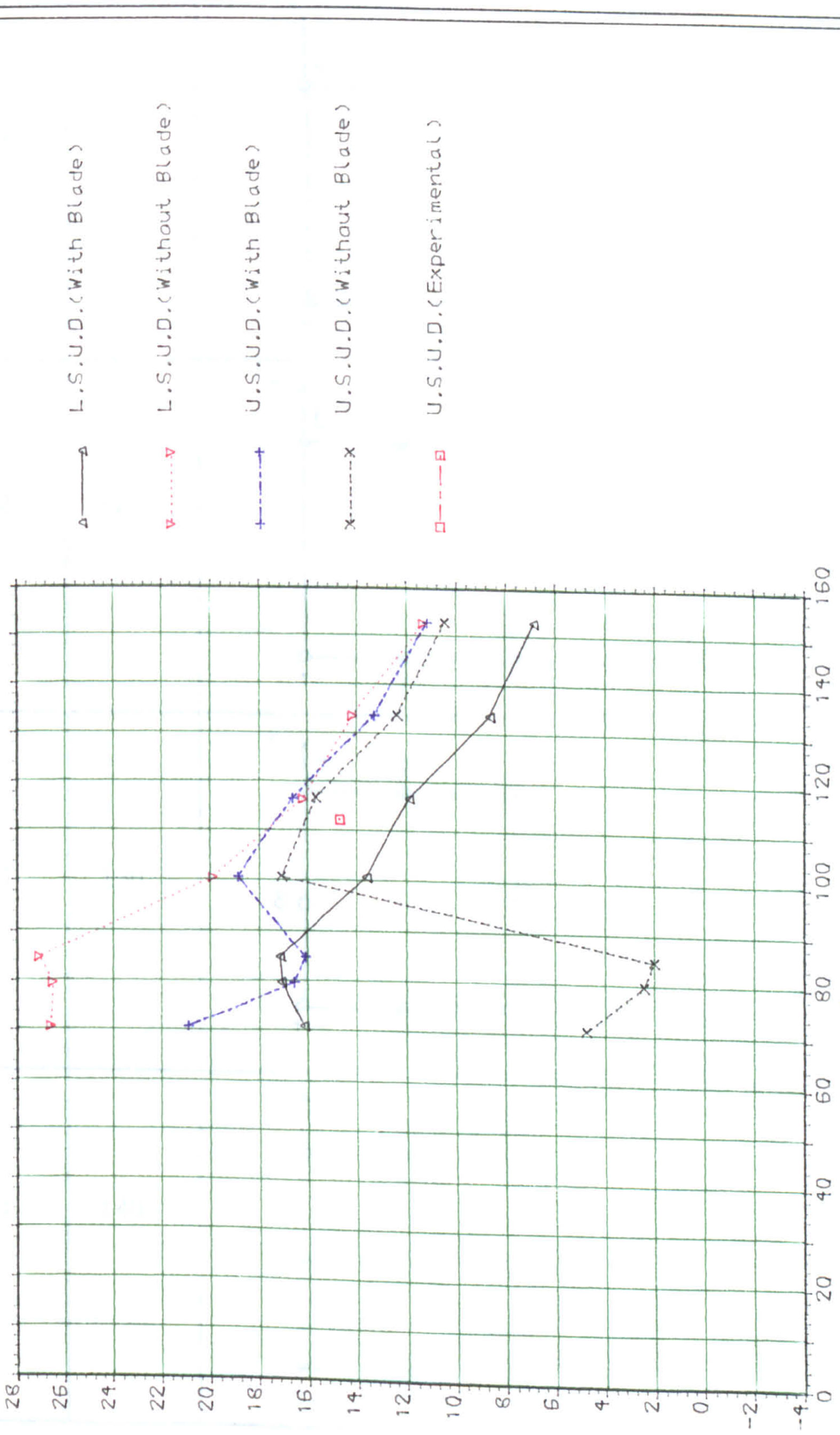

Figure.(8.47) Comparison Between Stresses OF Lower&Upper Surface OF Upper Disc.

No.	Package Code	Element	Name
1	110	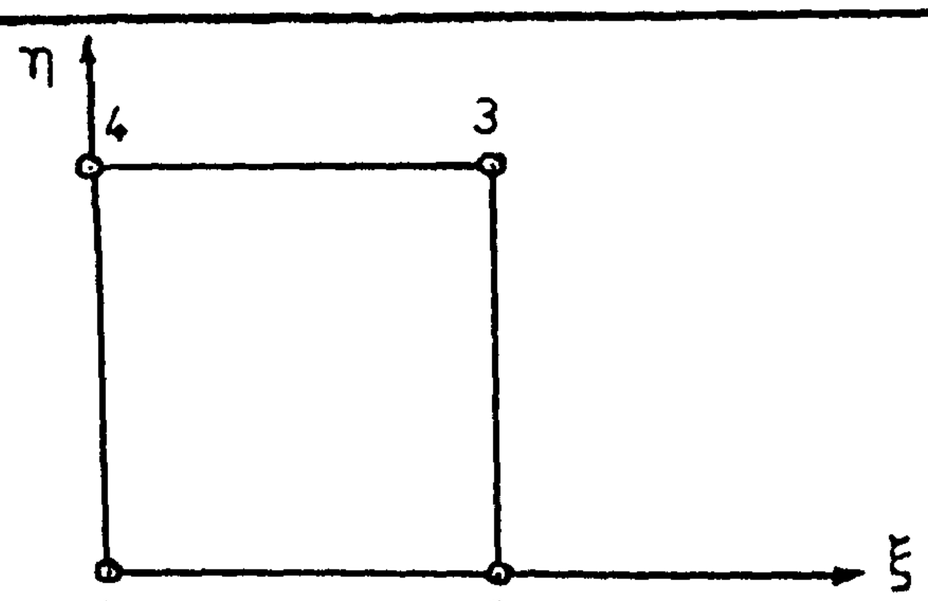	4-Node Quadrilateral
2	120	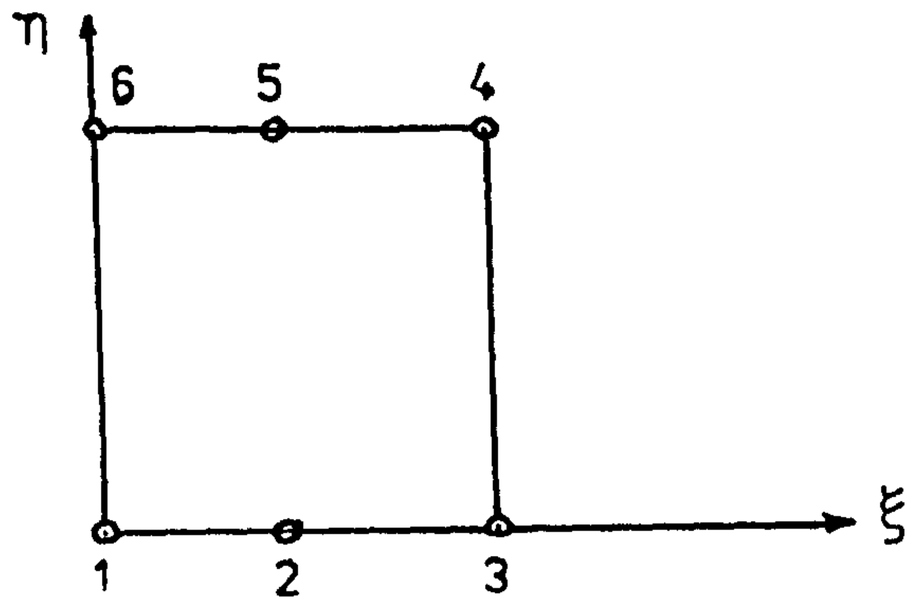	6-Node Serendipity
3	130	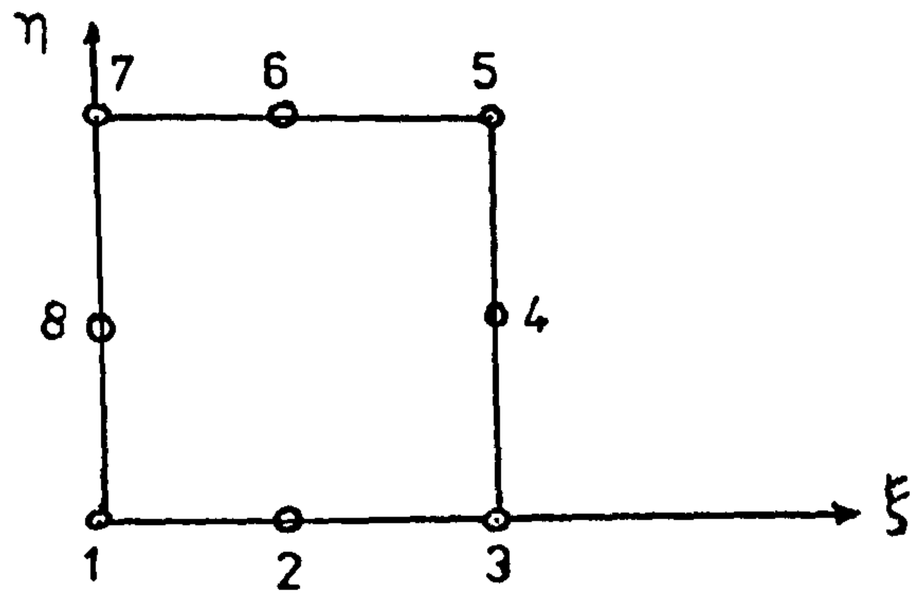	8-Node Serendipity
4	140	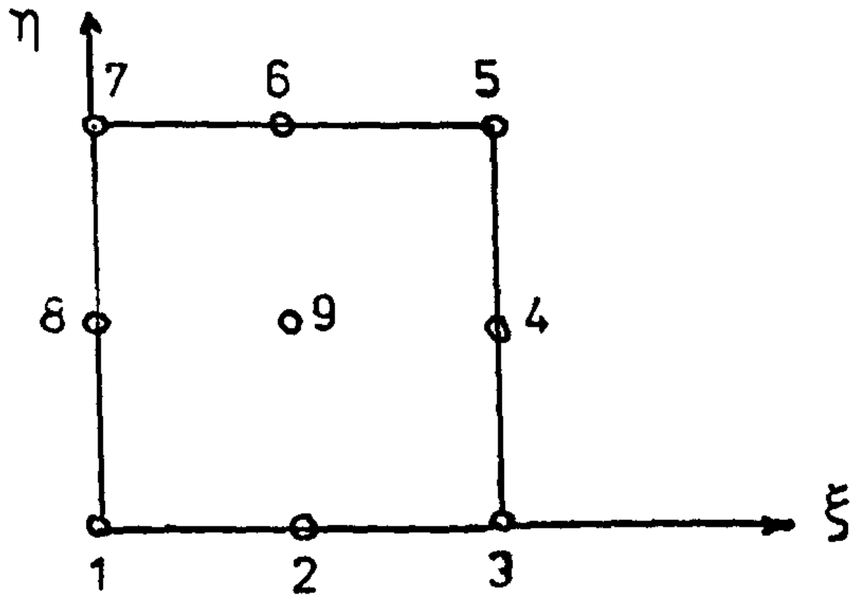	9-Node Lagrangian

Table 2.1 Quadrilateral Family (part 1)

No.	Package Code	Element	Name
5	150	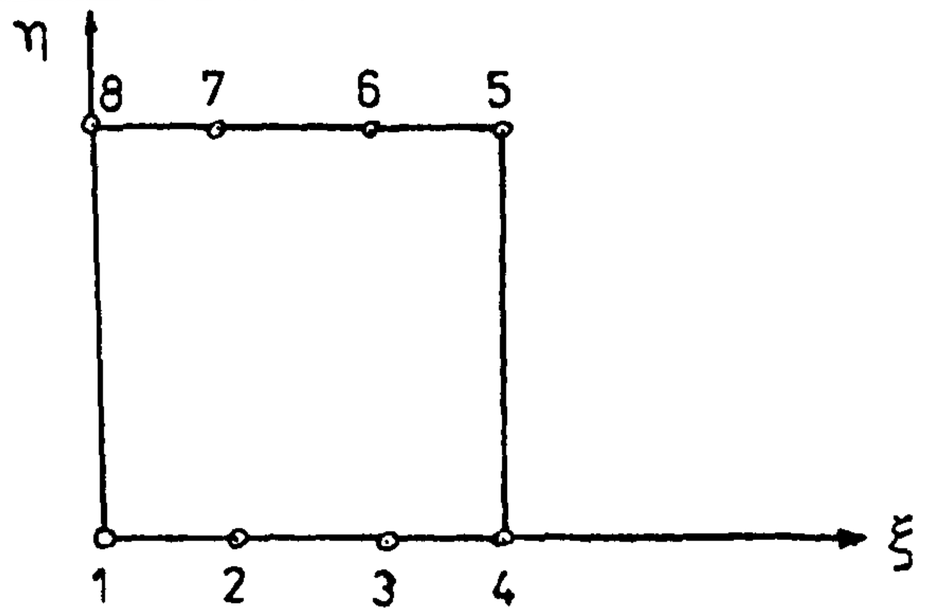	8-Node Serendipity
6	160	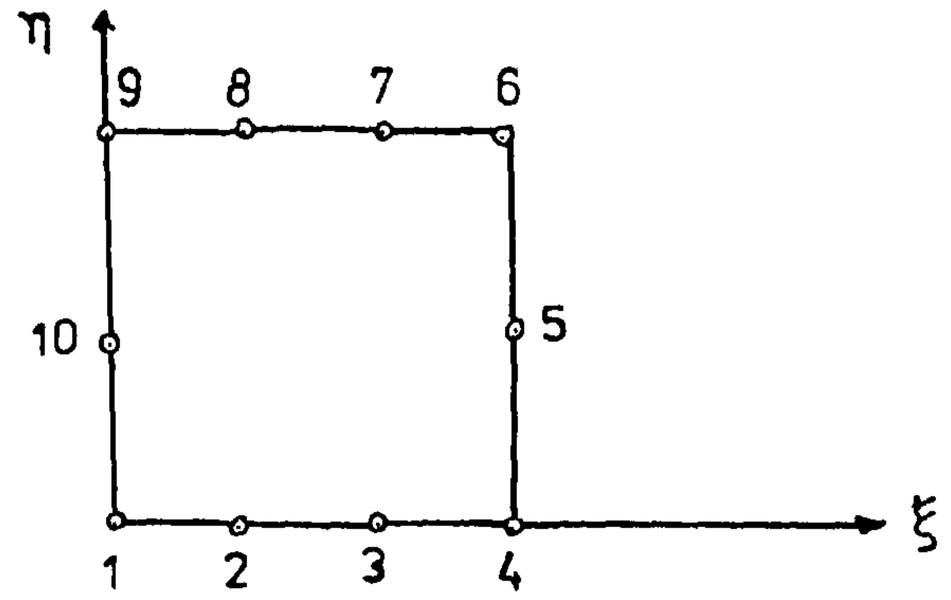	10-Node Serendipity
7	170	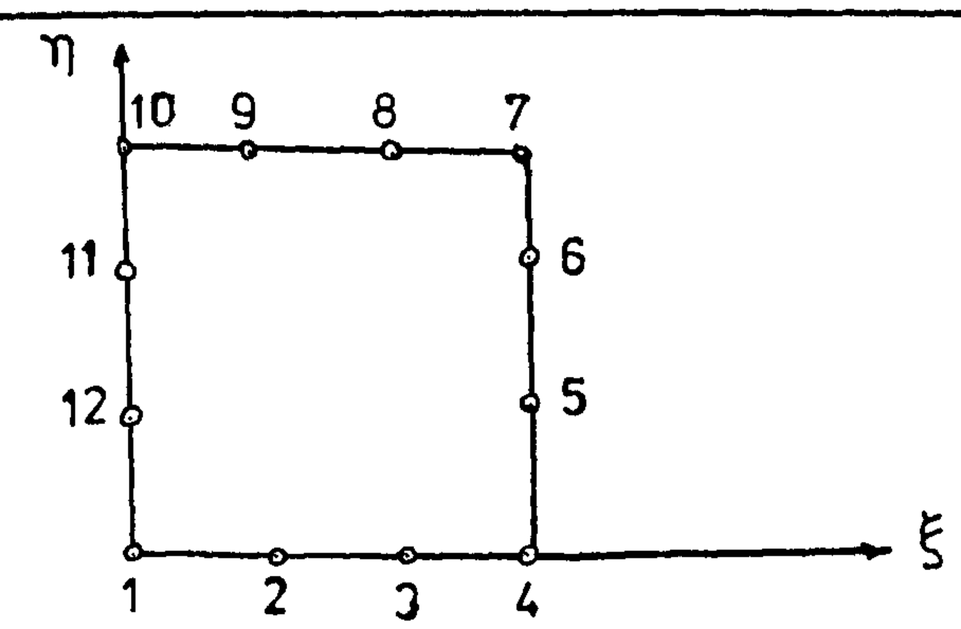	12-Node Serendipity

Table 2.2 Quadrilateral Family (part 2)

No.	package code	Element	Name
1	210	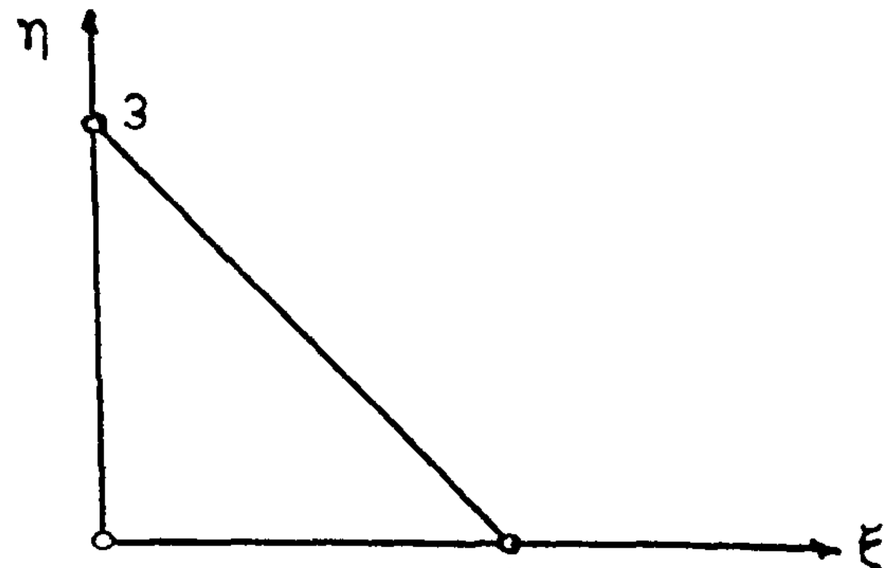	3-Node Linear
2	220	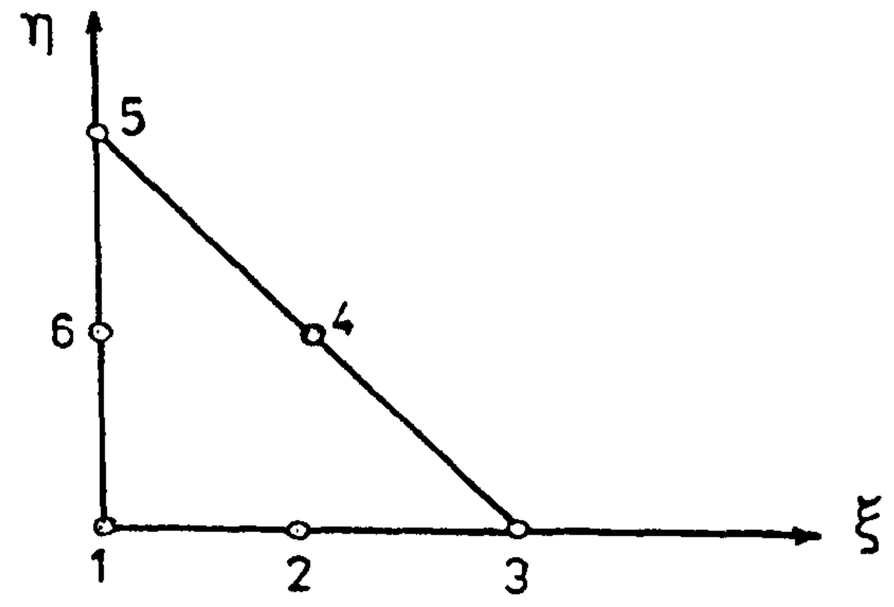	6-Node Quadratic
3	230	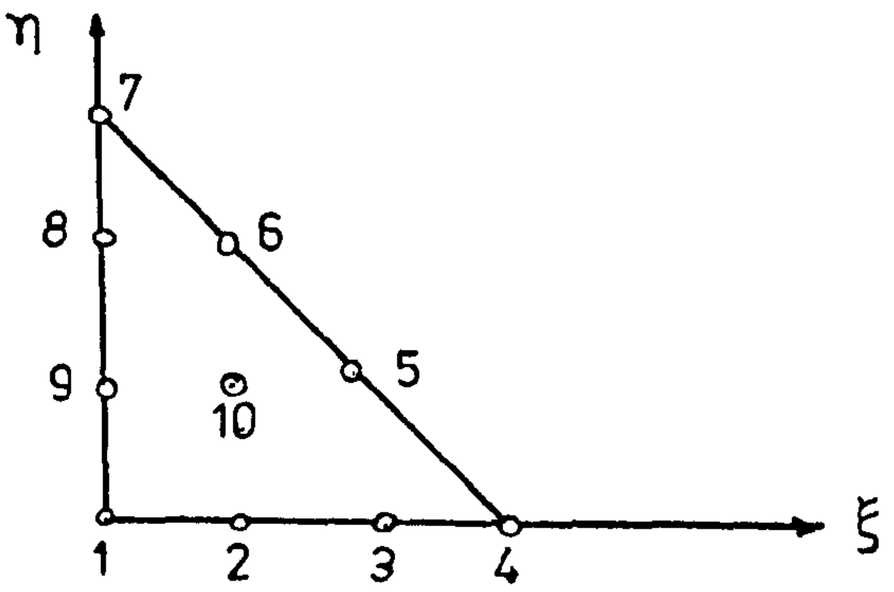	10-Node Cubic

Table 2.3 Triangular Family

No.	package code	Element	Name
1	310	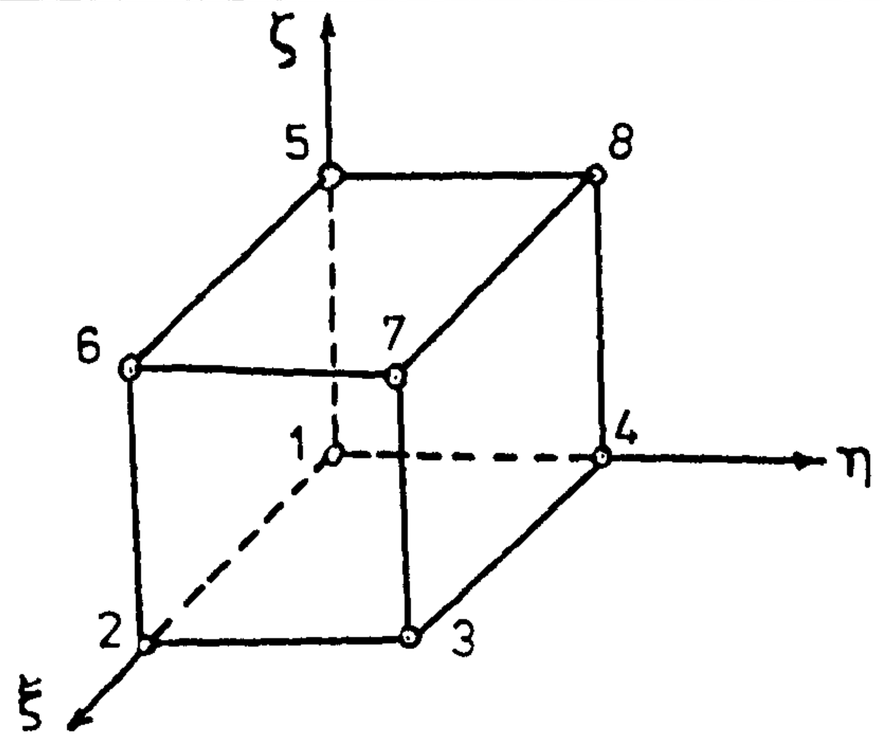	8-Node Lagrangian
2	320	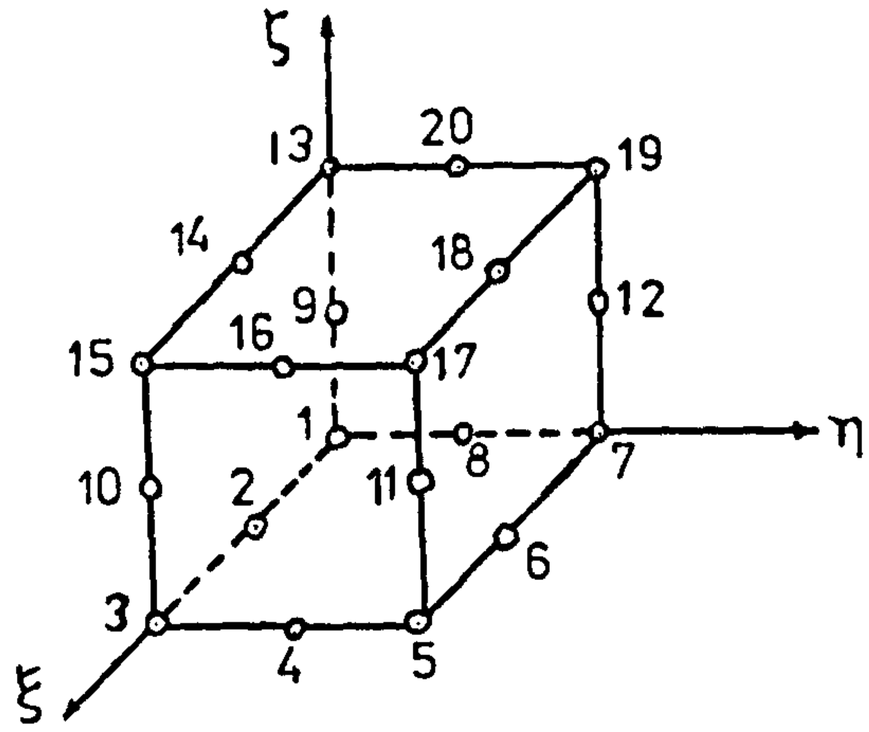	20-Node Serendipity

Table 2.4 Hexahedral Family

No.	package code	Element	Name
1	410	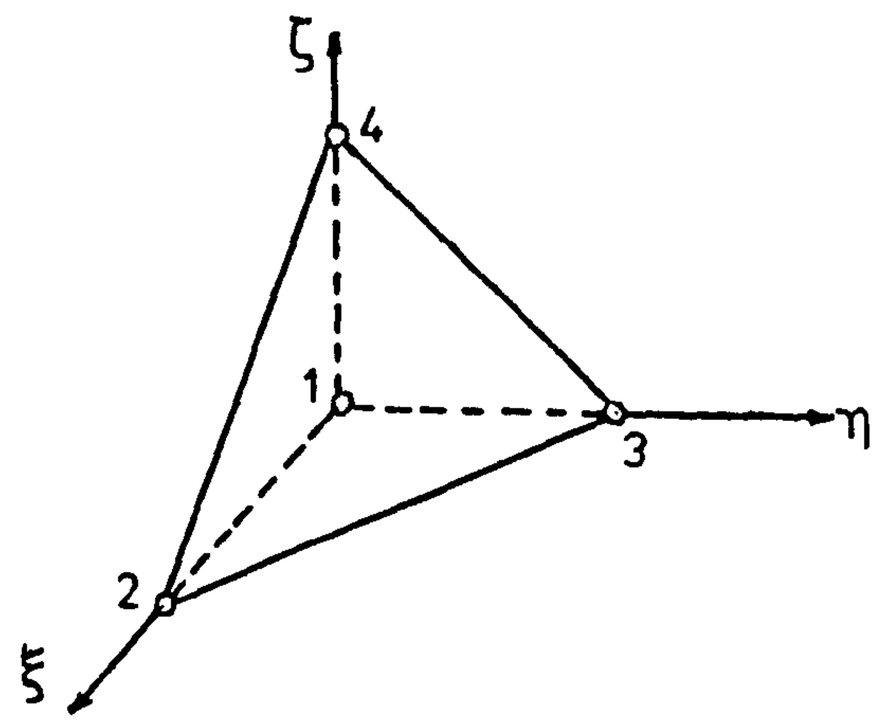	4-Node Tetrahedral
2	420	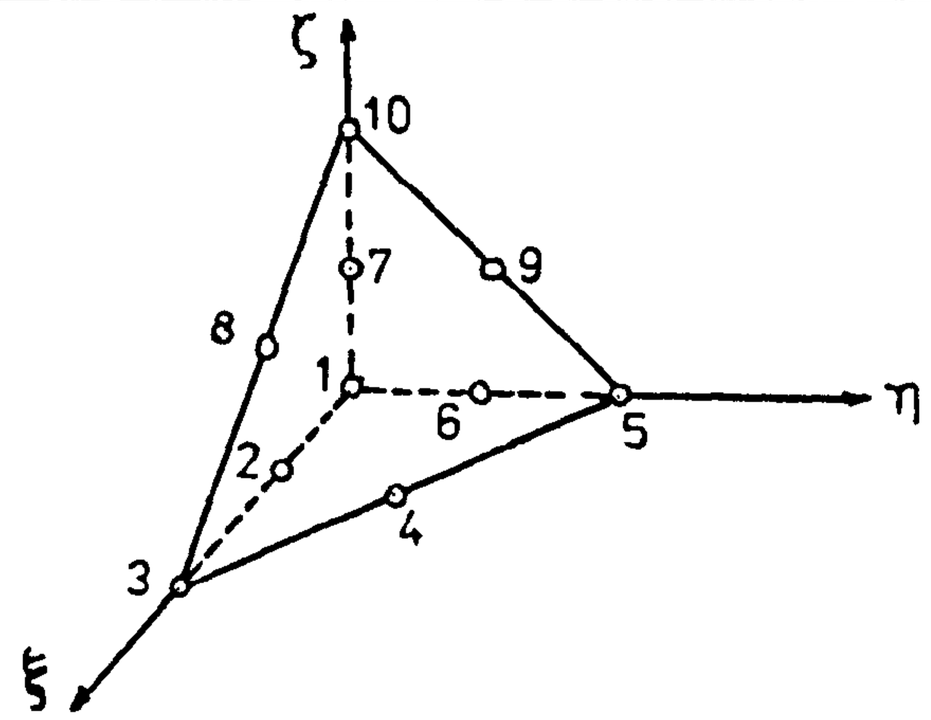	10-Node Tetrahedral

Table 2.5 Tetrahedral Family

No.	package code	Element	Name
1	510	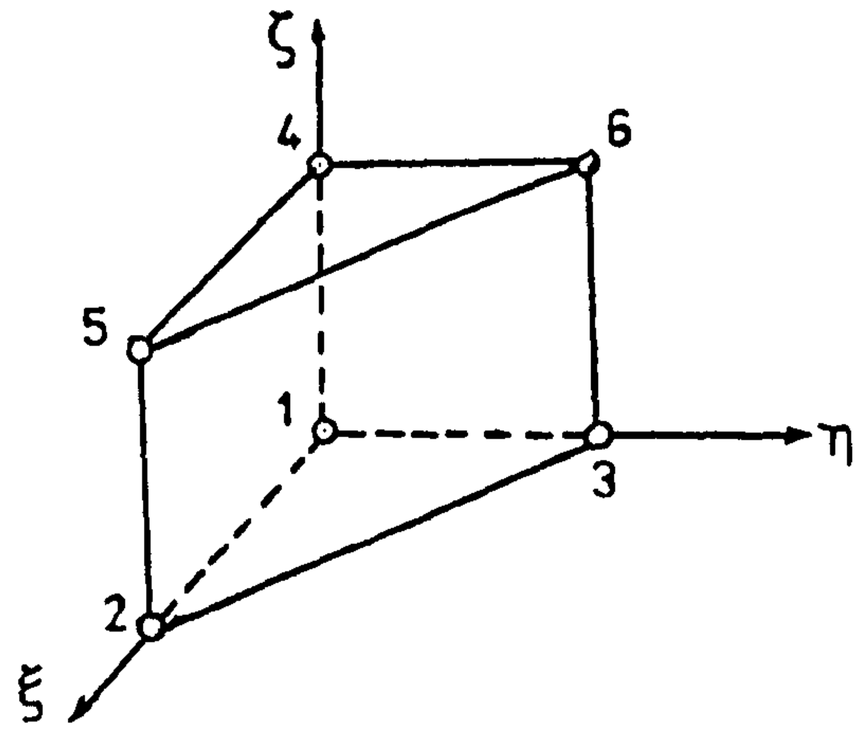	6-Node Pentahedral
2	520	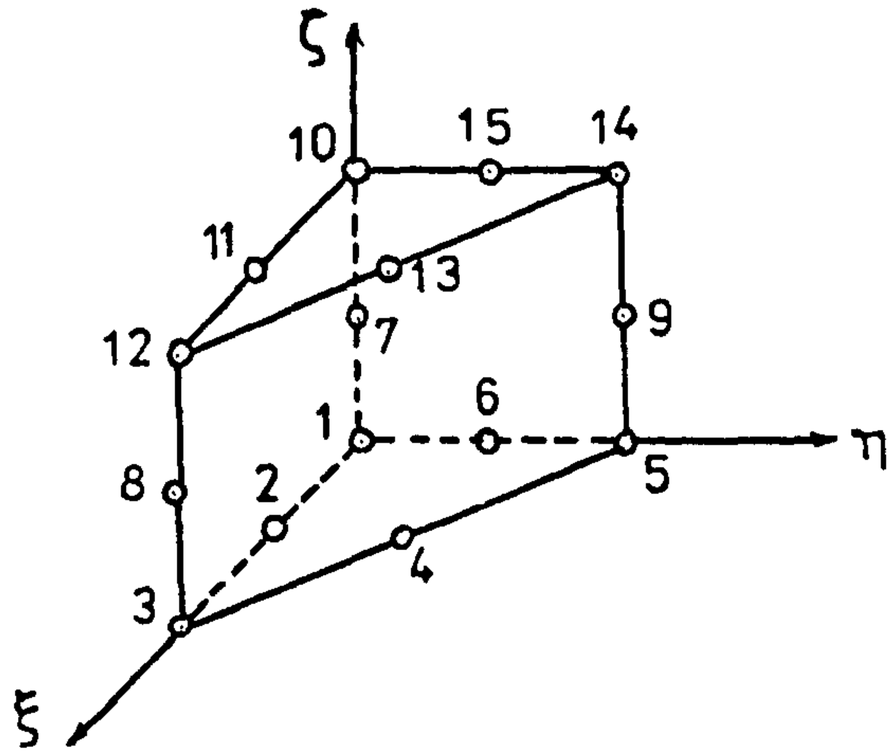	15-Node Serendipity

Table 2.6 Pentahedral Family

Type of Element	Number of Available Elements
Two-D (Plane-Stress,Plane-Strain)	10
Axisymmetric Elements	10
Mindlin Elements	10
Facet Thick Elements	10
Ahmad Elements	10
Kirchoff Elements	4
Facet Thin Elements	4
New Plate-Bending Elements	4
New Facet Elements	4
Three-D Cartesian Elements	6
Three-D Cylindrical-Polar Elements	6
Total	78

Table.7.1 Package Element Library

d1	Intrinsic Family
1	Lagrangian Quadrilateral Family
2	Lagrangian Triangular Family
3	Lagrangian Hexahedral Family
4	Lagrangian Tetrahedral Family
5	Lagrangian Pentahedral Family
6	Hermitian Quadrilateral Family
7	Hermitian Triangular Family

Table.7.2 Element First-Digit Code

Case Description	Holography Results (Hz)	FEM First Mesh Results (Hz)	FEM Second Mesh Results (Hz)
First Mode	1380	1272.6	1319.4
Second Mode	2729.7	2369.9	2435.6
Third Mode	4958.6	4134.8	4257.3

Table 8.1 Comparison Between Experimental and Theoretical Results for Blade Only.

Case Description	Holography Results (Hz)	FEM First Mesh Results (Hz)	FEM Second Mesh Results (Hz)
Diametral Mode	2418.1	2674.4	2550.4

Table 8.2 Comparison Between Experimental and Theoretical Results for Radial Impeller.